Remote sensing of supraglacial lakes on the Greenland Ice Sheet.

Selmes, Nick

Remote Sensing of Supraglacial Lakes on the Greenland Ice Sheet

Nick Selmes

Submitted in fulfilment of the requirements for the degree of Doctor of Philosophy

Swansea University
Department of Geography

August, 2011.

ProQuest LLC.
789 East Eisenhower Parkway
P.O. Box 1346
Ann Arbor, MI 48106 – 1346

Abstract

The dynamic mass loss from the Greenland Ice Sheet has prompted considerable research into the role of supraglacial lakes in causing dynamic thinning. These lakes can drain through 1000 m of ice to the bed and are thought to play an important role in connecting the surface and basal hydrologies of the ice sheet, allowing water to reach the bed and cause the ice to accelerate. Despite this apparent importance little research has been carried out on lakes outside of SW Greenland, and no research has examined the occurrence of lake drainage over the whole of Greenland. The aim of this thesis is to discover where lakes occur for the entire Greenland Ice Sheet, and how these lakes drain.

New remote sensing techniques for monitoring lakes through the melt season were developed and tested. The evolution of 2600 lakes (those lakes larger than > 0.125 km^2) was studied over five years (2005–2009) using 3704 MODIS images. Lakes were discovered to either drain fast to the bed, more slowly over the surface, or to freeze at the end of the melt season. There were 263 fast lake drainages per year of which 61% were in the SW region and a further 17% in the NE, both regions where mass loss is mainly due to surface mass balance. In the dynamically thinning SE region there were only three fast lake drainages per year along a 1300 km coastline. In the NW, fast lake drainage did not occur on five of the ten glaciers with the most rapid dynamic thinning. The results of this thesis show that the drainage of supraglacial lakes cannot have been responsible for dynamic mass loss from the Greenland Ice Sheet.

Acknowledgements

Several people made writing this thesis either possible or at least far less painful. First of all thanks goes to my supervisors Tavi and Tim, for selecting me for the project in the first place, sharing their expertise, and for turning around paper and chapter drafts within hours of first seeing them. Swansea Glaciology is fortunate to have a fantastic postgraduate and postdoctoral community. Thanks to all, you made writing this thesis far more pleasant. Thanks also to all those who invited me along on fieldwork, I was grateful to get my Greenland fix each summer. Apologies to family and friends in other parts of the UK for largely vanishing for a year during the write up, and thanks to my parents for their support. Finally, thank you to Amy for her support through all four years of my PhD and for putting up with my increasing absence as this thesis progressed, I think we can only be grateful that we were both writing up at the same time!

This project was funded by the Leverhulme Trust, through the GLIMPSE research group.

Contents

List of Figures

List of Tables

List of Abbreviations

ASTER	Advanced Spaceborne Thermal Emission and Reflection Radiometer
AWS	Automatic Weather Station
CREFL	Corrected Reflectance algorithm
E	East
Fa	Fast draining lakes
Fr	Freezing lakes
GrIS	Greenland Ice Sheet
IDL	Interactive Data Language
LST	Land Surface Temperature (referring to a MODIS data product)
MODIS	Moderate Resolution Imaging Spectroradiometer
N	North
NIR	Near Infra-Red
NSIDC	National Snow and Ice Data Center
P	Probability
p	Statistical p-value
S	South

Sl	Slow draining lakes
Un	Lakes of unknown drainage type
W	West

Chapter 1

Introduction and Aims

1.1 Mass loss from the Greenland Ice Sheet

Air temperatures over the Greenland Ice Sheet (GrIS) have increased significantly since 1990 resulting in increasing melt and runoff. However, there has also been a concurrent increase in accumulation (Hanna *et al.*, 2008). As a result the overall surface mass balance of the GrIS shows no significant trend (Hanna *et al.*, 2006; Box *et al.*, 2006). Despite no significant trend in surface mass balance, the GrIS is still losing mass. This mass loss from the ice sheet can be measured using the GRACE gravimetry satellites and laser altimetry.

Results from GRACE show a substantially negative mass balance. Wouters *et al.* (2008) found a mass loss of 179±25 Gt yr^{-1} for the period 2003-2008. The highest mass loss was in 2005 and 2007, with 279 and 328 Gt lost respectively over two month periods. Mass loss has also been found to be accelerating. The mass loss for 2002–2003 was 137 Gt yr^{-1}, however by 2007–2009 this had increased to 286 Gt yr^{-1} (Velicogna, 2009). These figures are in broad agreement with mass balance studies from lidar altimetry, with Sørensen *et al.* (2011) finding ice sheet mass balances in the range of 191 $\pm$ 23 Gt yr^{-1} to 240 $\pm$ 28 Gt yr^{-1} for the period October 2003 to March 2008. Rignot *et al.* (2008) attempted to model longer term trends in mass

balance, and estimated that the ice sheet lost 110 ± 70 Gt yr^{-1} in the 1960s, was in near balance 1970s–1980s, lost 97 ± 47 Gt yr^{-1} in 1996, and then that mass loss increased rapidly to 267 ± 38 Gt yr^{-1} in 2007.

Mass loss has been found to be spatially uneven. Mass loss increased considerably in the SE around 2003 (Velicogna and Wahr, 2006; Khan *et al.*, 2010), and a subsequent increase in mass loss commenced in the NW around 2005 (Wouters *et al.*, 2008; Khan *et al.*, 2010). Mass loss in the SE slowed in 2006, although it is still above pre-2003 levels (Khan *et al.*, 2010). Altimetry studies show that the ice sheet is generally thinning at lower altitudes (Abdalati *et al.*, 2001; Krabill *et al.*, 2004) and either stable (Krabill *et al.*, 1999, 2000) or thickening (Johannessen *et al.*, 2005) at higher elevations. Significant mass loss above 2000 m was observed by GRACE for the first time in 2007 (Wouters *et al.*, 2008), although the mass balance from GRACE above 2000 m was still positive over the period 2003–2010 (Schrama and Wouters, 2011).

Models of surface mass balance do not predict the increasingly negative mass balance (Hanna *et al.*, 2005), suggesting a dynamic element. Removal of surface mass balance and density change signals from the mass loss inferred from lidar (Pritchard *et al.*, 2009) and GRACE (van den Broeke *et al.*, 2009) has shown that the mass loss from the regions with greatest mass loss, the South East (SE) and North West (NW), must be dynamically driven as surface mass balance is not sufficiently negative in those regions. In the South West (SW) and North East (NE) regions of the ice sheet however, mass loss can be explained by a negative surface mass balance and therefore has little or no dynamic component. Mass loss being concentrated in the SE and NW is particularly interesting as both regions are dominated by tidewater glaciers, and Rignot *et al.* (2008) has shown that variations in glacier discharge cause 60% more variation in ice sheet mass balance than is caused by surface mass balance.

1.1.1 Changes in outlet glaciers

The discovery that mass loss has been concentrated in regions that are drained by tidewater glaciers has lead to considerable study of the behaviour of these outlets. Large-scale changes have been recorded at outlet glaciers in most sectors of the ice sheet. Moon and Joughin (2008) examined the frontal positions of 203 outlet glaciers over three periods: 1992–2000, 2000–2006, and 2006–2007. Between the first two of these periods, an increase in glacier retreat was noted for tidewater glaciers in the North (N), East (E), and SE regions. Land-terminating ice showed no change over the same period. By the period 2006–2007, retreat in the NW had increased further, whereas the SE region had switched to a period of mean advance. Howat and Eddy (2011) found that of a sample of 210 marine terminating glaciers, 90% retreated during the period 2000–2010. Nearly 100% of NW tidewater glaciers retreated during the same period.

Synchronous regional trends in glacial thinning, retreat, and acceleration have occurred. Tidewater outlet glaciers of the SE region commenced thinning in 2003, with associated retreat and acceleration over the following two years (Howat *et al.*, 2008; Hanna *et al.*, 2009; Murray *et al.*, 2010). Included in this retreat were the major outlets of Helheim and Kangerdlugssuaq Glaciers. This retreat was followed by a widespread regional slow down of the same glaciers, with thickening and frontal advance (Murray *et al.*, 2010). The synchronous nature of this retreat suggests the role of an external forcing mechanism.

1.2 The possible effects of mass loss from the Greenland Ice Sheet

1.2.1 Albedo

Any retreat in the GrIS would result in the increased exposure of either a bare land or ocean surface. As the albedo of snow and ice can be high (84% for dry snow and 40% for clean bare ice (Paterson, 1994)) it has a significant cooling effect on the regional climate. The loss of large areas of ice could trigger positive feedback mechanisms of warming as high albedo ice is replaced with lower albedo surfaces, which has been argued to be a potential forcing effect for rapid climate change through ice sheet disintegration (Hansen *et al.*, 2007).

1.2.2 Sea-level rise

Global sea-level rise for 1993–2003 was measured to be $3.1 \pm 0.7\,\mathrm{mm\,yr^{-1}}$ compared to the average for the 20^{th} Century of $1.7 \pm 0.5\,\mathrm{mm\,yr^{-1}}$, and of the 1993–2003 figure the component from the cryosphere is thought to account for $2.8 \pm 0.7\,\mathrm{mm\,yr^{-1}}$ (IPCC, 2007). As the GrIS loses the majority of its mass either through runoff to the sea or through calving, the potential effects on global sea-level are a major concern relating to the acceleration of mass loss. It has been estimated that in the scenario of the total loss of the GrIS, global sea-levels would rise approximately seven metres worldwide (IPCC, 2001). Models not including recent changes in outlet glacier dynamics have predicted total and possibly irreversible GrIS loss within 3000 years under IPCC predicted warming rates (Toniazzo *et al.*, 2004; Ridley *et al.*, 2005), and ice loss is likely to be more rapid if dynamic processes are included (Parizek and Alley, 2004). Sea levels during the last interglacial were five metres higher than present, and this has been estimated to have been as a result of ablation from Greenland, rather than from the West Antarctic Ice Sheet (Cuffey and Marshall, 2000). In 2006 the contribution of the GrIS to global sea-level rise was $0.7 \pm 0.4\,\mathrm{mm}$ (Rignot *et al.*,

2011), and the ice sheet is thought to be the single greatest contributor toward sea-level change in the cryosphere (Box *et al.*, 2006).

1.2.3 Ocean circulation

Some concern has surrounded the possibility that freshwater from the GrIS could interfere with the formation of the hyper-saline water of the North Atlantic Deep Water formation, an important part of the thermohaline circulation. The stalling of the thermohaline circulation has been associated with abrupt climate change in glacial history (Clark *et al.*, 2002). Monitoring of the North Atlantic drift shows that there is no significant change underway in the thermohaline circulation at present, and some models have suggested that the predicted rate of release of freshwater would be insufficient from Greenland alone to halt the thermohaline circulation (Ridley *et al.*, 2005). However, a recent model (Hu *et al.*, 2011) has shown that whilst current rates of melt are insufficient to influence Atlantic thermohaline circulation, very high rates of melt (increase of 7% per year) could be sufficient to slow circulation slightly.

1.3 Causes of mass loss

Simulations of Helheim Glacier have shown that acceleration and retreat are triggered at the calving front of the glacier, and propagate upstream (Nick *et al.*, 2009). Loss of ice from the calving front reduces backstress, thus increasing velocity. This leads to dynamic thinning at the terminus, steepening the surface slope and increasing driving stress leading to further acceleration. This ultimately leads to the ice near the terminus approaching flotation causing frontal retreat. Synchronous retreat of glaciers in SE Greenland was found to correlate with high sea surface temperatures (Howat *et al.*, 2010; Murray *et al.*, 2010), leading to speculation that ice-ocean interactions at the calving fronts of glaciers was responsible for the required initial frontal perturbation. Similarly, the doubling of velocity at Jakobshavn Isbræ in

1997 (Joughin *et al.*, 2004) coincided with an increase in warm water at depth in the fjord (Holland *et al.*, 2008).

An alternative hypothesis for the cause of dynamic mass loss is that surface melt water is delivered to the base of the ice sheet, causing the ice to accelerate. Whilst this effect is well known in temperate glaciers (e.g Iken and Bindschadler, 1986), it was previous thought that penetration of surface water through cold ice was unlikely (Hodgkins, 1997). Zwally *et al.* (2002) found summer accelerations in ice sheet flow that correlated with periods of higher melt, and it has since been shown that the process of hydrofracture allows surface melt to reach the bed (Alley *et al.*, 2005; van der Veen, 2007). These processes are discussed in greater detail in Chapter 2.

The theory that increasing melt due to a warming climate could cause ever increasing mass loss from the GrIS received attention in both the scientific literature (Parizek and Alley, 2004) and with policy makers (Stern, 2007). Whilst recent results have played down the possible role of the "Zwally Effect" in mass loss from the GrIS (Section 2.5), studies of supraglacial hydrology in SW Greenland still frequently use dynamic mass loss as a rationale (Georgiou *et al.*, 2009; Bartholomew *et al.*, 2011). The sudden drainage of supraglacial lakes is thought to be an important component of this process (Das *et al.*, 2008; Krawczynski *et al.*, 2009). However, lake drainage has not been studied outside of SW Greenland, presumably due to the very large numbers of satellite images required to be able to identify lake drainage events on the ice-sheet scale. As mass loss from SW Greenland can be explained by surface mass balance (Pritchard *et al.*, 2009; van den Broeke *et al.*, 2009), for fast lake drainage events to play an important role in dynamic mass loss they would need to be occurring in those regions where dynamic mass loss is occurring. This thesis aims to address this lack of knowledge about supraglacial lake drainage on the Greenland Ice Sheet.

1.4 Thesis aims

The objective of this thesis is to discover whether or not it is appropriate to generalize findings about supraglacial lakes, specifically their sudden drainage, over the entire Greenland Ice Sheet. This can be broken down into the following specific aims:

- To develop a method for monitoring the changing area of a large number of lakes in a large number of satellite images (several thousand of each).
- To map the positions of supraglacial lakes in all regions of the Greenland Ice Sheet, to see if lakes are equally common throughout.
- To investigate how common the phenomenon of sudden lake drainage is, and whether it is occurring in all regions of the ice sheet.
- To discover what happens to supraglacial lakes that do not drain suddenly.
- To investigate possible controls on lake position and drainage.

1.5 Thesis structure

The hydrology of the ice sheet and its effect on ice sheet velocity are described in Chapter 2. Studies of the surface, basal, and englacial hydrology of the ice sheet are so far rather limited, but those published to date are described in this chapter. Direct observations are supplemented by inferences from proxies such as proglacial discharge and ice velocity behaviour, and relevant studies from elsewhere in the Arctic and temperate valley glaciers are included. Thus Chapter 2 outlines the gaps in knowledge that this thesis will address, as described in the aims above.

The methods used in this thesis are split across two chapters. Chapter 3 describes the datasets used, and the preprocessing steps applied to them. Imagery from the MODIS sensor were used as the main data source for this study, so the characteristics of this sensor that made it the most appropriate choice are detailed. The remaining

non-MODIS datasets are also described. In general, the methods described in this chapter are standard procedures for processing the various datasets described. In contrast the methods presented in Chapter 4 are those that were developed for the specific challenges of this thesis. The difficulties of tracking the area of large numbers of lakes with a high temporal resolution are outlined. Previous approaches to lake classification from MODIS are described, and problems identified. The new methodology is presented, and compared with the previous methods. Sources of error are discussed, and quantified where possible.

The results of this thesis are presented in two chapters. Chapter 5 contains those results that relate to the size and distribution of lakes. Maps of the positions of the lakes in the dataset are presented at both ice sheet wide and region scales. Interannual variations in lake area are described, and differences between regions highlighted. Intra-annual variations in lake area and maximum lake elevation are demonstrated for subsets of the ice sheet. Results of melt extent and duration mapping are also discussed in this chapter. Chapter 6 contains results relating to the assignment of lakes to the drainage type classifications. The interregional and interannual variations are described, and the differences between the drainage types are explored both qualitatively and statistically through variables such as lake area and ice surface slope.

Chapter 7, analyses the results presented in Chapters 5 and 6. They are put into the context of the existing literature, and their importance for past and future research is discussed. Potential biases introduced by the methodology are also discussed. Chapter 8 contains the conclusions of this thesis. This recaps the motivation and aims of this study, and the conclusions that can be drawn from the results. This is followed by suggestions for further work that could build upon the findings of this thesis.

1.6 Publication from this thesis

Some of the methods, results, and discussion of this thesis are published as Selmes *et al.* (2011). Published material includes the following:

- The methodology relating to image selection, lake area classification, fast lake-drainage detection, and mapping melt extent.
- Results relating to interregional and interannual variations in lake position and total lake area.
- Results relating to interregional and interannual variation in fast lake-drainage.
- Discussion relating to the impact of the findings of this thesis on ice sheet dynamics.

Chapter 2

Greenland Hydrology

2.1 Introduction

The changing mass balance of the Greenland Ice Sheet was introduced in the previous chapter, where it was highlighted that the link between the supraglacial and subglacial hydrology has received considerable attention recently as having a possible role in dynamic mass loss from the GrIS. Supraglacial lake drainage to the bed has received particular attention as both a source of pressurized basal water, and as a means of opening conduits for surface melt to reach the subglacial environment. In this chapter, observations and inferences of the supraglacial, englacial, and subglacial drainage systems of the Greenland Ice Sheet are introduced. Observations from Greenland are often scarce, and so examples from Svalbard, Alaska, and temperate valley glaciers are also included where relevant.

Supraglacial lakes on the GrIS are described in Section 2.2, and the characteristics of these lakes including their distribution, size, and what is known about how they drain are introduced. As few direct observations of lakes draining on the GrIS have been made, inferences from proglacial hydrology and observations from Svalbard and Alaskan lakes are also included.

Hydrofracture, the process by which lakes can drain through 1000 m of cold ice, is

described in Section 2.3. This description includes both modelling studies of the process, and the field observations that support them. These fractures are thought to be the source of englacial conduits to the bed of the ice sheet. There are few published observations regarding Greenland englacial hydrology, but those that have been made are presented in Section 2.4. Inferences as to the nature of the englacial system can be made from the lag between melt intensity and the response of glacial velocity, these are also included in the englacial section.

The inferred nature of the subglacial hydrology is described in Section 2.5, as is the relationship between hydrology and glacial velocity. Recent observations have suggested that the subglacial drainage system of the GrIS may be similar to those of temperate valley glaciers, so observations from these glaciers have been included.

2.2 Supraglacial lakes

2.2.1 Observations of lake distribution and size

Supraglacial lakes on the Jakobshavn Isbræ catchment were described in some detail by Echelmeyer *et al.* (1991). They found numerous lakes between 600 m and 1450 m elevation. Below 1150 m lakes were formed on bare ice, between 1150 and 1300 m lakes rested on superimposed ice, and above this zone lakes were found on firn. Those on firn were partly ice covered for some of the summer. Surface areas were up to 10 km^2, with depths from 1 m deep up to 20 m over large crevasses. Lakes were found to remain in the same locations from year-to-year, leading to the suggestion that the positions of lakes in the Jakobshavn region are controlled by sub-glacial topography. Echelmeyer *et al.* (1991) and Lüthje *et al.* (2006) also noted that supraglacial lakes reduce the albedo of the ice; therefore lakes perpetuate their own existence through this positive feedback effect.

The sizes and depths observed by Echelmeyer *et al.* (1991) are similar to those described by subsequent studies. McMillan *et al.* (2007) used lidar measurements

of full and empty lake basins along with runoff modelling to estimate the depths of lakes in the Russell Glacier catchment, and found lakes to have mean depths ranging from $\sim$ 1 m in early summer to $\sim$ 4 m in August. Optical depth measurements of lakes with surface areas $\sim$ 0.5 km^2 in the Kong Oscar catchment found mean lake depth to be $\sim$ 2 m (Sneed and Hamilton, 2007). Box and Ski (2007) measured lake depths with both direct measurements using a boat-mounted sonar, and from a depth-reflectance relationship derived from the field and MODIS data. Direct observations gave depths for two lakes, both had a maximum depth of around 10 m. Lakes areas up to 9 km^2 were observed, and lake depths from MODIS were in the range of 5 - 10 m. Lake volumes were estimated to be in the 10^6–10^8 m^3 range. Georgiou *et al.* (2009) used optical depth estimation techniques - where the depth of water is estimated using the Lambert-Beer law combining the optical attenuation characteristics of water and the reflectance of the ice under the lake - for a lake in SW Greenland over several years to find lake depths up to 10 m, and volumes up to 18.6 x 10^6 m^3. Filling rates were estimated, and found to be 0.12 x 10^6 m^{3}d^{-1} for the first 80 positive degree days, with a tripling of the rate after this leading to drainage. This change in filling rate was interpreted to be a result of a switch of meltwater source from snow to ice.

Sundal *et al.* (2009) studied the onset of lake formation, and the maximum area of lakes present per day, for three regions of the ice sheet: subsections of the SW, N and NE regions. A close relationship between runoff and lake evolution was discovered: lakes formed later, and the maximum lake area per day was smaller, in years with low runoff. Regional differences were also noted. Lakes formed up to two weeks later in the N/NE than in the SW, and lakes formed at higher elevations in the latter region. In addition, the year with the greatest lake area was not the same in each region. A strong link was found between the percentage lake cover of a section of the ice sheet and slope angle, with more extensive lake cover where surface slopes were lower.

2.2.2 Lake drainage

The drainage of Greenland supraglacial lakes was noted by Thomsen *et al.* (1989), who described their tendency to "tap periodically". Moulins were found in the centres of the the drained lake sites, and Thomsen *et al.* (1989) suggested that these moulins may be sealed in winter by snow, allowing the same lake to reform the next year.

To date the only detailed published direct field observations of a Greenland lake drainage are those of Das *et al.* (2008), who monitored the drainage of a 5.6 km^2 lake in SW Greenland with depth logging, GPS, and passive seismic equipment. Lake level at first fell steadily for $\sim$ 16 hours, then increased considerably with the lake emptying in $\sim$ 1.4 hours. GPS data showed 1.2 m vertical uplift, and 0.8 m displacement normal to the direction of ice flow. This was followed by subsidence of the ice, and a temporary increase in horizontal velocity. The period of rapid lake drainage was preceded and coincided by an increase in seismic activity. This lead Das *et al.* (2008) to propose four steps of drainage. First a period of slow drainage as a connection to the bed is forced through hydrofracture, no uplift or acceleration was associated with this phase. Second, a connection to the bed is made, and rapid lake drainage occurs, this coincides with uplift and acceleration. A large uplifted block was found at the lake site which appeared to be associated with this stage. Third, most of the fractures probably closed at depth, whilst moulin formation occurred in the part of the fracture with greatest flow. Fourth, this moulin remained open and subsequent surface drainage was routed down this. Observations by Das *et al.* (2008) of this and other lakes found km scale fractures running through the drained lake sites, with moulins running through the fractures. Further field measurements of a lake near the JAR1 weather station (Section 3.5.6) have been made from an acoustic ranging device (Box and Ski, 2007). This lake drained suddenly in consecutive years, with near constant filling rates followed by drainage in 10 hours in 1996 and 8 hours in 1997.

The field observations of Das *et al.* (2008) are similar to those made by Boon and

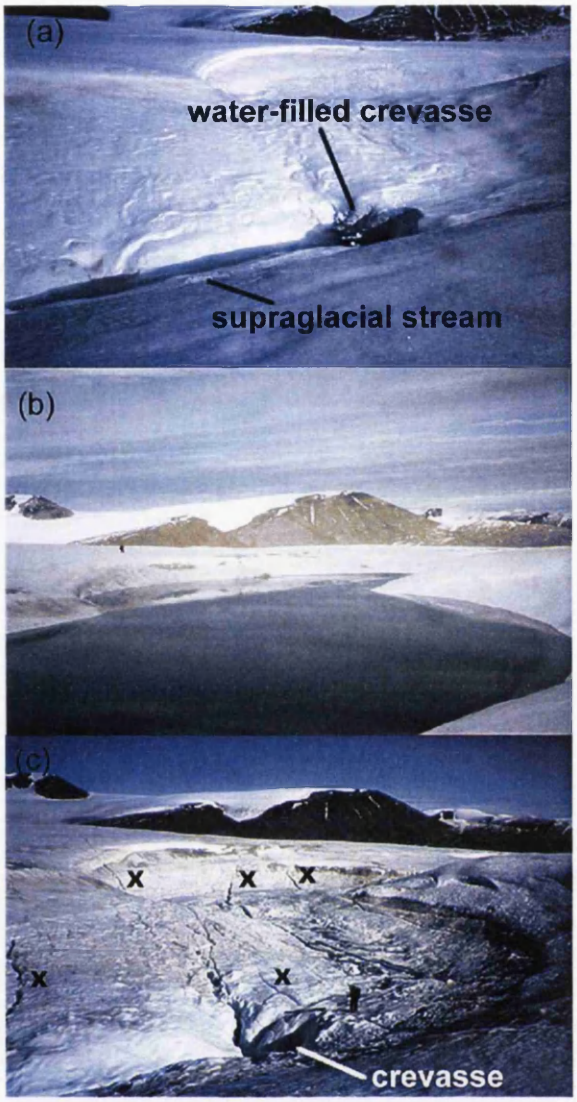

Figure 2.1: Lake growth and drainage on John Evans Glacier. (a) inital crevasse and supraglacial channel. (b) The lake at maximum extent. (c) The drained lake with fresh crevasses marked "x". From Boon and Sharp (2003).

Sharp (2003) on John Evans Glacier (Ellesmere Island), a glacier composed of predominantly cold ice (-15 °C at 15 m depth) $\sim$ 150 m thick. A supraglacial stream was observed running into a crevasse (Figure 2.1a). This took three days to fill before surface ponding commenced, resulting in a supraglacial lake with a diameter of $\sim$ 200 m after 11 days (Figure 2.1b). During this period a sequence of 8 partial drops in water level occurred that could not be explained by the surface inputs and outputs of the lake. Crevasses at the lake shore were noted to widen slightly (3 cm). These events suggest that crevasse propagation was starting, but the crevasses

were closed out before a basal connection was made. 13 days after the crevasse commenced filling, total lake drainage occurred within one hour, and several new crevasses were observed in the lake bed (Figure 2.1c).

Studies of lake drainages in Svalbard can help us understand the mechanisms at work in Greenland. Lakes on Brøggerbreen were found to drain catastrophically through a central drainage hole (Liestøl *et al.*, 1980). Any drainage hole was sealed in spring by the ingress of snow, followed by the refreezing of percolating meltwater causing a superimposed ice layer. Ice dammed lakes in Svalbard were also found to drain rapidly through a central moulin, with several draining around the same dates. Hambrey (1984) found that a fresh looking crevasse ran across two lakes, through which both appeared to have drained.

No studies of lake drainages have been conducted in Greenland on an ice-sheet scale with a high enough temporal resolution to determine if lake drainage was rapid or not. Some remote sensing studies with a high temporal resolution have been carried out in small regions of the ice sheet. Box and Ski (2007) used daily imagery for the period 2000–2005, for a $\sim$ 200 km section of the SW ablation area. Lake drainage events were detected as early as day 168, and as late as day 221. Lake drainage events were found to occur earlier at lower elevations, and the occurrence migrated inland. Around eight sudden lake drainage events were detected per year, with an average estimated volume loss of 15.7 x 10^6 m^3. As drainage events were detected visually, the authors suggest that a large number of drainage events will have been missed. The largest single drainage event detected was 97.4 x 10^6 m^3.

Bartholomew *et al.* (2011) examined a land-terminating region of the ice sheet with the aim of correlating lake drainage with pro-glacial hydrological discharge. They used 40 MODIS images between 31st May and 18th August 2009 to examine the drainage behaviour of lakes on the Leverett Glacier catchment, and compared these data to discharge at the glacial terminus. They found pulses of higher discharge, which correlated with periods of several lake drainages. Conversely Chu *et al.* (2009) found a poor link between remotely observed lake drainages in the Russell Glacier

catchment (SW GrIS) and sediment plumes in Kangerlugssuaq fjord, with only $\sim$ 10% of lake drainages causing a sediment response, from which it was inferred that drained surface water was either dissipated englacially or entered an inefficient subglacial drainage system.

This section has so far considered only the sudden catastrophic drainage of supraglacial lakes vertically through the ice. Lakes have also been observed to empty by draining over the surface. A lake on Finsterwalderbreen was observed over a 22 year period (Liestøl *et al.*, 1980). Once the lake reached a critical size surface drainage could occur, and the outlet channel became increasingly incised through the melt season until the lake was totally emptied. The lake observed reused the same canyon each year, which filled with snow each spring, damming the lake. After several years the outlet channel formed into an englacial tunnel.

Lake drainage through the downwasting of the outlet spillway can occur in both a stable and unstable mode. Raymond and Nolan (2000) showed that the spillway floor can incise at the same rate of the drop in lake level giving stable drainage, or the spillway can incise faster the the lake level drops giving unstable drainage. A lake on Black Rapids Glacier in Alaska with an area of 0.15 km^2 shrank to 0.07 km^2 in four days owing to overflowing and supraglacial discharge. Drainage was initially unstable with the spillway floor incising faster than the lake level was dropping, and later became stable. The spillway incised significantly forming a gorge, downwasting 5 m in the first day, 3 m on the second, and 1 m per day subsequently. The gorge, despite the depth (up to 16 m deep), was only $\sim$ 3 m wide. Raymond and Nolan (2000) demonstrated that if a lake exceeds a critical area, then unstable drainage occurs. The critical area was shown to be smaller if the lake water is warmer, or the gradient of the spillway is steeper.

These processes of supraglacial drainage of lakes have never been reported to occur on the GrIS, although there is no obvious reason why the processes should not be occurring. The occurrence of lake drainage on the GrIS has only been studied in certain regions of the ice sheet, and never over a large number of lakes. Therefore

no information as to the fate of the majority of the lakes on the ice sheet exists, so the dominant mode of drainage on the GrIS is unknown. If it is possible to substantially empty a lake in a matter of days over the surface of the ice in a deep but narrow channel as described above it may have significant consequences for the remote sensing observations of Greenland lakes. It is possible that previous studies reporting lake drainage from satellite imagery that have inferred drainage to the bed from coarse temporal resolution observations (for example Joughin *et al.*, 1996; McMillan *et al.*, 2007) may in fact have merely observed drainage over the ice surface from spillway downwasting. While this water may still reach the bed through moulins, it would not be delivered in a high pressure pulse as observed by Das *et al.* (2008), and therefore would be expected to have far less impact on glacial velocity (Section 2.5).

2.3 Hydrofracture

Studies of lake drainage have shown that hydrofracture is an important process for lake drainage. Original work on crevasse depth (Nye, 1957) found that closely spaced crevasses reach the depth where tensile stress is balanced by cryostatic pressure i.e.

$$d = \frac{2}{\rho_i g}\left(\frac{\dot{\epsilon}_x}{A}\right)^{1/n} \tag{2.1}$$

where d is crevasse depth, ρ_i is the density of ice, g is the acceleration due to gravity, $\dot{\epsilon}_x$ is the longitudinal strain rate and A and n are flow law parameters (the factor 2 was added by Paterson, 1994). Closely spaced crevasses "blunten" the tensile force experienced by neighbouring crevasses. Isolated crevasses do not experience this effect and can thus penetrate deeper (Weertman, 1973). The depth model of Nye (1957) in fact holds only for dry crevasses. As the density of water is higher than that of ice, the hydraulic pressure exerted by the water in a crevasse can overcome the stress balance at the crevasse tip and allow the crevasse to grow. In fact, if the crevasse is kept sufficiently full, this can continue until the crevasse reaches the ice

base. Weertman (1973) calculated that the crevasse must be 97.4% full for this to occur.

Linear elastic fracture mechanics (LEFM) has been used to study this process by van der Veen (2007). In LEFM, a stress intensity factor is calculated from the shear stress, cryostatic pressure and water pressure. A crevasse will propagate until the stress intensity factor is equal to the fracture toughness of ice, with the rate of the inflow of water as the main control on the rate of fracture propagation. Once a fracture is initiated, crevasses with sufficient water inflow can propagate independent of far-field tensile stress and the fracture toughness of ice. This is important as previously the blunted tensile stress in closely spaced crevasse fields was thought to prevent hydrofracture (Weertman, 1973). However, LEFM shows that hydrofracture can occur even in closely spaced crevasses (van der Veen, 2007). Refreezing is a significant process for fractures in cold ice, but it is not a major constraint on hydrofracture provided propagation is rapid enough (van der Veen, 2007). If the process takes more than a few days, the fracture will freeze up. The observations of Boon and Sharp (2003) give direct evidence that crevasse propagation to the bed, whilst possible, is not a trivial process. Even with a lake reservoir of water, several hydrofractures failed to reach the bed in a region where ice thickness was only 150 m, compared with the 1000 m thick ice of the GrIS ablation zone. Healed crevasses where hydrofracture appears to have occurred but not reached the bed are often seen in icebergs (Alley *et al.*, 2005).

If fracture propagation is controlled by water inflow rate, and the time window during which the crevasse can grow without freezing up is limited, it follows that for a fracture to reach the bed a sufficiently rapid inflow of water is crucial. The effect of different sizes of crevasses and moulins on the volumes of water required to force a crevasse through 1000 m of cold ice has been tested through LEFM (Krawczynski *et al.*, 2009). Smaller crevasses are easier to propagate due to the lower volumes of water required, which may indicate that crevasse propagation is easier in regions of lower tensile stress. The minimum crack opening diameter likely to be able to penetrate 1000 m of ice is $\sim$ 10 cm, and the cross section of water-filled crevasses

(unlike the V-shaped cross-sections of dry crevasses) is U-shaped i.e. crack width is relatively uniform at all depths (Krawczynski *et al.*, 2009).

Crevasse filling from a supraglacial channel has been observed in the field (Boon and Sharp, 2003), with a crevasse taking 3 days to fill. This rate of inflow is clearly insufficient for fracture propagation, as some fractures may heal in < 30 hours (Krawczynski *et al.*, 2009), and the volume of water required in the crevasse will increase as the fracture grows. It would therefore seem unlikely that an inflowing supraglacial stream alone could force hydrofracture. Lakes however have been shown to contain sufficient water to drive hydrofracture (Boon and Sharp, 2003; Das *et al.*, 2008). If a lake contains enough water to fill a crevasse once it has penetrated the full depth of ice, sufficient water inflow for fracture propagation is ensured. A 7 m deep, 200 m diameter lake contained sufficient water volume for hydrofracture in the observations of Boon and Sharp (2003); however that was through relatively thin ice. Observations of draining lakes in Greenland have involved much larger lakes (Das *et al.* (2008) - 5.6 km^2, Box and Ski (2007) - 1.3–8.5 km^2). For a crack of 10 cm opening width and length equal to lake diameter, Krawczynski *et al.* (2009) calculated that a lake of 250 - 800 m diameter (depending on the shear modulus used for ice) would be required to provide sufficient water for hydrofracture to the bed. It follows that wider crevasses would require larger lakes as a water supply.

The direct exploration of englacial conduit systems adds further credibility to the hydrofracture hypothesis. Very deep fracture systems have been explored in regions with extensional stresses and ready availability of meltwater, such as the Crystal Cave system of Hansbreen, Svalbard (Benn *et al.*, 2009). Here deep vertical fractures were found extending through 60 m of cold ice to the bed. Hydrofracture seems the most likely cause for this englacial system, as the entrance to the fracture system is associated with an annually draining supraglacial lake.

2.4 Englacial hydrology

Direct measurements of the englacial hydrology of the GrIS are rare. However, as described above, the englacial connection between the surficial and basal hydrology is thought to be through moulins formed from crevasses that have reached the ice base through hydrofracture.

Ground Penetrating Radar (GPR) surveying has shown apparently vertical features that are only present in the ablation zone of the GrIS, which have been interpreted as moulins (Catania *et al.*, 2008). These features were often found close to supraglacial lakes sites, especially over thicker ice (> 800 m). No moulins were reported above the equilibrium line of the ice sheet, despite lakes being present there. Note that the data presented by Catania *et al.* (2008) provides evidence of vertical structures only, not necessarily of a basal connection.

Whilst published observations of Greenland moulins or other conduits are rare, the response time of glacial velocity to increases in melt (Section 2.5) and lake drainage (Section 2.2.2) can be used to make inferences about the nature of the englacial hydrology. The rapid response of ice velocity to catastrophic lake drainage (Das *et al.*, 2008) shows that efficient drainage to the ice sheet base is possible, but reveals nothing about whether these connections remain open. The response time of velocity to increases in melt is more telling. van de Wal *et al.* (2008) noted responses to melt increases in the order of days, and Shepherd *et al.* (2009) found a delay of only hours with a diurnal velocity signal observed. A delay of days would suggest that moulins may partly close, and increases in melt may allow them to reopen. Diurnal responses to melt implies a large number of continuously open conduits to the bed with a high degree of efficiency. Taking the observations of van de Wal *et al.* (2008) and Shepherd *et al.* (2009) together it seems likely that both scenarios occur in Greenland, with those conduits with continuous water supply remaining open, and others partly closing during periods of lower melt. Indeed van de Wal *et al.* (2008) found differing response times to melt in different parts of the ice sheet, with faster responses at lower elevations where the ice is thinner. This

result would suggest that conduits are more likely to remain open over the thinner ice of the periphery, which fits with the lack of moulins at altitude as described (Catania *et al.*, 2008).

2.5 Subglacial hydrology and the effect on ice velocity

Direct observations of the basal hydrology of the Greenland Ice Sheet have not been possible, although some geophysical observations have been made of water at the bed of the ice sheet (Oswald and Gogineni, 2008). Despite the scarcity of direct observations, some inferences as to the nature of the basal hydrology of the ice sheet can be made through the transit time of melt water to proglacial streams, and through the time varying response of the velocity of the ice sheet to supraglacial melt.

Initial work on the relationship between supraglacial melt and ice velocity on the GrIS found a simple correlation between the amount of melt and glacial velocity. Summer speed ups of 25 - 50% were observed on the ice sheet (Zwally *et al.*, 2002; Joughin *et al.*, 2008), with more melt giving higher velocities (Figure 2.2). However, results from tidewater terminating regions show that whilst the summer speed-ups of these regions are of a similar absolute magnitude to those of the land-terminating regions, the relative speed up of these regions is smaller.

Whilst the relationship between melt and velocity initially seemed straightforward, GPS measurements from the Russell Glacier in SW Greeland (Shepherd *et al.*, 2009) showed that whilst the response of ice velocity to melt availability was fairly linear near the ice margin, at higher elevations ice velocities decreased throughout the season with the suggestion indicating the transition from an inefficient to an efficient drainage system. This result may mean that the GrIS behaves more like an alpine glacier than previously thought. Hydrological studies of valley glaciers have shown

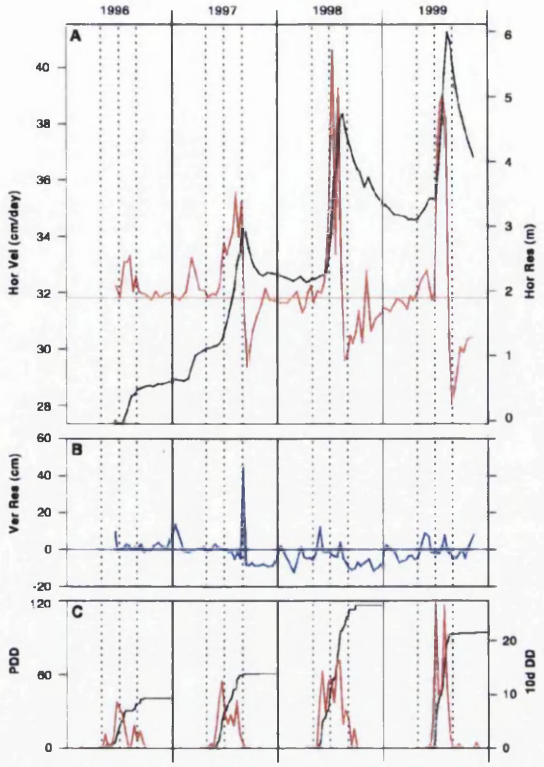

Figure 2.2: Velocity (red line in A), uplift (blue line in B) and PDD melt model results (red line in C, number of positive degree days per 10 day period) from 1996-1999 for the Swiss Camp region. From Zwally *et al.* (2002). Black lines show cumulative additional motion from melt forcing and cumulative Positive Degree Days. Periods of increased ice motion appear linked to periods of increased melt.

that the morphology of the subglacial drainage system affects the relationship between meltwater input from the surface and glacial velocity. Subglacial drainage and storage in linked cavities can occur at higher pressures than in channelised drainage (Kamb, 1987), which allows decreased effective pressure and acceleration of the ice (Iken *et al.*, 1983; Iken and Bindschadler, 1986). As water discharge increases, the subglacial drainage system switches to channelised flow (Lappegard and Kohler, 2005; Lappegard *et al.*, 2006), which transports water at lower pressures than distributed linked cavities (Kamb, 1987). This transition moves up the glacier as the snow line retreats (Nienow *et al.*, 1998), and is associated with a decrease in ice velocity (Anderson *et al.*, 2004). This process of flooding an inefficient distributed drainage system at the start of the melt season, which then evolves to an efficient channelized system, causes characteristic early-season glacial speedups known as spring events (MacGregor *et al.*, 2005).

Schoof (2010) modelled the Greenland subglacial system incorporating the dynamic switching from inefficient to efficient drainage. This model demonstrated that high rates of steady melt water influx would force the subglacial system to switch to a more efficient form once a critical hydrological discharge was reached, and that only sudden pulses of water (such as lake drainages) would then be able to cause accelerations. These modelled findings have been supported by ice velocities from field observations and remote sensing. van de Wal *et al.* (2008) found decreases in velocity on land-terminating ice in SW Greenland of 10% over a 17 year period, possibly as a result of surface thinning reducing the driving stress. No correlation was found between mean annual melt and mean annual velocity. Velocities from synthetic aperture radar intensity tracking (Sundal *et al.*, 2011) have shown that whilst melt related accelerations in early summer are similar from year-to-year, once a critical runoff threshold is reached (1.4 cm per day) ice velocity drops rapidly. This means that whilst higher velocities were observed in years of high melt, the period of higher velocities is shorter resulting in a lower mean velocity. Similar observations were made by Bartholomew *et al.* (2010), who discovered early summer is characterized by accelerating ice and vertical uplift, whereas the remainder of the melt season has subsidence of the ice surface, and declining velocities with occasional peaks. The transition between the two types of drainage system is also supported by observations of proglacial hydrological discharge (Bartholomew *et al.*, 2011). A 20 day delay occurred between the onset of positive air temperatures and any increase in proglacial discharge. Early discharge was slow, with high solute concentrations and little suspended sediment. This result was interpreted as evidence for slow transit times. This period was followed by a sudden increase in discharge, a drop in solute concentration and an increase in sediment load. This change was taken to be evidence of rapid water transit through a basal hydrological network. The presence of slow downs part way through the summer was noted by Zwally *et al.* (2002), who also attributed these events to a switch in subglacial drainage systems. These slow downs are visible in Figure 2.2, although no link between higher melt and shorter lived accelerations was made at the time.

The discovery that steady input of surface-melt to the bed has little impact on glacial velocity once the basal hydrological system has adapted, places rapid lake drainage to the bed in an important role. Even once the basal hydrology has adapted to summer levels of meltwater discharge, lake drainage to the bed can still cause temporary velocity increases by overwhelming the subglacial drainage network and causing decreased effective pressure. However, the fact that this phenomenon has only been observed in SW Greenland should inspire caution. With no published evidence that catastrophic lake drainages are common outside of the SW region, it is not appropriate to extrapolate these findings over the whole GrIS. More information is needed about the frequency of sudden lake drainage events in other regions of the ice sheet.

2.6 Chapter summary

A relationship between the production of meltwater at the surface of the GrIS and the velocity of the ice has been observed. Meltwater from the surface is hypothesised to propagate fractures to the bed through the process of hydrofracture, and once at the bed it is thought the water reduces the effective pressure and allows the ice sheet to flow faster. This so called "Zwally Effect" was thought to be a significant dynamic process which could explain the observed dynamic mass loss from the GrIS. However, the impact of this process is now thought to be less significant than initially suggested. Whilst pressurized subglacial water causes increased ice velocity, it also forces the reorganisation of the subglacial drainage system from a high-pressure linked-cavity system to a low-pressure channelized system. Once the switch has occurred the velocity of the ice is reduced. It has been demonstrated that in years of higher melt this switch occurs earlier, and may actually reduce the mean annual ice velocity.

In this process the drainage of supraglacial lakes plays two important roles. Firstly, the drainage of a lake by hydrofracture establishes the connectivity between the

surface and basal hydrologies. Secondly, even once the subglacial drainage system has been reorganised to efficient channelised drainage, the sudden pulses of melt water from lake drainages are significantly large enough to overwhelm the basal hydrology and cause speed ups.

Despite the apparent importance of supraglacial lakes on the GrIS, little is known of their occurrence and behaviour on the ice sheet scale. The distribution of lakes on the ice sheet has only been studied for selected regions, and little is known about their drainage behaviour. Whilst individual lakes have been observed to drain catastrophically, this process has not been reported outside of the SW region. Little is known about whether sudden lake drainage is a common process, or whether the majority of supraglacial lakes have an alternative fate. Without knowing how widespread the process of sudden lake drainage is, it is not appropriate to generalise the effects of this process over the whole ice sheet.

The uncertainties concerning supraglacial lakes that have been raised in this chapter will be addressed in the subsequent chapters of this thesis. The distribution and spatial characteristics of lakes on the whole GrIS are described in Chapter 5. Chapter 6 presents the results with regards to lake drainage processes, and their occurrence across the ice sheet. The significance of these findings is discussed in Chapter 7.

Chapter 3

Data Selection and Pre-Processing

3.1 Introduction

This chapter introduces the key datasets used in this thesis, the rationale for choosing them, and the preprocessing steps that were applied. The majority of the results presented in this thesis were derived from MODIS data. Section 3.2 introduces some of the basic characteristics that separate different satellite sensors, what characteristics are desirable for monitoring supraglacical lakes, and an introduction to why MODIS was ultimately chosen as the main data source for this study. The reasons behind this choice are brought together and discussed in Section 3.3. A thorough description of the characteristics of the MODIS data used are included in Section 3.4. Also included in this section are the preprocessing steps taken before the use of these data in further chapters, and the considerations that went into selecting particular images and MODIS data products. A range of other datasets were also used, which are outlined in Section 3.5. MODIS Land Surface Temperature data, a MODIS product developed from thermal infrared MODIS bands, are included in Section 3.5 as the preprocessing steps used differ to those for MODIS radiance data.

3.2 Desirable sensor characteristics for lake monitoring

One of the first choices that needed to be made in the methodology of this study was the choice of a satellite sensor to use as a data source for lake monitoring. In order to make an informed decision it was first appropriate to consider what was required of the data, and what characteristics of a sensor would be desirable for this purpose. In this section the various characteristics that mark the key differences between possible sensors are identified, and each characteristic is put into the context of the present study. The characteristics of the MODIS sensor are described to explain why MODIS was considered to be the most appropriate data source for this research.

3.2.1 Swath width

Swath width, the width across the ground that a sensor images in one pass, determines the number of scenes required to cover a given area. In this project the aim was to image the entirety of the GrIS at the chosen time interval, so a wider swath was desirable to reduce the number of images needed. The swath width is also an important component of temporal resolution as sensors with a large swath width can supply repeat imagery more frequently than their repeat cycle alone would suggest, which is discussed in the next section. The swath width of MODIS is very wide (2330 km), and can usually cover the whole ice sheet in one or two images.

3.2.2 Temporal resolution

There are two considerations when choosing a temporal resolution for monitoring lakes. The first is the duration that the lake exists, the second the speed of lake drainage to the bed. As Das *et al.* (2008) described lake drainage occurring within a 24 hour period, a very fine temporal resolution was required as the lake needed to be be imaged before and after drainage with a short enough lag to tell that the

lake had indeed drained catastrophically, or if it had drained more slowly over the surface. In addition, if the timing of acquisitions had been too sparse it was possible that lakes could have formed and drained without being detected at all.

The repeat time of a sensor is determined by the orbital characteristics, the swath width, and whether the sensor is pointable off nadir or not. For example, ASTER and Landsat are both carried by satellites with 16 day orbital repeat cycles. Landsat cannot be pointed off nadir, and so the repeat time of Landsat is 16 days. ASTER in contrast can be pointed so observations can be made more frequently - up to every 3 days. Pointable sensors (ASTER, Ikonos, Quickbird) are operated on an "on-demand" basis, and so despite their potentially rapid repeat time, archived data can be rather sparse being limited to previously requested sites. As a further example of sensors with different temporal resolutions despite the same orbital properties, both ASTER and MODIS are carried on the Terra satellite. MODIS has a much wider swath than ASTER (2330 km vs 60 km), and so despite not being pointable and having the same orbital characteristics, MODIS can image daily - in the case of polar regions several times a day due to the convergence of the satellite's orbital paths. This wide swath acquisition method allows for global indiscriminate imaging rather than the on-demand methods of pointable sensors, and so regularly repeated data for all areas is available from the archives.

3.2.3 Spectral considerations

The most significant division when considering what wavelengths to use is whether the solar reflective and thermal IR (0.4 - 14 μm) or microwave (1 mm to 1 m) components of the spectrum are used.

Microwave remote sensing has the distinct advantage of being able to image the ground through cloud cover and at night, both of which are not possible with the visible wavelengths. However, interpretation of microwave data over the margins of the ice sheet can be difficult due to the scattering by different glacial facies being complicated by surface water, superimposed ice, volume scattering in snow, and

ice inclusions from refreezing melt in the snowpack (Partington, 1998). While the different causes of high and low intensity returns can be interpreted, it is difficult to apply these interpretations automatically to large numbers of images. It was essential for this study that a consistent method can be applied to large volumes of imagery, and this would have been prohibitively difficult with microwave data.

Fortunately the frequency of cloud cover is relatively low over Greenland in comparison to other areas of the Arctic such as Svalbard (Scorer, 1988), so occasional lost observations to cloud were considered to be less important than being able to develop a classification scheme that could be used on large numbers of images without excessive user intervention.

It is demonstrated in Section 4.2.1 that an effective classification for detecting supraglacial lakes can be devised using red and/or green visible wavelengths. MODIS has bands both in the visible wavelengths and also in the thermal infrared wavelengths which allows the development of concurrent cloud masks, although the same can be said for several other optical sensors.

3.2.4 Spatial resolution

The spatial resolution of a sensor is the dimensions of the ground resolution cell, that is the area of the ground detected either at a given moment in time in an across track sensor, or by an element of the detector array in a pushbroom sensor. This in turn is a function of the instantaneous field of view - the cone angle over which energy is focused on the detector - and the altitude of the sensor. The size of this cell increases off nadir causing larger cells towards to the edge of an image which needs accounting for in post-processing (see Section 3.4.4). An increase in spatial resolution has a resulting increase in the resolving power of the sensor - the ability of a sensor to distinguish nearby objects. High spatial resolution is desirable as it allows the detection of smaller features to be made, and the measurement of a given area to be made with greater accuracy. In the case of supraglacial lakes this will decrease the minimum size at which a lake is likely to be detected, and increase

the chances of identifying drainage channels and other small features of interest. A compromise must be made regarding the relationship between image resolution and the size of the images on disk. For a given spatial coverage images with finer spatial resolution will take up more space, an important consideration when using large numbers of images. As a result of this trade-off, finer spatial-resolution data are not always the most practical choice depending on the number of images required. Note that sensors can resolve features smaller than the ground resolution cell if there is a high contrast between the feature and its background, which is the case of supraglacial lakes on light coloured ice.

MODIS data are available in different spatial resolutions depending on the wavelength, the finest being 250 m for the red and near infrared (NIR) Bands 1 and 2. Whilst this is a higher spatial resolution than other wide swath sensors such as AVHRR (1100 m), it is considerably lower than pointable sensors such as Quickbird (0.65 m). This coarse spatial resolution is a drawback of the MODIS sensor, and needs to be considered in the context of Greenland supraglacial lakes. Previous studies have reported large numbers of lakes being several kilometres in diameter (Echelmeyer *et al.*, 1991; Box and Ski, 2007), and linear elastic fracture mechanics (Section 2.3) has shown that for rapid lake drainage to occur a lake diameter of at least 250 m is required for drainage by hydrofracture through 1000 m of cold ice. This suggests that a spatial resolution of 250 m is adequate for monitoring supraglacial lakes.

3.3 Sensor choice

Unfortunately no sensor has yet been made available that has very high spatial and temporal resolution whilst offering global coverage, as such for the choice of sensor for a given task a compromise must be made. In the case of monitoring supraglacial lakes, frequent observations are vital to understand their drainage patterns, whilst lakes are known to be several kilometres across. This requirement for fine temporal

resolution combined with the large size of lakes means that spatial resolution can be sacrificed somewhat in favour of temporal resolution and the ability to store more images. With this in mind MODIS data were the most obvious choice - 250 m resolution data are available several times a day in high latitude regions owing to its substantial swath width. 250 m pixels still have sufficient resolving power to identify very large numbers of lakes on the ice sheet, and Krawczynski *et al.* (2009) estimated that 98% of lake volume in SW Greenland was contained within lakes detectable by MODIS. Restricted resolving power will mean that there are smaller lakes that are not included in this thesis. However, an area threshold would always have to be set otherwise ever smaller ponded areas would need to be classified. As Krawczynski *et al.* (2009) calculated that lakes need to be in the range of 250–800 m across to drain to the bed, the use of 250 m pixels will not compromise detecting these lake drainage events.

3.4 MODIS

3.4.1 The MODIS sensor

The Moderate Resolution Imaging Spectroradiometer (MODIS) is a NASA-operated whiskbroom instrument carried on both the Aqua and Terra satellites. Each satellite also has a payload of other instruments, most notably the ASTER (Advanced Spacebourne Thermal Emission and Reflection Radiometer) sensor on-board Terra. The orbits of the satellites - both polar-orbiting - are timed so that Terra crosses the equator from north to south in the morning, whilst Aqua passes the equator from south to north in the afternoon. The combination of two sensors and the very wide swath width allows observations of a single point on the ground several times each day. MODIS collects data across 36 spectral bands from 0.405 to 14.385 μm which are available at resolutions from 250 m to 1000 m dependent on wavelength (Table 3.1). These are distributed as a range of different products from virtually unprocessed (Level-1) to higher level products each with a specific purpose, and

Table 3.1: The < 1 km resolution MODIS bands

Band	Wavelength (μm)	Resolution (m)	Common name
1	0.62–0.67	250 m	Red
2	0.84–0.88	250 m	NIR
3	0.46–0.48	500 m	Blue
4	0.55–0.57	500 m	Green
5	1.23–1.25	500 m	NIR
6	1.63–1.65	500 m	SWIR
7	2.11–2.16	500 m	SWIR

are described as being processed to levels one, two, and three. Level-1 data have undergone the least processing. Level-1A data are radiance counts with information regarding bad or missing pixels, instrument modes, and raw engineering and spacecraft data. Level-1B data are processed further to give calibrated and geolocated at-aperture radiance. Level-2 files are derived from their Level-1 equivalents - each pixel in a Level-2 file is located in the same position as in their source Level-1 file, but is atmospherically corrected and with an algorithm applied for a specific purpose e.g. snow mapping. Level-3 data are composited: Level-2 data are combined over 1 day, 8 days, 1 month, or 1 year into a grid whenever quality control conditions such as a lack of cloud cover are met. The Level-3 data has the advantage of reduced likelihood of data gaps at the cost of a loss of temporal resolution. Each product has a short name, for example the calibrated radiance product is MOD02 or MYD02. Data from Aqua are represented by the prefix MYD, whereas data from Terra data are prefixed MOD. Products derived from images from both satellites are prefixed MCD to show that they are combined products.

3.4.2 MODIS data product selection

As there is no product developed specifically for water mapping on ice sheets, a suitable alternative product must be chosen. Three MODIS products were identified that could be used for lake detection, these and other products mentioned in this thesis are outlined in Table 3.2. MOD/MYD02, the Level-1B calibrated radiance data

are available for every MODIS acquisition at 250 m resolution, although it requires atmospheric correction and conversion into reflectance before use. MOD/MYD09, the Level-3 reflectance product is available daily at 250 m resolution and is ready to use requiring no further corrections. MCD43, the Level-3 albedo product gives surface albedo at 500 m resolution, and is composited from 16 days of data from both Aqua and Terra. Whilst the MCD43 albedo product is the most refined and least likely to exhibit data gaps, the 500 m data every 16 days is too large a compromise on both spatial and temporal resolution. Both MOD02 and MOD09 are available daily at 250 m resolution. MOD02 is available for every pass of Terra (several times a day), and MOD09 was composited from MOD02 to make daily images. For this study MOD02 data were chosen. This choice was to allow sub-daily observations if required, and because supraglacial lakes are a phenomena which can change in a few hours a composited product could be made up of observations before and after the drainage of a lake.

As previously described in Section 3.4.1, data from MODIS are available from either the Aqua and Terra satellites. Owing to the frequent overpasses by both satellites over the latitudinal range of the GrIS, data are only really required from a single satellite. For this study, only data from Terra was used - the primary reason for this was to allow concurrent observations from the ASTER instrument (also onboard Terra, Section 3.5.2) for the evaluation of the classification method (Sections 4.2.4 and 4.2.5).

3.4.3 Timing of images

As already described, owing the high latitude of Greenland and a wide swath MODIS images are available at a range of times throughout the day. In midsummer in the polar regions any of these times can be used owing to 24 hour daylight. At lower latitudes, and early and late in the year lower sun zeniths cause long shadows to be cast. This occurs in mountainous areas causing problems around the outlet glaciers (Figure 3.1(a)), and very low angles cause shadowing in depressions on the ice sheet,

Table 3.2: A description of the MODIS products described or used in this thesis

Code	Name	Description
MOD02	Calibrated radiances	Calibrated and geolocated at-aperture radiances. Used as the main source of data for lake identification.
MOD09	Surface reflectance	Atmospherically corrected surface reflectance, available as a daily, 8 day, or monthly composited product
MCD43	BDRF/albedo	Bidirectional Reflectance Distribution Function (BRDF) produced from 16 days of both Terra and Aqua data
MOD03	Geolocation dataset	This is the dataset used to georeference the MOD02 data, providing geolocation information and as solar azimuth/zenith
MOD35	Cloud mask	1 km cloud mask product. Used for producing cloud coverage figures in this thesis.
MOD11B1	Land surface temperature and emissivity	Daily land surface temperature product, calculated with day and night images
MOD11A1	Land surface temperature and emissivity	Daily land surface temperature product, calculated with a split window algorithm. Used in this thesis for calculating melt.

the same depressions that surface lakes form in. Shadows are easily misidentified as lakes when working solely on spectral characteristics and so minimizing them is key. Solar azimuth and zenith are known for each image, but the available elevation data are not detailed enough to allow shadow masking to be performed. To minimize these problems, only images from the middle of the day were used. Optimum coverage of Greenland from Terra tends to be around midday, so images between 13:00 and 17:00 UTC or 10:00 and 14:00 local time were used for the best combination of favourable illumination and coverage. Figure 3.2(a) shows the coverage for a day in July, 2010. This shows optimum coverage at 14:30 UTC, or 11:30 local time, at this point the ice sheet is totally imaged in two scenes, and is also an excellent time for favourable solar illumination. This optimum point varies slightly from day to day, but only by $\sim \pm$ 1 hour, as demonstrated by Figure 3.2(b). Despite being from a different year

(2009) and different month (June), preferential coverage occurs only an hour later at 15:25. This figure also shows the number of alternative scenes available on a given day. Full coverage of the GrIS was aimed for twice in every day, usually amounting to four scenes. This frequency allows for cloud to move between images increasing the chances of cloud-free data, and enabled sub-daily measurements of lakes where possible.

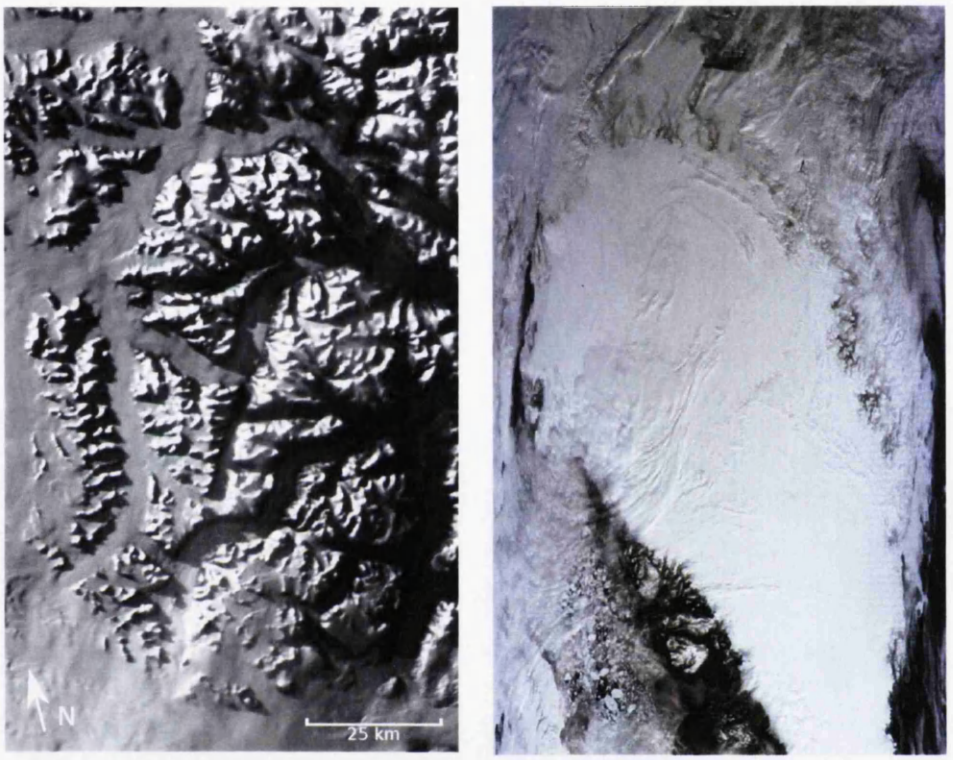

(a) Severe shadowing from a low sun angle in SE Greenland

(b) Varying illumination over Greenland, also showing a sinusoidal projection

Figure 3.1: Illumination effects in Level 1B MODIS imagery

3.4.4 MODIS preprocessing

Geolocation and "Bow-Tie" correction

All images and other datasets were projected into a polar stereographic projection, with a latitude of true scale of 71°N, and a central longitude of 45°W. This was resampled and subsetted to a 4875 x 9235 pixel grid with each pixel corresponding to

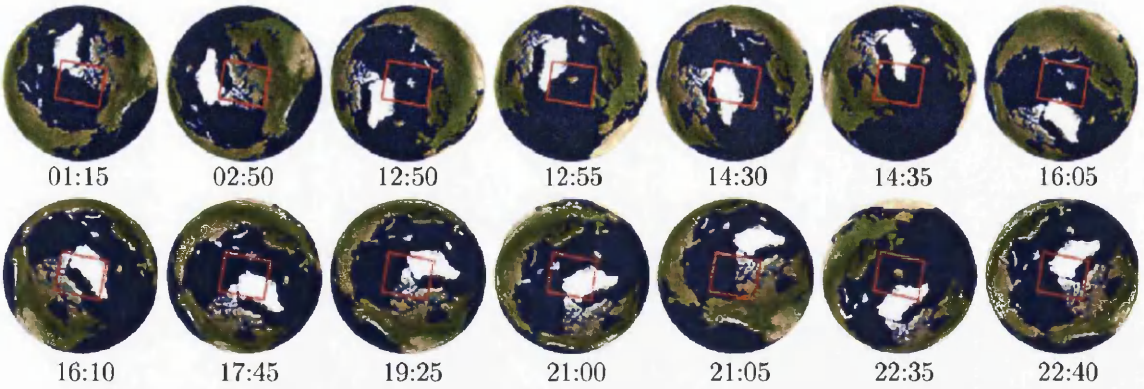

(a) Day 212, 2010

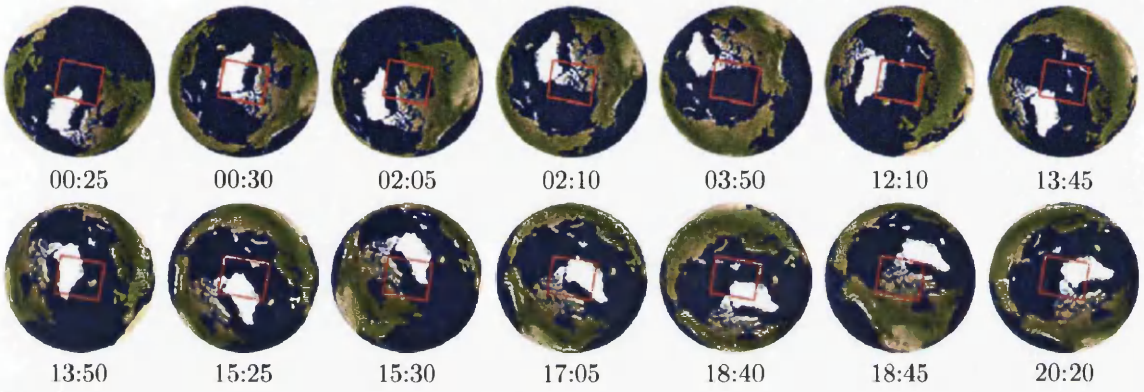

(b) Day 160, 2009

Figure 3.2: Footprints of available MODIS scenes from Terra covering GrIS. Shown in (a), on day 212 in 2010, preferential coverage occurs at 14:30/14:35 UTC imaging the whole ice sheet in two scenes. On day 160 in 2009 (b), preferential coverage occurs at 15:25/15:30 UTC, also covering GrIS in two scenes. These two days were selected to represent the variability in coverage

250 m x 250 m on the ground. By projecting all geographic data onto a standard grid, the Interactive Data Language (IDL, a programming language used for almost all data processing in this thesis) can be used to process the datasets without referencing the geographic projection. Whilst the geographic location of any pixel can be located when necessary, pixel to pixel comparisons between datasets are far more common.

The geolocation of the MODIS imagery was performed using the MODIS Reprojection Tool Swath developed by the Land Processes Distributed Active Archive Center (`https://lpdaac.usgs.gov/lpdaac/tools/modis_reprojection_tool_swath`). This requires as an input the MODIS geolocation dataset (MOD03) which contains geodetic coordinates, and solar and satellite azimuth/zenith information

on a 1 km grid. Owing to the increase in the ground resolution away from nadir, towards the edges of an uncorrected MODIS image the cells of one line of samples overlaps those of the adjacent lines - the length of each swath is 10 km at nadir, and $\sim$ 20 km at the image edge. Each swath thus has a bow-tie shape, and duplication of data is found towards the edges of the image across track - the appearance of this can be seen in Figure 3.3. This duplication is eliminated as part of the geolocation process performed by the MODIS reprojection algorithm.

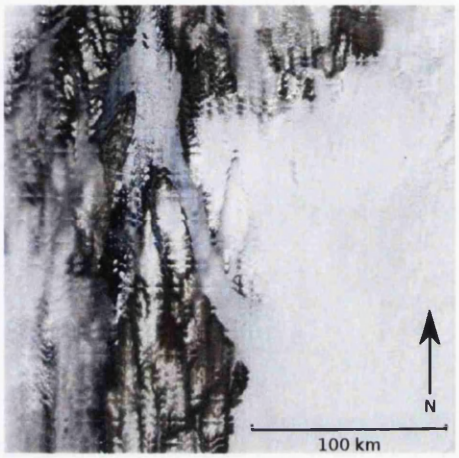

Figure 3.3: An image of Petermann Glacier showing bowtie distortion in Level 1B MODIS imagery. North direction is approximate owing to high latitude

Atmospheric correction and conversion to reflectance

For the majority of remote sensing applications the primary property of interest of a given material is its reflectance. Reflectance is the dimensionless ratio of incoming radiation of a specific wavelength that is reflected back away from the material's surface. The exact nature of reflectance depends on the viewing and solar angles as well as the surface properties; reflectance as detected by satellites is bidirectional in nature: the reflectance changes depending on the viewing angle and solar azimuth and zenith. Albedo is a similar concept but refers to bihemispherical reflectance i.e. the ratio of incoming and outgoing radiant fluxes over the whole hemisphere (Schaepman-Strub *et al.*, 2006). Different reflectance values at different wavelengths allow surface types to be identified in an image. Unfortunately reflectance is not

measured directly by a satellite based sensor. These sensors record spectral radiance, the amount of energy measured at the sensor over an area on the ground in $W{\cdot}sr^{-1}{\cdot}m^{-2}{\cdot}nm^{-1}$ (where W are watts, and sr are steradians). This needs to be converted to reflectance before analysis of these data can be performed. The primary concern in this process is correcting for the effects of the atmosphere, to give bidirectional surface reflectance as if the atmosphere was not present.

All radiation detected by remote sensors must pass through the atmosphere, and in doing so radiation is subjected to absorption and scattering. The degree and mechanism of scattering of an electromagnetic wave by atmospheric particles are functions of the size of the particles and the wavelength of the wave, and can be Rayleigh scattering (shorter wavelengths scattered at the molecular level), Mie scattering (scattering of longer wavelengths by aerosol particles), or non-selective scattering (scattering of all wavelengths by larger particles such as water droplets).

Atmospheric absorption involves the loss of energy at particular wavelengths to the atmosphere, most significantly by ozone, water vapour and carbon dioxide. Absorption differs across the electromagnetic spectrum, with the atmosphere being opaque to certain wavelengths, rather those wavelengths that experience little atmospheric absorption must be used. Useful "atmospheric windows" occur in the visible, infrared and microwave components of the spectrum.

Scattering and absorption have significant, but opposing effects on the radiance received from a point on the ground by a spacebourne sensor. Scattering adds "path radiance", i.e. radiance is measured from the atmosphere rather than from the object of interest, whereas absorption attenuates the energy that would otherwise be detected by the sensor. Before reflectance can be calculated from radiance, these effects must be accounted for.

Once downloaded, MODIS Level-1B data were converted to reflectance using the Corrected Reflectance Science Processing Algorithm (CREFL) developed by the Goddard Space Flight Centre (`http://directreadout.sci.gsfc.nasa.gov`). This performs a basic atmospheric correction which corrects for Rayleigh scattering and

absorption by atmospheric water and ozone. While the MOD09 land surface reflectance product uses a more complex algorithm requiring input of meteorological data and performs better in the presence of aerosols, both CREFL and MOD09 use the 6S Radiative Transfer Model (Vermote *et al.*, 1997) and give similar results in clear atmospheric conditions.

Conversion to reflectance is an essential step to be taken before classifying an image based on spectral characteristics. Another important aim of the conversion to reflectance is the elimination of differential illumination over the ice sheet early and late in the year as the furthest north regions leave and enter polar night. Figure 3.1(b) shows the effect of variable illumination on radiance detected over the GrIS, and Figure 3.4 shows the varying solar zeniths throughout the year at the northern and southerly extents of the ice sheet that cause this variation.

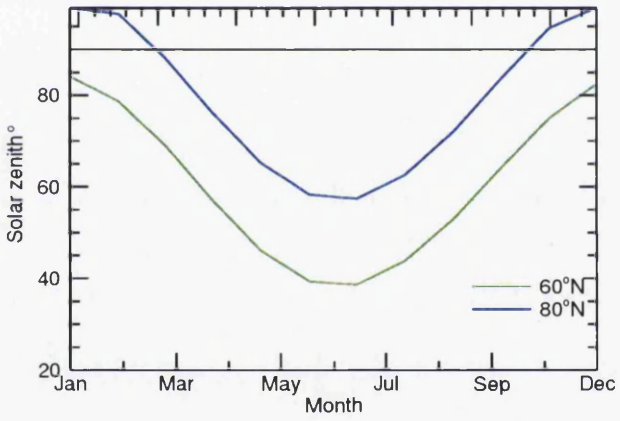

Figure 3.4: Solar zeniths at 14:00 UTC at 60°N and 80°N along the longitude of 45°W during 2009. This represents varying solar illumination at the northerly and southerly extents of the GrIS. 14:00 UTC was chosen for this figure, as many images acquired around this time were used. Zeniths were extracted from the MODIS geolocation product (MOD03) metadata. The horizontal black line represents a zenith of 90°, zeniths higher than this will result in darkness at the time of day (in mountainous regions this will occur at lower zeniths).

Masking

Although a MODIS cloud mask product is available at 1 km resolution, this was a coarser resolution than desirable. For this study, cloud masking was performed by

thresholding 500 m MODIS Band 7 data coincident with the Band 1 image being used and resampled to 250 m. Band 7 thresholding is also used for snow/ice/cloud distinction for the MODIS sea ice product by the NSIDC. Pixels with Band 7 reflectance > 0.06 were, after some experimentation, assumed to be cloud and marked as NaN. Box and Ski (2007) used a similar method, thresholding MODIS Band 6. This study used Band 7 data for the same purpose, but using Band 7 allows the use of the same methods for Aqua as Terra if necessary: Aqua has a degraded Band 6 sensor (Riggs and Hall, 2004).

Using Band 7 for cloud masking worked well over the ablation area and gave similar results to the coarser resolution MODIS cloud mask product (MOD35). For an unknown reason however the relationship failed over the higher ice. Therefore to examine the density of cloud cover over the whole ice sheet (e.g. Figure 4.10) the MOD35 MODIS cloud mask product was used.

A land/ice mask was applied to all MODIS imagery. The mask was a simple binary image created manually by the author, by digitizing areas of bedrock such as nunataks and the coastal regions from a 100 m resolution Landsat image mosaic produced by Dr. Adrian Luckman. Removing land pixels from the imagery simplified the classification process described in later chapters.

3.5 Other data sources

While the bulk of the results of this thesis were obtained through the use of MODIS data, for some results and cross-comparisons other data sources were used. Datasets described here are ice thickness and elevation at lakes (Section 3.5.1), ASTER data used when higher spatial resolutions were required (Section 3.5.2), melt extent and duration (Sections 3.5.3), modelled surface mass balance (Section 3.5.5), meteorological data from weather stations on the ice sheet (Sections 3.5.4 and 3.5.6), strain rate and ice sheet velocity (Section 3.5.7), and glacier catchments (Section 3.5.8).

3.5.1 Digital elevation model and ice thickness

A 5 km spatial resolution digital elevation model (DEM) and ice thickness dataset was collected as part of the Program for Arctic Regional Climate Assessment (PARCA) (Bamber *et al.*, 2001). The DEM was produced through a combination of lidar (ATM), radar altimetry (Geosat) and airborne photogrammetry. Ice thickness was collected by a University of Kansas airborne radar system and this thickness was used for exploring the reasons behind the drainage of certain lakes in Section 6.5. Whenever elevation is referred to in this thesis, these values have been obtained from this DEM. An alternative elevation dataset was available in the form of the 1 km ICESat DEM (Dimarzio *et al.*, 2007), however the advantages of the higher resolution of that dataset were offset by the requirements of applying a 7.5 km low pass filter before use, and poor performance in the complex terrain of the east coast.

3.5.2 ASTER

The Advanced Spacebourne Thermal Emission and Reflectance Radiometer or ASTER is a sensor onboard the Terra satellite. It has range of spectral channels from the visible through to the thermal infrared, and a NIR sensor pointing both nadir and backwards for DEM generation. ASTER was used in this study as a high resolution comparative dataset for testing the classification method used with MODIS (Section 4.2.4), and for more detailed observations of phenomena observed using MODIS. As already described in Sections 3.2.1 and 3.2.2, ASTER is a pointable sensor with a limited swath width, and as such the high spatial resolution is achieved at a cost of smaller image footprints. ASTER data are acquired on demand by pointing the sensor off track, and so the data archive is limited to that data which has previously been requested. Fortunately the interest in the GrIS in recent years means that a great deal of data acquisition over Greenland has been made. Only the visible and NIR bands were used in this study (Bands 1-3), as these are available at 15 m spatial resolution. Either the ASTER reflectance product was

used (ASTER07), or the unprocessed Level-1 data were converted to reflectance using algorithms available as part of the ENVI software package (an ITT Visual Information Solutions product built in the IDL programming language).

3.5.3 MODIS land surface temperature product

Studies of melt extent frequently use passive microwave data (e.g. Steffen *et al.* (2004)), which measures both melt at the surface and sub-surface. The latter will usually refreeze in-situ (Joshi *et al.*, 2001). The former is of more interest to this study, and can be measured using the MODIS Land Surface Temperature (LST) products (Hall *et al.*, 2006).

MODIS LST has previously been used for melt extent studies over Greenland (Hall *et al.*, 2006, 2008). The ablation zone of SW Greenland was also one of the test sites for the MODIS LST algorithms (Wan, 2004). MODIS LST is used in this thesis to estimate melt season length across the ice sheet (Section 3.5.4), and for determining the likelihood of a lake freezing (Section 4.6.2).

There are a range of MODIS LST products varying either by the algorithm used, the processing level (1 or 2), and the number of days over which the Level-3 products are composited. The product selected for use in this thesis (MOD11A1) is calculated using the generalized split window algorithm of Wan and Dozier (1996) which corrects for atmospheric effects by comparing the absorption of adjacent infrared bands - in the case of MODIS the bands used are 31 and 32. Some MODIS LST products such as MOD11B1 calibrate LST by comparing emissivity across a range of infrared wavelengths from both night and day images. This is obviously problematic for high latitude remote sensing where night time imagery is not available, so the use of the split window algorithm is preferable. The night/day method was developed by Wan and Li (1997) owning to errors in land surface temperatures derived from the split window algorithm over semi-arid and arid areas resulting from highly variable surface emissivity. However, Wan and Li (1997) state that the same problems do not occur over snow/ice. These data are available as a Level-2 swath product, but

owing to the conservative cloud mask described below the level-3 daily composited product (MOD11A1) was used to limit data gaps. MOD11A1 is produced on a 1 km resolution grid.

Owing to the sensitivity of the MODIS LST method to cloud contamination, cloud is masked out before the product is calculated using the standard MODIS cloud mask (Ackerman *et al.*, 1998) which Hall *et al.* (2006) reports to be rather conservative and tend to classify as cloud any pixel where uncertainty exists. This means that the product should strictly be referred to as *clear sky* land surface temperature as no records of ice temperature under cloud cover are included, with warmer temperatures usually occurring under cloud cover (Hall *et al.*, 2006). For brevity LST will be used from now on with this proviso.

MOD11A1 is supplied with a quality assurance layer as metadata, with each pixel comprising of a bitfield describing if the pixel is potentially cloud contaminated and giving the estimated error in emissivity and LST. Only pixels with a bitfield of "00" were used in this thesis, this is the highest level of quality control and requires there to be no suspected cloud contamination, estimated LST error of ≤ 1 K and estimated emissivity error of ≤ 0.01.

Wan *et al.* (2002) found that when compared to field measurements (including over snow) from thermal infra-red radiometers, MODIS LST error was usually < 1 °C, and occasionally up to 2 °C i.e. land surface temperature inferred from MODIS was usually within 1 °C of that measured concurrently with a field radiometer in clear sky conditions.

3.5.4 Melt extent and duration

The usual dataset used for Greenland melt extent is derived using passive microwave brightness from sensors such as the Special Sensor Microwave/Imager (SSM/I) (Abdalati and Steffen, 2001). This data product was not available beyond 2007 at the time of writing, so melt extent and duration was calculated from MODIS data

instead.

The duration of the melt season at each pixel was calculated from the MODIS LST data described in Section 3.5.3 in a method similar to that used by Hall *et al.* (2008). As the error in MODIS LST was assumed to be ± 1 °C, the melt season was taken to begin at the first surface temperature value of the year above -1 °C at each point, and to end at the last temperature value higher than -1 °C. This also takes into account the fact that melt can occur with surface temperatures below 0 °C in some circumstances. Restricting melt to positive surface temperatures resulted in unrealistically small melt extents. The time elapsed between these two days was taken to be the length of the melt season in this pixel. To obtain a value for the combined extent and duration of the melt season over a whole region or catchment, the sum of the melt duration values for all pixels assigned to that region was taken. The result of the summation is referred to in this thesis as "melt extent and duration".

3.5.5 Modelled surface mass balance

Modelled surface mass balance data were provided by Edward Hanna of Sheffield University. These data were based on a modified version of the model described in Hanna *et al.* (2005) with a retention factor built into the runoff model based on Janssens and Huybrechts (2000), and were provided on a 5km x 5km grid, separated into accumulation, runoff, and surface mass balance. Modelled melt and refreezing data were also available. The modelled surface mass balance components were used to estimate the ablation area of the ice sheet for comparison with patterns in lake occurrence in Section 7.3.1. Ablation area was taken as the area where modelled surface mass balance was ≤ 0 m/yr.

3.5.6 GC-Net automatic weather station network

GC-Net is a collection of automatic weather stations (AWS) located around the Greenland Ice Sheet and maintained by the Cooperative Institute for Research in Environmental Sciences (CIRES). Each station records energy fluxes, temperature, wind speed and direction, humidity, pressure, and accumulation. This gives adequate data to calculate energy balance or degree day based melt models at points around the ice sheet; unfortunately these points are highly sparse and temporal coverage differs considerably between stations. In this thesis data from the JAR1 AWS of this network are used as a comparative dataset to MODIS Land Surface Temperature product (LST) in its use as a proxy for melt season duration (Section 4.6.2).

3.5.7 Ice sheet velocity

Longitudinal strain rate ($\dot{\epsilon}_{xx}$) is used in Section 6.5.5 while investigating the reasons why certain lakes drain. Strain rate was calculated from the over-winter (2005–2006) velocity map from the interferometry and speckle-tracking of RADARSAT data (Joughin *et al.*, 2010). The velocity map is distributed as annual displacement in x and y components. These were converted into maps of speed and direction, and strain rate in the down-flow direction was calculated. For this purpose, flow direction was restricted to queen's case i.e. in multiples of 45° away from the central pixel, resulting in a mean and standard deviation difference between the observed flow direction and that used for strain rate calculations of $9.9 \pm 6.7°$. Strain rate was calculated as

$$\dot{\epsilon}_{xx} = \frac{\partial u}{\partial x} \tag{3.1}$$

where u is velocity and x is the distance along the flow line. ∂u was taken as the difference in velocity between two adjacent pixels along the flow line in the velocity map, and ∂x as the distance between the pixel centres.

3.5.8 Glacial drainage catchments and ice sheet regions

Throughout this thesis references are made to various glacial catchments i.e. regions of the ice sheet drained by a given outlet glacier. The catchment boundaries are those derived by Dr. Suzanne Bevan of Swansea University. A catchment has been determined for most of the major outlet glaciers of the GrIS (Figure 3.5). However for some regions, especially those regions typified by large numbers of smaller outlets such the NW GrIS, there are no catchments defined. For this reason when presenting results by catchments, the spaces between catchments are used as catchments for this purpose otherwise large areas of the ice sheet can appear devoid of data.

From the glacial level catchments, five larger ice sheet regions were defined: South West (SW), North West (NW), North (N), North East (NE), East (E), and South East (SE). These separated the ice sheet into logical sectors based upon the catchment boundaries and major geographical features (Figure 3.5).

3.6 Chapter summary

The majority of the results of this thesis were produced from 250 m MODIS data from the Terra satellite. This imagery was chosen owing to the compromise between regular coverage of the ice sheet and spatial resolution. Before further use the images were corrected for atmospheric and geometric effects and reprojected onto a uniform grid. A range of other datasets were also used in this thesis to support the MODIS derived datasets, these have been outlined in this chapter. Only the preprocessing steps applied to to these data are described in this chapter; the more advanced processing steps leading to the final results are described in Chapter 4. The results are then presented in Chapters 5 and 6.

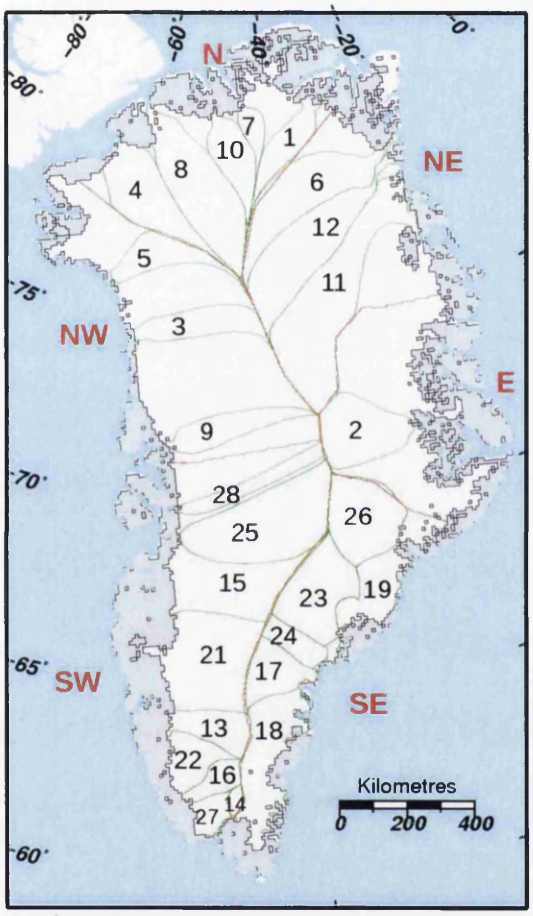

1	Academy
2	Daugaard-Jensen
3	Hayes
4	Humboldt
5	Kong Oscar
6	Nioghlvfjerdsbræ
7	Ostenfeld
8	Petermann
9	Rink
10	Ryder
11	Storstrømmen
12	Zachariae
13	Narssap
14	Nordbogletscher
15	Nordenskiöld
16	Sermilik
17	Koge Bugt
18	South East Fjords
19	Schweizerland
20	Johan Peterson Fjord region
21	Narssap Sermia region
22	Frederikshåb Isblink region
23	Helheim
24	Ikertivaq
25	Jakobshavn
26	Kangerdlugssuaq
27	Arsuk Bræ region
28	Sermeq Avangnardleq

Figure 3.5: Map of catchments and regions used in this thesis. Green lines show catchment boundaries. Red lines show region boundaries.

Chapter 4

Methodology of mapping and monitoring lakes on the Greenland Ice Sheet

4.1 Introduction

In this chapter the methods used for the classification and monitoring of the lakes on the Greenland Ice Sheet are discussed. In Chapter 3, the preprocessing steps performed on the data used in this thesis were described. Most of the methods presented in that chapter were standard procedures for the various datasets. In this chapter however, many of the methods presented were developed specifically for this thesis, or existing methods were adapted to address the particular challenges of this study. The results presented in Chapters 5 and 6 are the direct output of the methodology presented here.

First the process of choosing a classification method based on previous studies, the optical properties of ice and water, and a series of experiments is described (Section 4.2). The errors inherent in the classification are described in the same section, and comparisons with an existing method are made. Applying this method to a

very large number of images without classification errors proved problematic, and a new two stage approach had to be developed. The first stage was mapping the locations of the lakes on the GrIS at a relatively coarse temporal resolution, with considerable manual intervention, and is described in Section 4.4. The second stage was using the lake centres found in the first stage to track these lakes through a much larger number of images, with much less user input (Section 4.5). Finally lakes were classified according to how they drained (or did not drain), this process is detailed in Section 4.6.

4.2 Methods used for lake classification

4.2.1 The optical properties of water with regard to image classification

When attempting to distinguish two land cover types based on spectral properties, it is desirable to have a significant contrast between the reflectance of the two surfaces. In the case of distinguishing water and ice, the generally high albedo of ice and low albedo of water gives the opportunity for contrasting reflectance. To enhance this a wavelength must be chosen for which the absorption by water is as high as possible, and the reflectance by snow and ice is as high as possible giving the strongest contrast available.

The reflectance values from each of the 500 m MODIS bands were taken over a deep lake, an area of adjacent ice, and and an area of snow in the same catchment. These values are summarized in Table 4.1 and Figure 4.1. These data show that the greatest contrast between the reflectance of ice and water occurs in the wavelength range of Band 1. This finding is further demonstrated by the lake cross profiles in Figure 4.2b, where Band 1 reflectance was strongly depressed across the lake, whereas Band 3 was far less affected. This would suggest that an effective classification scheme can be developed using MODIS Band 1, or a ratio of MODIS Bands 1 and 3.

Table 4.1: Reflectance values from 500m L1B MODIS data over lake, snow/firn, and ice sheet pixels. The spectral separation of ice and water is also reported ($r_{(ice)}$-$r_{(water)}$).

MODIS band	λ (μm)	$r_{(water)}$	$r_{(ice)}$	$r_{(snow)}$	$r_{(ice)}$ - $r_{(water)}$
1	0.62–0.67	0.13	0.71	0.86	0.57
2	0.84–0.88	0.08	0.59	0.77	0.51
3	0.46–0.48	0.46	0.75	0.87	0.29
4	0.55–0.57	0.26	0.75	0.89	0.48
5	1.23–1.25	0.04	0.23	0.40	0.19
6	1.63–1.65	0.01	0.04	0.07	0.03
7	2.11–2.16	0.00	0.02	0.03	0.01

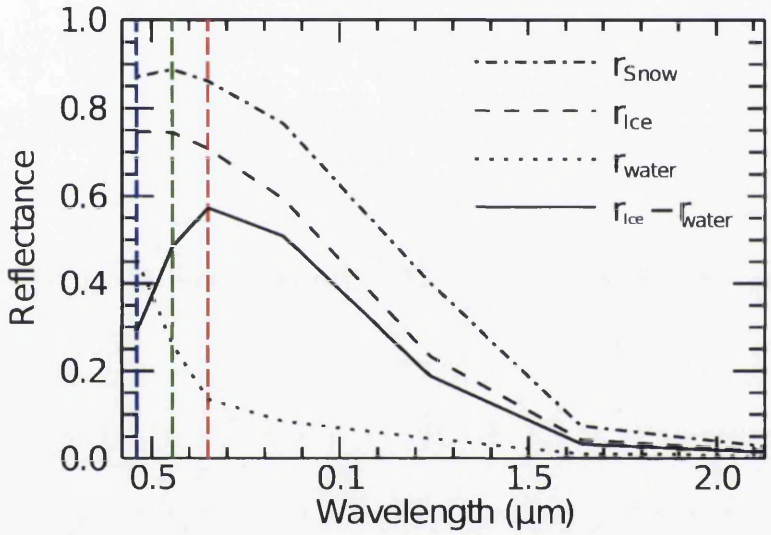

Figure 4.1: Experimentally derived reflectance over snow, ice, and water for different wavelengths. The visible wavelength bands are shown (RGB=Bands 1,4,3). Note the peak in the spectral separability of ice and water ($r_{(ice)}-r_{(water)}$) at the wavelength of Band 1 (red).

4.2.2 Methods of previous MODIS-based studies of supraglacial lakes

From examining Figure 4.1 and Table 4.1, a substantial difference in reflectance over water can be seen between the blue ($\sim$ 0.46 μm) and red ($\sim$ 0.65 μm) wavelengths. This means that by ratioing red and blue wavelengths an effective classification can be formed, and this has formed the basis for the methodology of previous studies. The lack of a 250 m resolution MODIS band in the blue wavelengths has led previous

researchers (Box and Ski, 2007; Sundal *et al.*, 2009) to use a resolution sharpening algorithm (Gumley *et al.*, 2007) to infer detail from the 250 m red band (Band 1) into the 500 m blue band (Band 3). This approach will be subsequently referred to as the "ratio method". Box and Ski (2007) classified lakes using a Band 3/Band 1 ratio with a threshold varying in the range of 1.05–1.25, replacing this where classification failed with Band 1 thresholded in the 0.5–0.7 reflectance range. Thresholds were altered within these ranges between images or even between lakes to avoid misclassification. Sundal *et al.* (2009) also used the Band 3/Band 1 ratio along with Band 1, and performed the classification using a propriety fuzzy classification package (Definiens eCognition).

As part of choosing a classification method for this study, the use of resolution sharpened MODIS Band 3 ratioed with native 250 m resolution Band 1 as described above was trialled. This method resulted in some smaller lakes being omitted. Further analysis showed that during the sharpening process the relationship between the presence of water and Band 3 reflectance was being biased by Band 1, presumably as a result of the sharpening process. This is demonstrated in Figure 4.2. Figure 4.2a shows a cross section through a lake in MODIS 500 m data with the visible wavelength Bands 1, 3, and 4. This shows the desired relationship for classification with Bands 1 and 3 having similar reflectance over ice at the lake margin, and diverging over the deeper water as Band 1 reflectance is depressed more than Band 3. Figure 4.2b shows the same lake in sharpened data. Note how Bands 3 and 4 now follow the curve of Band 1 - the desired relationship has been diminished and the use of the sharpening algorithm is the only difference between these data. In fact, the source of the sharpening method used by previous studies (Box and Ski, 2007; Sundal *et al.*, 2009) deliberately makes no argument as to the scientific integrity of the algorithm, stating rather that it is intended for visualization purposes (Gumley *et al.*, 2007). As a result of these findings the use of resolution sharpening was ruled out. As a 250 m resolution was desirable (see Section 3.2.4), the ratio method with 500 m resolution data was also unsuitable, so a classification using a single MODIS band was chosen.

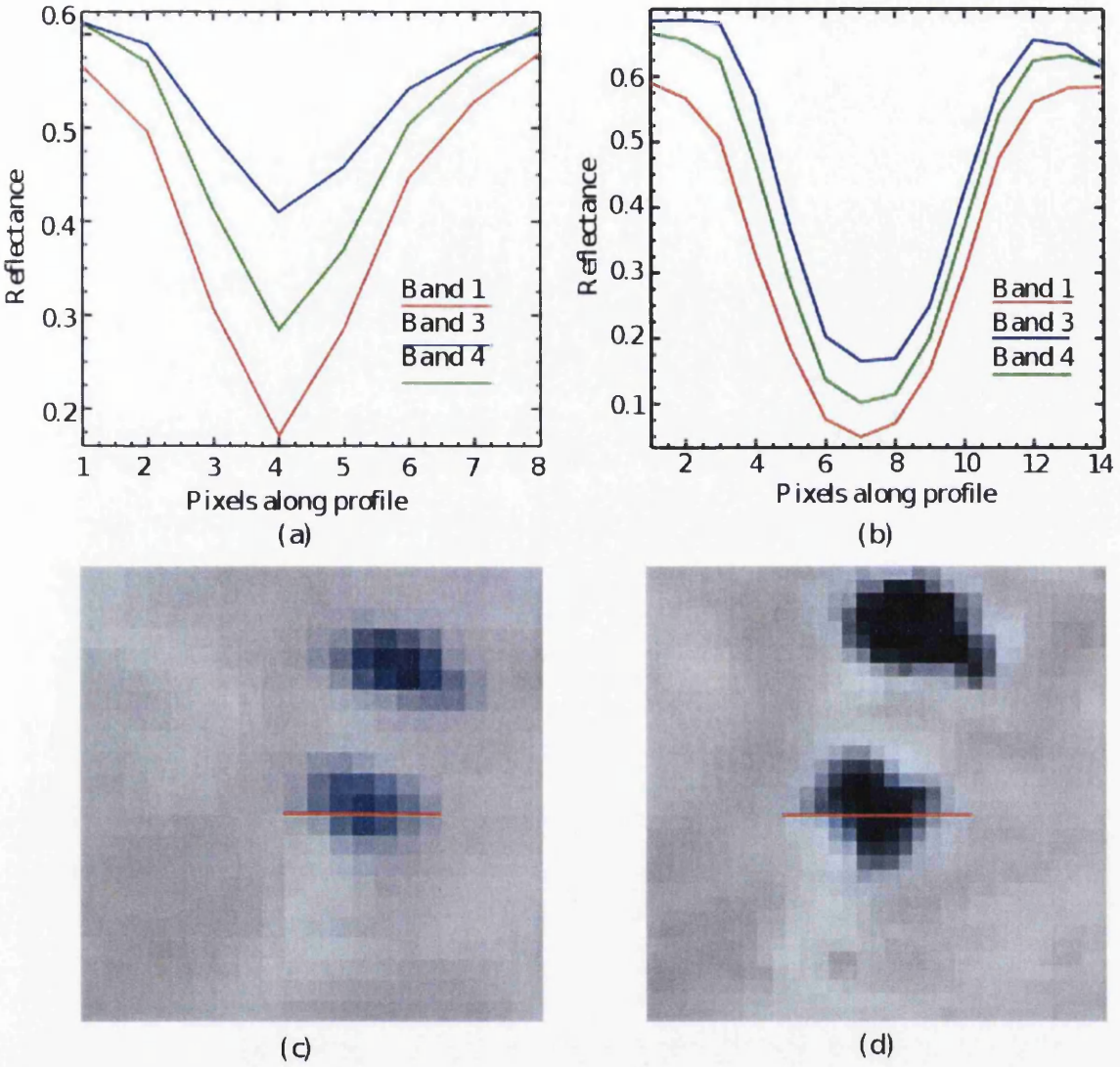

Figure 4.2: Spectral profiles across a lake. (a&c) Profile through a lake in 500 m data, note the separation of Bands 1 and 3 over the lake. (b&d) Profile through the same lake in sharpened data (250 m). Note that Band 3 now follows the curve of Band 1 more closely.

4.2.3 Classification choice

Owning to the limited range of MODIS bands available at 250 m resolution and the shortcomings of resolution sharpening highlighted in Section 4.2.2, classification of lakes was performed using only one band. MODIS Band 1 was chosen, owing to a strong contrast between ice and water in the wavelength range of this band (Table 4.1 and Figure 4.1). Using one band rather than two also had considerable advantages when using several thousand images, as only half the data storage was

required. Whilst the use of only one spectral band would be problematic in a more spectrally complex environment, once land and cloud pixels had been masked from each image the water/ice contrast of supraglacial lakes was the most obvious feature of the ice sheet at this wavelength. A reflectance threshold therefore needed to be chosen to mark the division of water and ice.

Although separating deep water from fresh snow in terms of spectral characteristics is straightforward, both flooded and non-flooded areas of the ice sheet have a range of reflectances. Whilst reflectance of the deepest part of a large lake is low, the shallower the water is the closer the reflectance becomes to that of the surrounding ice. Indeed shallow supraglacial water bodies have a spectral signature composed of both the absorption of the water column and the albedo of the underlying ice (Sneed and Hamilton, 2007). Conversely, whilst fresh snow has very high reflectance, a melting ice surface has a lower reflectance and the presence of cryoconite and dust inclusions in the ice lowers this further (Wientjes and Oerlemans, 2010). The reflectance ranges of dark ice and shallow water can become very close, this tends to occur as the melt season progresses because the albedo of the ice falls as surface melt intensifies (Stroeve *et al.*, 1997). As such different threshold values were necessary throughout the melt season (Figure 4.3). Spatial differences in required threshold values also occurred, as a result of different parts of the ice sheet being at different stages in the melt season at any one time. Box and Ski (2007) used a different threshold value on a image-by-image and lake-by-lake basis for this reason, but for this study this was not practical due to the large number of images being used.

Rather than use a range of fixed thresholds, a dynamic threshold was chosen based upon the mean reflectance of the surrounding ice. This means that to be classified as flooded, a pixel in an area of dust-covered ice must have a lower reflectance than if the surrounding pixels represent fresh snow. The relationship of the reflectance of a given pixel to that of its surroundings can be obtained by filtering MODIS Band 1 with a 21x21 pixel low pass filter, and ratioing the result with the original data. This was performed after the masking procedures described in Section 3.4.4 to avoid contamination of the filter window by cloud or nunataks. The 21 pixel

window size was chosen experimentally as the smallest window size to give an approximation of ice reflectance without high frequency detail (i.e. lakes). The output was converted into a binary classification by applying a threshold value. The choice of threshold value is discussed in Section 4.2.4. Using a dynamic threshold had an advantage when considering the pixels around the periphery of the lake, which had a reflectance that was a mixture of ice and water surfaces. With a fixed threshold, if the surrounding ice was dark, mixed pixels were more likely to be classified as a lake. When the albedo of the surrounding ice was higher, mixed pixels were more likely to be classified as ice. With a dynamic threshold as used here, this effect was reduced (Figure 4.3). In addition, reflectance over shallow water is partly a function of the reflectance of the lake bottom (applicable if the lake is shallower than approximately five metres at the wavelength used (Green *et al.*, 1996)), which is likely to have a similar reflectance to the surrounding ice (Sneed and Hamilton, 2007). Therefore it was logical to take into account the reflectance of the surrounding ice.

4.2.4 Comparison of classification methods and threshold choice

A range of threshold values were tested to examine whether one threshold applied to the mean reflectance of the surrounding area (referred to from this point as the "dynamic threshold" method) would work universally for classifying lake area. The areas of 173 lakes were calculated by performing a supervised classification on 15 m resolution ASTER data. Lakes from several ASTER images were used, on different dates at different times of the day. These images were from the SW and NE, as these regions had the most image choice in the ASTER archives. The images used were from 01/08/2001 (Nordenskiöld catchment, SW Greenland), 01/07/2007 (Sermeq Avangnardleq area, W Greenland), 17/07/2009 (Academy Glacier, N Greenland), and 08/07/2009 (Nordenskiöld catchment, SW Greenland). Concurrent MODIS data were then classified using the proposed method with a range of threshold values. As a comparison, the ratio of MODIS Band 1 and sharpened Band 3 as used by

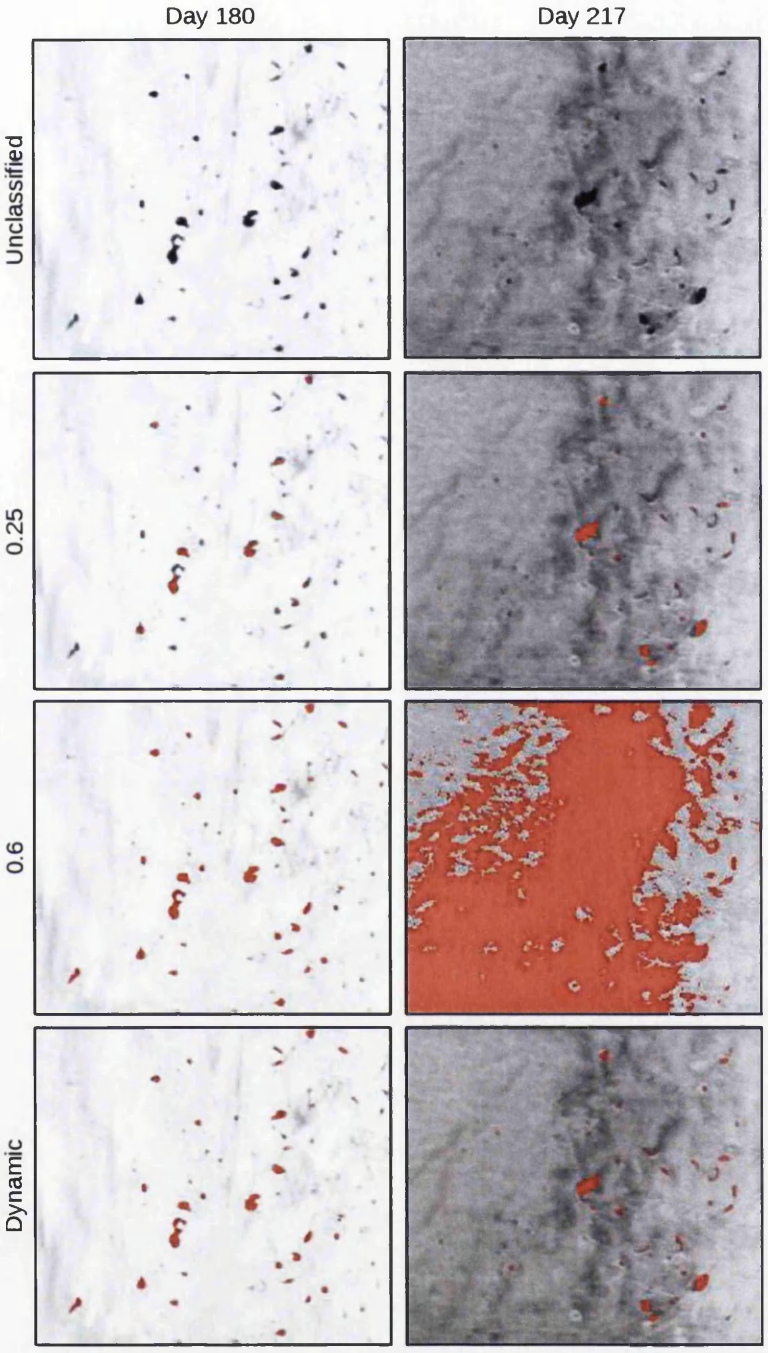

Figure 4.3: A comparison of different static and dynamic thresholds in images from the same region on different dates. Pixels classified as lakes are shown in red. Note that the background albedo is higher on day 180 than 216. Day 180 required a reflectance threshold of 0.6 to classify lake extent. For day 217 this threshold was too high and resulted in severe errors, a value of 0.25 was more appropriate. This value resulted in an underestimate of lake area for day 180. The dynamic threshold method performed well for both days.

Box and Ski (2007) was also tested with a range of threshold values. The results of this analysis are shown in Table 4.2 and Figure 4.4. Total area calculated from ASTER was used as validation. The percentage deviation from this total area, the Root Mean Square Error, the Spearman's Rank Correlation Coefficient, and the percentage of lakes detected were used to rate the performance of each method and threshold value.

Table 4.2: Comparison of different threshold values for the ratio and dynamic threshold methods.

Method	Total area	% difference	RMSE	Corr. Coeff.	% detected
ASTER	144.49	-	-	-	-
Dynamic 0.6	127.1	12.2	0.19	0.96	93.7
Dynamic 0.65	141.4	2.16	0.17	0.96	96.5
Dynamic 0.7	162.6	12.5	0.24	0.94	98.8
Ratio 0.7	85.8	41.4	0.43	0.86	60.7
Ratio 0.75	121.2	16.1	0.36	0.85	73.4
Ratio 0.8	178.8	23.8	0.57	0.82	87.3

The use of a threshold of 0.65 of mean local reflectance performed the best overall, with 97.8 % of the total area from ASTER, and a RMSE of 0.17 km^2. 96.5 % of lakes were detected. Using a higher threshold of 0.7 increased the percentage of lakes detected to 98.84 %, but with a loss of accuracy in area measurement (RMSE = 0.24 km^2). Lakes measured in the ASTER data and not in the MODIS data area were the smallest in the dataset. Mean lake area for this test was 0.84 km^2 with a median area of 0.54 km^2, mean area of lakes not detected at 0.65 of mean local reflectance was 0.16 km^2 with a median area of 0.17 km^2. Other lakes in this size range were successfully detected by MODIS; the omitted lakes were presumably shallower than those detected as shallow water will attenuate less radiation (Smith and Baker, 1981). Several of those lakes that were omitted were visible in the imagery, but had similar reflectances to areas of darker ice making them difficult to classify.

The dynamic threshold method outperformed the ratio method in terms of greater success in detecting lakes, lower RMSE, and higher correlation coefficients. The lowest RMSE for the ratio method was 0.36 km^2. However, this corresponded to

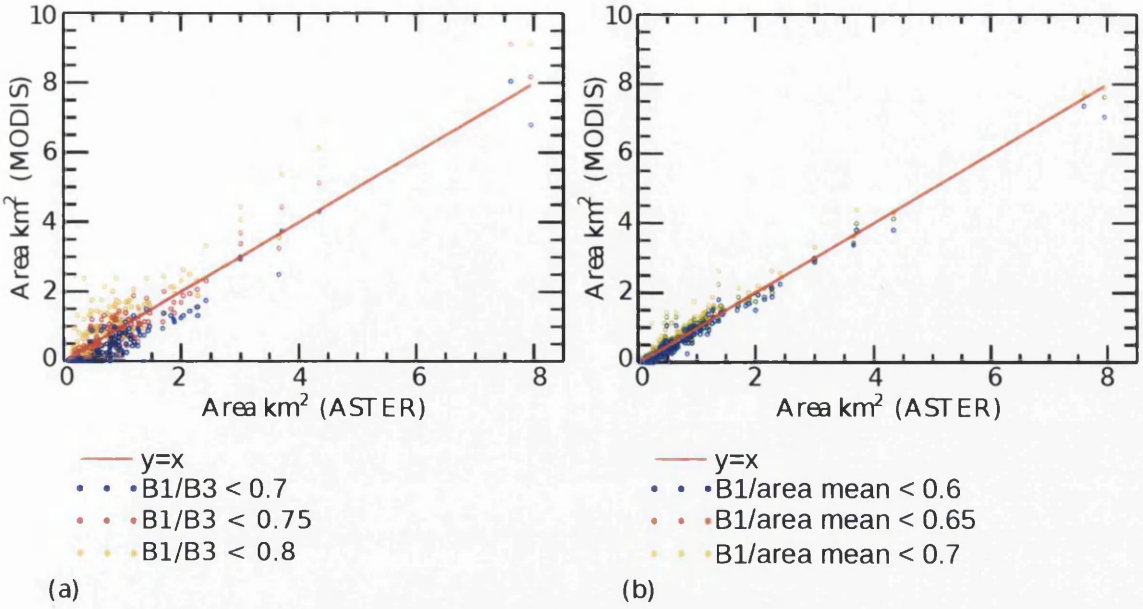

Figure 4.4: Comparison of threshold values for the ratio (a) and dynamic threshold (b) methods. MODIS bands 1 and 3 are represented as B1 and B3. Three threshold values are tested for each method. The red line represents $y = x$. Note the greater degree of variance shown by the ratio method, and the cluster in the ratio plot (a) where y=0 relating to lakes that could not be detected by MODIS with that method. There are far fewer points relating to undetected lakes (y=0) for the dynamic threshold method (b).

only 73.4 % of lakes being detected. All thresholds used with the ratio method showed lower correlation with the area from ASTER than with the dynamic threshold method. This is reflected in the wider spread around the line $y = x$ in Figure 4.4a than in Figure 4.4b.

As a result of this experiment, it was decided that using the dynamic threshold method with a threshold of 0.65 was optimal, and this was the classification method chosen for this study.

4.2.5 Classification errors

Errors in the classification method have been divided into errors in the estimation of individual lake areas, and errors of omission and commission. Errors of omission and commission are the erroneous omission of lakes from the classification, and

erroneous inclusion (commission) of non-lake areas with similar spectral properties. Whilst some errors in individual lake area are essentially errors of commission and omission of individual pixels, they are discussed separately.

Errors in the measurement of lake area

As MODIS data has a relatively course resolution, pixel size was a source of error in the measurement process. To quantify this, a comparison was made between the areas obtained from MODIS using the methods described in this chapter, and those derived from a much higher resolution sensor. Ideally field derived lake boundaries would have be used for this stage, however these were not available. Using a similar approach to the threshold choice in Section 4.2.4, the areas of 100 lakes were extracted from both MODIS data using the method selected in Section 4.2.3, and from concurrent ASTER data using a supervised classification. No images or lakes were reused from the threshold choice experiment. Seven ASTER images were used, which were acquired on different years and from both the SW and NE regions of the ice sheet. In the previous section all lakes visible in the ASTER data were included, and MODIS classification methods were judged in part by their ability to detect smaller lakes. In this experiment the selection of test lakes was made according to what could be detected in the MODIS data, to assess the errors relating solely to classification accuracy and pixel size rather than including errors of classification omission.

The combined areas of all of the 100 lakes measured from ASTER and MODIS were both 75.69 km^2. However, this does not mean that there were no deviations between the measurements. RMSE was 0.14 km^2 per lake, although there was no evidence of systematic error in this test (Figure 4.5). There was no evidence to suggest that measurement errors varied from year to year.

Some errors in the measurement of area were harder to quantify, namely the effect of cloud, and the effect of floating ice on the surface of lakes. These errors are independent of any classification error. If a lake was obscured by cloud on the day

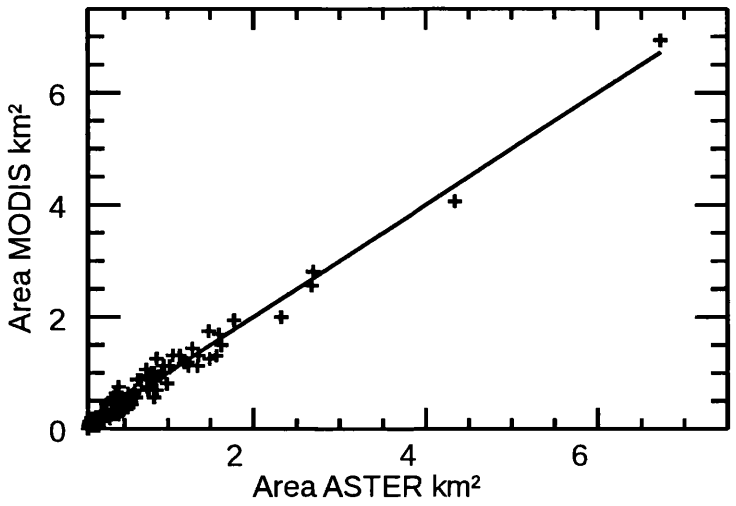

Figure 4.5: Final classification method using a threshold of 0.65 plotted against the area of the same lakes from concurrent ASTER data.

of maximum extent, then the area of that lake will have been measured on the day of the largest cloud-free extent. Unfortunately the effect of this cannot be quantified, although it will always result in an underestimate of lake area. Areas of the ice sheet and periods where fewer observations could be made will have had an increased likelihood for errors in area measurements from this source. The availability of cloud-free data is described in Section 4.5.1.

At the highest elevations, a cap of ice partially covered the surface of some lakes (as described by Echelmeyer *et al.* (1991)), which reduced the area recorded for these lakes. Sundal *et al.* (2009) is the only study since Echelmeyer *et al.* (1991) to mention this phenomenon, and these lakes were omitted from their dataset. These lakes were included in this study, since partial measurement of a lake is more accurate than its omission. In addition, these lakes were often observed ice-free at some stage of the melt season. This meant that whilst the full extent of the lake may not have been measured when the lake was at its greatest size, the full extent could be measured at some stage. Nevertheless this did represent a potential error in the measurement of lake area, albeit one that only affected those lakes at higher elevations.

Problems of misclassification

Errors in the estimation of lake area are discussed briefly in Section 4.2.5. Another source of error lay in misclassification, which is separable into errors of omission and commission. Whilst errors in estimating lake area are errors in the omission and commission of individual pixels, this section will discuss the omission of entire lakes, and the false identification of lakes caused by factors such as shadowing.

The main source of errors of omission was small lake area, i.e. lakes that never grew to a sufficient size to be detected in the classification. The absence of the smaller lakes did have the advantage of setting the lower size limit for inclusion in the dataset which would have to be set even if using data of infinitely fine resolution, otherwise ever smaller melt-ponds and flooded crevasses would have needed to be included.

A second cause for the absence of a lake from the data could be occlusion by cloud. The risk of this was minimized as far as possible by using frequent observations and working on a lake-by-lake basis. The availability of cloud-free data is shown in Section 4.5.1.

The sources of errors of omission could not be avoided. However, the various errors of commission however could be dealt with more effectively. For example, it was difficult to distinguish between shadowing and liquid water over ice based solely on spectral characteristics with the wavelengths available. As such misclassification due to shadowing occurred in many images (Figure 4.6). The main sources for shadowing over the ice sheet were topographic shadowing around the margins, and cloud shadowing. Topographic shadowing was especially problematic in the complex topography of the E coast (Figure 4.6d), particularly on the glacier tongues of the Schweizerland Alps and the region just N of Scoresby Sund. This effect was mitigated to some extent by using only imagery with the highest possible solar zeniths, but remained a problem early and late in the melt season when solar zeniths were at their lowest. Shadowing could also occur in the hollows where lakes form (Figure

4.6a), although this tended to only occur after the last lakes had frozen as very low sun angles were required. Cloud shadowing however could occur anywhere on the ice sheet (Figure 4.6b), and occurred independently of the time of year. Areas of very dark ice due to dust or cryoconite could also have low enough reflectance to be misclassified as water, however this was unusual, and tended to occur in the same sites each year so this was straightforward to control. It was particularly prevalent in regions of the SW where dust inclusions in the ice result in a lower than expected albedo (Wientjes and Oerlemans, 2010).

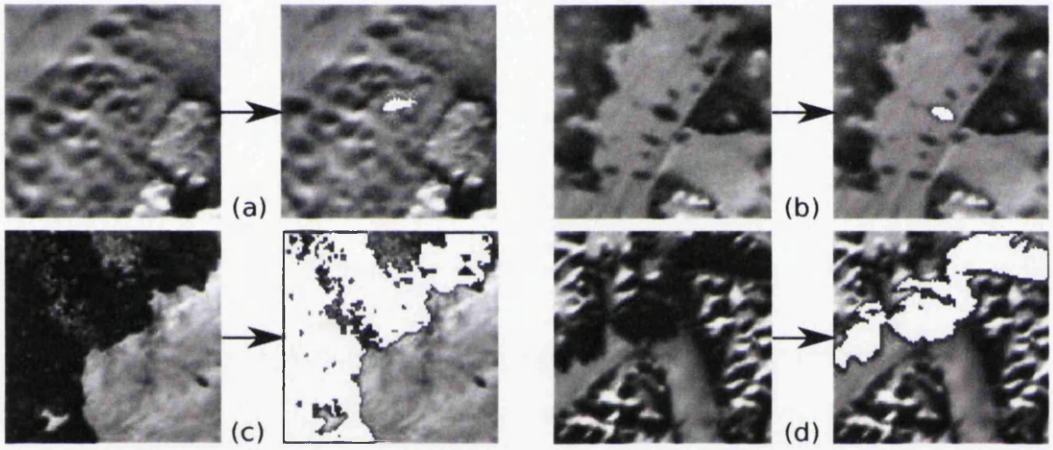

Figure 4.6: Examples of problems with the classification process. Low solar zenith and surface hollows late in the year (a). Cloud shadowing (b). An unusual example where a lake site from 2005 calved away, causing the ocean to be classified as a lake at this site (c). Topographic shadowing in the mountainous eastern GrIS (d).

Finally areas of what appears to be saturated snow and firn were observed at the upper limit of the lake zone, particularly in SW Greenland, and were sometimes classified as lake water. Whilst this is obviously part of the supraglacial hydrological system, for the purpose of lake monitoring these slush zones were ignored by omitting them during manual intervention in the classification process (Sections 4.4.3 and 4.5.3).

The problem of false positives was circumvented in different ways at different stages of this methodology. The simplest method was to manually remove misclassified areas, which was implemented in the early stages of the methodology (Section 4.4.3). However, this was time consuming, and impractical to apply to a large number of

images. The problem of correcting errors in classification over a large number of images with a high degree of confidence required the development of a novel approach to lake monitoring, this is introduced in the next section.

4.3 General approach to lake monitoring

A method was required that would allow a high degree of confidence to be afforded to the classification without necessitating checking every image. The solution to this problem stems from the finding of Echelmeyer *et al.* (1991) that supraglacial lakes maintain their position over periods of many years. This finding was verified for several regions of the ice sheet before proceeding with this methodology, and results are presented in Section 5.2. This stability means that if the locations of the lakes of interest are known, only these specific locations need to be classified in every image. This lead to a two-stage solution. In the first stage, the lakes to be studied were mapped. This process is discussed in Section 4.4. As lake area changed through the melt season, and not all lakes were present at any one time the lake extent needed to be mapped several times throughout the year. Once the central coordinates of the lakes were found, then the area of the lake at that site could be extracted from any number of images. This methodology is presented in Section 4.5. By classifying each lake in isolation, the probability of erroneously including false positives into the dataset was greatly reduced.

4.4 Methods used for lake identification

This section describes how the positions of lakes were determined. The decisions behind image selection for this stage are discussed in Section 4.4.1. The application of the classification is described in Section 4.4.2, and the subsequent manual editing of this classification is described in Section 4.4.3. This classification was used to find the coordinates of each lake, which is described in Section 4.4.4.

4.4.1 Image choice

To ensure that all lakes were detected at this stage, the temporal separation of the imagery used was important. Whilst the lake studied by Das *et al.* (2008) lasted ~ 1 month before draining, no data on the duration of other lakes is currently published. To avoid the risk of a lake forming and draining between the dates of consecutive images, approximately two images per week through the melt season were used (Figure 4.7). This decision was made after inspecting more frequent imagery to establish approximate lake duration.

The best (i.e. cloud-free) images available were selected for this stage. The size of Greenland means it is very unusual to obtain ice sheet wide cloud-free imagery. Therefore the GrIS was divided up into the regions described in Section 3.5.8 and the most suitable images selected for each region (Figure 4.7). Owing to the latitudinal range of the SW, SE, and NW regions, these areas were each divided into N and S sections for the purpose of image selection.

When no totally cloud-free images were available for a desired date, images were sampled more frequently until full coverage for that time period was guaranteed. The frequency of cloud-free observations used at this stage is shown in Figure 4.8.

4.4.2 Application of the classification

Once the most appropriate imagery had been selected, the classification process was started. Each masked and georeferenced image was filtered with a 21x21 low pass filter (Section 4.2.3). The original image was then divided by the filtered image and the output thresholded with a value of 0.65, giving a binary image. This binary image was then converted into a shapefile of preliminary lake classification.

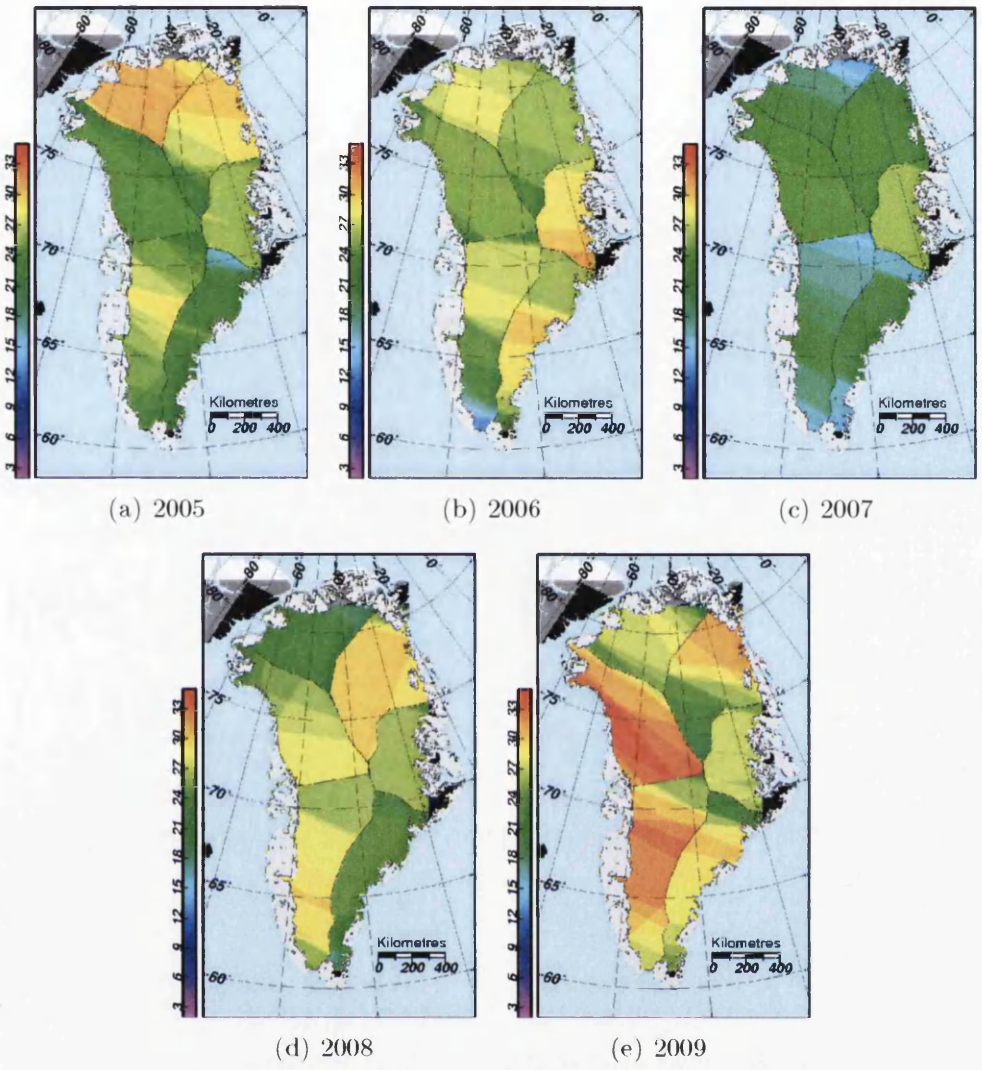

(a) 2005 (b) 2006 (c) 2007

(d) 2008 (e) 2009

Figure 4.7: Image coverage used for the initial identification of lakes. The regions of the GrIS are shown. Each pixel is coloured according to the number of images that overlapped that pixel.

4.4.3 Manual editing

For each of the images used, a 250 m "true colour" image (red, green, and blue represented by MODIS bands 1,4, and 3) was produced as described in Section 4.2.2. These data are easier for a human operator to interpret than the grayscale or two-band 250 m data available otherwise. Each shapefile was overlain on the corresponding true-colour image. This process allowed the comparison of the classification with the MODIS imagery. All areas of misclassification (Section 4.2.5) were then manually deleted from the shapefile.

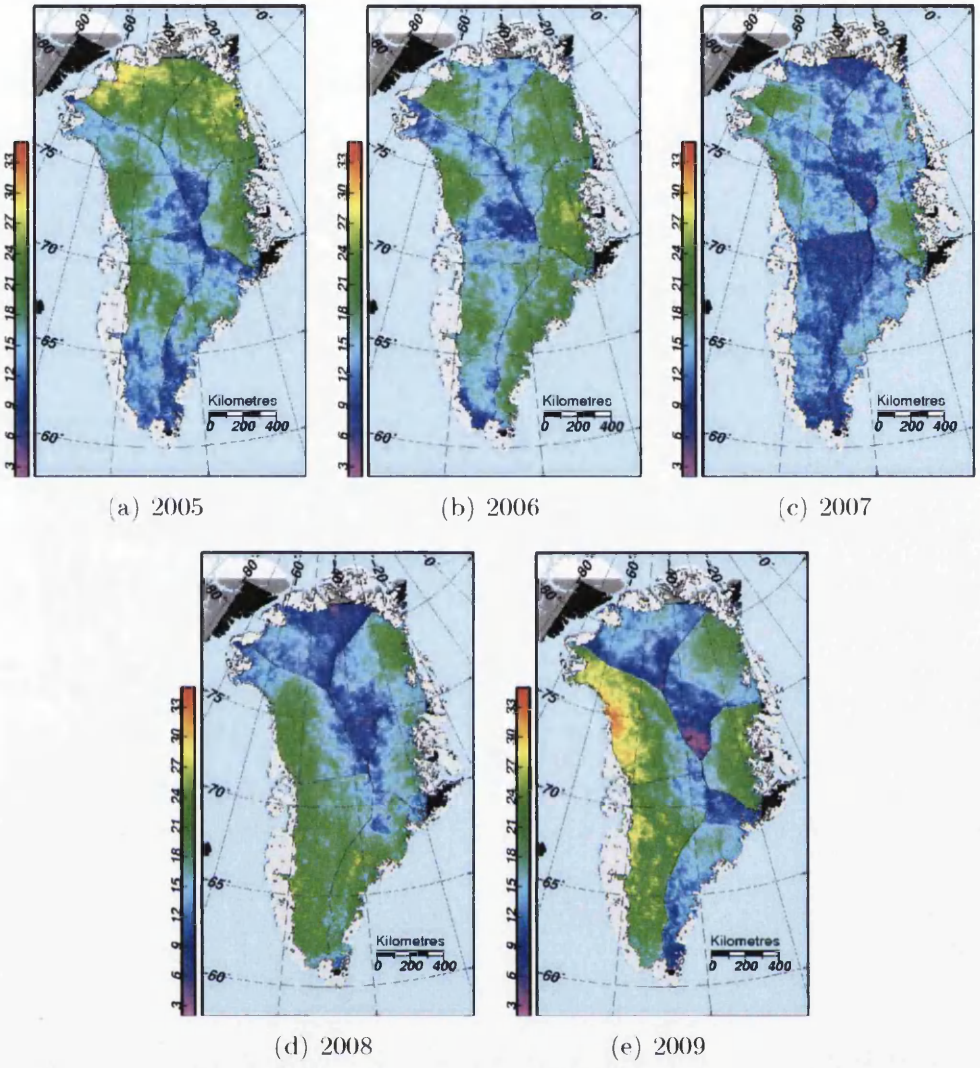

(a) 2005 (b) 2006 (c) 2007

(d) 2008 (e) 2009

Figure 4.8: Cloud-free pixel density for the images used for the initial identification of lakes. Each pixel is coloured according to the number of times that overlapped that point could be imaged without cloud.

4.4.4 Obtaining lake coordinates

Each edited shapefile of lake extents was converted back into a binary raster image. Total lake extent per year was calculated by summing the pixels of the binary images. To reduce the chances of missing a lake due to an extended period of cloud, a very short lake lifespan, or lakes not occurring every year, the data from all five years were combined by summing the five lake extent images. This image was thresholded to show the positions of lakes over the five years.

For lakes with a maximum size similar to the pixel size of MODIS (0.0625 km^2), it was difficult to infer changes both interannually and intra-annually. As such lakes that did not reach a maximum area of two pixels (0.125 km^2) at any point in the five year period were omitted at this stage. This procedure left the 2600 largest lakes in the dataset.

A segmentation algorithm was run over the remaining classification to give each lake an identification number. These IDs were used at every stage of the analysis when dealing with individual lakes. For each ID number, the corresponding lake was found, and the location of the centre point was calculated by taking the median of the x and y coordinates of the constituent pixels. The coordinates were predominately kept as pixel coordinates owing to the shared coordinate system (Section 3.4.4) and extent of all imagery and other data used, although they were also converted to latitude/longitude.

4.5 Monitoring the evolution of individual lake areas

As previously described in Section 4.2.5, classifying lakes in an image had significant potential for error without manual intervention, and as such extracting lake area image-by-image with satisfactory accuracy was laborious. In Section 4.4.4 the locations of supraglacial lakes in the melt seasons of 2005–2009 were determined. With the positions known, the remaining information required to examine the draining behaviour of these lakes was the changing area through time, and when the lakes formed and drained. Obtaining this information obviously required the use of a greater number of images than in the method described in Section 4.4. Rather than applying the method in Section 4.4 to more imagery, the positions already determined were used to "seed" a classification over more images.

For each image in the dataset, an attempt to grow a region around the coordinates

of each lake site was made. From the central point, each adjacent pixel that met the required spectral parameters was stored as a lake pixel. Regions could only grown into connected pixels, so other nearby lakes are omitted.

The standard region growing algorithm from IDL was used, and growth through 8 adjacent pixels (i.e. queen's case) was allowed. The spectral parameters used were the same as in Section 4.4, i.e. for a pixel to be a lake it must have MODIS Band 1 reflectance less than 65% that of the mean reflectance over a 21 x 21 pixel window (or 5.25 x 5.25 km). Once the number of 250 m pixels that correspond to each lake was known, this it was multiplied by 0.0625 to give the lake area in km^2.

It was possible that a lake might have developed in such a way that the central point at its maximum extent would not fall within the boundaries of the lake earlier in the melt season, resulting in the lake being missed. To avoid this a degree of snapping was allowed. A 5 x 5 pixel window was defined around each central point, the dimensions of which were decided upon based on the minimum spacing of lakes on the ice sheet. Within this window, the pixel with the lowest reflectance was chosen as the new central point, allowing lakes to be detected even if the central point used was not central to the lake on that date.

Cloudy pixels had already been masked out by this stage (see Section 3.4.4) but to reduce the risk of including cloud shadows in the classification, any pixels where mean MODIS band 7 thermal reflectance in a surrounding 21 x 21 pixel window (or 5.25 x 5.25 km) was greater than 0.06 were rejected as being at risk from contamination.

4.5.1 Images used for region growing and frequency of cloud-free imagery

The criteria for the choice of imagery are presented in Section 3.4.3. Figure 4.9 shows the distribution of this imagery. A total 3704 images were used. Note that the centre of the ice sheet had greater coverage owing to the more peripheral images

overlapping. Differing degrees of cloud between regions and between years meant that the usable coverage varied, the number of days when cloud-free observations could be made is presented in Figure 4.10.

The occluding presence of cloud could affect several of the stages of the methodology presented in this chapter. Missing a day or more of observations for a lake may have meant that the maximum extent of a lake was missed (Section 4.2.5), or a rapid drainage event may have occurred without being observed with sufficient detail to be interpreted as such. Whilst the exact degree to which these events occurred in this dataset cannot be directly measured, it was possible to quantify variations in the number of days missed due to cloud. This can be expressed by each region of the ice sheet, by year, or by periods of a melt season. By quantifying the number of days missed due to cloud, it is possible to identify possible spatial and temporal biases in the availability of cloud-free images, and therefore biases in the potential for the errors described above.

Previous studies (Box and Ski, 2007; Sundal *et al.*, 2009) have attempted to find imagery that is cloud-free across whole study regions. This limits the number of available scenes. By working on a lake-by-lake basis, it did not matter for the observation of an individual lake if the rest of the ice sheet was cloud covered, as long as that lake site was cloud-free. This meant that it was possible to obtain data through small gaps in cloud, and with the very high temporal resolution used it was possible to image around drifting cloud as well. This approach means that this method allowed the maximum number of observations possible using optical imagery.

Figures 4.10 and 4.11 give an insight into the spatial and temporal availability of cloud-free imagery. Cloud-free data were consistently more frequent in the N of the ice sheet than the S, especially in the NE. Fewer cloud-free images were available in the SW than the SE. This pattern was consistent across the whole observation period with similar distributions each year, although fewer cloud-free observations could be made during 2009 (Figure 4.10). Periods of image unavailability were not biased

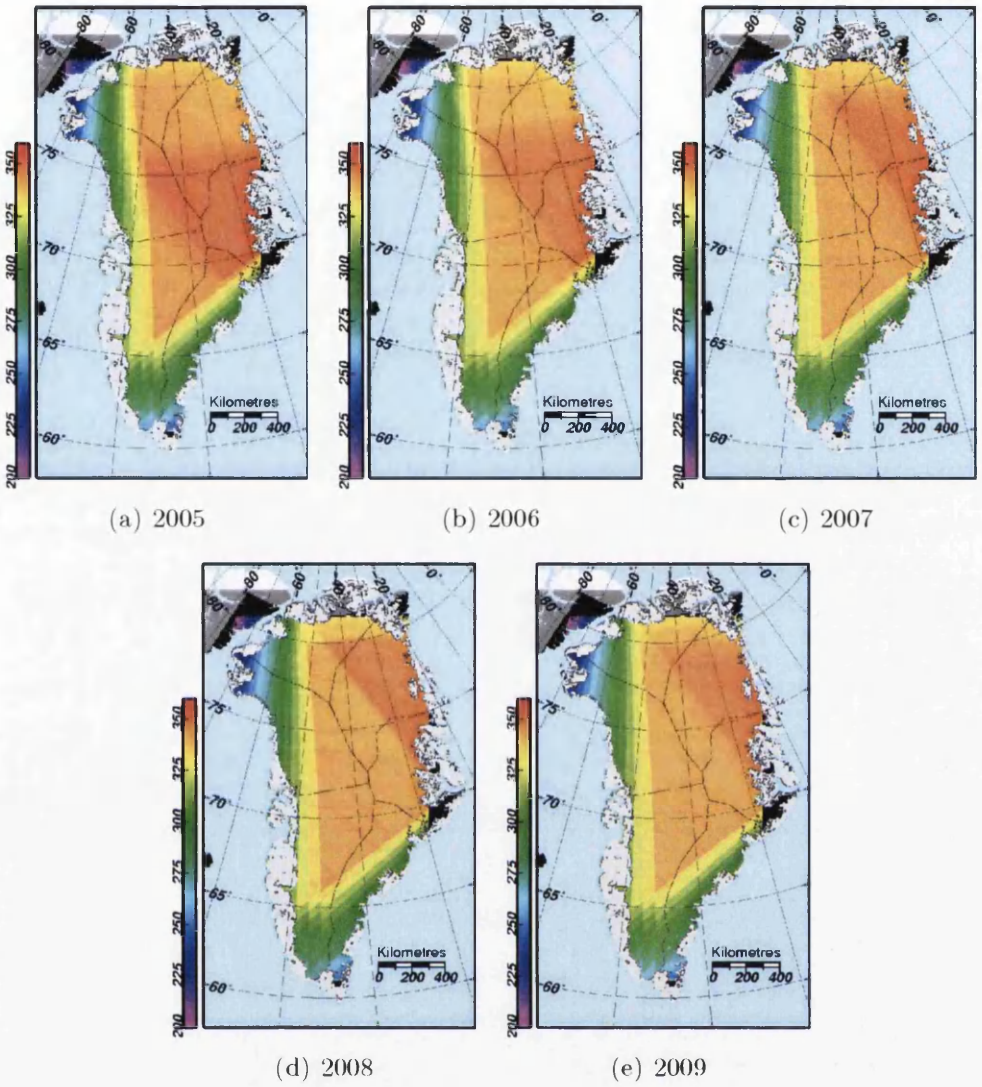

(a) 2005 (b) 2006 (c) 2007

(d) 2008 (e) 2009

Figure 4.9: Number of images used for region growing. Each pixel has a value equal to the frequency of image coverage at that point on the ice sheet. The angular patterns show that images were often acquired along very similar paths. The higher image density in the upper central regions if the GrIS result from the overlapping of more peripheral images, and converging MODIS paths at higher latitudes.

towards particular periods of the melt season, and did not persist from year-to-year (Figure 4.11).

4.5.2 Production and use of thumbnail images

To aid in the interpretation of the area data, a series of thumbnail images were produced for each lake. A 101x101 pixel area was extracted from each of the images

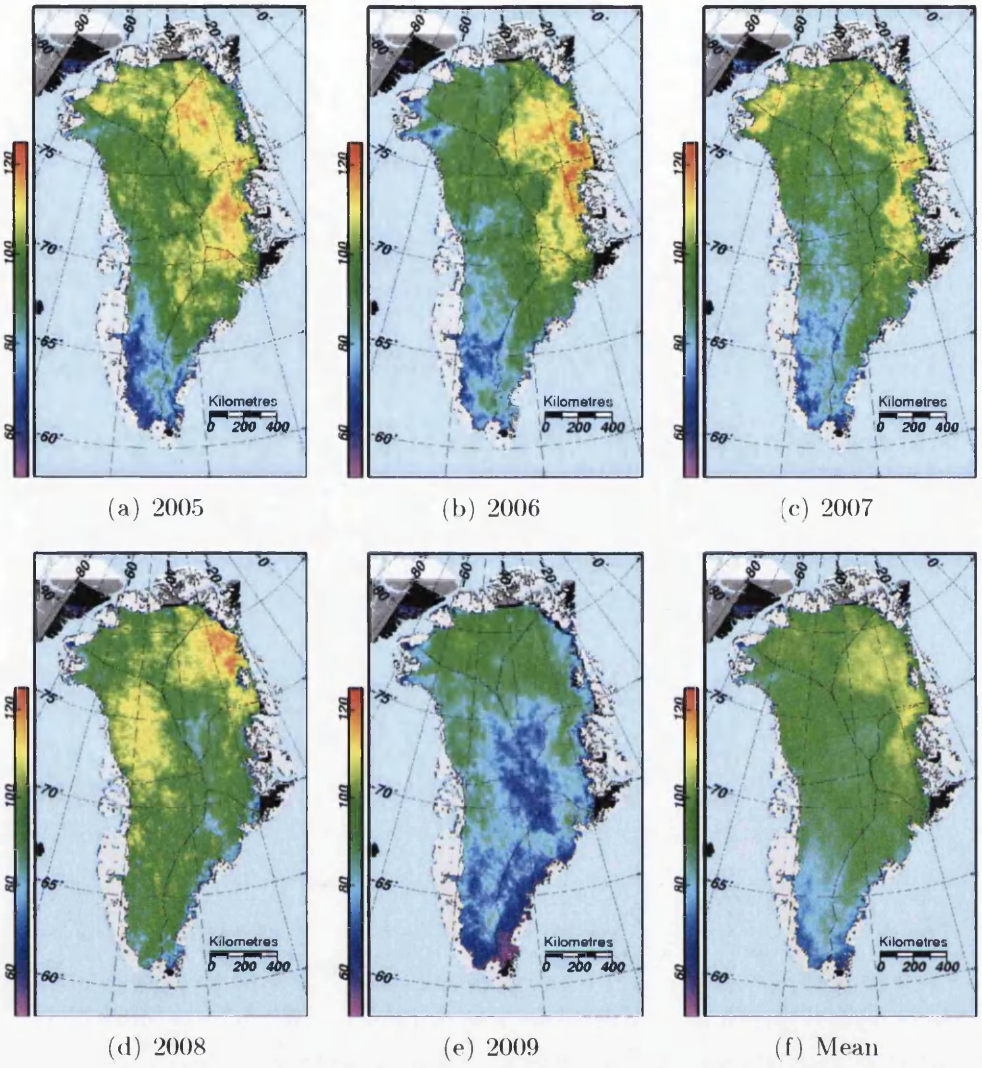

(a) 2005 (b) 2006 (c) 2007

(d) 2008 (e) 2009 (f) Mean

Figure 4.10: Number of cloud-free days per pixel per year. Note this is cloud-free days rather than cloud-free images. The observation period was 140 days.

for each lake where cloud-free observations could be made and stored as a greyscale JPEG image. These could be flicked through rapidly to help interpret the area data, and were used as part of the error elimination process described in Section 4.5.3.

4.5.3 Classification verification and error elimination

Once a time series of area data was available for each lake, a series of error elimination tests were undertaken. When cloud and topographic shadows were erroneously classified as lakes they typically had a very large area. Therefore lake area values

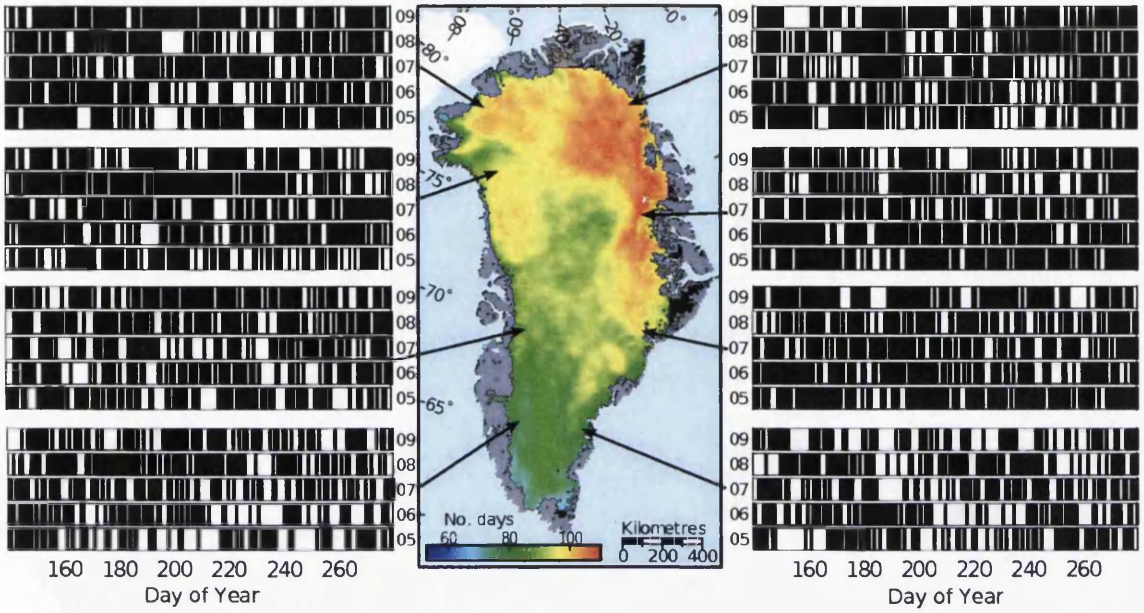

Figure 4.11: Cloud free days at lake sites around the ice sheet. Each horizontal of black and white blocks represents a year at each lake, from 2005 (bottom) to 2009 (top). Black blocks consist of vertical lines indicating days when a cloud-free observation was made during the melt season. Central image is the mean number of days with a cloud-free observation per melt season per pixel.

that were too large to plausibly represent a lake were treated with suspicion, as were area values that were much larger than other measurements for that lake site.

As a first step in identifying unusual values, the median absolute deviation of the surface area data for each lake was taken. Any values that fell outside of 6 deviations from the median were considered suspicious and investigated further. This threshold was chosen after experimenting with different values for separating topographic shadowing from the largest lakes observed. Very early and late measurements (i.e. before day 150 and after day 250) were also treated as suspicious, as the low solar elevations early and late in the Arctic summer can result in shadowing within the hollows where lakes form. This could have resulted in misclassification before and after lake formation and termination (Section 4.2.5).

Any area measurements considered suspicious in these tests were investigated visually by means of the thumbnail images described in Section 4.5.2. The thumbnails corresponding to each measurement to be checked were copied into a folder. A copy

of each thumbnail was also displayed alongside with the lake classification overlain. Any images that displayed an error in the classification were deleted, and the corresponding data point was removed automatically.

The maximum area of each lake per year is an important metric that was used extensively in the production of the results presented in Chapters 5 and 6, as such ensuring the accuracy of these values was desirable. The maximum area per year for each lake was found, and the thumbnail from the corresponding lake copied into a folder, along with a copy of the image with the classified lake overlain as above. As before, deletion of a thumbnail resulted in the removal of the corresponding data point, however in this case the maximum area for that lake was recalculated and the thumbnail for the new date loaded. Through this method it was possible to manually check the most critical values in the dataset, without the need to check all data points. The same method was applied to all metrics critical for the results presented in this thesis. It was used to check the first and last occurrences of each lake, to ensure that lake duration was measured accurately. The earliest and latest observations were the most sensitive to errors of commission. The earliest owing to the presence of areas of slush (Section 4.2.5), and the latest as low sun angles at the end of the melt season sometimes lead to false classifications owing to shadowing in the hollows of the lake site. Likewise the same checking process was performed for the maximum lake elevation data presented in Section 5.7. By the end of the error elimination process, 0.76% of images had shown a classification error requiring the corresponding area value to be removed.

4.6 Interpreting changes in lake area over time

Part of this study identified three major methods by which lakes disappear: fast drainage, slow drainage, and freezing. As this is a result of this thesis, this topic is discussed in Chapter 6 (Section 6.2). Presented here is the methodology used to classify all the lakes in the dataset into these three categories, plus a fourth category

of "unknown".

For each class of lake, there were both qualitative and quantitative criteria for the classification, these are detailed below. Lakes were assigned an initial class based on the change in their area over time and the stage of the melt season, these being the quantitative criteria. Once these were assigned, all fast draining lakes and any other lakes where class assignment was uncertain based on their area/time graph were checked manually using the thumbnails described in Section 4.5.2. The most common reason for needing manual intervention in the classification was distinguishing between slow draining lakes late in the melt season, and freezing lakes. At this stage the qualitative criteria were used. Lakes were classified by the dominant means of lake termination. This means that while a lake may have partially drained slowly through the melt season, if the majority of the surface area observed was lost through freezing it was assigned to the freezing category.

4.6.1 Fast-draining lakes

A fast-draining lake was one which drained completely or almost completely in less than two days (Figure 4.12a). For a lake to be assigned to this category the time from the lake being observed full for the last time, to the lake basin being observed to be empty had to be less than 48 hours. This requirement for rapid reimaging of the lake site eliminated the possibility that if a lake drained slowly during a period of extended cloud it might have appeared to have drained rapidly, and also ruled out the possibility of massive supraglacial runoff from the failure of a lake across the surface. All fast draining lakes were checked visually in the thumbnails for signs of drainage over the surface. It was assumed that for a lake to drain over the surface in $\sim$ 48 hours that the resulting channels would be large enough to be visible in MODIS data, a scenario that was very occasionally observed during this study.

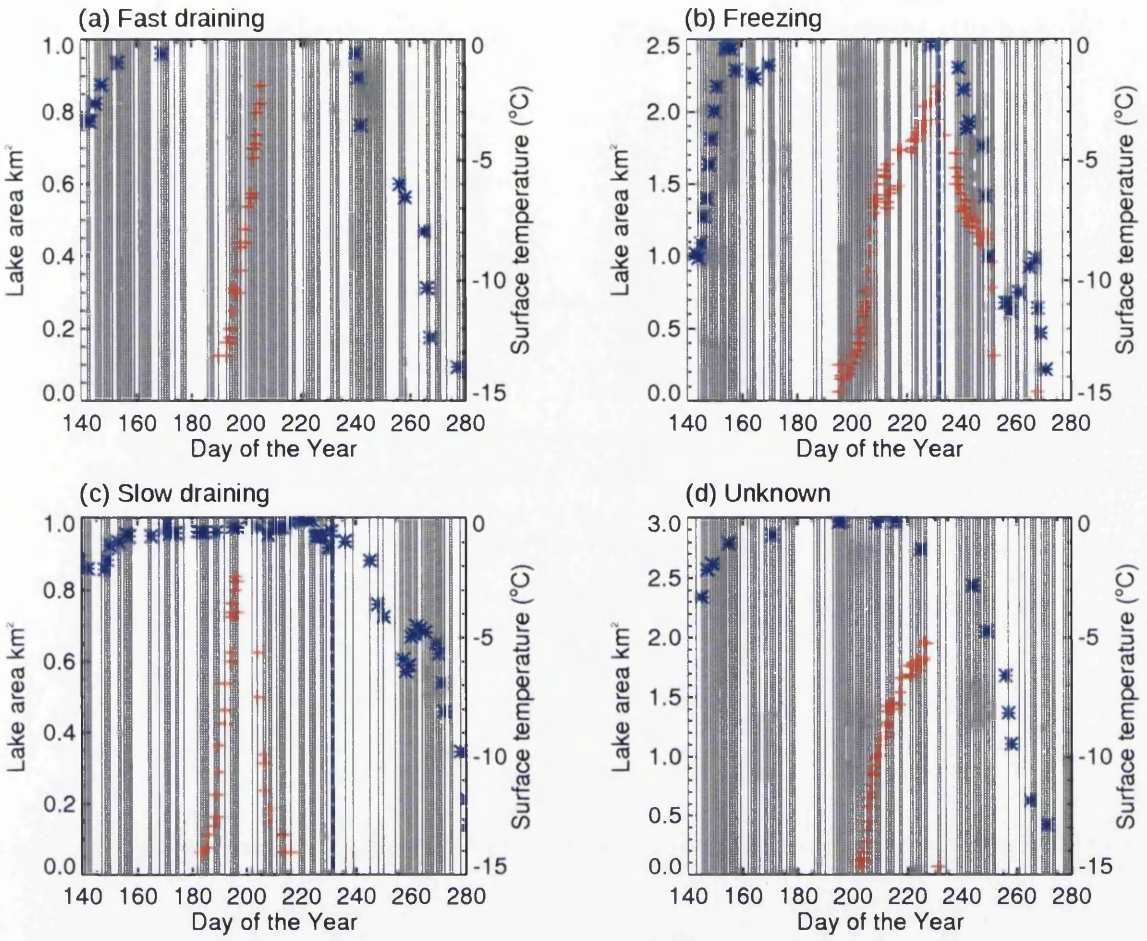

Figure 4.12: Plots of lake area over time for lakes of different drainage types. Lake area is plotted in red. MODIS LST is plotted in blue, with the blue vertical line in b and c showing the estimated end of the melt season. Vertical grey lines show cloud-free images at the lake site.

4.6.2 Freezing lakes

Some lakes were found to survive the melt season without draining and to refreeze at the end of the melt season. This phenomenon appeared in the area data as a gradual decline in surface area over time, at the end of the melt season (Figure 4.12b). The initial classification of lakes as freezing-type was made using MODIS LST data. An assumption was made that given a melting ice surface has a surface temperature of 0 °C, and the MODIS LST product is reported to have an error over ice of ~ 1 °C (Wan *et al.*, 2002), that the end of the melt season can be represented by the last day of the year LST ≥ -1 °C. This assumption is supported by comparing air temperature and surface energy balance data from the JAR1 automatic weather

station (Figure 4.13).

This initial criterion can be enhanced by the use of several qualitative factors, to help differentiate freezing and slow draining lakes which both have a steady decline in surface area over time. Firstly, lakes that were freezing over often showed visible signs of this process such as patches of ice on the lake surface, or an increase in reflectivity presumably owing to the formation of a thin film of ice on the surface prior to disappearing.

The state of surrounding lakes was sometimes indicative. If all the lakes in the immediate area declined in area at the same time, it was assumed that the melt season for that region was over. This freezing of lakes was often accompanied by an increase in the reflectivity of the surrounding ice as melting ceased and accumulation increased.

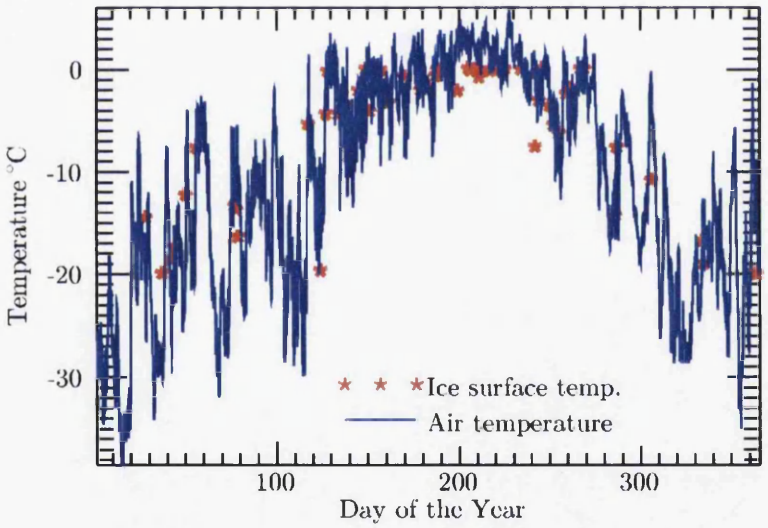

Figure 4.13: MODIS LST (red stars) over the JAR1 AWS shown with concurrent air temperature from that weather station for 2006. Whilst LST is measuring ice surface temperature, it also corresponds well to air temperature at the same location while ice surface temperature is below 0 °C.

4.6.3 Slow-draining lakes

Slow-draining lakes were those that lost volume (inferred from surface area) over a longer period of time, i.e. 3 days to several weeks. These were classified by a gradual

decline in surface area with time during a period when MODIS LST was $> -1°C$ (Figure 4.12c), inferring that the lake was unlikely to have frozen. The qualitative tests used for testing for freezing lakes applied for slow-draining lakes as well. If the surface area of a lake was declining, but the areas of the surrounding lakes were stable or increasing, it was unlikely that the lake was freezing and would therefore be categorized as a slow draining lake.

4.6.4 Uncertainty

Lakes which could not be assigned to one of these categories were assigned to the category "unknown". This was usually a result of too much cloud cover during the drainage period, and lakes in this category probably belong to the fast or slow draining categories. An example is shown in Figure 4.12d. Here a lake has probably drained, however the mode of drainage could not be determined owing to a gap in available cloud-free imagery during the drainage process. Freezing lakes were less likely to be assigned to this class as a slow rate of areal decline made short periods of cloud cover less important, and the time of the year and LST helped with the classification.

Whilst most lakes in the "unknown" category could not be assigned to another class due to cloud contamination, any lakes where the mode of termination could not be assigned with sufficient confidence to one of the other three classes for any other rea son were also assigned to this class.

4.7 Chapter summary

Previous methods for the classification of lakes from MODIS data were trialled, and a shortcoming with a resolution sharpening algorithm used in other studies was discovered. An alternative method of identifying bodies of water on an ice surface from MODIS data was developed taking into account the reflectance of the

surrounding ice-sheet surface. This method was applied to MODIS Band 1 data, as of the higher resolution MODIS bands this band allowed the greatest contrast between ice and water. The method was tested against classifications from higher resolution imagery. RMSE was 0.14 km^2 per lake, and the method performed well against existing methods in both the detection of smaller lakes, and the accuracy of area estimation.

A new approach was developed for applying this classification to a very large number of images whilst keeping classification errors to a minimum. The locations of the lakes through each of the five melt seasons studied were determined in images of limited temporal resolution with considerable manual editing for the reduction of classification errors. Only lakes which grew large enough to be represented by two or more MODIS pixels were chosen, which amounted to 2600 lakes. The centre of these lakes were used to "seed" a classification system based on the growth of regions around the lake centre points satisfying the previously determined spectral requirements. This method of monitoring lakes on an individual basis made it possible to track lake area through a much higher number of images per year than have been used by previous studies (3704 images used), and over the whole ice sheet rather than for limited regions. Once the sequence of surface area for each lake through the melt seasons of 2005–2009 was recorded, each lake was assigned a class based upon if and how it drained.

The results from the methods described here are presented in the following two chapters, and the implications are discussed in Chapter 7.

Chapter 5

Area and distribution of supraglacial lakes

5.1 Introduction

This chapter presents the results of this thesis relating to lake distribution and area on the GrIS. These results come from a combination of simple mapping (Section 4.4) and the monitoring of individual lake area over time through region growing (Section 4.5). The theory that lakes remain in the same positions from year-to-year rather than advecting with ice flow was important for the methodology of this thesis, a test of this is included as Section 5.2. Melt extent and duration, as produced in Section 3.5.4, is an important comparative dataset for studying lake distribution. The melt extent and duration calculated for the study period is presented in Section 5.3, and is used in Section 5.6 as well. Maps showing lake distribution as mapped in Section 4.4 are presented in Section 5.4, and are split into ice-sheet scale and regional-scale mapping. Full ice sheet and regional-scale mapping includes the positions and extents for lakes in the highest and lowest melt extent years. Patterns in the lake distribution are identified and discussed. The sizes of individual lakes are considered in Section 5.5, with frequency distributions of lake size, and interannual

and interregional variations in mean lake size. Lake size was also amalgamated into total lake area for whole regions and catchments. These results are presented in Section 5.6, and interannual and interregional variations are demonstrated. As well as interannual variations, changes in intra-annual lake distribution were calculated. In Section elevation the zone of lakes reached are presented.

5.2 Persistence in the location of individual lakes between years

It has been previously observed that lakes in SW Greenland do not advect downstream with ice flow, rather they stay in the same position every year leading to the theory that the positions of lakes are determined by bedrock depressions (Echelmeyer *et al.*, 1991). This lack of advection is important for the methodology used in this thesis, and so the results of this hypothesis test are presented here for several areas of the ice sheet.

Images from the temporal limits of MODIS (2000–2010) were compared for evidence of lake advection by finding comparable lake extents in the 2000 and 2010 imagery and attempting to identify lakes common to both images and comparing their locations to the distance and direction ice should have advected based on the winter velocities from 2005–2006 (Joughin *et al.*, 2010). In each region lakes could be found which were in the same locations 10 years apart. Lake advection was not found either on the very fast flowing outlet glaciers (Figure 5.1) where ice velocity was recorded up to 11 km per year, or on the slow moving parts of the ice sheet (Figures 5.2 and 5.3) where over-winter ice velocity was < 100 m per year. Note that the ice will have advected further than indicated on Figures 5.2 and 5.3, as seasonal increases in ice velocity are not taken into account.

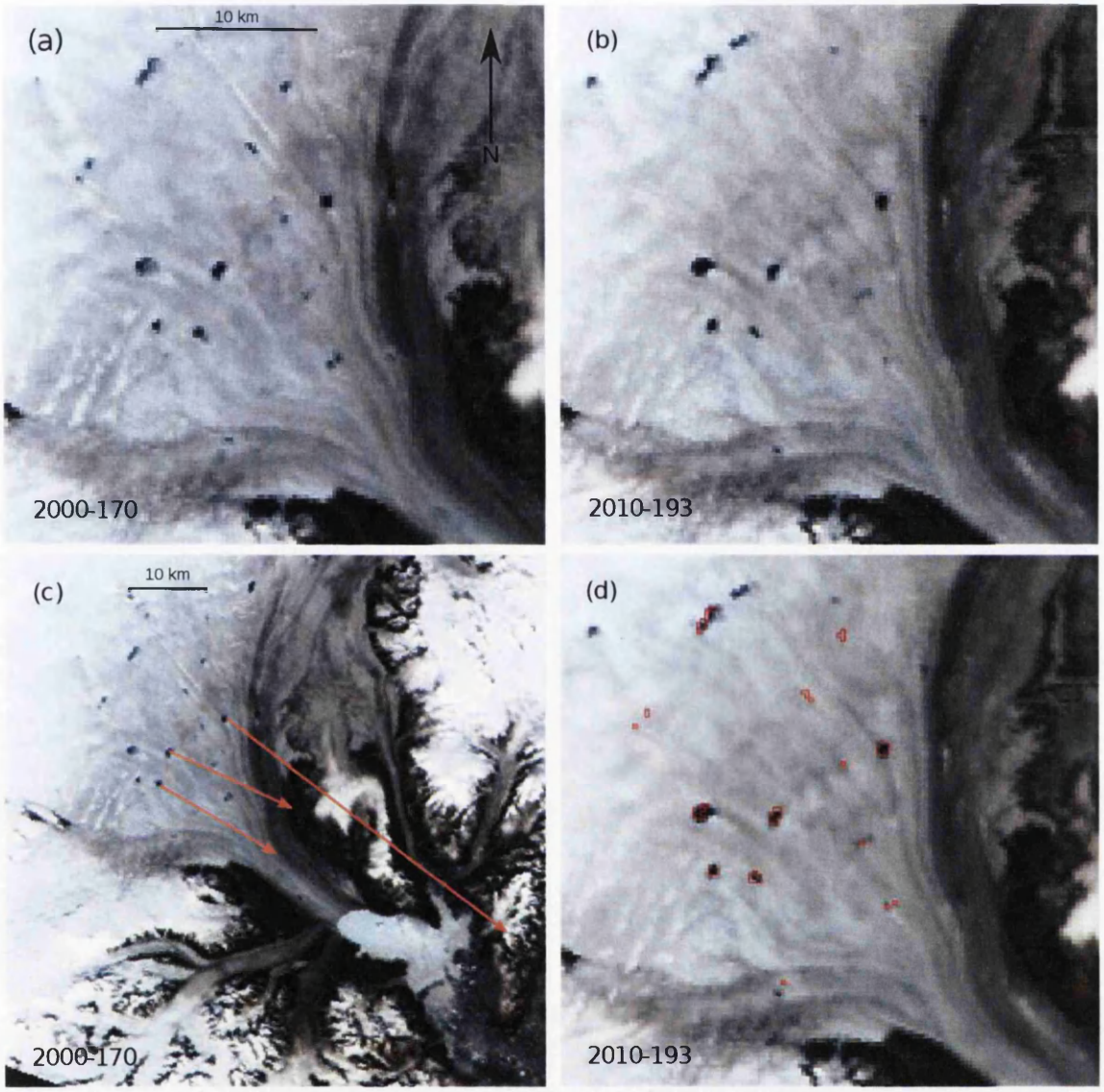

Figure 5.1: MODIS images of Kangerdlugssuaq Glacier from 2000 and 2010 showing a lack of lake advection. Similar patterns of lakes are seen 10 years apart (a+b). (c) Vectors are winter ice flow 2005–2006 extrapolated over the 10 year period showing how far the ice at lake sites in 2000 would have moved by 2010. (d) Lake positions from 2000 are shown on 2010 imagery.

5.3 Melt extent and duration

Melt extent and duration (defined here as the melt days per pixel summed over each region) was calculated for the each year of during the period 2005–2009 from MODIS LST (Section 3.5.4), and is shown in Figure 5.4. These data were compared with melt extent and duration from SSM/I passive microwave data (Abdalati, 2007)

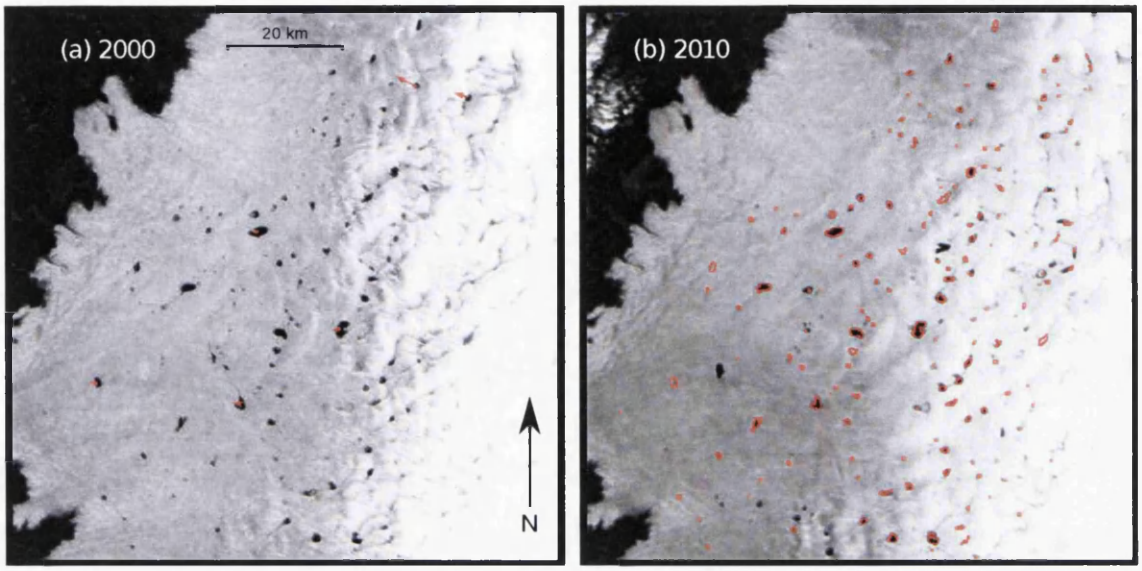

Figure 5.2: MODIS images of the Jakobshavn Isbræ region from 2000 (a) and 2010 (b) showing a lack of lake advection. Similar patterns of lakes are seen 10 years apart. Vectors (in red on a) are winter ice flow 2005–2006 extrapolated over the 10 year period showing how far the ice at lake sites in 2000 would have moved by 2010. Lake positions from 2000 are shown on the 2010 imagery in red (b).

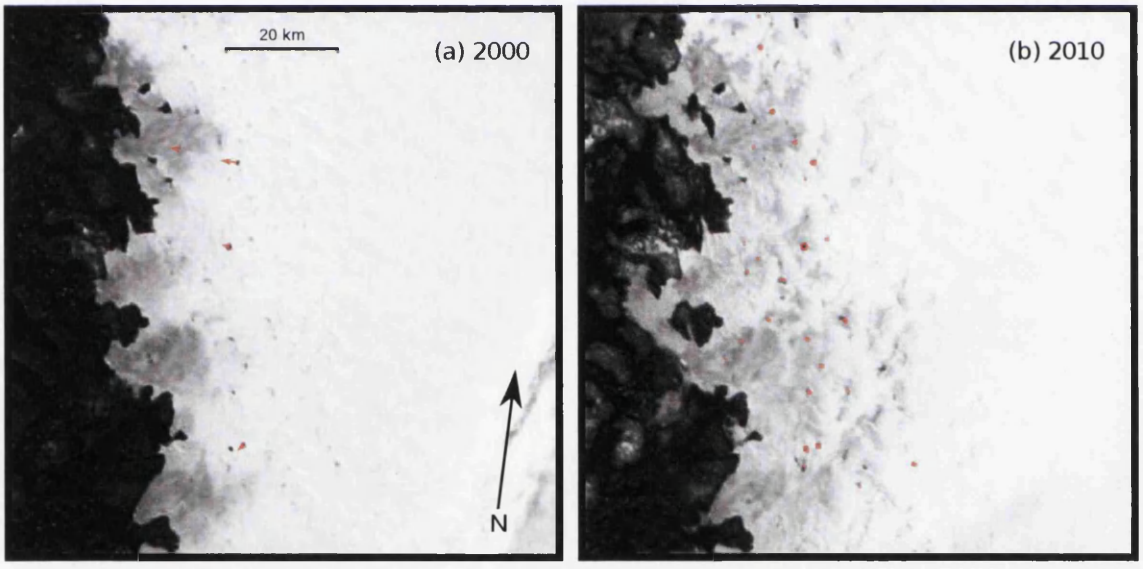

Figure 5.3: MODIS images of the NW region from 2000 (a) and 2010 (b) showing a lack of lake advection. Similar patterns of lakes are seen 10 years apart. Vectors (in red on a) are winter ice flow 2005–2006 extrapolated over the 10 year period showing how far the ice at lake sites in 2000 would have moved by 2010. Lake positions from 2000 are shown on the 2010 imagery in red (b).

by resampling MODIS melt extent to the same resolution as that dataset (25 km pixels), and then summing the melt duration for all pixels for each region per year

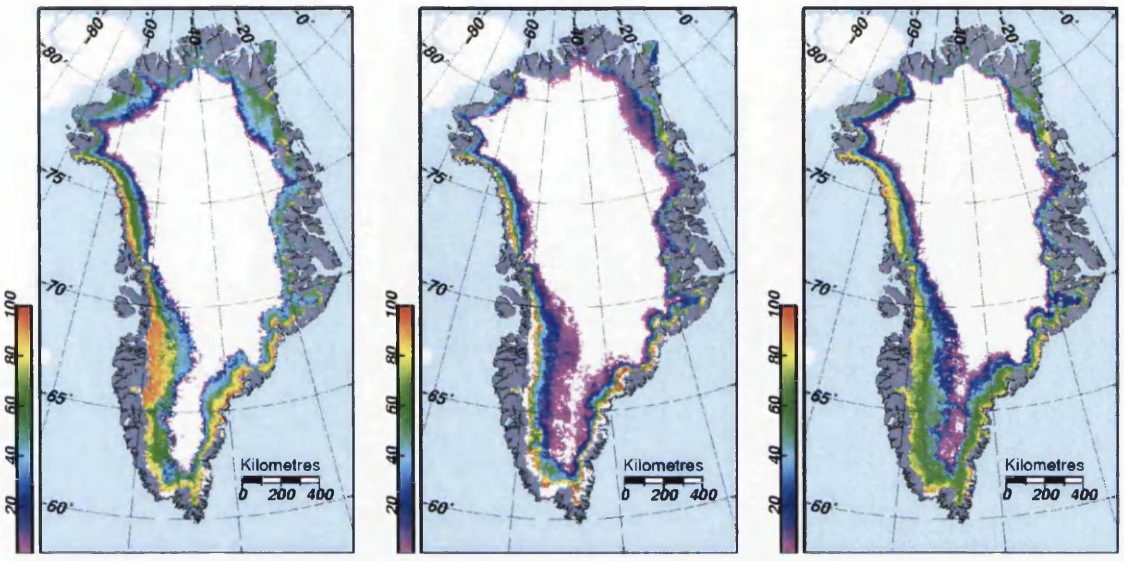

(a) Days of melt - 2005 (b) Days of melt - 2006 (c) Days of melt - 2007

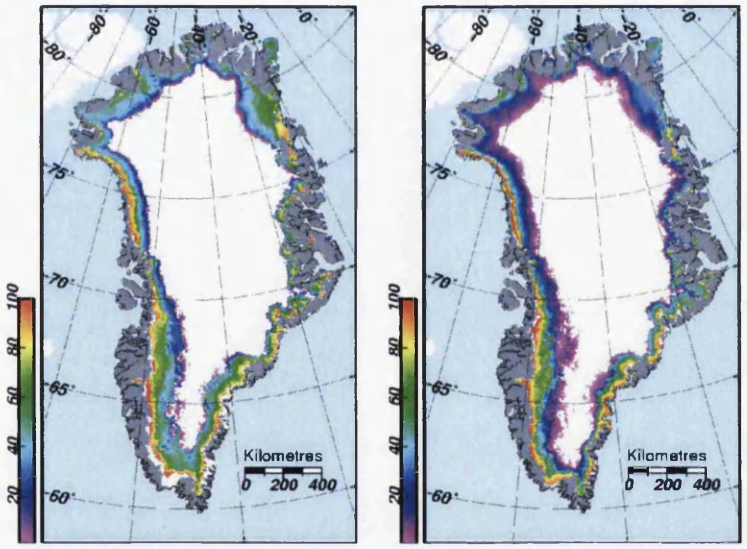

(d) Days of melt - 2008 (e) Days of melt - 2009

Figure 5.4: Maps of melt season extent and duration (days) for the period 2005–2009 from MODIS LST data.

for both data sources. The dataset of Abdalati (2007) was chosen over other SSM/I melt extent datasets as it had the most overlap with the study period of this thesis. These data were compared over the three years where the records overlap. A strong correlation between the melt extent calculated from MODIS and that from passive microwave was found (Spearman's Rank Correlation Coefficient $[r_s]$=0.95, Figure 5.5), and despite differences in the absolute values shown, both datasets show the same interannual trend (Figure 5.6).

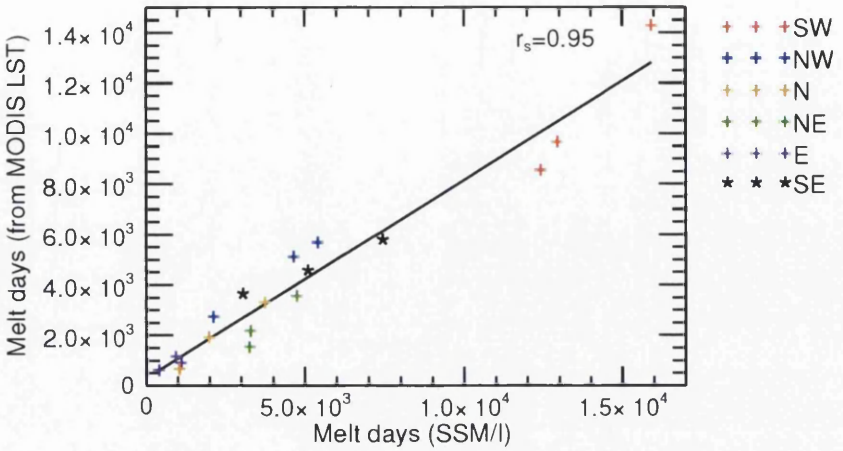

Figure 5.5: Comparison of melt extent and duration values from SSM/I melt data (Abdalati, 2007) and MODIS LST. A best fit line and Spearman's Rank Correlation Coefficient (r_s) are shown.

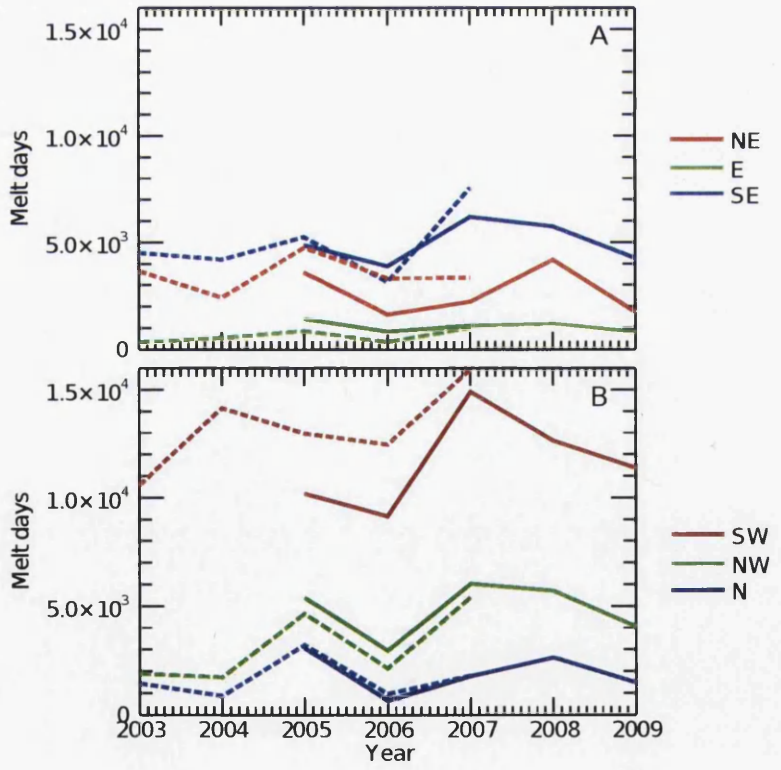

Figure 5.6: The overlapping period (2005–2007) of SSM/I (dashed lines) and MODIS (solid lines) melt extent and duration observations. The plot is split into groups of three regions for clarity. Whilst there are differences between the datasets, the interannual variation they show is similar.

Spatial and temporal variations in melt can be seen in the maps of Figure 5.4, and summed over each region in Figure 5.6. The most intense melt was in 2007 for most of the ice sheet, namely the SW, NW, and SE regions. In the remaining northern regions (N and NE) melt was most intense in 2008. Melt was low in all regions during 2006 and 2009. The E region showed little interannual variation in melt extent and duration compared with other regions.

5.4 Maps of the distribution of supraglacial lakes

5.4.1 Ice sheet scale

The location of each lake in a high (2005) and low (2006) melt year as detected during the initial mapping stage (Section 4.4) is shown on Figure 5.7. While melt was higher in 2007 than 2005 in the SW, and higher in 2008 in the north, 2005 had consistently high melt across all regions of the ice sheet making it the most suitable year to display in this figure. Data from only these 2005 and 2006 are shown here to avoid repeated similar figures, but the lakes detected in all years are included in Appendix A as Figures A.1–A.5. From Figure 5.7 the general patterns in the distributions of lakes are visible. Lakes were detected in the melt zones of most parts of the ice sheet. However spatial variations in the occurrence of lakes are apparent. Particularly of note is the contrast between the SW and SE regions, with many lakes in the SW, and very few in the SE. Lakes were present nearly the full length of the W coast, in a concentrated area of the NE, and on the upper sections of outlet glaciers on the N and E coasts. Some temporal variation can be seen in this figure and those in Appendix A, especially the maximum elevation of the lake zone in the SW in 2005, and the substantial interannual variation of the NE region.

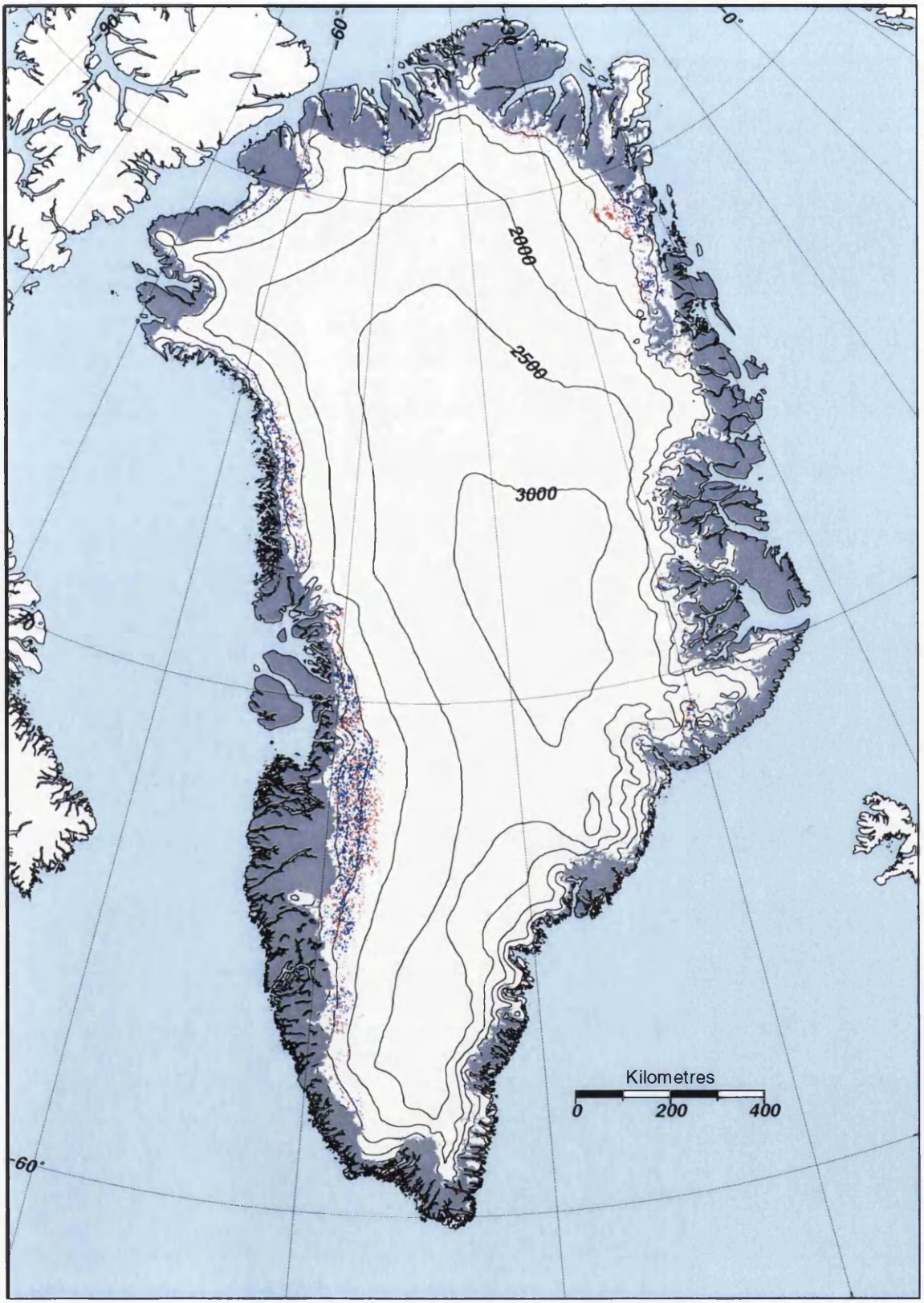

Figure 5.7: Lakes on the GrIS for a high melt year (2005 in red) and a low melt year (2006 in blue).

5.4.2 Regional scale

Maps of the maximum extent of each lake per year from the initial mapping stages are shown on regional scale MODIS imagery in Figures 5.8–5.13. For each figure, the lakes from maximum and minimum melt years (Figure 5.6) are shown for comparison. The maximum year is always shown in red, the minimum in blue. Note that the minimum year is plotted above the maximum year to avoid it being obscured, explaining the apparent absence of some lakes at lower elevations in the maximum year.

South West Greenland

A considerable number of lakes were found in SW Greenland (Figure 5.8), especially in the Nordenskiöld and Narssap sermia catchments. Lakes were not restricted to the outlet glaciers, rather they extended in a wide zone reaching up to around 1500 m a.s.l. in 2009, and up to around 2000 m a.s.l. in the high melt year of 2007 demonstrating large interannual variation in distribution. Far fewer lakes were evident in the southernmost part of this region. Note in Figure 5.8 the large areas of land-terminating ice in this region.

North West Greenland

Lakes were detected along most of the NW coast (Figure 5.9). This section of the ice sheet is largely tidewater terminating with many outlets, and lakes were detected uniformly along the length of the coast in most parts of the melt zone. A discontinuity in the distribution of lakes occurred in all years just N of Rink Isbræ. Higher melt years such as 2007 (in red on Figure 5.9) merely resulted in a uniform spread a short distance up the ice sheet. In fact seasonal variation in this region appears rather limited in Figures 5.7 and 5.9.

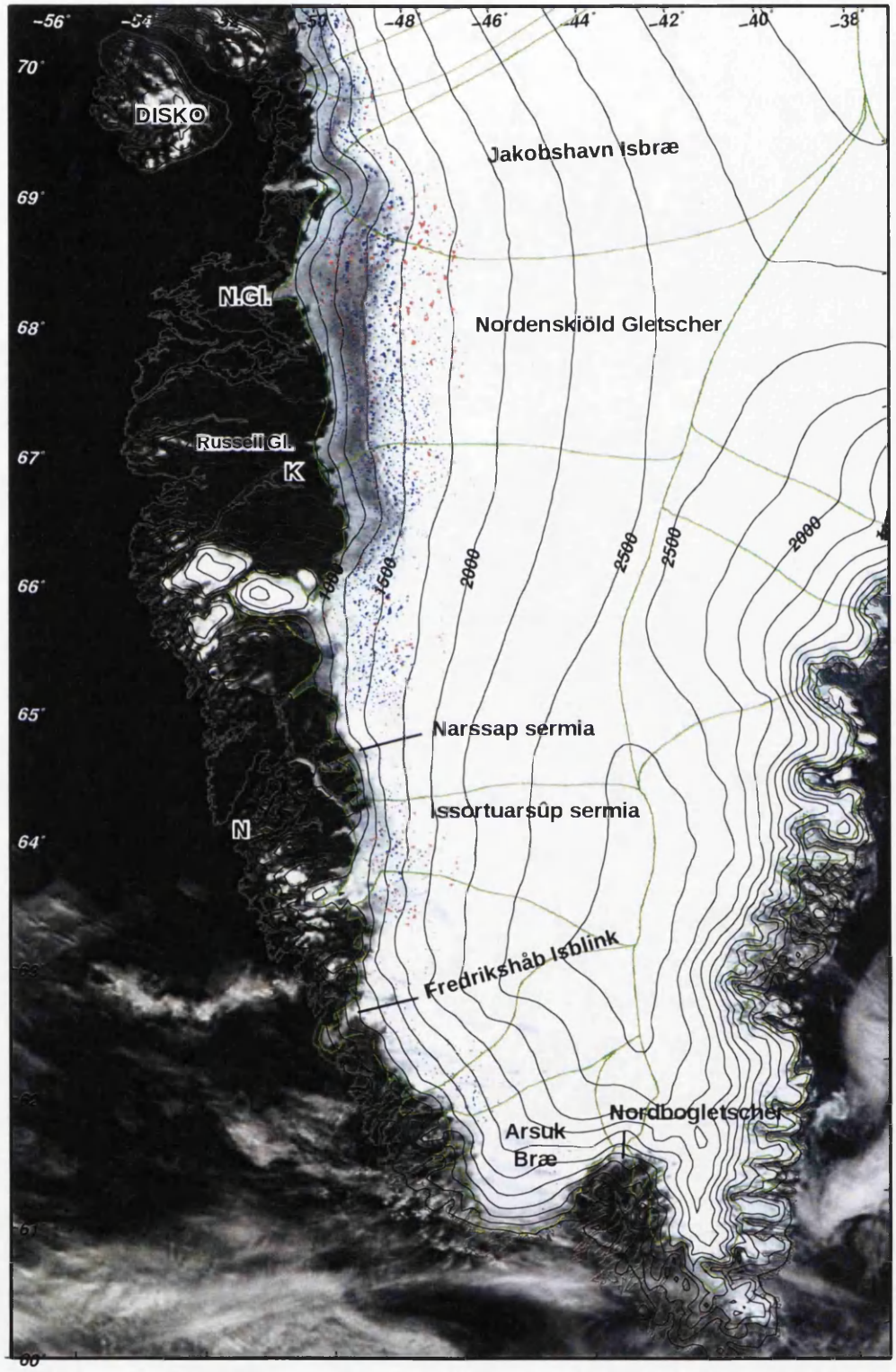

Figure 5.8: Multi-temporal map of lakes at their largest extent in the SW region of GrIS during low melt (2009, blue) and high melt (2007, blue) years. Kangerlussuaq (K). Nuuk (N).

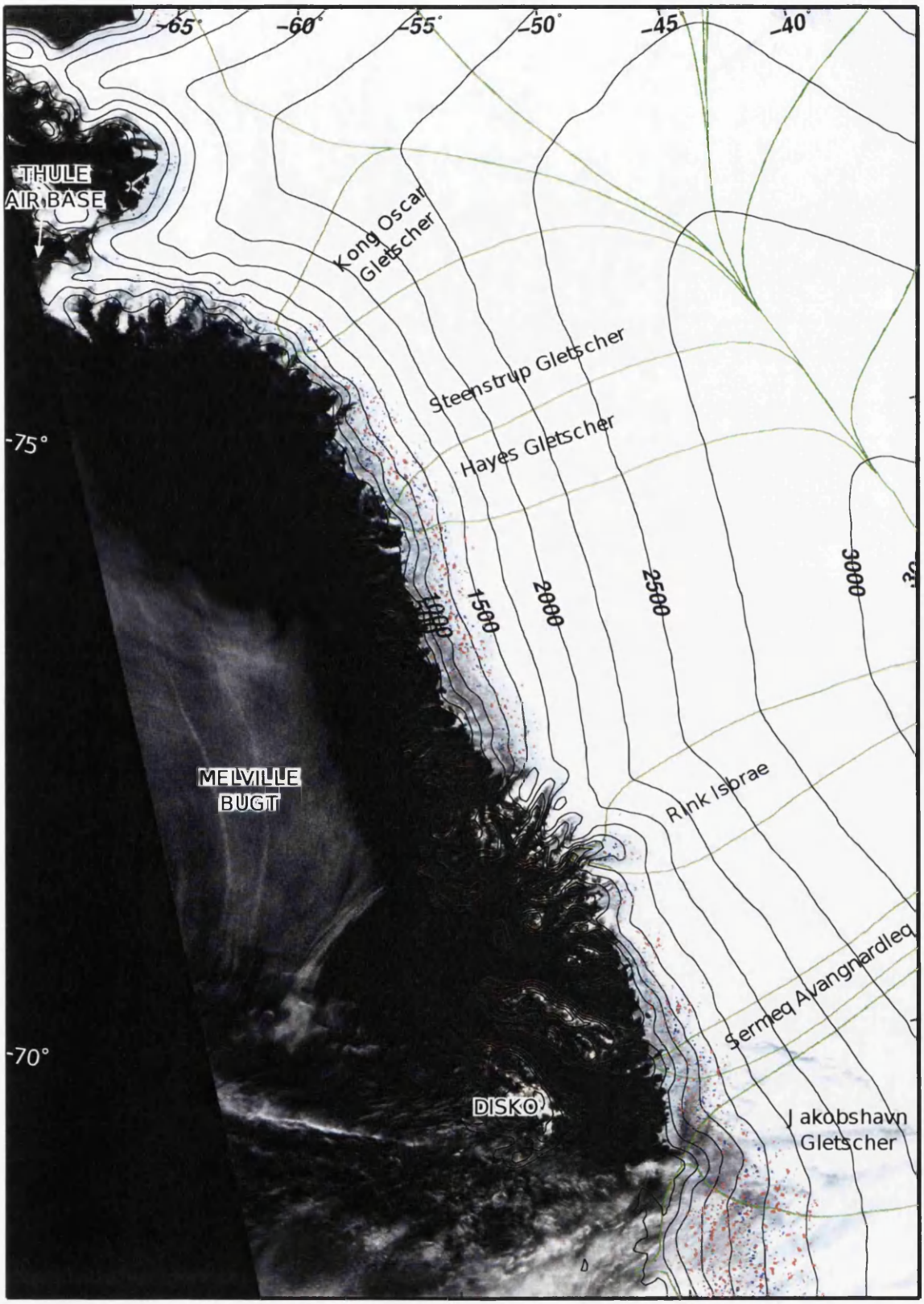

Figure 5.9: Multi-temporal map of lakes at their largest extent in the NW region of GrIS during low melt (blue, 2006) and high melt (red, 2007) years.

Northern Greenland

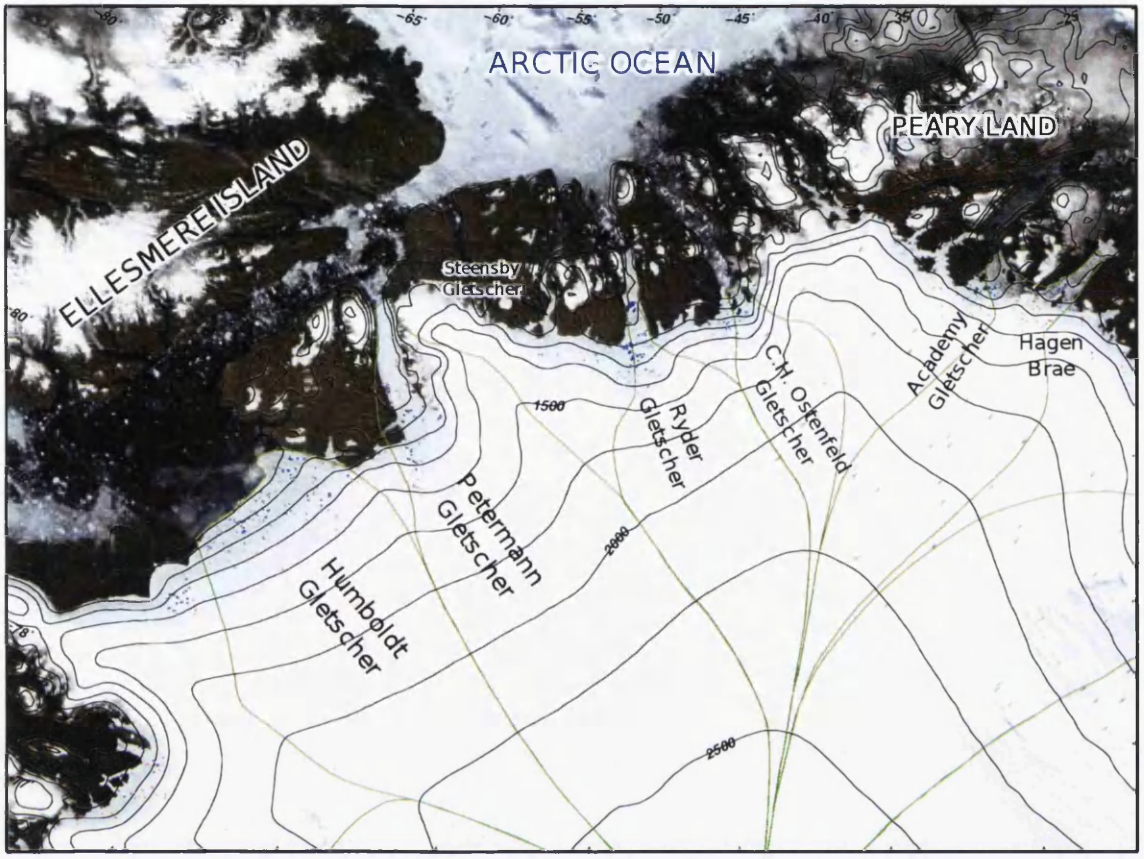

Figure 5.10: Multi-temporal map of lakes at their largest extent in the northern region of the GrIS during low melt (2006, blue) and high melt (2008, red) years.

Lake formation along the Northern coast of the GrIS was mainly restricted to the drainage basins of the large outlet glaciers: Humboldt, Petermann, Ryder, C. H. Ostenfeld, and Academy Glaciers (Figure 5.10). One of the largest lakes on the ice sheet formed on the Ryder Glacier tongue. Unexpectedly this grew to a much larger extent in lower melt years, as can be seen in Figure 5.10.

North East Greenland

Lake formation in the NE was concentrated between Kronprins Christian Land and Dronning Louise Land, on the three outlets that make up the terminal area of the NE Ice Stream: Nioghalvfjerdsbræ, Zachariae Istrøm, and Storstrømmen. The difference between a low melt (e.g. 2006) and high melt (e.g. 2008) year in terms

of lakes in this region is the most striking of any region of the ice sheet. The area covered by lakes on Nioghalvfjerdsbræ advanced the furthest horizontal distance in a high melt year of any part of the ice sheet. This spread included the formation of several large lakes that did not form in low melt years. This difference can also be seen on ice sheet scale mapping (Figure 5.7).

Eastern Greenland

The E coast of the GrIS, north of Kangerdlugssuaq Glacier and up to and including Walterhausen Glacier, is typified by high mountains and tidewater glaciers terminating in long fjords. Lakes forming in this region (Figure 5.12) are found exclusively on the outlet glaciers, especially on Kong Christian IV, Daugaard-Jensen and Walterhausen Glaciers. Unlike in the N and NE regions, where lakes form some distance up the ice sheet from the main outlet, lakes on these glaciers only form on the glacier tongues. Note from Figure 5.12 that there is little difference in the extent of lake formation in this region between high and low melt years.

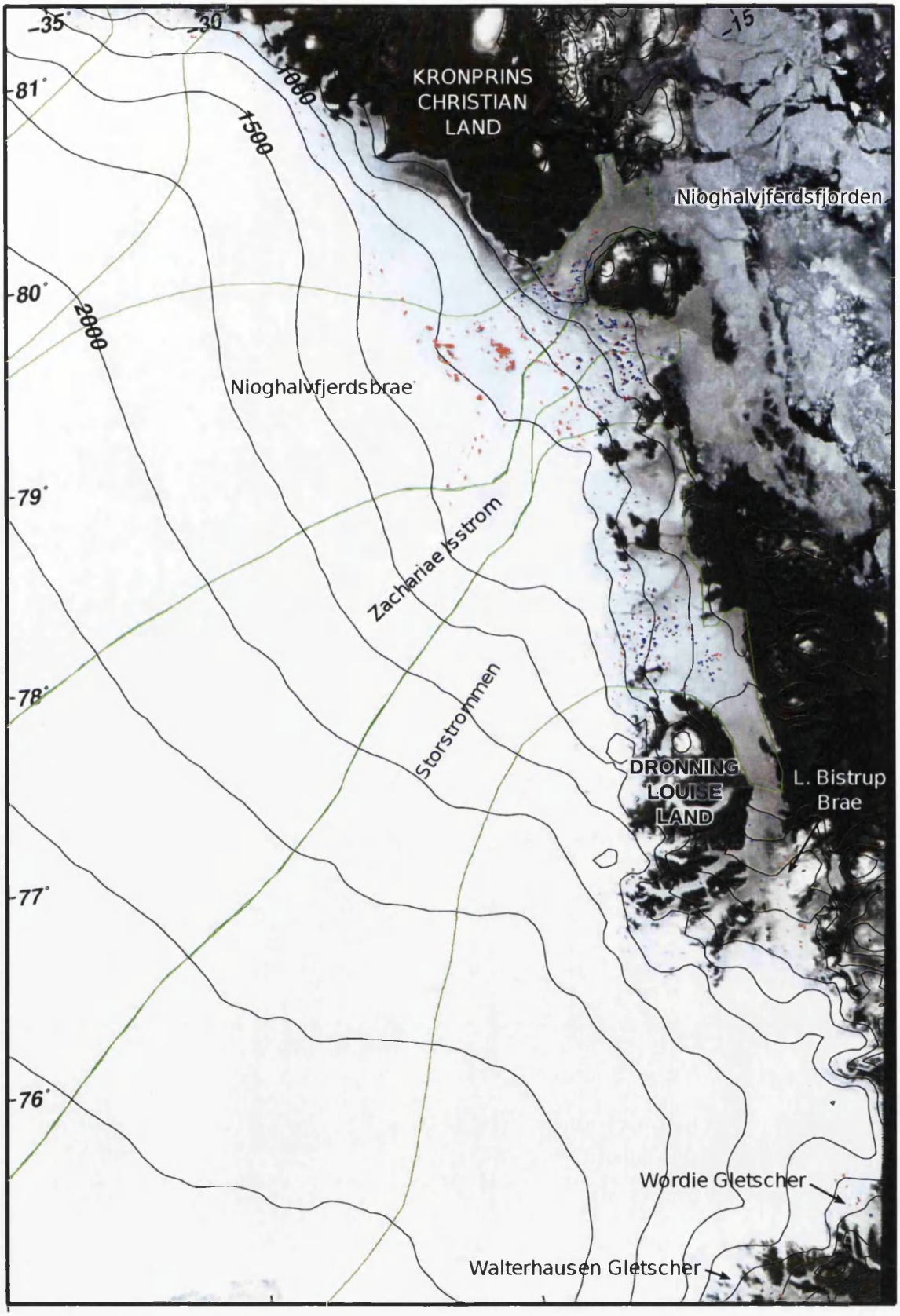

Figure 5.11: Multi-temporal map of lakes at their largest extent in the NE region of the GrIS, during high melt (2008, red) and low melt (2006, blue) years.

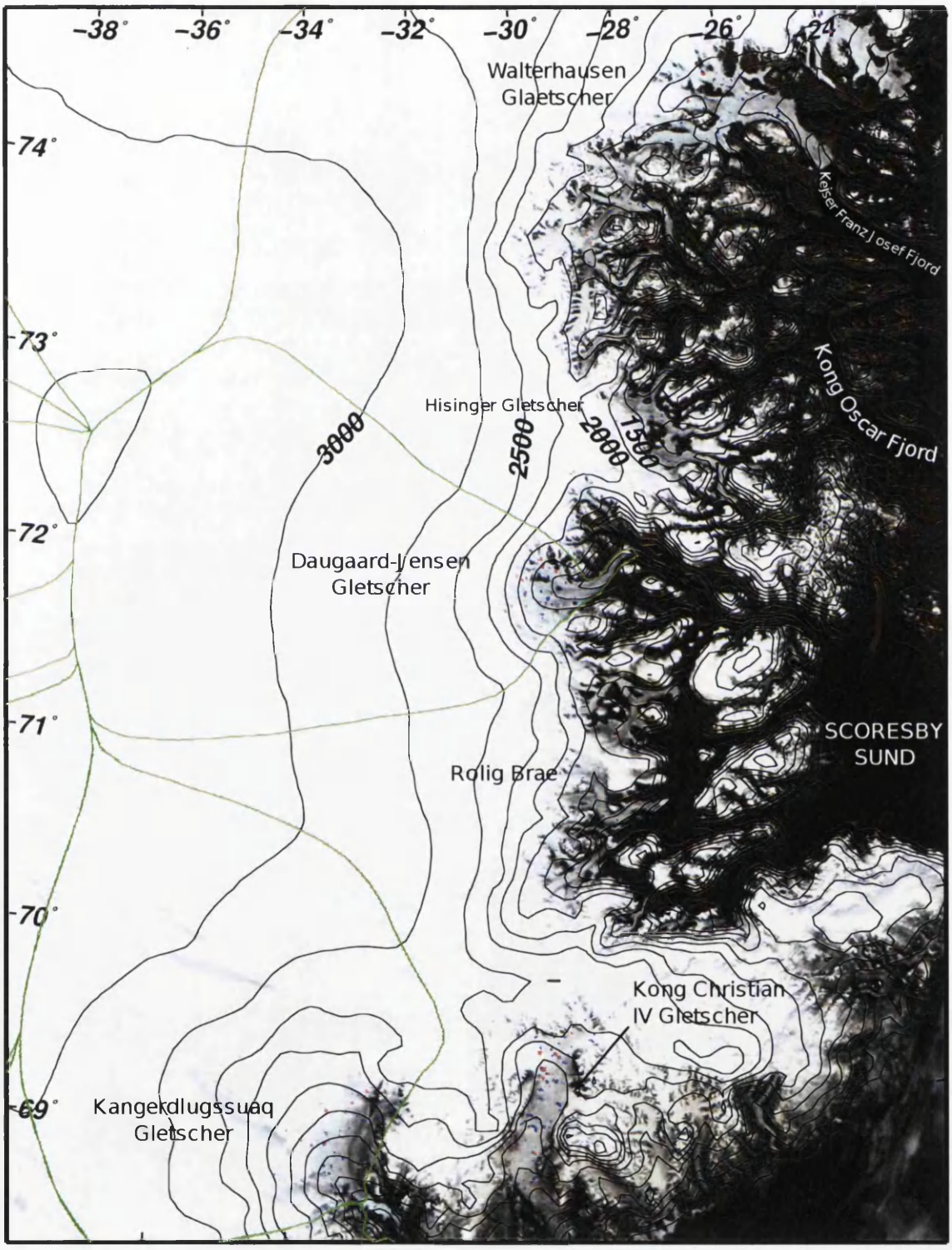

Figure 5.12: Multi-temporal map of lakes at their largest extent in the E region of the GrIS, during high melt (2007, red) and low melt (2009, blue) years.

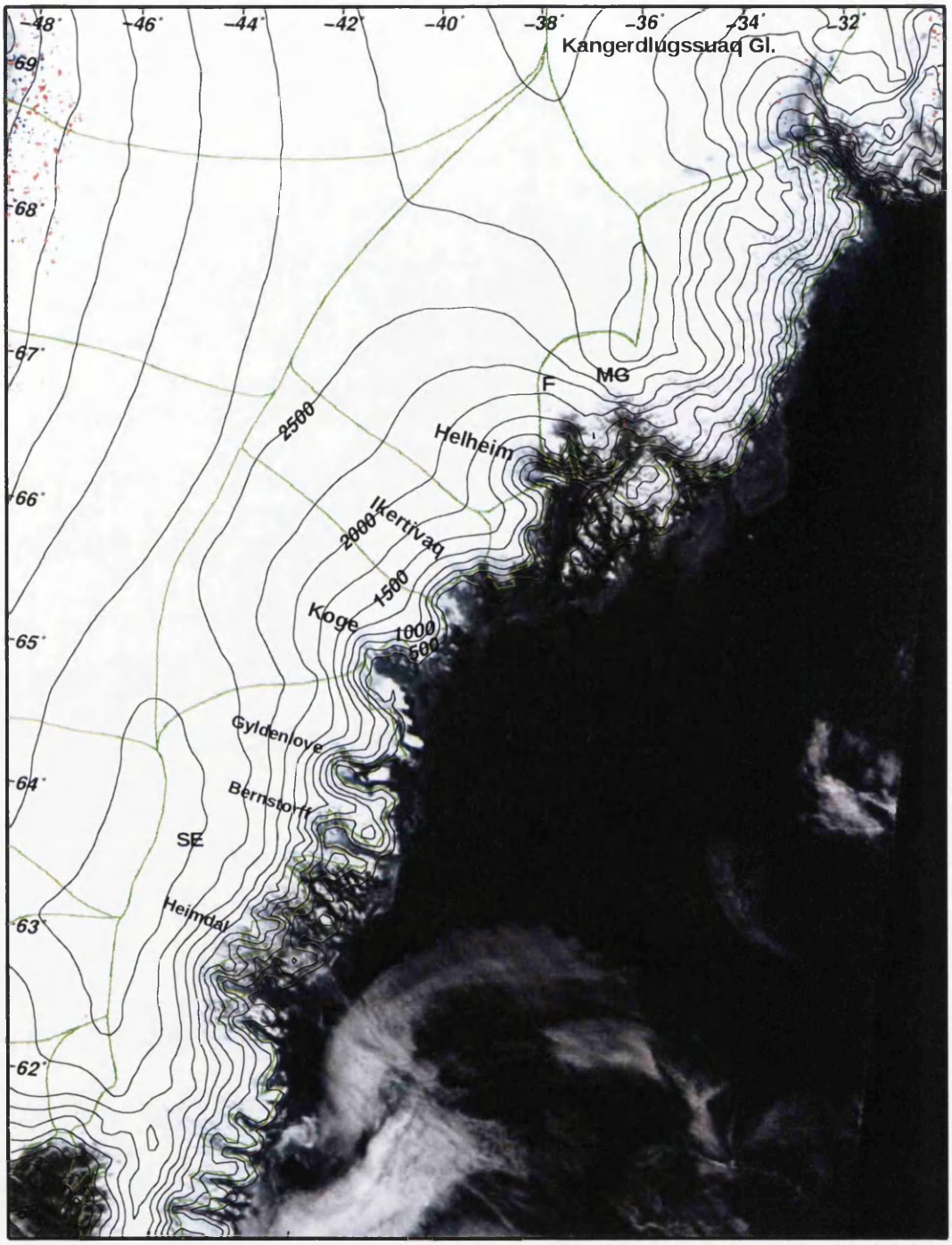

Figure 5.13: Multi-temporal map of lakes at their largest extent in the SE region of GrIS, during high melt (2007, red) and low melt (2006, blue) years. Fenris Glacier (F). Midgaard Glacier (MG).

South East Greenland

The distribution of lakes in SE Greenland is shown in Figure 5.13. Immediately apparent is the contrast with the SW region on the opposite coast (Figure 5.8). A considerable number of lakes were mapped on the tongue of Kangerdlugssuaq Glacier, however few lakes were detected in the remainder of SE Greenland. Those lakes which were found were located on the tongues of outlet glaciers, particularly in the Schweizerland region on Fenris and Midgaard Glaciers. Small numbers of lakes were detected on the tongue of Helheim Glacier, and on the glaciers of the SE fjords, including Heimdal Glacier. Interannual variations in lake distribution can be seen on Kangerdlugssuaq Glacier, but are difficult to observe further south.

5.5 Sizes of individual lakes

The frequency distribution of lake area was positively skewed (skewness=+5.07, see Figure 5.14a), with a mean area of 0.80 km^2 and a median of 0.56 km^2 (Figure 5.14b). A normal distribution can be obtained through a natural log transformation of the lake areas (Figure 5.14b), which allowed the use of parametric statistical tests. The geometric mean (Table 5.1) is a more appropriate measure of central tendency for log-normalised data than the arithmetic mean, and is calculated by taking the arithmetic mean of the log transformed data, and converting it back to the original scale by using the exponential function i.e. the mean of the set

$$\{a_1, a_2 \ldots, a_n\} \tag{5.1}$$

can be calculated as

$$\exp\left[\frac{1}{n}\sum_{i=1}^{n}\ln a_i\right] \tag{5.2}$$

The geometric mean for the full dataset including all years was 0.52 km^2. Throughout the rest of this thesis the geometric mean will be used whenever data have a skewed distribution, while the arithmetic mean will be still be referred to as simply

"the mean". While the median could be used as an alternative to the geometric mean, the ANOVA test is used extensively in the following chapters which when applied to log transformed data is testing for significant differences between geometric means, making this latter measure of central tendency more meaningful to include than the median.

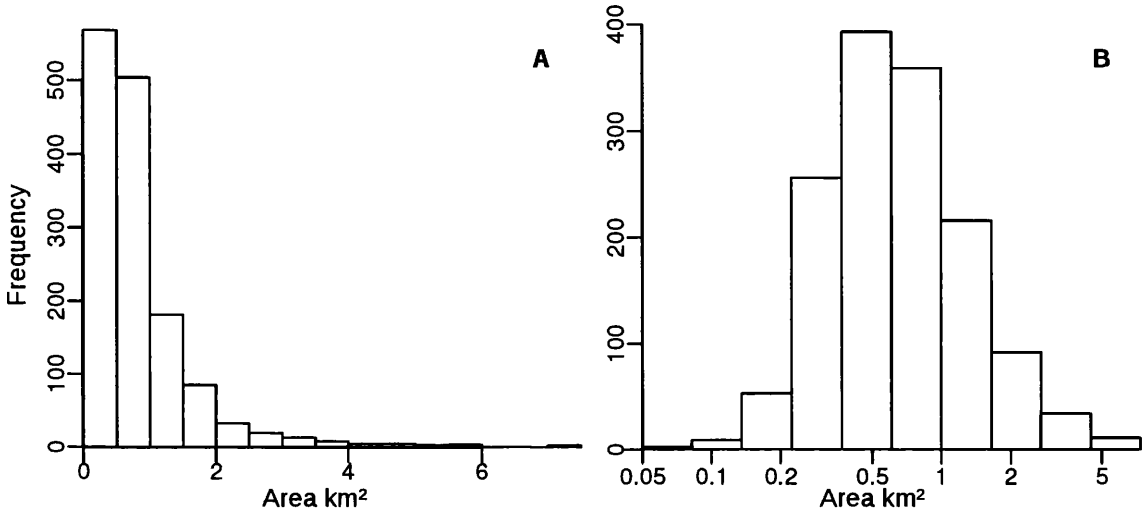

Figure 5.14: (A) Frequency distribution of lake areas for the whole ice sheet. Arithmetic mean area 2005–2009 is used for each lake. Note the pronounced positive skew. (B) Frequency distribution lake area on a natural log scale. Being able to log normalize the data allowed parametric statistical tests to be used.

5.5.1 Interregional variation in mean lake area

There was pronounced variation in the geometric means of individual lake areas between regions (Figure 5.15, Table 5.1). The lakes in the NE had the largest geometric mean area, whereas the largest single lake was in the SW. The SE had the smallest lakes of any region. The statistical significance between the sizes of lakes of different regions was examined first using the ANOVA test, and as this showed a significant difference (p <0.001) the significance of differences between individual pairs of geometric means was tested using the Tukey's Honestly Significant Difference (Tukey's HSD) test (Table 5.2). Tukey's HSD is a post-hoc multiple comparison test, analogous to performing multiple Student's T-Tests between the pairs used in the ANOVA test, which protects against the increasing probability of Type I

errors associated with multiple comparisons. The use Tukey's HSD is described in Townend (2002), and a full mathematical definition in given in Hsu (1996). Owing to the skewed nature of the lake areas, the data were log normalised and geometric means used. The SW, NE, and SE regions were each found to have significantly different geometric mean lake areas to all other regions. The geometric mean lake areas for the NW, N, and E regions were not significantly different from each other.

Table 5.1: Geometric mean area of individual lakes 2005–2009 (km^2)

Region	2005	2006	2007	2008	2009	All years
SW	0.56	0.53	0.55	0.59	0.5	0.55
NW	0.43	0.41	0.49	0.47	0.41	0.44
N	0.51	0.37	0.47	0.5	0.46	0.46
NE	0.67	0.5	0.56	0.77	0.57	0.62
E	0.47	0.46	0.47	0.46	0.44	0.46
SE	0.28	0.22	0.35	0.26	0.26	0.27
GrIS	0.53	0.48	0.53	0.57	0.48	0.52

Table 5.2: p values of Tukey HSD test for interregional differences in mean lake size. Comparisons of pairs of means can be made using the Tukey HSD test as ANOVA tests were significant at $p < 0.001$ for all regions. p values < 0.05 indicate a significant difference in geometric means at the 95% confidence level, and are highlighted in *italics*. Data were aggregated from all years (2005–2009)
, and rounded to 3.d.p.

	SW	NW	N	NE	E	SE
SW	-	*0.000*	*0.001*	*0.001*	*0.002*	*0.000*
NW		-	0.931	*0.000*	0.962	*0.000*
N			-	*0.000*	1.000	*0.000*
NE				-	*0.000*	*0.000*
E					-	*0.000*
SE						-

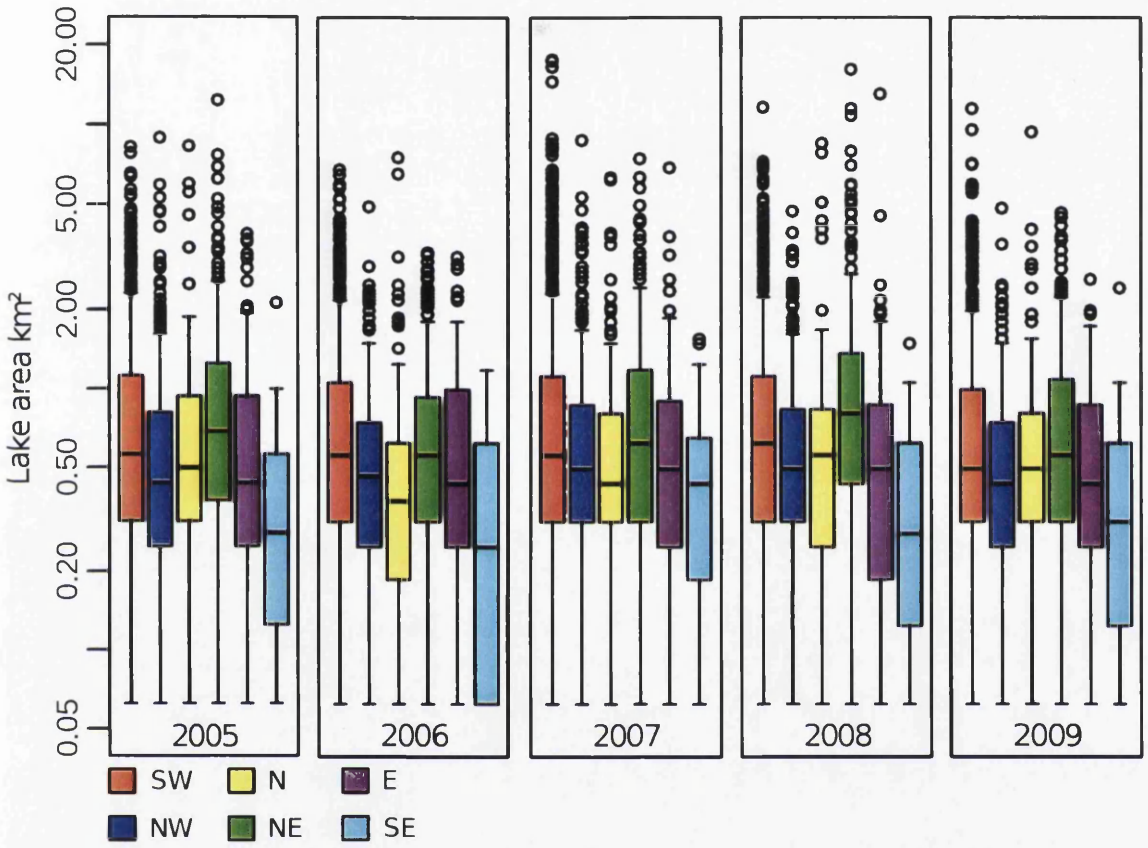

Figure 5.15: Box and whisker plot of individual lake sizes, arranged for comparison between regions. Note the logarithmic scale, and large positive outliers. All box and whisker plots in this thesis are produced using the standard settings of the R Project for Statistical Computing. The central horizontal line indicates the median, and the "box" shows the interquartile range. The range of the data minus outliers is shown by the length of the "whiskers". Outliers are plotted as circles, and are calculated as those values that are more than 1.5 times the interquartile range above the upper quartile and below the lower quartile.

5.5.2 Inter-annual variation in mean lake area

The geometric mean lake area also varied interannually for each region (Figure 5.16, Table 5.1), although this variation was not statistically significant in the E and SE regions (Table 5.3). Lakes were smallest in all regions in either 2006 or 2009. Lakes were at their largest in 2008 in the SW, N, and NE. Lakes in the NW were largest in 2007.

Table 5.3: Results of ANOVA tests for interannual differences in mean lake size. p values < 0.05 show significance at the 95% confidence level (indicated in *italics*) i.e. interannual variation in mean lake size was not significant in the E and SE regions.

	SW	NW	N	NE	E	SE
F	13.6	3.2	3.5	16.0	1.3	0.4
p	*0.000*	*0.012*	*0.008*	*0.000*	0.279	0.774

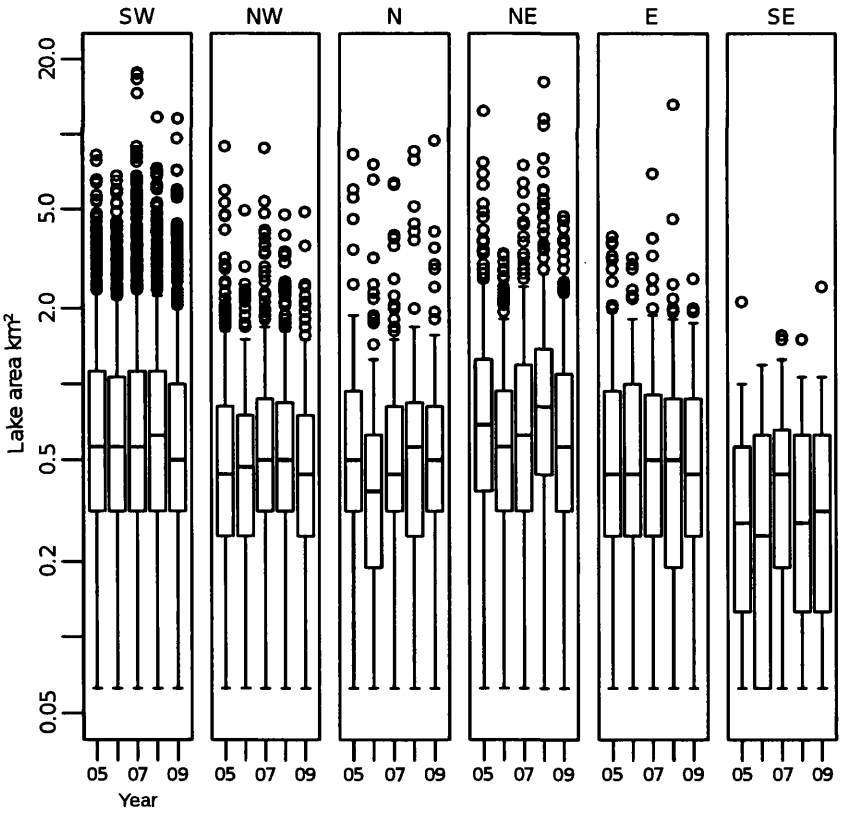

Figure 5.16: Box and whisker plots showing the relative sizes of individual lakes in the six regions of the ice sheet, with log y axis and arranged for interannual comparisons.

5.6 Lake area and frequency composited per year

The maximum areas of all the lakes in the dataset were summed over each region and catchment for each year and the result was used as the main metric for lake distribution in this thesis, and will be subsequently referred to as total maximum lake area. This is a function of the number of lakes that form, and the maximum size of these lakes. Note that these area values are multi-temporal, and do not refer to an area of lakes present on any single day during the melt season.

5.6.1 Region scale

Total maximum lake area per region of the ice sheet is shown in Table 5.4 and Figure 5.17, and as percentages of total maximum lake area for the GrIS in Table 5.5. When looking at mean area, the SW stands out with $\sim$ 60 % of the total lake area and more than three times the lake area of any other region. The NW and NE regions had similar total maximum lake areas (around 25 % the total lake area for the SW), with the NE having a slightly larger mean area. The N and E regions also had similar total maximum lake area ($\sim$ 5 % of lake area for GrIS), with the N having slightly greater lake area in each year. The SE stood out as having the smallest total maximum lake area, with $<$ 1 % of GrIS total lake area.

Table 5.4: Total maximum lake areas (km^2) for regions of the GrIS. These data are also presented graphically and compared with melt extent and duration in Figure 5.17.

Region	2005	2006	2007	2008	2009	Mean
SW	1020	972	1239	1068	879	1036
NW	267	234	310	259	231	260
N	104	73	98	107	90	94
NE	311	172	237	379	242	268
E	82	72	81	82	64	76
SE	16	15	20	16	17	17
Total	1800	1539	1985	1911	1523	1752

Table 5.5: Percentage per region of total maximum area of all lakes on the GrIS.

	2005	2006	2007	2008	2009	Mean
SW	56.7	63.2	62.5	55.9	57.7	59.1
NW	14.8	15.2	15.6	13.5	15.2	14.9
N	5.8	4.8	4.9	5.6	5.9	5.4
NE	17.3	11.2	11.9	19.8	15.9	15.3
E	4.6	4.7	4.1	4.3	4.2	4.4
SE	0.9	1.0	1.0	0.8	1.1	1.0

Total maximum lake area was found to vary interannually for each region. Maximum lake area was in 2007 in the SW, NW, and SE, and it was 2008 in the N and NE. Minimum lake area was 2009 in the SW, NW, and E, and it was 2006 in the N, NE, and SE. This approximately follows the general trend of the melt data shown on Figure 5.17.

Inter-annual variations were small when compared to interregional differences. The largest interannual variation for any region was 360 km^2 in the SW, whereas the lowest area in the SW (879 km^2 in 2009) was 500 km^2 larger than the next highest value from another region (379 km^2 during 2008 in the NE). Inter-annual variations were more important when comparing areas that had very similar area values, namely the NW and NE. The range of values for the NW and NE overlapped. Maximum total lake area was larger in the NW in 2006 and 2007, and larger in the NE in 2005, 2008, and 2009.

The interregional differences observed above could be a result of the sizes of the regions chosen. To test if the observed patterns were an artefact of the regional sizes or geometry, observed and expected frequencies of lake occurrence per region were compared. The expected frequency was calculated by multiplying the total number of lakes on the GrIS by the proportion of the ice sheet's margin in each region (Table 5.6). Ice margin length was chosen as it takes into account the different size and shape regions used, thus removing sampling bias. Whilst the NW region had an observed frequency close to that expected, other areas differed considerably with only the SW and NE regions having more lakes than the expected distribution.

The significance of this deviation was tested with Chi Square analysis, and the lake occurrence between regions was found to differ from the expected lake distribution at the 99.9 % confidence level (Table 5.6). Different normalizations methods and their effect on the results are discussed in Section 7.4.4.

Table 5.6: Observed and expected frequencies of lakes by region, as used for Chi Square analysis. χ^2=1807, degrees of freedom=5, $p< 0.001$

Region	Ice margin length (km)	Proportion of total length	Expected frequency (E)	Observed frequency (O)	$\frac{(O-E)^2}{E}$
SW	1331	0.21	435	1126	1100
NW	1193	0.19	390	390	0
N	923	0.15	302	117	112
NE	476	0.08	156	267	79
E	985	0.16	322	101	152
SE	1329	0.21	434	37	363
Total	6237	1	2038	2038	1807

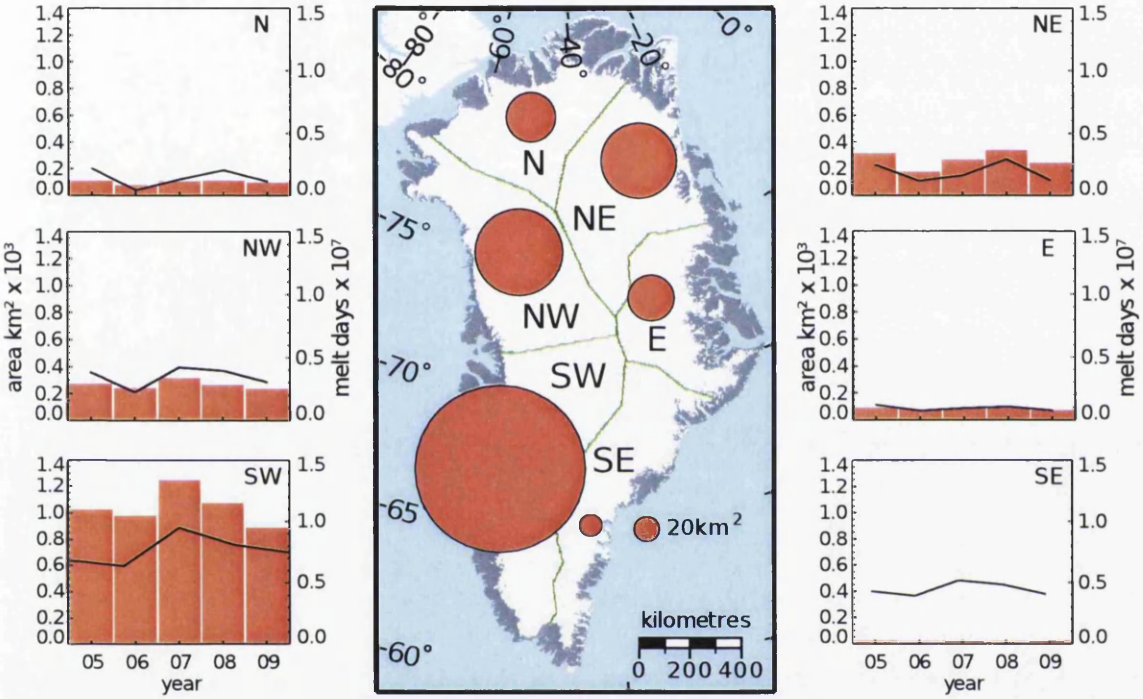

Figure 5.17: Lake distribution on the Greenland Ice Sheet by region. Circles on the central figure show the total maximum lake area in each region, averaged over the five year observation period. Side plots show the interannual variation in lake area (red bars) for each region, compared with melt extent and duration (black line). Vertical scales are deliberately held the same for all regions to emphasise the difference between regions. The area values used in this plot are also presented in Table 5.4.

5.6.2 Catchment Scale

Total maximum lake area per catchment is presented in Figures 5.18–5.23, and in Tables 5.7 and 5.8. The catchments are presented by region, which allows assessment of whether the regional variations presented in Section 5.6.1 are part of a region-wide synchronous signal across several catchments, or a product of several differing patterns.

Table 5.7: Total maximum lake area per catchment. Only true glacial catchments are presented here (for clarification on this point see Section 3.5.8). Figures 5.18–5.23 also include data for the areas between the defined catchments. Catchment ID numbers are included on Figures 5.18–5.23.

No.	Catchment	2005	2006	2007	2008	2009	Mean
1	Academy	4.0	1.2	5.9	3.1	2.6	3.4
2	Daugaard-Jensen	10.6	6.8	12.1	6.8	5.2	8.3
3	Hayes	19.9	20.1	34.3	19.4	20.1	22.8
4	Humboldt	23.1	18.1	26.4	26.8	20.9	23.1
5	Kong Oscar	1.9	3.6	6.4	4.9	4.1	4.2
6	Nioghlvfjerdsbræ	115.7	23.0	48.3	139.3	75.3	80.3
7	Ostenfeld	1.9	1	2.3	0.5	1.8	1.5
8	Petermann	17.9	11.2	14.9	15.3	15.3	14.9
9	Rink	11.9	9.6	15.8	11.3	9.6	11.6
10	Ryder	21.7	15.8	15.5	22.1	17.6	18.5
11	Storstrømmen	76.1	71.1	95.3	106.3	76.9	85.1
12	Zachariae	57.6	35.3	36.9	58.6	32.7	44.2
13	Narssap	27.3	35.9	55.3	37.1	2	35.9
14	Nordbogletscher	0	0	0	0	0	0
15	Nordenskiöld	473.1	425.2	514.9	436.1	397.6	449.4
16	Sermilik	2.4	6.3	6.0	9.1	6.2	6.0
17	Koge Bugt	0	0	0	0	0	0
18	SE Fjords	0.1	0.6	0.5	1.3	1.2	0.7
19	Schweizerland	1.4	2.0	3.3	2.9	3.6	2.7
20	Johan Peterson Fjord region	0	0	0	0	0	0
21	Narssap Sermia region	282.1	295.9	352.8	365.1	259.6	311.1
22	Frederikshåb Isblink region	21.0	16.0	44.3	26	21.6	25.8
23	Helheim	0.3	0.3	0.8	0.6	0.6	0.5
24	Ikertivaq	0	0	0	0	0	0
25	Jakobshavn	98.6	83.0	116.2	76.8	61.7	87.3
26	Kangerdlugssuaq	14.1	11.8	14.6	10.9	11.9	12.7
27	Arsuk Bræ region	0.7	1.4	2.7	2.3	1.3	1.7
28	Sermeq Avangnardleq	24.1	29.3	30.6	28.8	21.9	26.9

Table 5.8: Percentage per catchment of total maximum area of all lakes on the GrIS.

No.	Catchment	2005	2006	2007	2008	2009	Mean
1	Academy	0.2	0.1	0.3	0.2	0.2	0.2
2	Daugaard-Jensen	0.6	0.4	0.6	0.4	0.3	0.5
3	Hayes	1.1	1.3	1.7	1.0	1.3	1.3
4	Humboldt	1.3	1.2	1.3	1.4	1.4	1.3
5	Kong Oscar	0.1	0.2	0.3	0.3	0.3	0.2
6	Nioghlvfjerdsbræ	6.4	1.5	2.4	7.3	4.9	4.6
7	Ostenfeld	0.1	0.06	0.1	0.03	0.1	0.1
8	Petermann	1.0	0.7	0.8	0.8	1.0	0.9
9	Rink	0.7	0.6	0.8	0.6	0.6	0.7
10	Ryder	1.2	1.0	0.8	1.2	1.2	1.1
11	Storstrømmen	4.2	4.6	4.8	5.6	5.1	4.9
12	Zachariae	3.2	2.3	1.9	3.1	2.2	2.5
13	Narssap	1.5	2.3	2.8	1.9	1.6	2.1
14	Nordbogletscher	0	0	0	0	0	0
15	Nordenskiöld	26.3	27.6	25.9	22.8	26.1	25.7
16	Sermilik	0.1	0.4	0.3	0.5	0.4	0.3
17	Koge Bugt	0	0	0	0	0	0
18	SE Fjords	0.01	0.04	0.03	0.07	0.08	0.04
19	Schweizerland	0.08	0.1	0.2	0.2	0.2	0.1
20	Johan Peterson Fjord region	0	0	0	0	0	0
21	Narssap Sermia region	15.7	19.2	17.8	19.1	17.0	17.8
22	Frederikshåb Isblink region	1.2	1.0	2.2	1.4	1.4	1.5
23	Helheim	0.02	0.02	0.04	0.03	0.04	0.03
24	Ikertivaq	0	0	0	0	0	0
25	Jakobshavn	5.5	5.4	5.9	4.0	4.1	5.0
26	Kangerdlugssuaq	0.8	0.8	0.7	0.6	0.8	0.7
27	Arsuk Bræ region	0.04	0.09	0.1	0.1	0.1	0.1
28	Sermeq Avangnardleq	1.3	1.9	1.5	1.5	1.4	1.5

SW Greenland

The Nordenskiöld and Narssap sermia catchments dominated the lake distribution of the SW (Figure 5.18). Indeed the Nordenskiöld catchment had the largest total lake area of any catchment of the ice sheet, with Narssap sermia - the catchment adjacent to the south - having the second largest (Table 5.7). These two catchments alone accounted for 43 % of the total maximum lake area of the GrIS, and 73 % of the lake area of the SW. The Jakobshavn catchment was the next most significant, accounting for 5 % of the GrIS lake area. Each catchment south of Narssap sermia contained

progressively less total lake area, with the Arsuk Bræ catchment containing only 0.1 % of the GrIS lake area.

In the majority of SW catchments the interannual variations followed the trend of the whole SW region (Section 5.6.1) and the melt extent and duration trends for each respective catchment (Figure 5.18). The most notable exception to this trend was in the Narssap sermia catchment where maximum lake area was recorded in 2008. This was contrary to the melt trend and the rest of the SW where 2007 was the year of maximum lake area. Also of note, total lake area was higher in 2008 than in 2009 in the Nordenskiöld catchment whereas the opposite trend is observed in the melt extent and duration data, although this was a marginal trend with only slight differences between the two years.

NW Greenland

All catchments of the NW region contained significant lake area (Figure 5.19). Whilst total lake area is largest in catchments 30, 31, and 32, this is probably explained by the larger area of these catchments. Interannual variations in this region appear to be well explained by variations in the melt extent and duration data shown.

N Greenland

All of the major catchments of the northern region contained significant lake area, especially the Humboldt, Petermann, and Ryder catchments (Figure 5.20). Most catchments had a maximum area in 2008, and a minimum in 2006, in keeping with the regional trend and the melt extent and duration data shown.

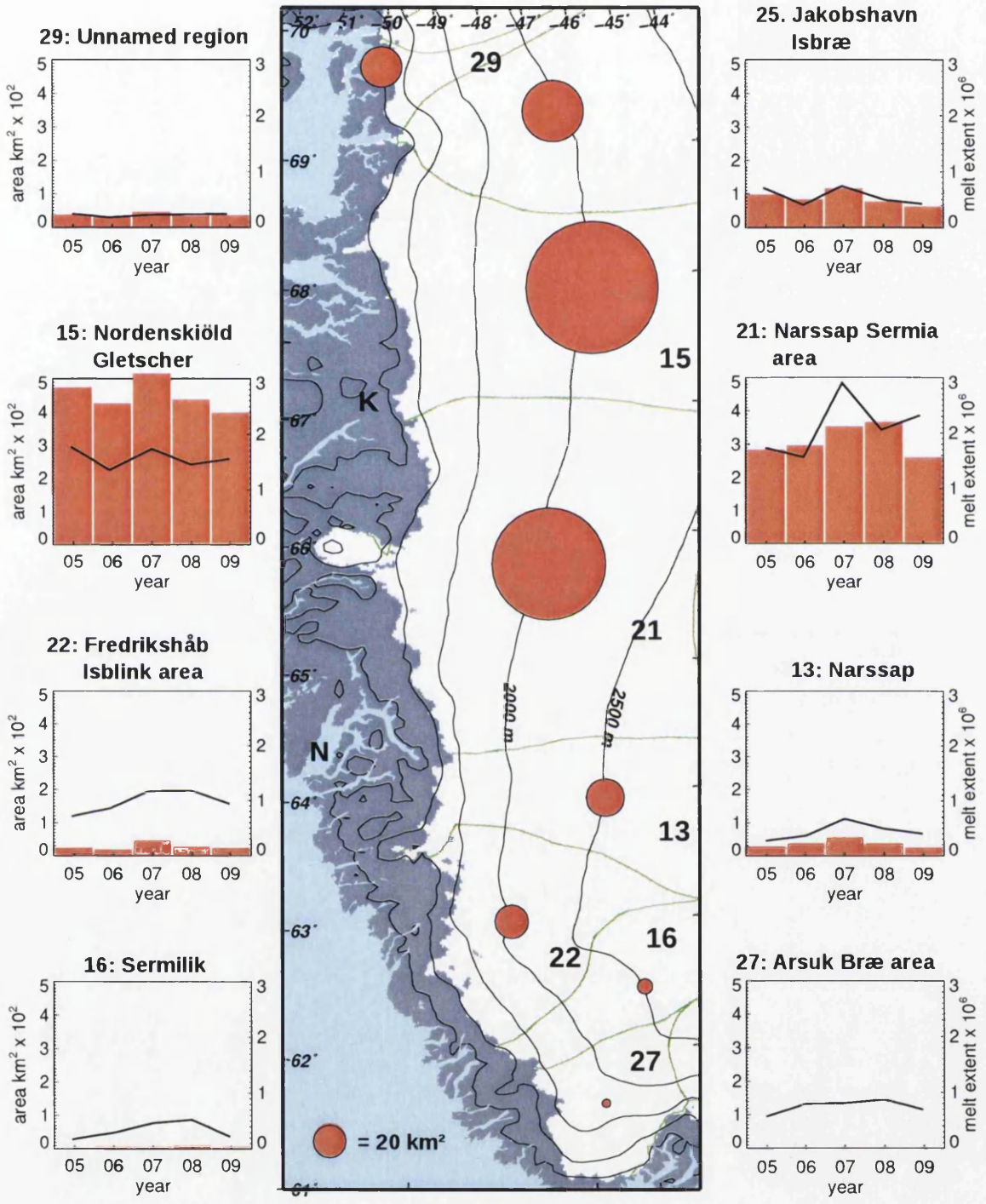

Figure 5.18: Distribution of lake area in SW Greenland, showing mean lake area (red circles) and interannual variations (bar charts). Melt extent and duration plotted as black line. All bar charts for Figures 5.18–5.23 are plotted on the same scale for easy comparison.

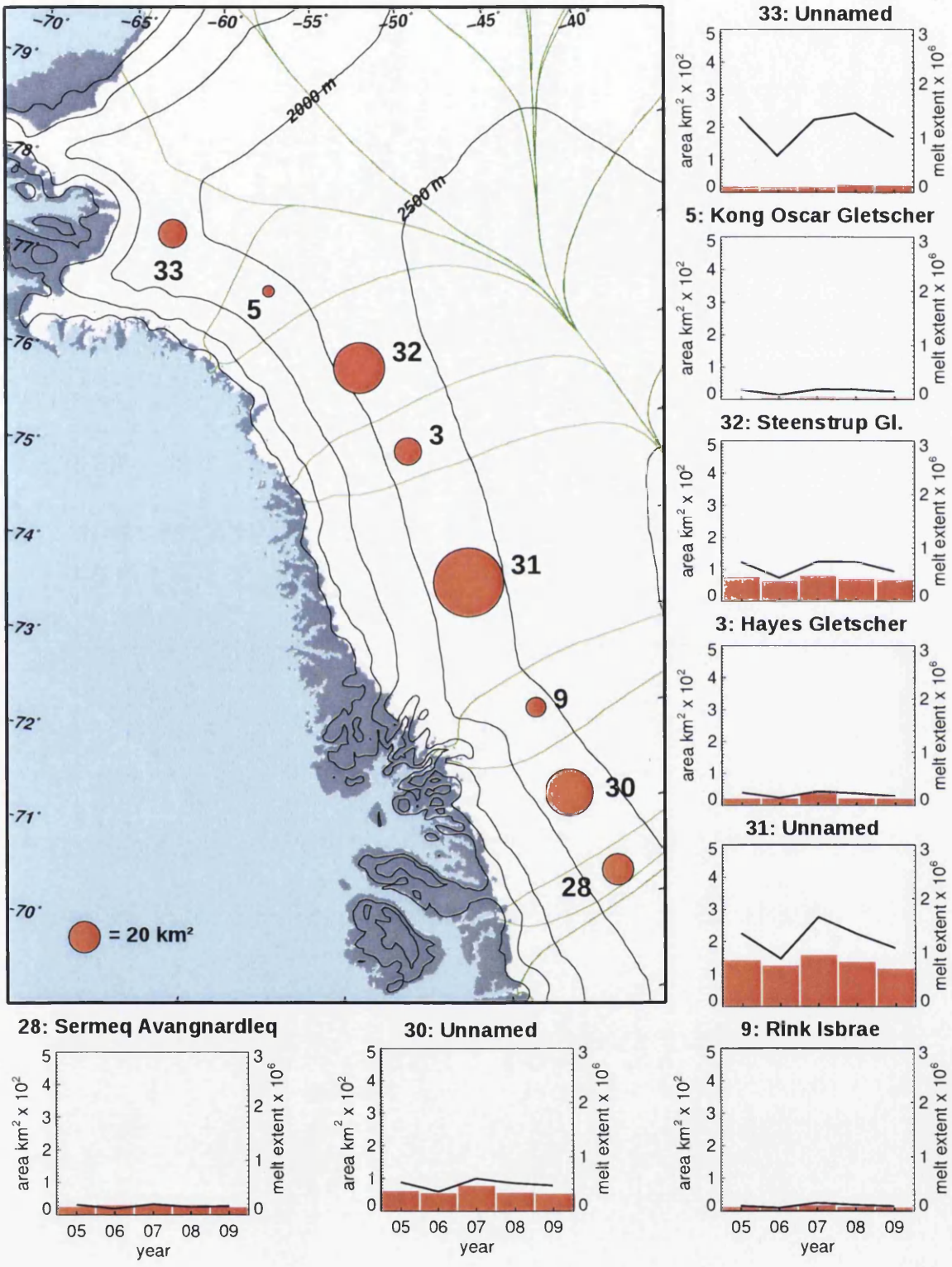

Figure 5.19: Distribution of lake area in NW Greenland, showing mean lake area (red circles) and interannual variations (barcharts). Melt extent and duration plotted as black line.

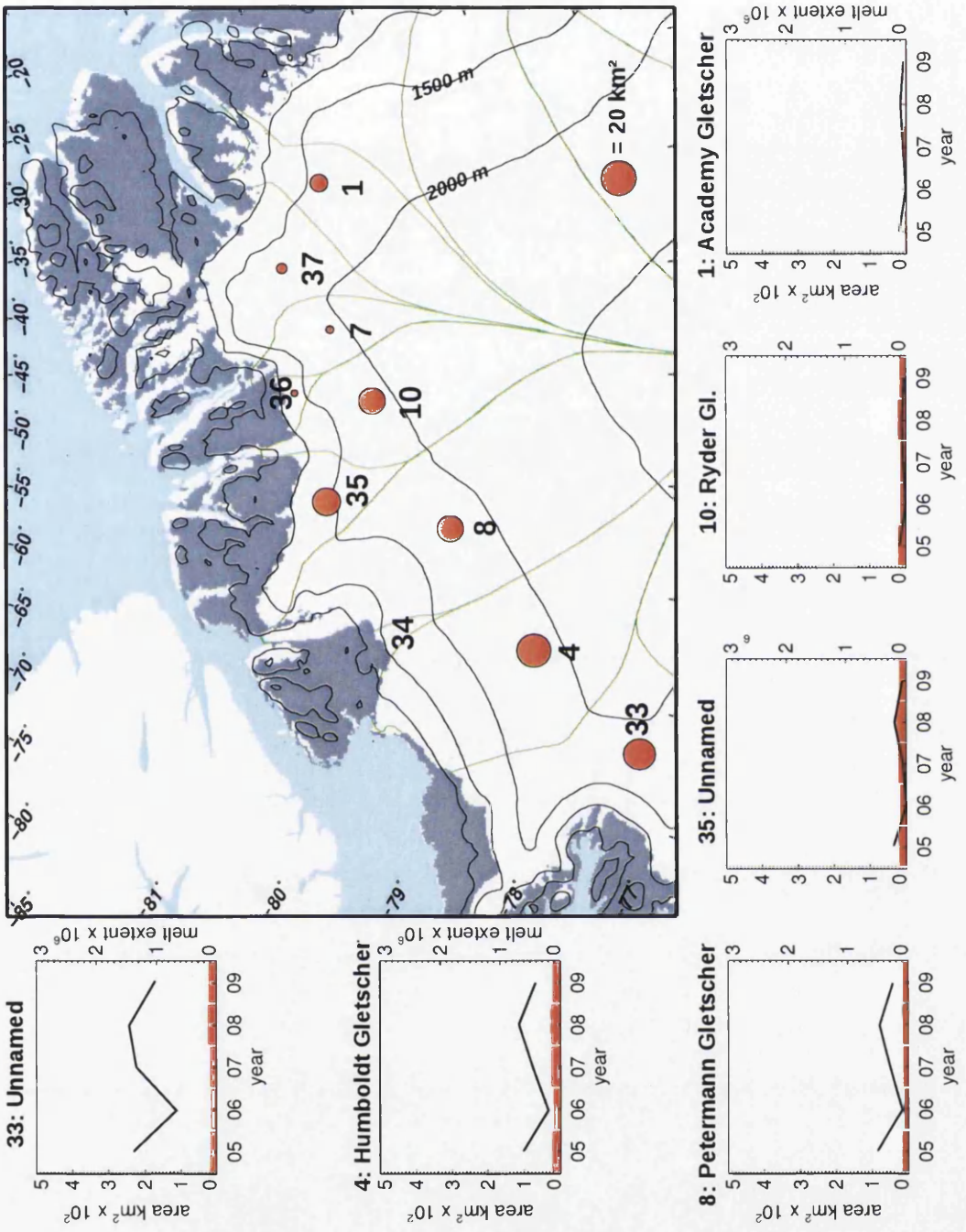

Figure 5.20: Distribution of lake area in North Greenland, showing mean lake area (red circles) and interannual variations (bar charts). Melt extent and duration plotted as black line. All barchart axes are the same, some are omitted for clarity. No barchart for catchments 7, 34, 36, or 37 are included, as the areas were too small to plot on these axes.

NE Greenland

The catchments of the Nioghalvfjerdsbræ, Zachariae Istrøm, and Storstrømmen glaciers accounted for a large proportion of total GrIS lake area, especially when considering the relatively modest width of each of these catchments. Catchment 40 contained a large proportion of total lake area for its size. This is not a glacial catchment as such, rather the gap between the glacial catchments of Storstrømmen and Zachariae Istrøm. The combination of Nioghalvfjerdsbræ, Zachariae Istrøm, Storsrtrømmen, and the intermediary catchments 39 and 40 accounted for 16.3 % of the total GrIS lake area.

Interannual variations in lake area in this region were large. Total lake area was six times larger in 2008 than in 2006 in the Nioghalvfjerdsbræ catchment, no other catchment showed interannual variations on this scale. Lake area was also 1.7 times larger in 2008 than in 2006 in the Zachariae Istrøm catchment.

E Greenland

Only two catchments are fully in the E region, both of which show a slight peak in total lake area in 2007. Catchment 41, containing Walterhausen Glacier, is also partly in the NE region and has a peak in lake area in 2008, in keeping with the melt extent and duration trend that it shares with the other NE catchments.

SE Greenland

As shown in Figure 5.23, total lake area was small in all SE catchments, and no lakes were detected in the Koge, Ikertivaq or Johan Peterson Fjord catchments. The greatest lake area was found in the Schweizerland area, however this only accounted for 0.15 % of the total GrIS lake area. The total lake area in these catchments is too small to visualise on the axes used, but interannual variations can be seen in Table 5.7. Whilst variations found in the Helheim and Schweizerland areas roughly

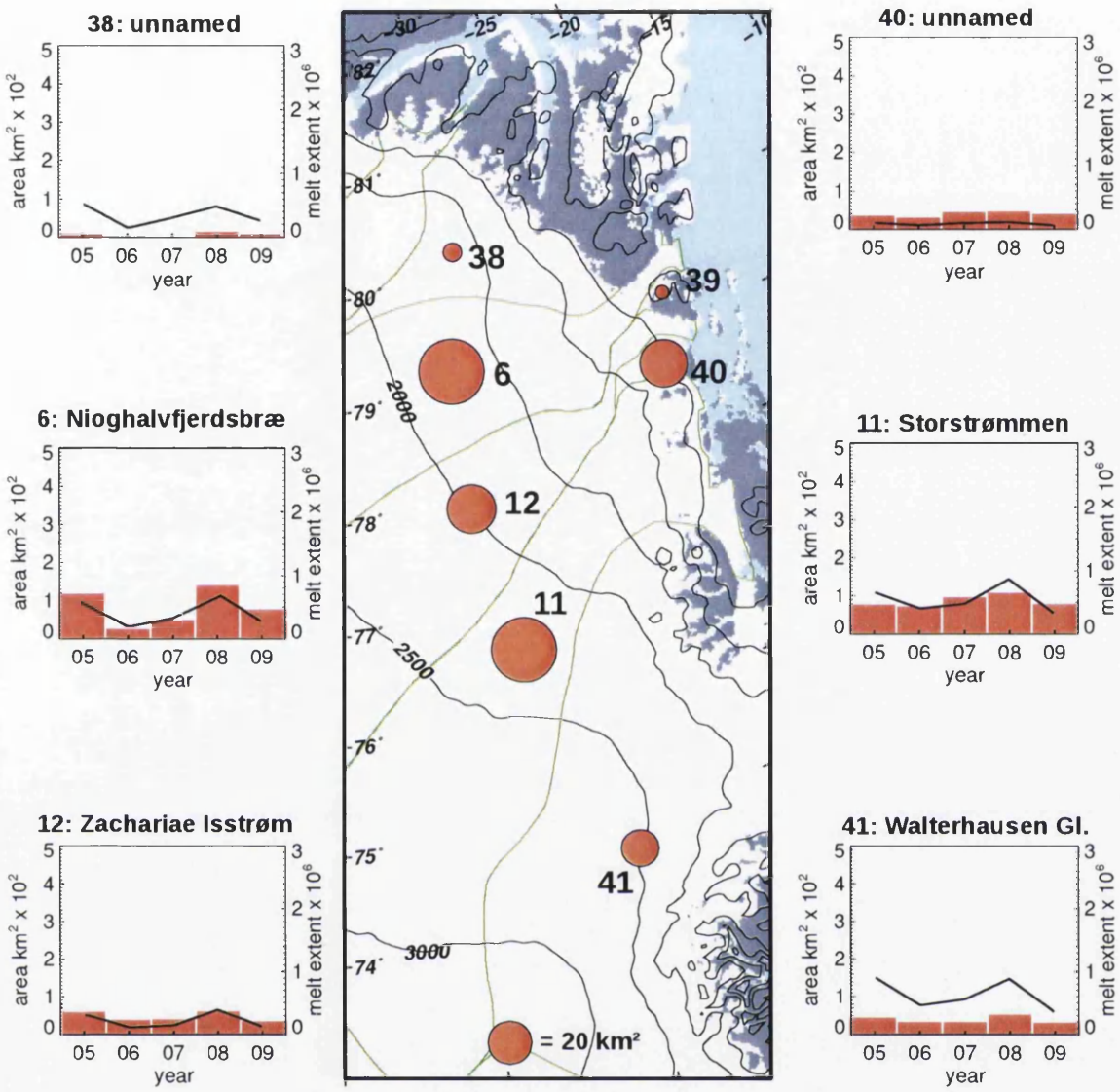

Figure 5.21: Distribution of lake area in NE Greenland, showing mean lake area (red circles) and interannual variations (bar charts). Melt extent and duration plotted as black line. Barplot for catchment 39 is omitted, as the area was too small to plot. Catchment 41 also appears on Figure 5.22.

followed the regional and melt trends, the "SE fjords" catchment showed variation independent of these trends.

The barplots in this section were deliberately kept at the same scale for comparison. As this means that for the catchments of the SE they are essentially blank, similar plots using different scales are available as Figure 6.11.

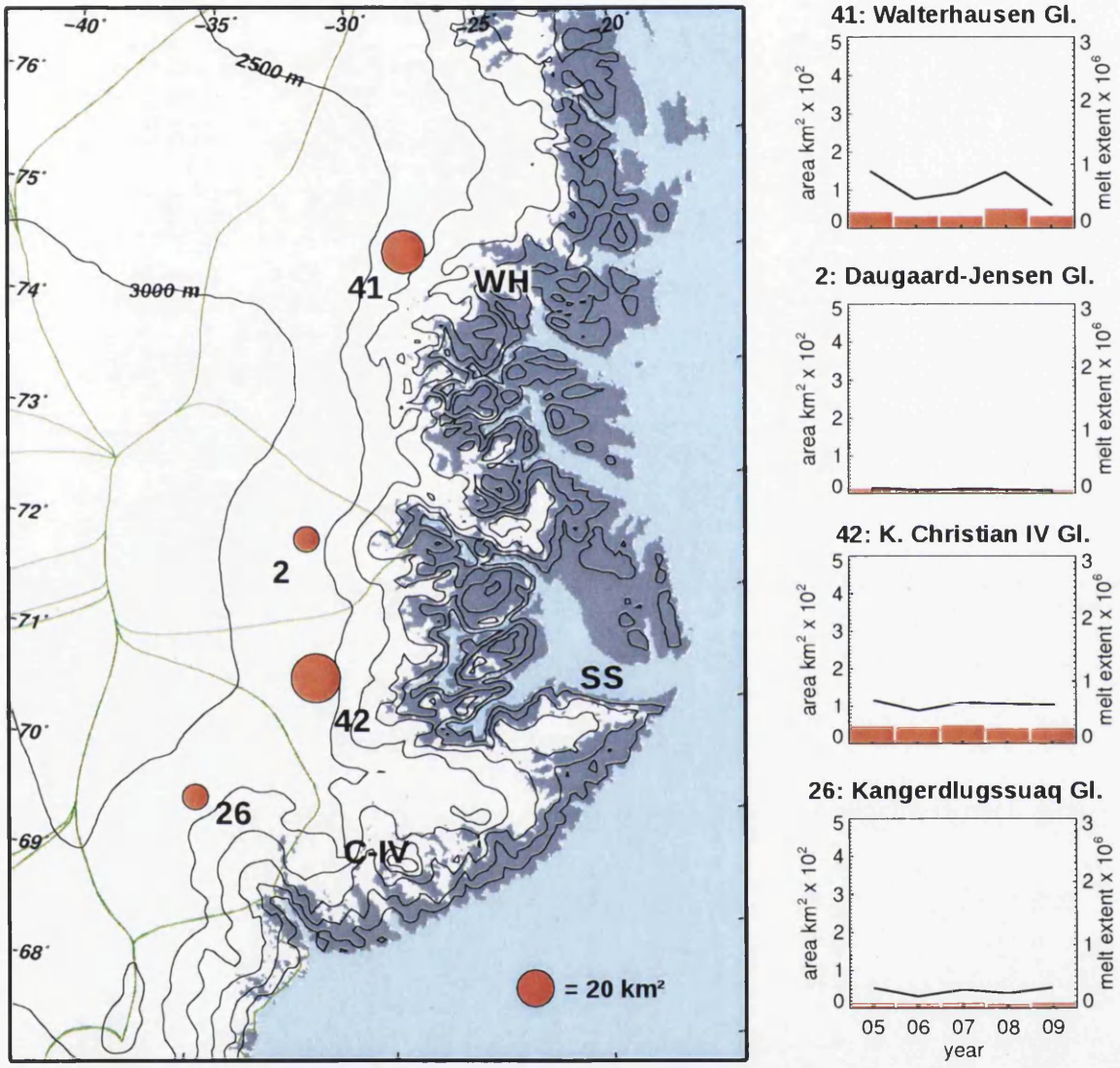

Figure 5.22: Distribution of lake area in E Greenland, showing mean lake area (red circles) and interannual variations (bar charts). Melt extent and duration plotted as black line. Kong Christian IV Gl. (C-IV), Scoresby Sund (SS), and Walterhausen Gl. (WH) are marked. Catchment 41 also appears on Figure 5.21. Kangerdlugssuaq Gl. (26) is included on this figure, but was part of the SE region for analysis purposes.

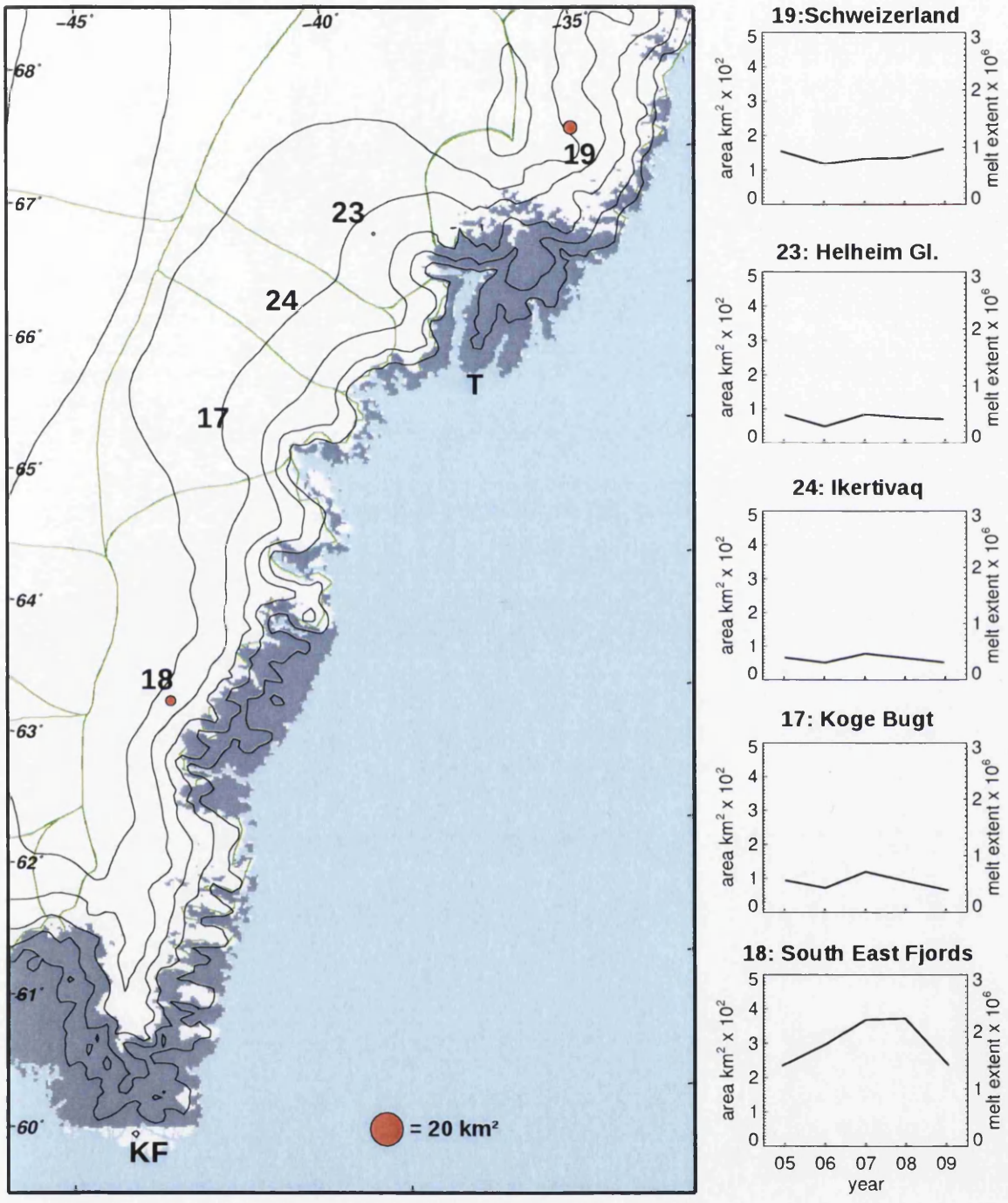

Figure 5.23: Distribution of lake area in SE Greenland, showing mean lake area (red circles) and interannual variations (bar charts). Melt extent and duration plotted as black line. Tasillaq (T) and Kap Farvel (KF) are marked. Kangerdlugssuaq Gl. was included in the SE region, but is shown on Figure 5.22.

5.7 Changes in lake distribution throughout the melt season

Results so far in this chapter have ignored the specifics of the seasonal changes of the lakes on the GrIS, with area being represented as the sum of the maximum areas of all lakes. In this section, the time varying nature of lake elevation and area within each melt season (i.e. intra-annual variations) is examined. Observations in this section are instantaneous, for example any area values relate to the total area in a given region on a specific day. To carry out this analysis cloud-free images of whole sections of the ice sheet were required. To maximize the number of cloud free images, small subsets of the regions used so far were chosen (Figure 5.24). Where obvious glacial catchments existed, a whole catchment was used. This was the case for the Ryder Glacier (in the N region), the NE Greenland Ice Stream outlets, Daugaard-Jensen Glacier (in the E region), and Kangerdlugssuaq Glacier (in the SE region). In the SW and NW regions glacial catchments are more poorly defined, and thus arbitrary boundaries were chosen. In regions with many lakes (e.g. SW and NW) the region subsets were chosen to be as representative of the wider region as possible. However, in regions with fewer lakes (e.g. SE), subset were chosen where there were sufficient lakes. For example, in the SW, Kangerdlugssuaq was chosen as other possible subsets would have contained no lakes. Note that the sizes of the sub-regions used were different (Figure 5.24), so comparisons of area between the regions would be meaningless. Also note that requiring totally cloud-free imagery significantly restricted the temporal resolution, which further demonstrates the advantage of a lake-by-lake approach as used elsewhere in this thesis.

Figure 5.25 shows the maximum elevation at which any lake occurred for days where cloud-free observations could be made. As expected, as the melt season develops, lakes form at higher altitudes until a plateau is reached. However, whilst it might be expected that at the end of the melt season the highest lakes would disappear first as freezing onsets, in higher altitude lakes (although not always the very highest) were often the last to disappear.

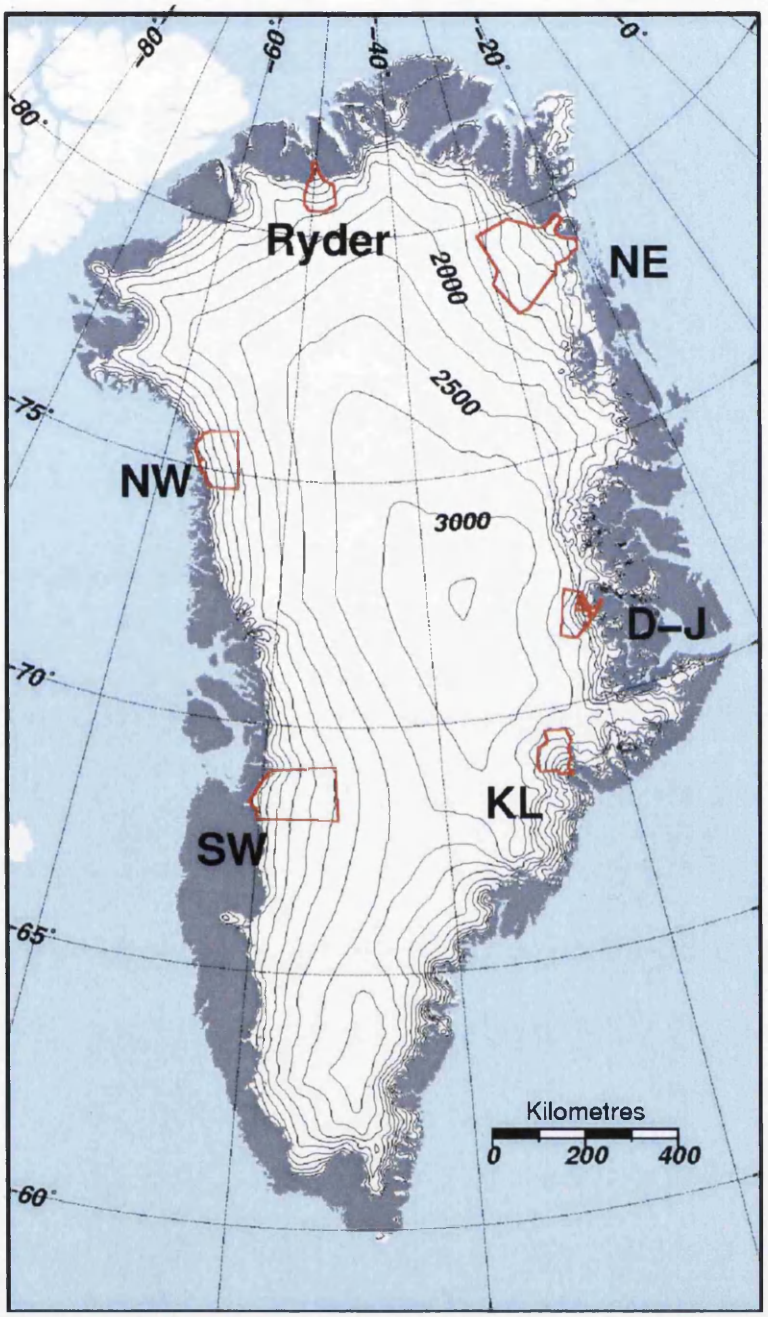

Figure 5.24: The regions used for examining intra-annual changes in lake area and elevation. D-J = Daugaard-Jensen Glacier. KL = Kangerdlugssuaq Glacier. The regions used were very different sizes, so direct comparisons of lake area are inappropriate. Kangerdlugssuaq, Ryder, and Daugaard-Jensen were used as whole catchments, whereas the NE, NW and SW regions contained several outlets.

The maximum elevation reached showed more interannual variation in some regions than in others, with little variation in the NW, and considerable variation in the NE. In general, lakes formed at higher elevations in more southern regions. The rate at which the zone of lakes spread up the ice sheet varied from year to year in most regions, with a particularly late onset in all regions in 2006, and in 2009 for Ryder Glacier and the NE.

Observations of daily lake area are shown in Figure 5.26. Significant interannual differences can be observed in the maximum area, the date of maximum area, and the rate of the onset of lake area growth. Spikes in the data can be observed in several plots (e.g. Kangerdlugssuaq Glacier during 2007). These spikes sometimes had no obvious cause, especially where there were many lakes (e.g. SW). Where there were few lakes (e.g. Kangerdlugssuaq Glacier) large dips in area were a result of lake drainage: the drainage of one lake had more effect on total lake area when fewer other lakes were present.

The year of maximum daily lake area was not always the same as the year of maximum melt, or the year of maximum total lake area presented in Section 5.6. For Kangerdlugssuaq Glacier, maximum daily lake area occurred in 2005 and 2007. These are the same years as the maximum total lake area, and the years of highest melt. Similarly, in the NE, extensive lake area was sustained in 2005 and 2008, which is to be expected given the total lake area and melt extent results. Ryder Glacier had similar maximum daily lake area for each year, with the exception of 2007 which was lower. However, the timing of the day of maximum area varied considerably: this day was later in low melt years. Very little variation was evident in the NW, although the rate of lake growth varied from year to year and was much slower in the low melt years of 2006 and 2009. Daugaard-Jensen Glacier had similar lake extents and rates of lake growth from year to year, with the exception of 2005 (a high melt year) which had a much larger lake area than any other year, which was sustained over a longer period. In the SW the results were harder to intepret. 2006, a low melt year, had lower lake area and a later onset than other years, although the lakes lasted until later in the year. 2007, the year of highest melt and largest total

maximum lake area, had the earliest and most rapid lake growth. 2008 however, a year of low melt, had the largest daily lake area.

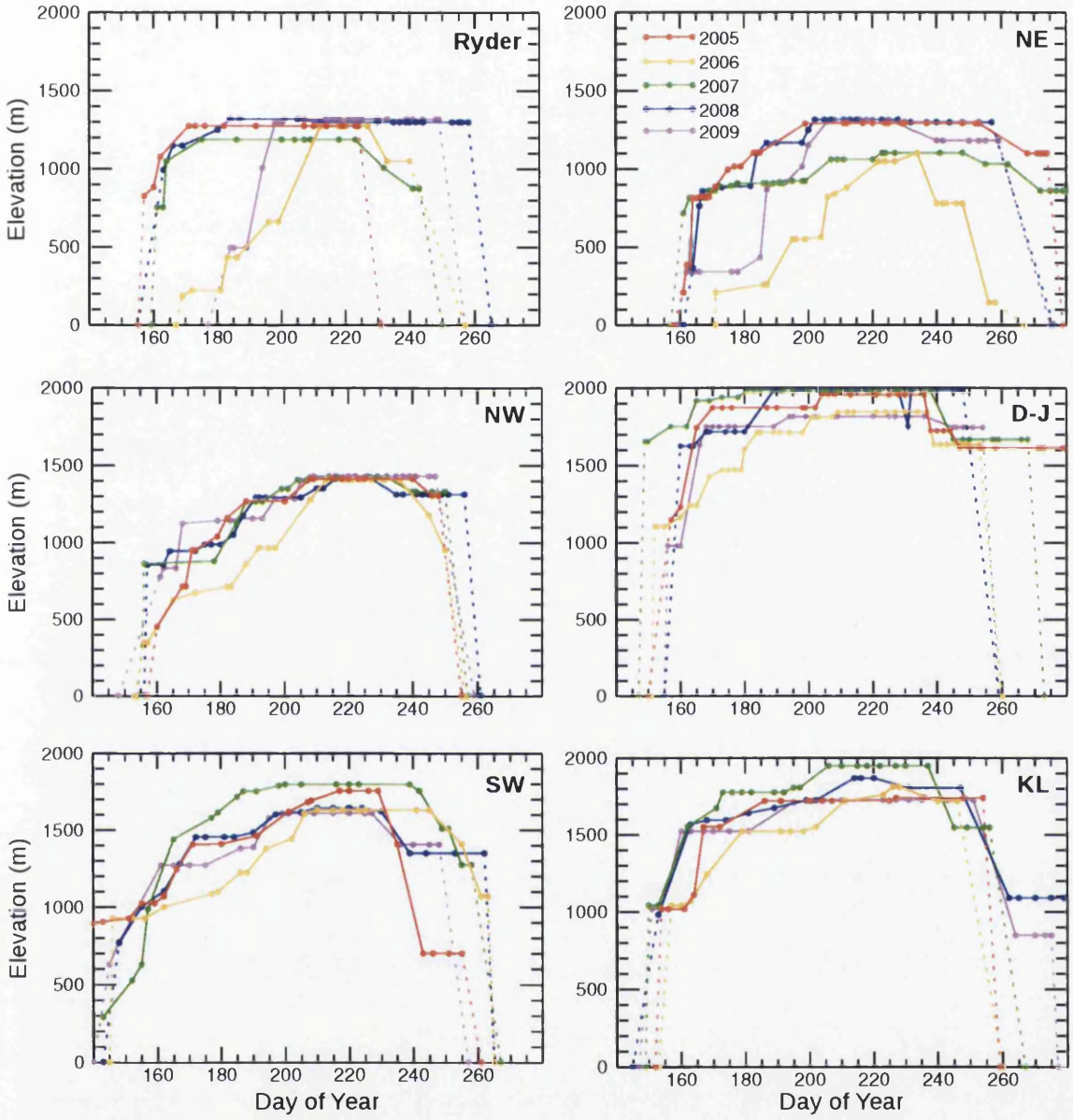

Figure 5.25: Observations of instantaneous maximum lake elevation through the melt seasons of 2005–2009 for six areas of the ice sheet. Dashed lines indicate that the first lakes appeared or the last lakes disappeared in that period. D-J=Daugaard-Jensen Glacier. KL=Kangerdlugssuaq Glacier.

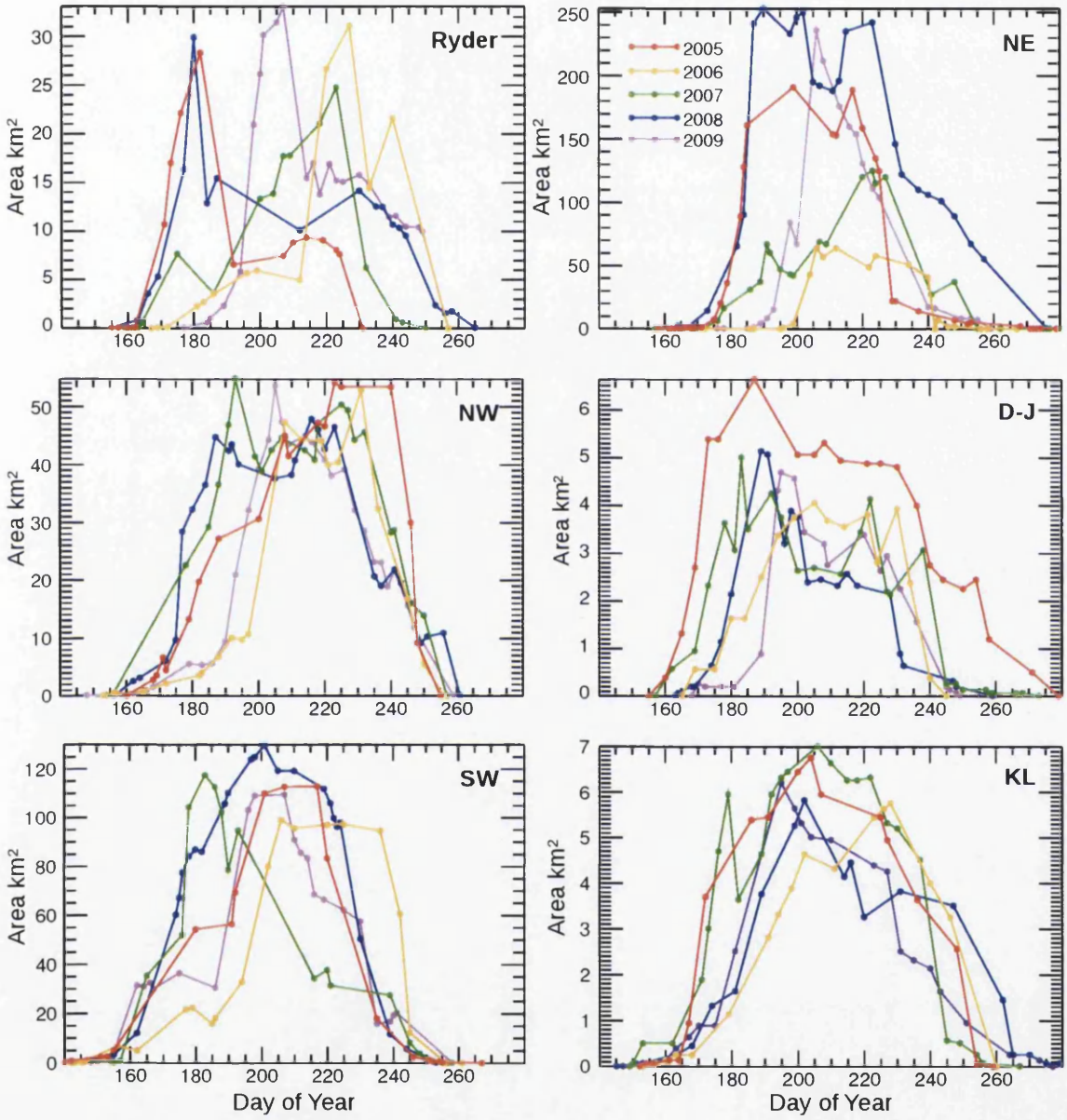

Figure 5.26: Observations of instantaneous lake area through the melt seasons of 2005–2009 for six areas of the ice sheet. D-J=Daugaard-Jensen Glacier. KL=Kangerdlugssuaq Gl.

5.8 Chapter summary

Lakes were mapped in the ablation zones of most of the ice sheet, and the finding of Echelmeyer *et al.* (1991) that lakes do not move down glacier over time was confirmed. Melt data produced from MODIS LST showed that 2005 was a year of extensive melt in all parts of the ice sheet, and 2006 was conversely a low melt year in all regions. The year of maximum melt extent varied between regions: 2007 was the year of greatest melt extent in the S of the GrIS, whereas in northern regions 2008 had the most extensive melt. Melt from MODIS LST was found to compare favourably with the more commonly used SSM/I melt extent data.

The size and frequency of occurrence of lakes varied considerably, both in space and time. The difference between the SW and SE regions was the most striking contrast, with the SW accounting for 60 % of total lake area, and the SE region containing $< 1\%$ of the total lake area. The NE contained the next largest percentage of lake area, followed by the NW, N, and then E regions. Total lake area was controlled by the frequency and size of lakes. Significant differences in lake frequency were found, with only the SW and NE regions having a greater than expected frequency of lakes. Lake size was also found to vary significantly between regions. Lakes in the NE and SW regions were the largest, and lakes in the SE were found to be the smallest. Lake size did not vary significantly between the NW, N, and E regions.

Both the total lake area and the area of individual lakes varied interannually, although variation in the latter was not significant for the E and SE regions. Both of these variables predominantly followed the yearly trend in melt extent and duration. The magnitude of interannual variations in total lake area were not equal in all parts of the ice sheet: the NE in particular showed very large interannual variation, whereas the E region showed considerably less variation from year to year.

Intra-annual variations in lake elevation were analysed. Unsurprisingly lakes tended to form at higher elevations at lower latitudes and in higher melt years. The highest lakes were usually the last lakes to disappear at the end of the melt season. Intra-

annual variations in lake area were also recorded. In general high melt years were associated with early lake growth and more extensive lake area, but this was not the case in all regions.

This chapter has discussed the results of this thesis that can be presented with no knowledge of the drainage behaviour of the lakes studied. The following chapter, Chapter 6, contains those findings that could be made once the drainage behaviour of each lake had been established.

Chapter 6

Patterns in Lake Drainage and Freezing

6.1 Introduction

While the previous chapter described the locations and sizes of lakes on the GrIS, this chapter details those results that were be obtained once lakes had been classified by their mode of termination. First the identification of different drainage and freezing modes is described in Section 6.2. Each lake was assigned one of these classifications in every year. Spatial patterns in lake termination type are described in Section 6.3, presented at both ice sheet and regional scales. The differences between lake termination types are explored in Section 6.5 through factors such as lake area, lake duration, and surface slope. The persistence of lake termination types inter-annually is examined in Section 6.6. Finally, the apparently coupled fast drainage of groups of lakes is described in Section 6.7.

6.2 Different characteristics of lake termination

Initially the aim of this study was to identify those lakes that drained rapidly in the style of that studied by Das *et al.* (2008). Once the lakes had been subdivided into those lakes that drained rapidly and those that did not, the question of what happened to the remaining lakes remained unanswered, as no studies have been published relating to the fate of supraglacial lakes on the GrIS that do not drain suddenly. From recording lake area over time (Section 4.5), and comparing with the JPEG thumbnails described in Section 4.5.2, it became apparent that lakes could be subdivided into further classes. These classes were lakes that disappeared suddenly, those that appeared to freeze over at the end of the melt season, and those that shrank in area gradually without freezing. The classifications of lake drainage types used in this thesis as detailed in Section 4.6 were based on the observations described here. Note that "drainage types" is used for brevity to describe the mode of termination of a given lake, and includes freezing over as a "drainage type".

6.2.1 Lakes with rapidly declining area

Lakes that drained suddenly were straightforward to identify, owing to the characteristic sudden disappearance of the lake in a few hours. With this type of lake drainage, the largest surface area was almost exclusively the last data point recorded for the lake before drainage. Examples of fast-draining lakes are shown in Figure 6.1, with both example MODIS imagery before and after drainage, and with lake area plotted against time. Note that in Figure 6.1a two adjacent lakes drain simultaneously in the same 24 hour period.

6.2.2 Lakes with gradually declining area

Those lakes that were not classed as fast-draining lakes reduced in area more slowly, with several data points being recorded between the maximum lake extent and the

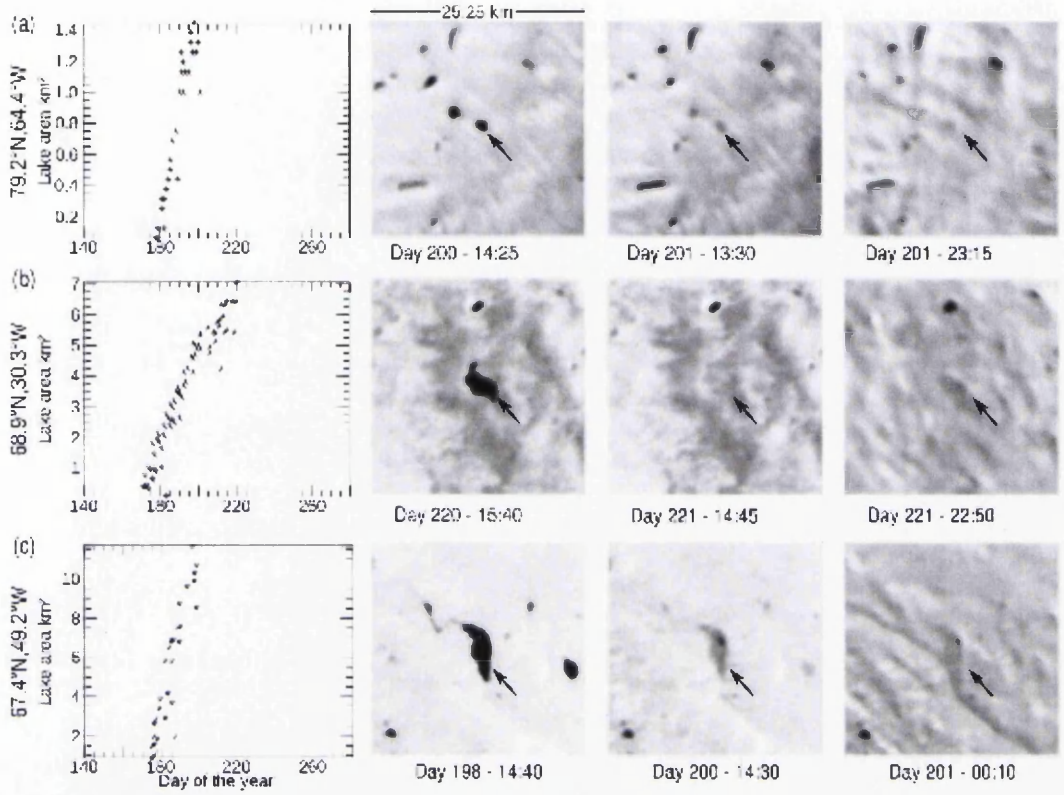

Figure 6.1: Examples of lakes that drain suddenly in 2008. All images are at the same scale and show MODIS band 1 250m images before and after drainage events. Note simultaneous drainage in (a) and (c), and a possible drainage moulin in (c). The area/time plots correspond to the lakes indicated by arrows.

eventual disappearance of the lake. The most obvious cause for this decline in area is the freezing of a lake at the end of the melt season, and indeed many lakes survived until the onset of the winter freeze up before the surface area was observed to decline (Figure 6.2). These lakes were assumed to have frozen over, and with larger lakes the spread of ice over the surface can be clearly distinguished (e.g. Figure 6.2a and c). A further characteristic of freezing lakes is that the neighbouring lakes reduce in area at the same time, again this is clearly visible in Figure 6.2.

Some lakes however exhibited a gradual decline in surface area in the middle of the melt season, with no decline in the surface area of the surrounding lakes (Figure 6.3) and comparison with melt data shows that this areal decline can occur in a period of consistent melt availability. The timing of this loss of area makes freezing over unlikely, and thus is interpreted as a loss of area through drainage. This

drainage is much slower than that of the fast drainage described above, and will be referred to subsequently as "slow drainage". There is no evidence that drainage through the ice to the bed should take several days. Slight drops in water level were observed by both Boon and Sharp (2003) and Das *et al.* (2008) associated with the propagation of fractures, but the drops in volume reported would not be of the magnitude observed in slow-draining lakes. The sudden increase in ice velocity and uplift associated with drainage as observed by Das *et al.* (2008) shows that total drainage in a short period of time is possible into an inefficient high pressure subglacial environment, as the ice can be displaced to make room for the water. Therefore, the slow drainage described above is interpreted to be supraglacial. Observations of unstable supraglacial drainage have shown that total drainage of a lake can occur over the ice surface through downwasting of the lake spillway in four days (Raymond and Nolan, 2000), which is compatible with the decline in surface area observed. The compatible time span, evidence against freezing, and lack of evidence for slow draining to the bed make supraglacial drainage the most likely cause of slow lake-drainage. However, the narrow width of supraglacial channels and the probably presence of more stable channels exiting fast draining and freezing lakes make testing this hypothesis through remote sensing problematic.

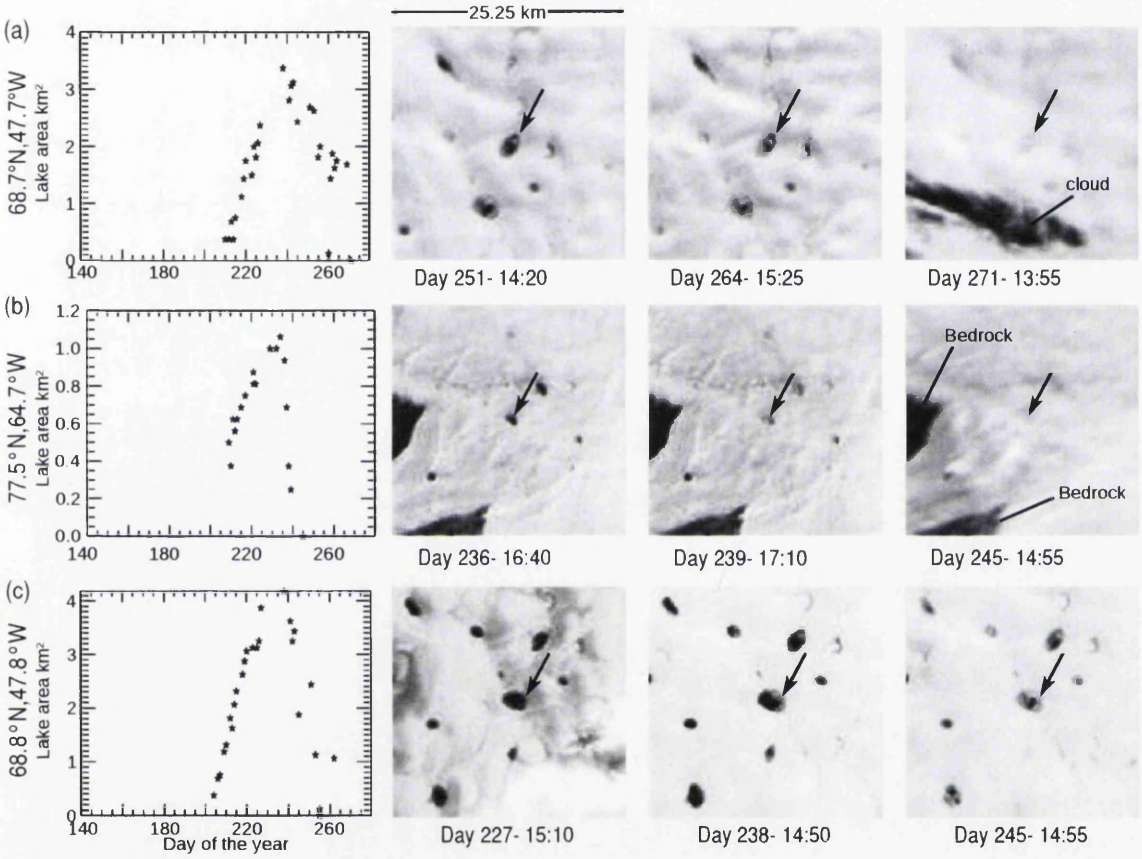

Figure 6.2: Examples of lakes that were observed freezing over at the end of the 2006 melt season. Note that in each case all of the lakes in the image have declining area at the same time, this is taken as strong evidence of freezing as opposed to supraglacial drainage. Also note in examples a and c that ice can be seen encroaching on the lake surface. Example c also shows a general increase in the albedo of the surrounding ice which is indicative of the end of the melt season.

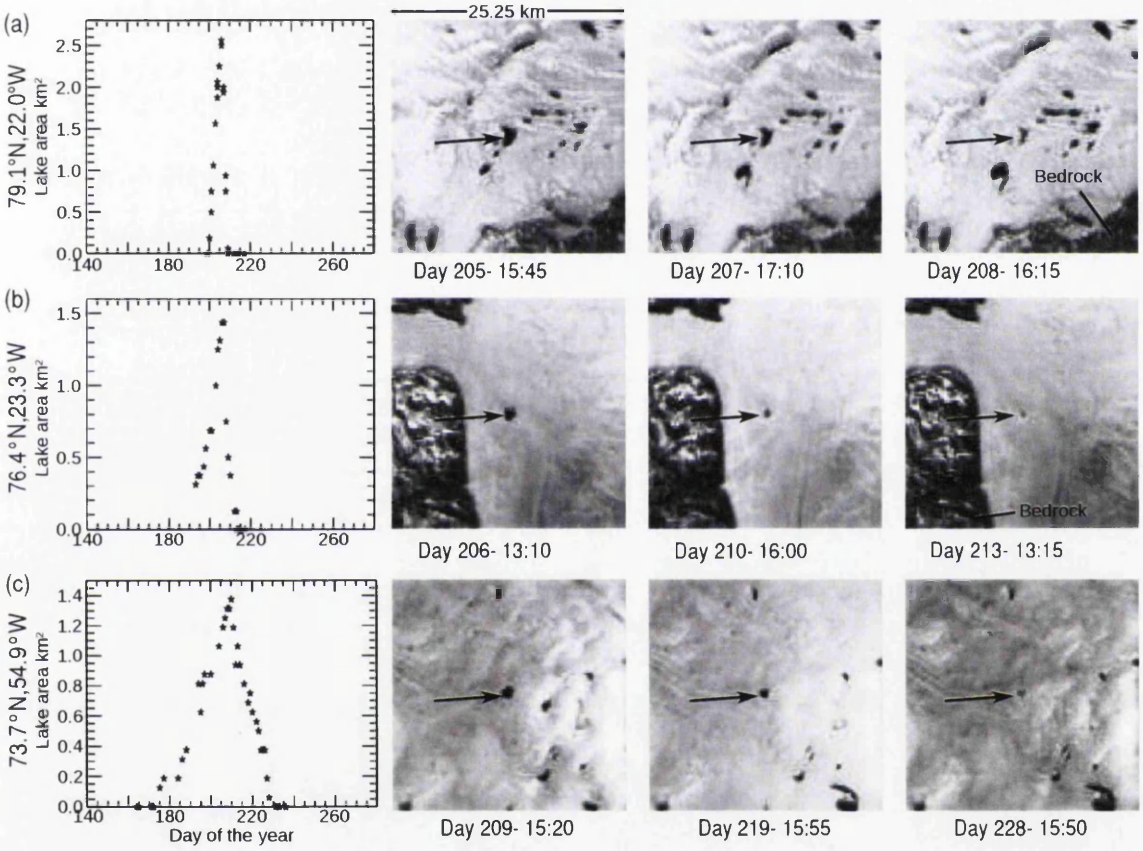

Figure 6.3: Examples of lakes that were observed draining slowly during the 2006 melt season. Note that in examples a and c other lakes in the surrounding area do not lose area, providing strong evidence that the lake in the central of the image is draining rather than freezing. The albedo of the surrounding ice in each example remains relatively low indicating a melting surface.

6.3 Patterns in lake termination type

6.3.1 Ice sheet scale

A map of the distribution of lakes of different drainage types in 2005 is presented as Figure 6.4. To avoid repetition of similar figures in the main body of the thesis, maps from all years are included in the appendices as Figures A.1–A.5. The pattern of the overall distribution of lakes is described in Section 5.4.1, this section will focus on the distribution of the different drainage types.

The most striking pattern in the distribution of lake drainage types as visible in Figure 6.4 (and Figures A.1–A.5) is that for several regions the highest lakes froze in each year. This pattern occurred in the SW, NW, N, and NE regions. In the E and SE regions lakes of all drainage types appear to have occurred equally at different heights. In those parts of the ice sheet where the highest lakes appeared to freeze, this occurred in every year during the period 2005–2009. Fast and slow-draining lakes appear to have formed at lower elevations than those which froze. Fast-draining lakes in particular were conspicuously absent from the highest elevations in all but a handful of cases.

Visually inspecting distribution maps such those in Figures A.1–A.5 it is difficult to judge the proportions of the various drainage types as they vary between years. This variation is addressed in the following section (6.3.2) by compositing the lake frequency and area by type across different regions, and across smaller catchments in Section 6.3.3.

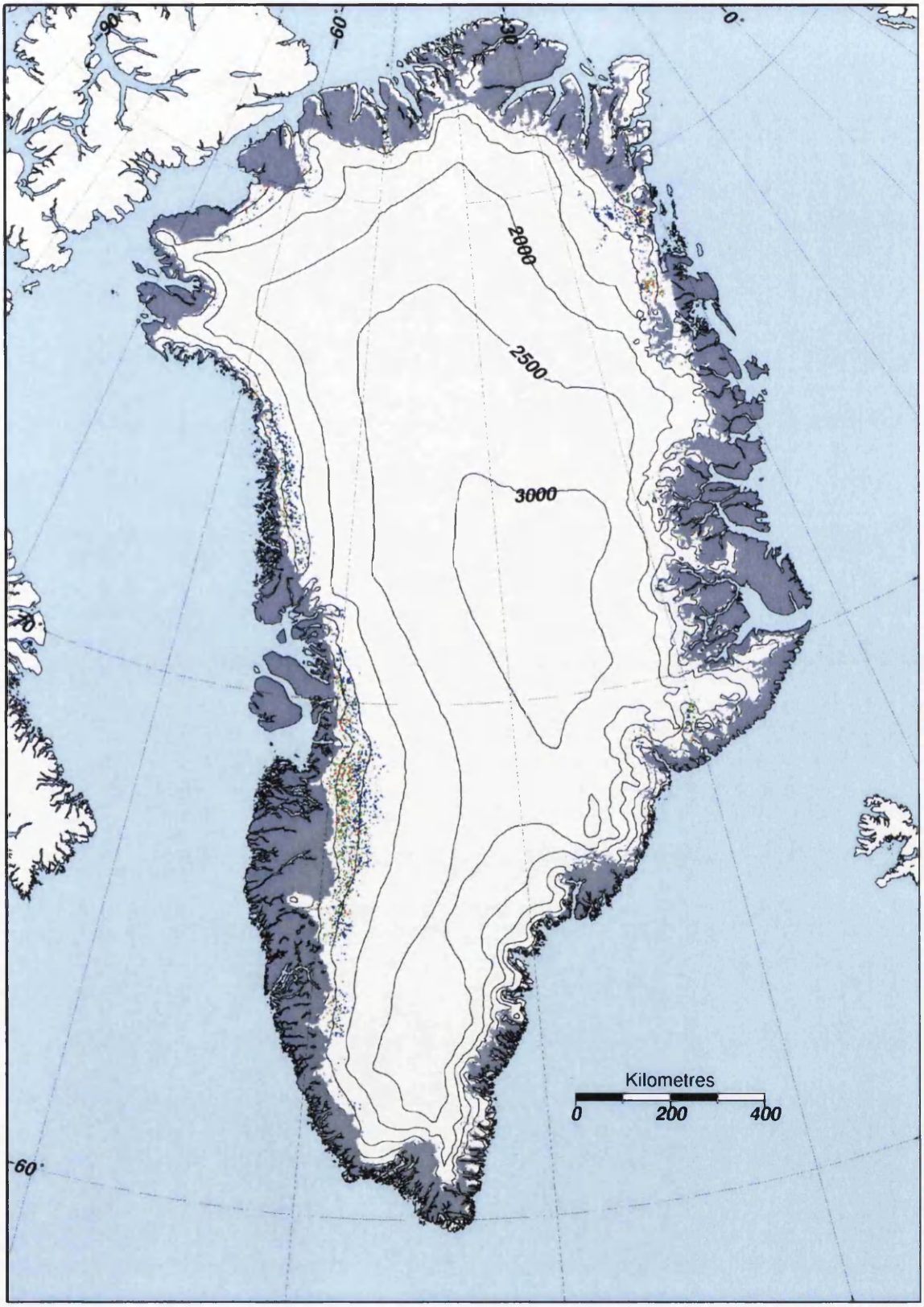

Figure 6.4: Distribution of different drainage types in 2005, showing fast-draining lakes (red), slow-draining lakes (green), freezing lakes (blue), and lakes of unknown drainage type (black). Maps showing the same data for all years are included in the appendices as Figures A.1–A.5.

6.3.2 Regional scale

The distribution of different lake drainage types is summarized in Figure 6.5 and Table 6.1. Lakes that froze over were most prevalent, accounting for nearly half of all lakes (46%), closely followed by slow drainage accounting for 34% of all lakes. Fast drainage accounted for 13% of all lakes on the ice sheet, and < 7% of lakes could not be assigned a category and were thus classed as "unknown". While for most regions it was the case that the freezing category was the largest, followed in order by slow draining, fast draining, and unknown, the exact proportions varied between regions. Lakes were most likely to drain rapidly in the NE (17%), SW (14%) and N (14%), and least likely in the NW (7%) and SE (8%). The highest and lowest frequencies of slow lake drainage were all on the E coast, with 48% of lakes draining slowly in the SE, 42% in the E, but only 27% in the NE. A larger proportion of lakes froze in the northern regions, with 57% in the NW, 55% in the N, and 52% in the NE.

The differing proportions of drainage type between regions were tested using a χ^2 analysis (Tables B.1–B.4), and found significant for fast draining, slow draining, and freezing lakes at the 99% confidence level. No significant difference in the proportions of unclassified lakes occurring between regions was found at the 95% confidence level. For the drainage types with significant differences in proportional occurrence between regions (fast draining, slow draining, and freezing), the expected frequency of occurrence normalised by the total number of lakes in each regions helps highlight patterns in the occurrence of the different drainage types (Tables B.1–B.4). The SW, NE, and to a lesser extent the N, had more fast-draining lakes than expected when normalised by the total number of lakes. The SW, E, and SE had more slow-draining lakes than expected when normalised by the total number of lakes. Finally, NW, N, and NE had more freezing lakes than expected when normalised by the total number of lakes.

By far the most fast-draining lakes were found in the SW region, indeed 61% of all fast-draining lakes were found in that region. 17% and 11% of fast-draining lakes were found in the NE and NW regions, and only 1% were in the SE region. To

Table 6.1: Frequency of fast draining (Fa), slow draining (Sl), freezing (Fr), and unknown (Un) lakes, from 2005–2009 per region and for the whole ice sheet. Mean frequency over 5 years is given for each drainage type as a percentage of the total number of lakes in that region.

2005	Fa	Sl	Fr	Un	Total
SW	128	426	477	86	1117
NW	27	103	236	16	382
N	20	35	58	13	126
NE	55	93	139	9	296
E	14	53	37	5	109
SE	3	15	15	4	37
GrIS	247	725	962	133	2067

2006	Fa	Sl	Fr	Un	Total
SW	146	309	591	86	1132
NW	29	92	256	13	390
N	7	13	76	17	113
NE	30	35	153	4	222
E	10	26	63	2	101
SE	3	15	18	2	38
GrIS	225	490	1157	124	1996

2007	Fa	Sl	Fr	Un	Total
SW	218	495	370	113	1196
NW	21	146	211	26	416
N	11	18	70	10	130
NE	41	65	113	5	274
E	10	54	30	2	71
SE	3	19	14	1	34
GrIS	304	797	808	157	2069

2008	Fa	Sl	Fr	Un	Total
SW	187	474	469	40	1144
NW	31	148	187	23	416
N	18	32	63	11	130
NE	59	97	137	12	274
E	7	32	58	5	71
SE	3	16	14	4	34
GrIS	305	799	928	95	2069

2009	Fa	Sl	Fr	Un	Total
SW	119	395	445	57	1016
NW	38	114	213	18	383
N	26	34	53	2	115
NE	42	60	156	28	286
E	5	35	50	5	95
SE	2	22	11	1	36
GrIS	232	660	928	111	1931

Mean	Fa	Sl	Fr	Un
SW	14%	37%	40%	8.1%
NW	7.4%	31%	57%	5.0%
N	14%	22%	55%	8.8%
NE	17%	27%	52%	3.9%
E	9.7%	42%	45%	3.4%
SE	7.7%	48%	40%	4.9%
GrIS	13%	34%	46%	6.7%

Table 6.2: Observed and expected frequencies for fast draining lakes. χ^2=321, df=5, critical value (p=0.001)=20.52. As χ^2 is greater than the critical value, there is a significant difference in fast-draining lake frequency between regions.

Region	Ice margin length (km)	Proportion of total length	Observed freq. (O)	Expected freq. (E)	O-E	$\frac{(O-E)^2}{E}$
SW	1331	0.21	160	56	104	191
NW	1193	0.19	29	50	-21	9
N	923	0.15	16	39	-22	13
NE	476	0.08	45	20	25	32
E	985	0.16	9	41	-32	25
SE	1329	0.21	3	56	-53	50
Total	6237	1.00	263	263		321

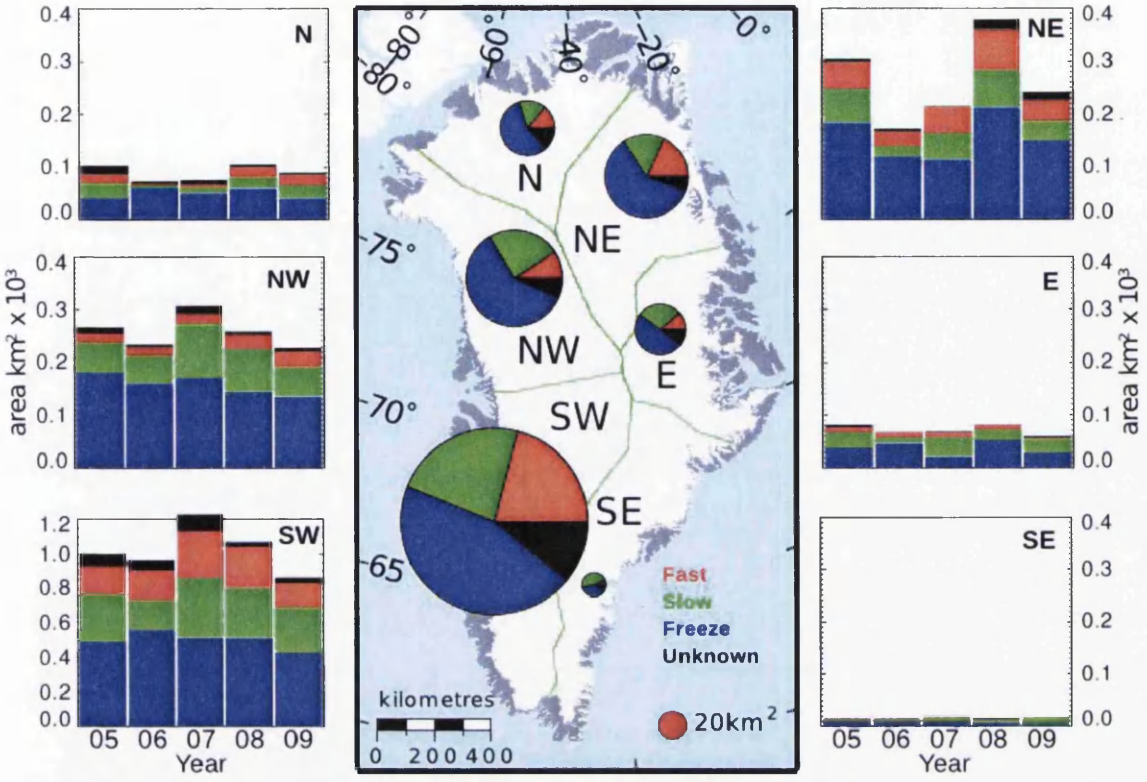

Figure 6.5: The distribution of lake drainage types on the GrIS. Lakes are represented by maximum surface area in each year. The central figure shows the mean area and proportions of lake types over the period 2005–2009. The bar charts show the area and proportions of lake drainage type per year. Fast-draining lakes (red), slow draining lakes (green), and freezing lakes (blue) are shown. Lakes of unknown drainage type are also shown (black). Note that a different vertical scale is used for the SW bar chart for clarity. On the same scale as the other plots the bars for the SW would be 3x larger. As a contrast, compare this figure with Figure 5.17, which shows the same area data on a consistent vertical scale.

test the significance of this difference, expected frequencies based on the ice margin length of the different regions were calculated and are shown in Table 6.2. Despite the NW accounting for 11% of fast-draining lakes, there were 21 less drainage events in that region than expected per year, showing that the number of fast-draining lakes in that region is partly explained by the region's large area. In contrast, the SW and NE regions were the only regions to have more fast-draining lakes than expected: 104 and 25 more than expected respectively. This variation in the distribution of fast-draining lakes normalized by margin length was significant at the 99.9% confidence level (χ^2 test used, Table 6.2). Similarly significant differences were found for slow draining, freezing, and unknown lakes (Tables B.5–B.7).

6.3.3 Catchment scale

The distribution of different drainage types by area is presented in Figures 6.6–6.11. Both frequency and area of lakes of different drainage type by catchments are presented in Tables 6.3–6.5 averaged over the five year observation period. Frequency of fast-draining lakes for all years is presented in Table 6.6. Similar tables for slow draining, freezing, and unknown lakes are included Appendix B as Tables B.8–B.10.

All catchments of the SW region show a similar (and large) proportion of lakes draining rapidly. Over the whole region 14% of lakes drained rapidly, on the catchment scale between 5% and 22% of lakes were fast draining, with most catchments in the SW having more than 10% of lakes draining rapidly. Freezing accounts for around half of all lake disappearance in the SW region, a pattern observable in the majority of catchments. In the Jakobshavn Isbræ catchment freezing is especially prevalent by area, with 70% of lake area freezing (Table 6.4). The percentage frequency of lakes freezing in the Jakobshavn catchment was 54% showing that freezing lakes in this catchment area are particularly large. Lakes that could not be classified (type unknown) were relatively unusual in the northern part of the SW region, with catchment 29 and Jakobshavn having 10.8% and 7.8% of lake frequency and 5.9% and 7.0% of lake area unclassified. Fredrikshåb Isblink however had 23% frequency and 19% lake area unclassified, Sermilik had 25% of frequency and 26% lake area unclassified, and Arsuk Bræ had 24% of frequency and 18% of lake area unclassified. This made these three of the most difficult to classify catchments on the ice sheet, and all three are clustered at the southern tip of the ice sheet. The catchments of Narssap sermia and Nordenskiöld contained the largest number of fast-draining lakes of any catchments of the ice sheet, accounting for 20% and 26% of all fast-draining lakes respectively. This large number of fast-draining lakes was partly due to the large number of lakes in both catchments, although a large proportion of lakes in both catchments drained (16% and 15% of lakes, 22% and 20% by lake area).

The distribution of fast-draining lakes in the NW region was not even. Fast-draining lakes were reasonably common in catchments 28 (Sermeq Avangnardleq), 30, 31, and

Table 6.3: Lake drainage types by frequency and area for all catchments of the GrIS. Catchments are presented in clockwise order from the southern tip of the ice sheet, using the catchment numbers from Figure 3.5. Catchments are grouped into regions, which are divided by horizontal lines. Data are averaged over all five years

			Frequency				Area km^2			
Region	No.	Name	Fa	Sl	Fr	Un	Fa	Sl	Fr	Un
	14	Nordbogletscher	-	-	-	-	-	-	-	-
	27	Arsuk Bræ	0.2	1.0	2.2	0.6	0.1	0.4	0.9	0.2
	16	Sermilik	-	4.4	4.6	1.4	-	2.4	2.4	1.1
	22	Frederikshab Isblink	5.2	11.2	21.2	6.4	3.3	5.9	13.1	3.5
SW	13	Narssap	4.2	15.4	23.2	3.6	3.5	10.6	18.4	3.3
	21	Narssap sermia	53.8	125.0	122.4	30.4	69.7	83.5	128.5	27.5
	15	Nordenskiöld	67.2	193.0	169.2	22.0	93.3	128.9	206.5	16.5
	25	Jakobshavn	8.4	21.4	49.8	3.4	9.9	13.9	59.9	2.4
	29	Unnamed	12.6	21.0	18.0	4.0	10.0	9.5	14.7	1.8
	28	Sermeq Avang.	3.2	7.8	19.4	0.8	2.7	4.4	18.0	1.0
	30	Unnamed	4.4	21.8	45.8	4.0	3.8	11.3	40.9	2.9
	9	Rinks	0.2	3.4	11.2	0.4	0.3	3.5	7.4	0.3
NW	31	Unnamed	13.6	70.6	107.0	10.6	8.8	40.2	79.7	4.5
	3	Hayes	0.8	8.6	25.0	0.2	0.4	5.7	16.4	0.2
	32	Steenstrup	12.8	26.8	54.2	4.4	10.8	15.6	41.3	2.6
	5	Kong Oscar	-	2.8	3.6	0.6	-	1.0	3.0	0.2
	33	Unnamed	1.8	9.0	22.8	2.8	1.0	4.9	11.6	1.3
	4	Humboldt	9.4	7.2	20.6	4.4	3.7	3.7	12.9	2.6
	34	Unnamed	-	-	-	-	-	-	-	-
	8	Petermann	2.8	6.6	12.2	1.6	1.0	4.3	8.5	1.1
	35	Unnamed	0.8	2.2	6.4	0.2	5.2	4.2	8.9	0.2
N	10	Ryder	0.6	4.0	9.4	2.2	1.0	2.5	10.8	3.6
	36	Unnamed	0.4	1.0	0.8	-	0.1	0.3	0.3	-
	7	Ostenfeld	-	0.2	2.0	-	-	0.0	1.1	-
	37	Unnamed	0.2	0.2	-	0.6	0.2	0.2	-	0.2
	1	Academy	0.2	0.4	2.6	1.0	0.2	0.4	1.6	0.2
	38	Unnamed	0.4	2.2	5.8	0.2	0.2	1.4	4.7	0.3
	39	Unnamed	-	1.0	0.6	0.2	-	0.3	0.2	0.0
NE	6	Nioghlvfjerdsbræ	4.8	9.0	49.4	2.8	4.4	5.2	68.8	1.1
	40	Unnamed	8.6	6.6	23.6	2.0	9.2	6.2	22.2	1.5
	12	Zachariae	6.8	8.0	19.2	1.2	10.3	6.5	24.1	1.5
	11	Storstrømmen	22.6	34.4	31.8	4.0	22.5	25.3	29.2	5.1
	41	Walterhausen	5.8	25.0	21.2	2.4	4.4	13.3	17.0	1.0
E	2	Daugaard-Jensen	1.2	4.4	10.4	0.0	0.7	2.0	5.0	0.0
	42	K. Christian IV	4.0	19.4	23.8	2.6	4.4	13.1	21.1	1.5
	26	Kangerdlugssuaq	2.0	10.0	12.6	0.4	1.2	5.3	6.0	0.1
	19	Schweizerland	0.6	4.4	1.4	0.8	0.1	1.7	0.2	0.4
	23	Helheim	0.2	1.2	-	0.4	0.0	0.4	-	0.1
SE	20	Johan Peterson	-	-	-	-	-	-	-	-
	24	Ikertivaq	-	-	-	-	-	-	-	-
	17	Koge	-	-	-	-	-	-	-	-
	18	SE Fjords	-	1.6	0.4	0.4	-	0.4	0.1	0.1

Table 6.4: Lake drainage types by frequency and area for all catchments of the GrIS, expressed as a percentage of all lakes in each catchment. Catchments are presented in clockwise order from the southern tip of the ice sheet using the catchment numbers from Figure 3.5. Data are averaged over all five years.

			Frequency				Area km^2			
Region	No.	Name	Fa	Sl	Fr	Un	Fa	Sl	Fr	Un
	14	Nordbogletscher	-	-	-	-	-	-	-	-
	27	Arsuk Bræ	5.0	25.0	55.0	15.0	6.9	21.5	57.7	13.8
	16	Sermilik	-	42.3	44.2	13.5	-	40.6	41.1	18.3
	22	Frederikshab Isblink	11.8	25.5	48.2	14.5	12.7	22.8	51.0	13.5
SW	13	Narssap	9.1	33.2	50.0	7.8	9.6	29.6	51.5	9.3
	21	Narssap sermia	16.2	37.7	36.9	9.2	22.5	27.0	41.6	8.9
	15	Nordenskiöld	14.9	42.8	37.5	4.9	21.0	29.0	46.4	3.7
	25	Jakobshavn	10.1	25.8	60.0	4.1	11.5	16.2	69.5	2.8
	29	Unnamed	22.7	37.8	32.4	7.2	27.8	26.3	40.9	5.0
	28	Sermeq Avang.	10.3	25.0	62.2	2.6	10.3	17.0	69.0	3.7
	30	Unnamed	5.8	28.7	60.3	5.3	6.4	19.2	69.4	5.0
	9	Rinks	1.3	22.4	73.7	2.6	2.5	30.3	64.4	2.8
	31	Unnamed	6.7	35.0	53.0	5.3	6.6	30.2	59.8	3.4
NW	3	Hayes	2.3	24.9	72.3	0.6	1.9	24.9	72.2	1.0
	32	Steenstrup Gl.	13.0	27.3	55.2	4.5	15.3	22.3	58.7	3.7
	5	Kong Oscar	-	40.0	51.4	8.6	-	23.7	71.8	4.5
	33	Unnamed	4.9	24.7	62.6	7.7	5.3	26.0	61.6	7.1
	4	Humboldt	22.6	17.3	49.5	10.6	16.3	16.3	56.1	11.4
	34	Unnamed	-	-	-	-	-	-	-	-
	8	Petermann	12.1	28.4	52.6	6.9	6.8	29.0	56.9	7.3
	35	Unnamed	8.3	22.9	66.7	2.1	28.3	22.9	47.8	1.0
N	10	Ryder	3.7	24.7	58.0	13.6	5.4	13.8	60.6	20.2
	36	Unnamed	18.2	45.5	36.4	-	18.3	45.0	36.7	-
	7	Ostenfeld	-	9.1	90.9	-	-	1.1	98.9	-
	37	Unnamed	20.0	20.0	-	60.0	26.1	41.3	-	32.6
	1	Academy	4.8	9.5	61.9	23.8	7.0	16.6	69.0	7.5
	38	Unnamed	4.7	25.6	67.4	2.3	2.3	21.1	71.9	4.7
	39	Unnamed	-	55.6	33.3	11.1	-	65.0	30.0	5.0
NE	6	Nioghlvfjerdsbræ	7.3	13.6	74.8	4.2	5.6	6.6	86.5	1.4
	40	Unnamed	21.1	16.2	57.8	4.9	23.5	16.0	56.9	3.7
	12	Zachariae	19.3	22.7	54.5	3.4	24.4	15.3	56.9	3.5
	11	Storstrømmen	24.4	37.1	34.3	4.3	27.4	30.8	35.6	6.3
	41	Walterhausen	10.7	46.0	39.0	4.4	12.3	37.2	47.7	2.7
E	2	Daugaard-Jensen	7.5	27.5	65.0	-	8.5	25.9	65.6	-
	42	K. Christian IV	8.0	39.0	47.8	5.2	10.9	32.7	52.7	3.7
	26	Kangerdlugssuaq	8.0	40.0	50.4	1.6	9.5	41.8	47.7	1.0
	19	Schweizerland	8.3	61.1	19.4	11.1	4.7	70.5	10.0	14.7
	23	Helheim	11.1	66.7	-	22.2	2.8	80.6	-	16.7
SE	20	Johan Peterson	-	-	-	-	-	-	-	-
	24	Ikertivaq	-	-	-	-	-	-	-	-
	17	Koge	-	-	-	-	-	-	-	-
	18	SE Fjords	-	66.7	16.7	16.7	-	71.1	8.9	20.0

Table 6.5: Lake drainage types by frequency and area for all catchments of the ice sheet, expressed as a percentage of all lakes of that drainage type for the whole GrIS. Catchments are presented in clockwise order from the southern tip of the ice sheet using the catchment numbers from Figure 3.5. Data are averaged over all five years.

			Frequency				Area km^2			
Region	No.	Name	Fa	Sl	Fr	Un	Fa	Sl	Fr	Un
	14	Nordbogletscher	-	-	-	-	-	-	-	-
	27	Arsuk Bræ	0.1	0.1	0.2	0.5	0.0	0.1	0.1	0.3
	16	Sermilik	-	0.6	0.5	1.1	-	0.6	0.3	1.2
	22	Frederikshab Isblink	2.0	1.6	2.2	5.2	1.1	1.3	1.4	3.9
SW	13	Narssap	1.6	2.2	2.4	2.9	1.2	2.4	2.0	3.7
	21	Narssap sermia	20.7	18.1	12.8	24.7	24.4	19.0	14.2	30.6
	15	Nordenskiöld	25.9	27.9	17.7	17.9	32.6	29.4	22.8	18.3
	25	Jakobshavn	3.2	3.1	5.2	2.8	3.5	3.2	6.6	2.7
	29	Unnamed	4.8	3.0	1.9	3.3	3.5	2.2	1.6	2.0
	28	Sermeq Avang.	1.2	1.1	2.0	0.7	0.9	1.0	2.0	1.1
	30	Unnamed	1.7	3.1	4.8	3.3	1.3	2.6	4.5	3.3
	9	Rinks	0.1	0.5	1.2	0.3	0.1	0.8	0.8	0.4
NW	31	Unnamed	5.2	10.2	11.2	8.6	3.1	9.2	8.8	5.0
	3	Hayes	0.3	1.2	2.6	0.2	0.2	1.3	1.8	0.3
	32	Steenstrup	4.9	3.9	5.7	3.6	3.8	3.6	4.6	2.9
	5	Kong Oscar	-	0.4	0.4	0.5	-	0.2	0.3	0.2
	33	Unnamed	0.7	1.3	2.4	2.3	0.3	1.1	1.3	1.5
	4	Humboldt	3.6	1.0	2.2	3.6	1.3	0.9	1.4	2.9
	34	Unnamed	-	-	-	-	-	-	-	-
	8	Petermann	1.1	1.0	1.3	1.3	0.4	1.0	0.9	1.2
	35	Unnamed	0.3	0.3	0.7	0.2	1.8	1.0	1.0	0.2
N	10	Ryder	0.2	0.6	1.0	1.8	0.3	0.6	1.2	4.0
	36	Unnamed	0.2	0.1	0.1	-	0.0	0.1	0.0	-
	7	Ostenfeld	-	0.0	0.2	-	-	0.0	0.1	-
	37	Unnamed	0.1	0.0	-	0.5	0.1	0.1	-	0.2
	1	Academy	0.1	0.1	0.3	0.8	0.1	0.1	0.2	0.2
	38	Unnamed	0.2	0.3	0.6	0.2	0.1	0.3	0.5	0.3
	39	Unnamed	-	0.1	0.1	0.2	-	0.1	0.0	0.0
NE	6	Nioghlvfjerdsbræ	1.8	1.3	5.2	2.3	1.5	1.2	7.6	1.2
	40	Unnamed	3.3	1.0	2.5	1.6	3.2	1.4	2.5	1.6
	12	Zachariae	2.6	1.2	2.0	1.0	3.6	1.5	2.7	1.6
	11	Storstrømmen	8.7	5.0	3.3	3.3	7.8	5.8	3.2	5.7
	41	Walterhausen	2.2	3.6	2.2	2.0	1.5	3.0	1.9	1.1
E	2	Daugaard-Jensen	0.5	0.6	1.1	-	0.2	0.5	0.6	-
	42	K. Christian IV	1.5	2.8	2.5	2.1	1.5	3.0	2.3	1.7
	26	Kangerdlugssuaq	0.8	1.4	1.3	0.3	0.4	1.2	0.7	0.1
	19	Schweizerland	0.2	0.6	0.1	0.7	0.0	0.4	0.0	0.4
	23	Helheim	0.1	0.2	-	0.3	0.0	0.1	-	0.1
SE	20	Johan Peterson	-	-	-	-	-	-	-	-
	24	Ikertivaq	-	-	-	-	-	-	-	-
	17	Koge	-	-	-	-	-	-	-	-
	18	SE Fjords	-	0.2	0.0	0.3	-	0.1	0.0	0.1

Table 6.6: Frequency of fast lake-drainages for all years studied (2005–2009), presented by catchment. Catchments are presented in clockwise order from the southern tip of the ice sheet (Kap Farvel). Similar tables for slow and freezing lakes are given in Appendix B as Tables B.8, B.9, and B.10.

No.	Name	2005	2006	2007	2008	2009
14	Nordbogletscher	-	-	-	-	-
27	Arsuk Bræ	-	-	-	-	1
16	Sermilik	-	-	-	-	-
22	Frederikshab Isblink	1	6	10	4	5
13	Narssap	2	4	7	5	3
21	Narssap Sermia	33	52	67	79	38
15	Nordenskiöld	67	58	93	72	46
25	Jakobshavn	7	8	12	7	8
29	Unnamed	12	12	14	13	12
28	Sermeq Avangnardleq	1	2	6	3	4
30	Unnamed	5	3	8	4	2
9	Rinks	1	-	-	-	-
31	Unnamed	12	16	10	15	15
3	Hayes	-	1	-	2	1
32	Steenstrup	11	11	9	12	21
5	Kong Oscar	-	-	-	-	-
33	Unnamed	3	1	2	2	1
4	Humboldt	12	3	7	8	17
34	Unnamed	-	-	-	-	-
8	Petermann	3	1	2	4	4
35	Unnamed	1	-	-	2	1
10	Ryder	-	1	-	2	-
36	Unnamed	-	-	-	1	1
7	Ostenfeld	-	-	-	-	-
37	Unnamed	-	-	-	-	1
1	Academy	1	-	-	-	-
38	Unnamed	1	1	-	-	-
39	Unnamed	-	-	-	-	-
6	Nioghlvfjerdsbræ	7	2	5	8	2
40	Unnamed	6	5	8	14	10
12	Zachariae	9	-	9	14	2
11	Storstrømmen	29	19	18	21	26
41	Walterhausen	9	6	4	5	5
2	Daugaard-Jensen	1	1	3	-	1
42	K. Christian IV	6	5	4	4	1
26	Kangerdlugssuaq	3	2	2	1	2
19	Schweizerland	-	1	1	1	-
23	Helheim	-	-	-	1	-
20	Johan Peterson	-	-	-	-	-
24	Ikertivaq	-	-	-	-	-
17	Koge	-	-	-	-	-
18	SE Fjords	-	-	-	-	-

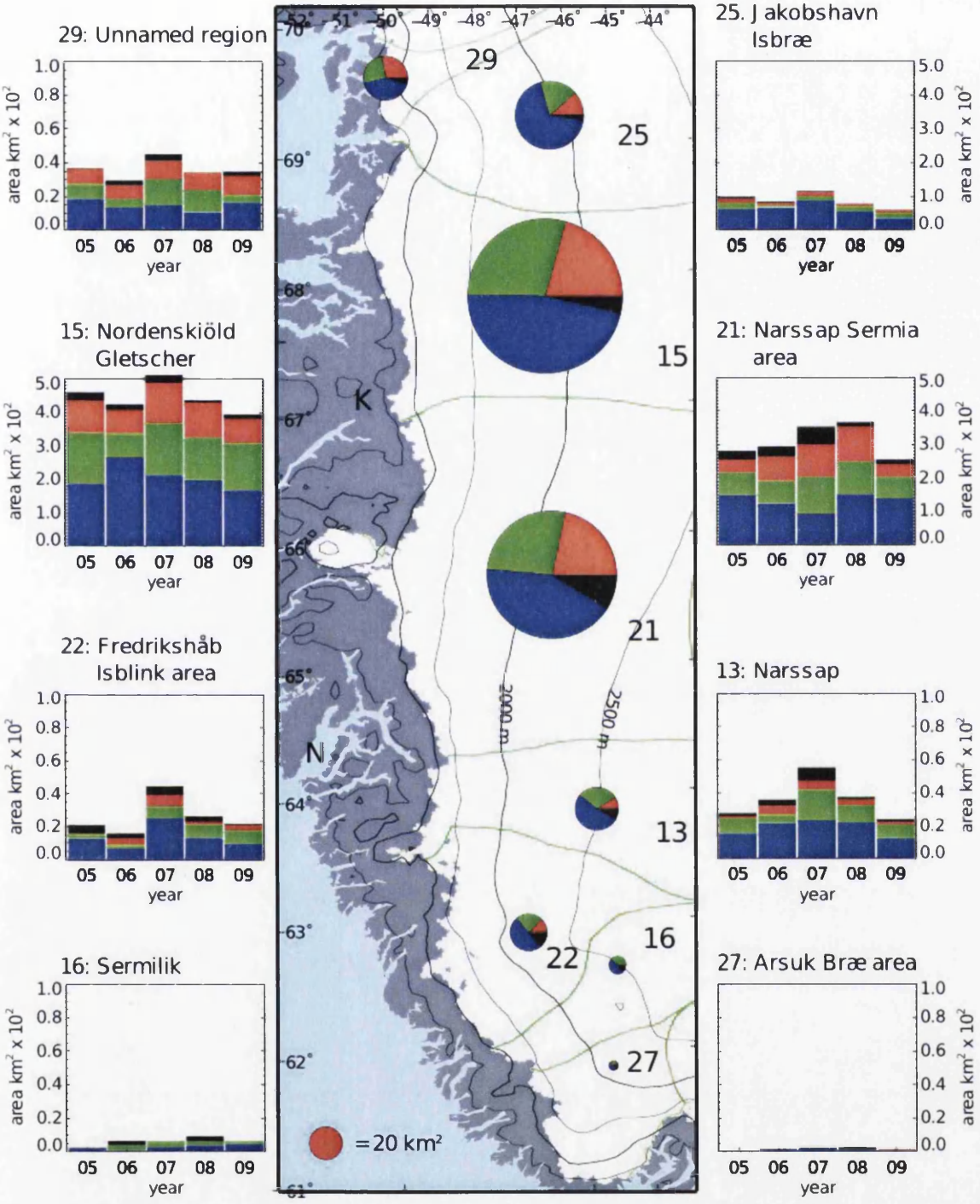

Figure 6.6: The distribution of lake drainage types in SW Greenland. Lake size is represented by maximum surface area for each year. The pie charts on the central figure have an area proportional to the mean total maximum lake area in that catchment, and divided into fast draining (red), slow draining (green), freezing (blue), and unknown lake types. The bar charts show the area and proportions of lake drainage type per year. Note that catchments 15, 21, and 25 are shown with a different vertical scale. The same areas are shown on consistent vertical scales in Figure 5.18. K=Kangerlussuaq. N=Nuuk.

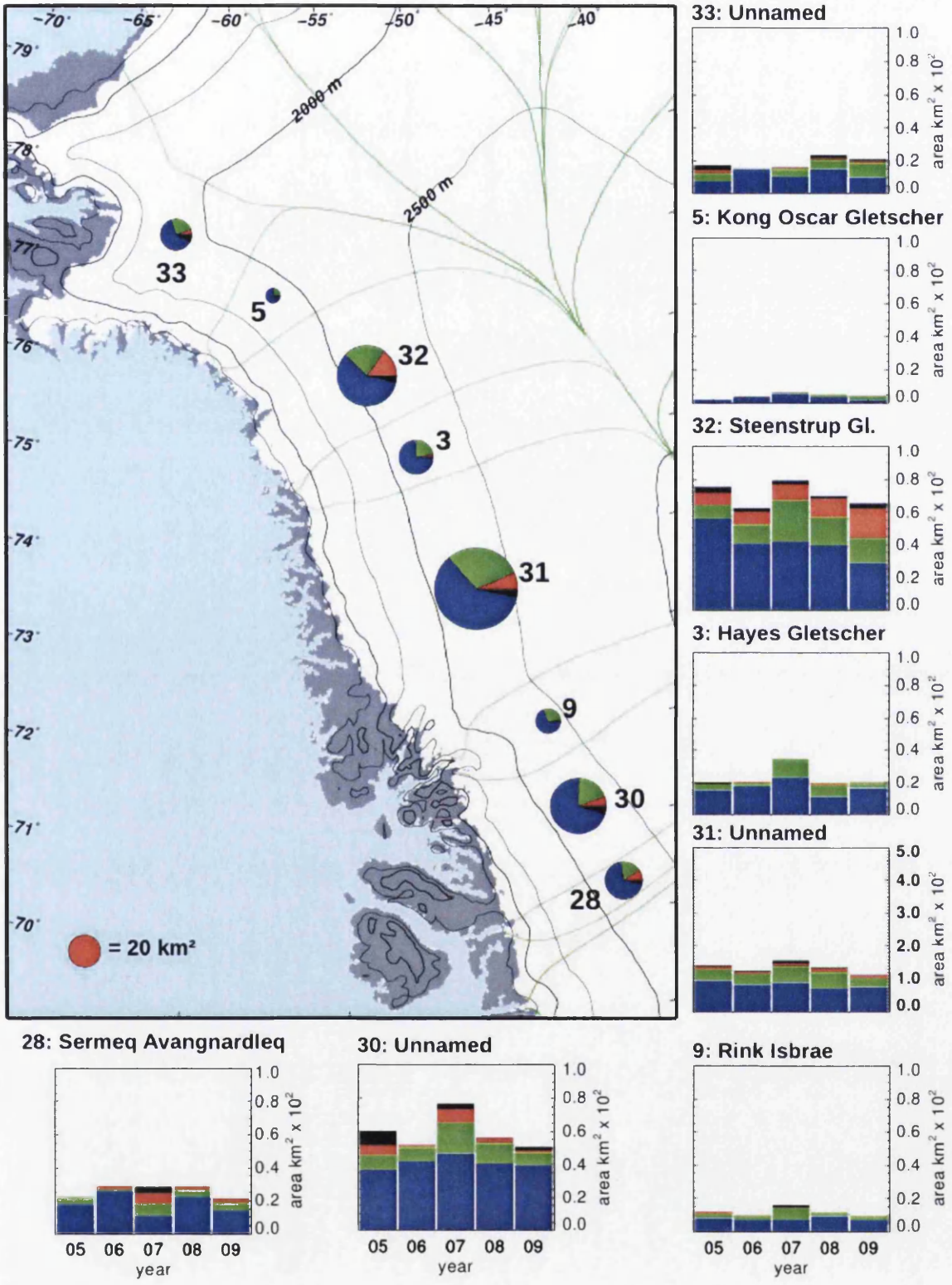

Figure 6.7: The distribution of lake drainage types in NW Greenland, showing fast draining (red), slow draining (green), freezing (blue), and unknown (black) lakes. Note that catchment 31 is shown with a different vertical scale. The same areas are shown on consistent vertical scales in Figure 5.19.

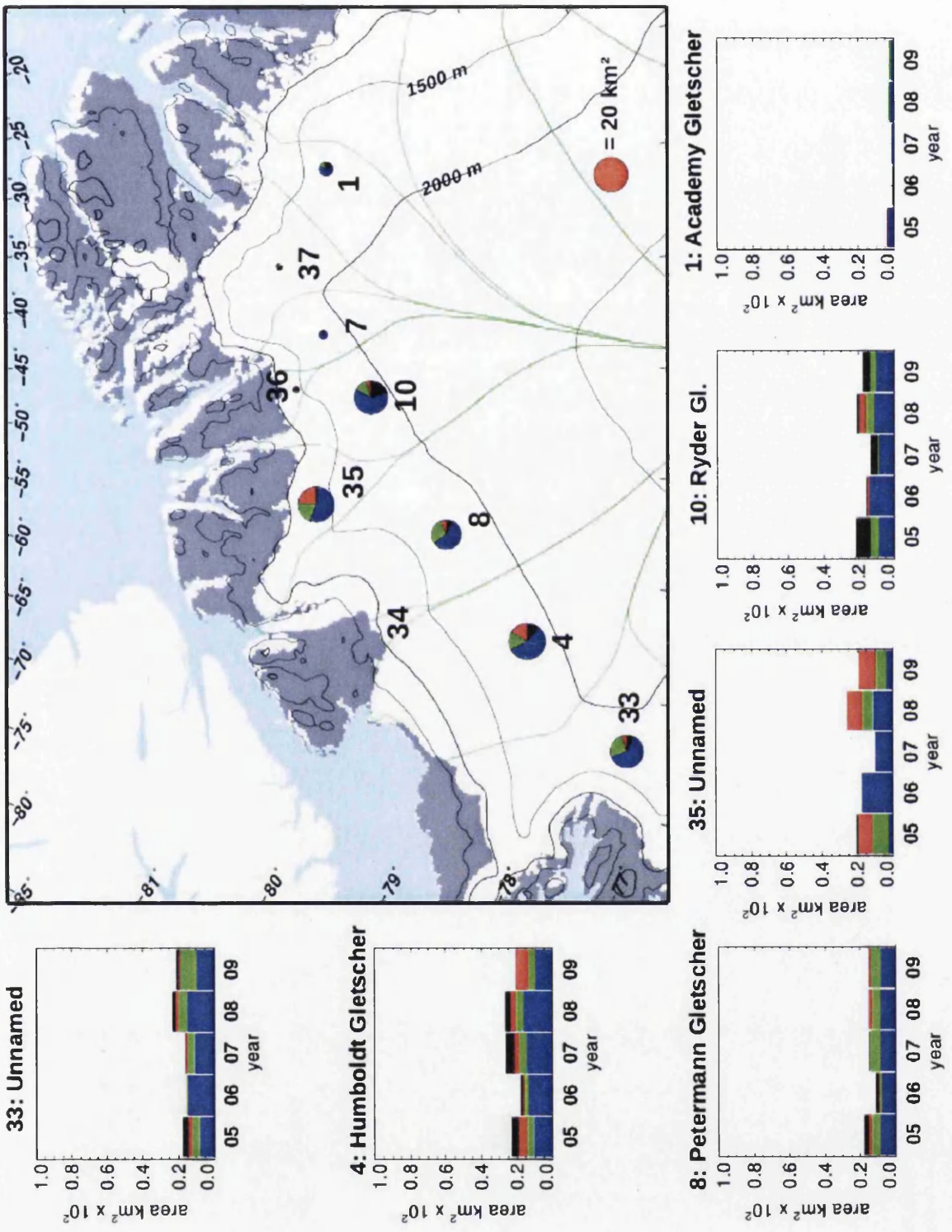

Figure 6.8: The distribution of lake drainage types in N Greenland, showing fast draining (red), slow draining (green), freezing (blue), and unknown (black) lakes. The total lake area of some catchments was too small to be plotted, hence the barplots are omitted.

32 (Steenstrup Gl.), indeed catchments 31 and 32 (Steenstrup Gl.) each contained $\sim$ 5% of all fast-draining lakes on the GrIS (Table 6.5). Fast-draining lakes were however very rare in catchment 3 (Haye's Gl.), and only one occurred in all five years in catchment 9 (Rink Isbræ), and none occurred in catchment 5 (Kong Oscar Gl.). Other drainage types largely followed regional trends, with a large proportion of the lakes in each region freezing, the smallest percentage frequency of freezing was 51% in the Kong Oscar catchment, the largest was 74% in the Rinks catchment.

The small number of lakes in the N region caused considerable variation in the differing proportions of drainage types, as a few lakes of a given drainage type were sufficient to cause large changes in the percentage of the lakes in a catchment with that drainage type. The Humboldt catchment had a large number of fast-draining lakes in each year studied, and accounted for 3.6% of all fast-draining lakes on the GrIS (Table 6.5).

Whilst catchments 38 and 39 in the NE contained few fast-draining lakes, fast-draining lakes were very prevalent in the remaining catchments of that region. The Zachariae, no. 40, and Storstrømmen catchments each had around 20% of lakes draining rapidly, and accounted for 9, 3, and 3% of all fast-draining lakes on the ice sheet respectively. Contrary to this overall pattern, no lakes drained rapidly in the Zachariae catchment in 2006, and only two did so in 2009 (Table 6.6). In Nioghlvf-jerdsbræ catchment fewer lakes drained rapidly (7%) despite these drainages being so common on the other two NE Ice Stream outlets (Zachariae and Storstrømmen). Instead, 75% of all lakes in the Nioghlvfjerdsbræ catchment froze, 5% of all freezing lakes on the GrIS were in this catchment (8% by lake area).

Fast lake-drainage events occurred in all E Greenland catchments, ranging from $\sim$ 1 per year on Daugaard-Jensen Gl., to $\sim$ 6 per year in the (large) Walterhausen catchment. No fast lake-drainages were detected on Daugaard-Jensen Gl. in 2008 (Table 6.6), yet three were detected in 2007.

Of the seven catchments of the SE region, only Kangerdlugssuaq had lakes draining rapidly in all years studied (Table 6.6). In all years but 2009, three lakes drained

rapidly in the SE region. These three lakes always included at least one in the Kangerdlugssuaq catchment, the remainder were usually in the Schweizerland area, and one fast lake-drainage was observed on Helheim Gl. in 2008. Whilst fast lake-drainages in the SE were most prevalent on Kangerdlugssuaq, this catchment still only accounted for $< 1\%$ of all fast-draining lakes, and only $< 0.5\%$ of fast draining lakes by area.

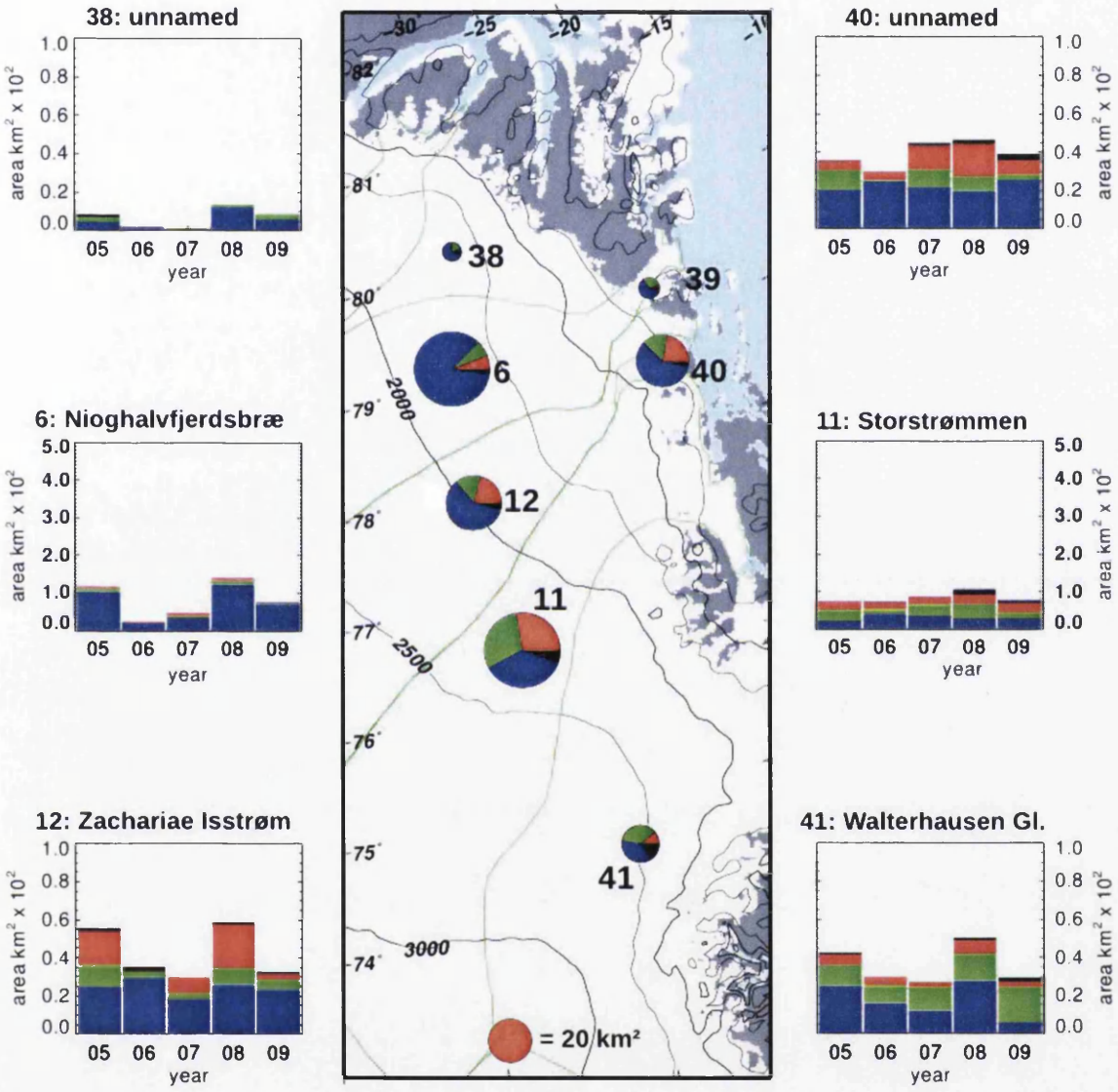

Figure 6.9: The distribution of lake drainage types in NE Greenland, showing fast draining (red), slow draining (green), freezing (blue), and unknown (black) lakes. Note that catchments 6 and 11 are shown with a different vertical scale. The same areas are shown on consistent vertical scales in Figure 5.21.

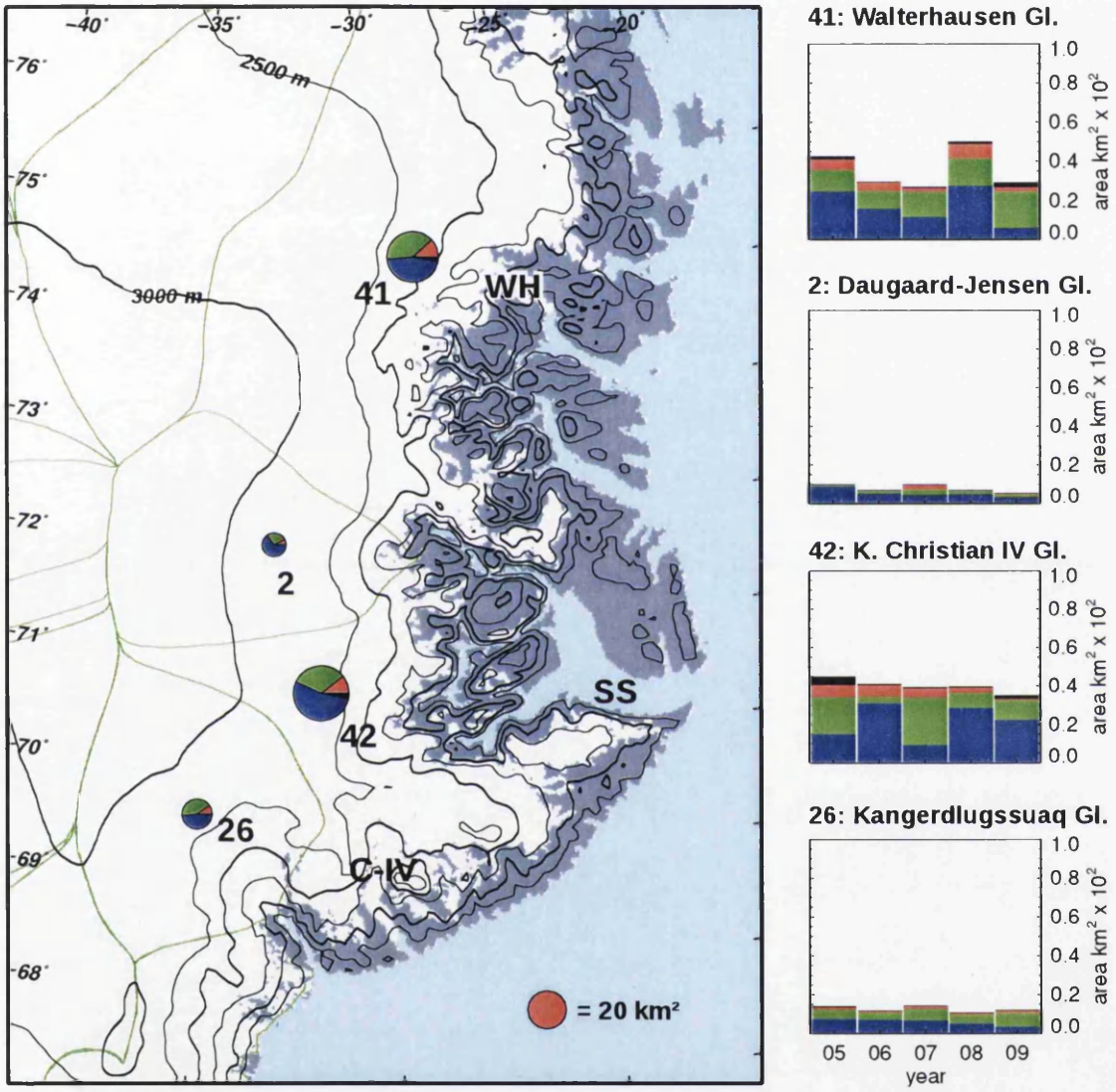

Figure 6.10: The distribution of lake drainage types in E Greenland, showing fast draining (red), slow draining (green), freezing (blue), and unknown (black) lakes. WH=Walterhausen Gl. SS=Scoresby Sund. C-IV=Christian IV Gl.

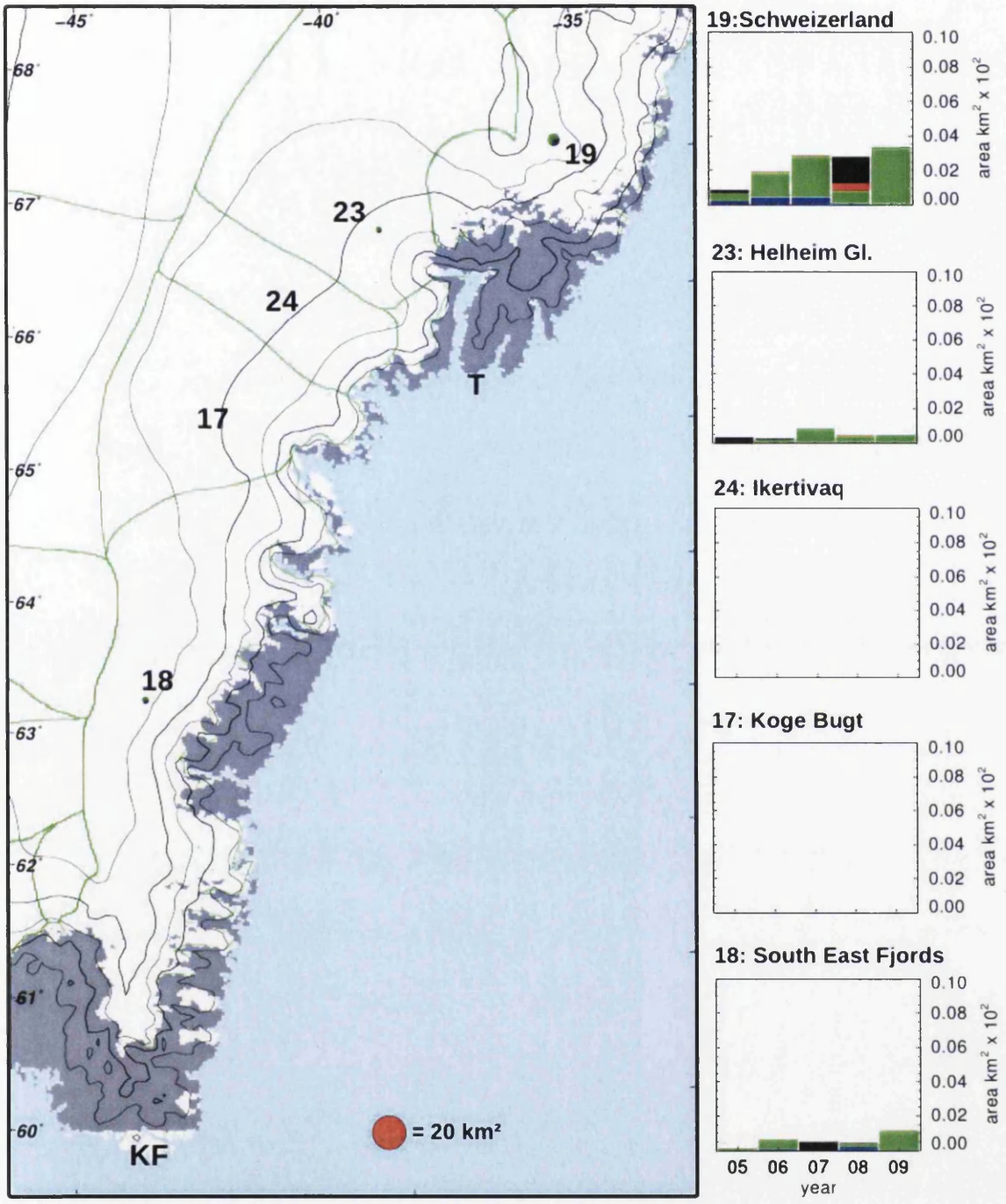

Figure 6.11: The distribution of lake drainage types in SE Greenland, showing fast draining (red), slow draining (green), freezing (blue), and unknown (black) lakes. Note that all barplots in this figure are on a different scale to Figures 6.6 - 6.10 owing to the very low number of lakes in this region.The same areas are shown on consistent vertical scales in Figures 5.23. T=Tasillaq. KF=Kap Farvel.

6.4 Intra-annual variation in fast lake-drainage

As the depths of the lakes studied are not known it is not possible to calculate the volume of water draining to the bed on each day; however the surface area of the lakes can be used as a proxy for lake volume. For each day of the melt season during the period 2005–2009, the total area of lakes draining rapidly in each region was summed, and is presented as Figure 6.12.

Given that 61% of all fast-draining lakes were found in the SW region, it is not surprising to discover that in most years far more lake area drained per day in the SW than in any other region. This was more pronounced in some years than others. In 2005, 2006, and 2008 there was at least double the area drained in one day in the SW than on any day in any other region. In 2007, on one day in the NE 19.6 km^2 of lake area drained rapidly, compared with a maximum of 31.7 km^2 in the SW. In 2009, there was the least variation in lake area draining rapidly per day between regions.

The day on which most water was delivered to the bed varied interannually, but was around day 200 (mid-July) in most years, and around day 180 (late-June) in the high-melt year 2007.

6.5 Characteristics of lakes of differing types

This section examines possible forcing factors behind different drainage types, i.e. testing hypotheses for why some lakes drain fast, while others freeze or drain slowly. Several plausible factors were chosen and tested. For each factor the rationale for choosing that factor is described, and then the results are presented graphically as a series of box and whisker plots, and then statistically through ANOVA and Tukey HSD tests to test whether differences in the mean of each variable between drainage types were significant. Interannual variation was tested using all the lakes in the dataset, from all regions. Interregional variation was tested for one year: 2005.

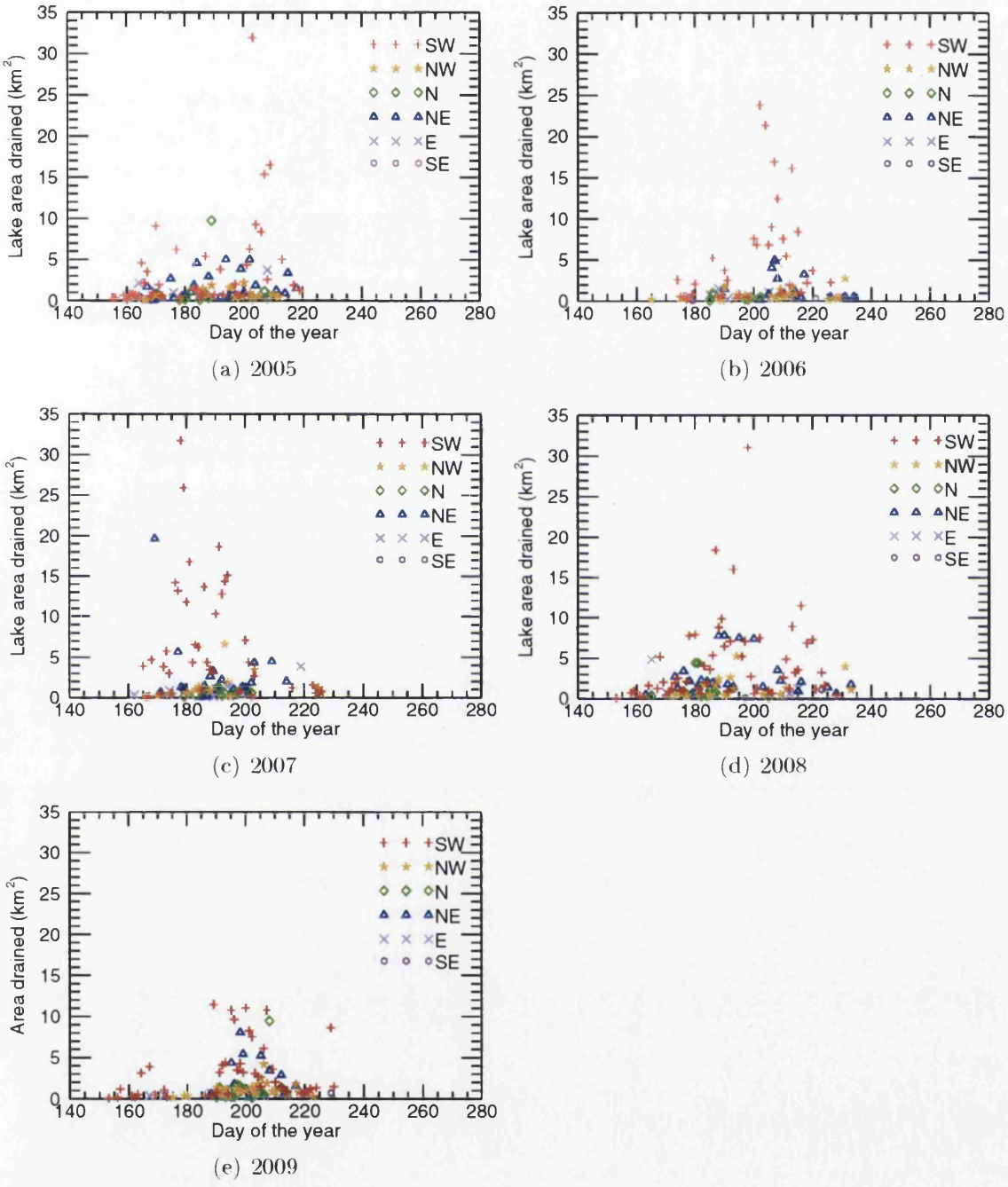

(a) 2005

(b) 2006

(c) 2007

(d) 2008

(e) 2009

Figure 6.12: The area of lakes draining rapidly per day, for each of the regions of the ice sheet, for the period 2005–2009.

The following hypotheses were tested.

- Do lakes need to reach a critical size before drainage can occur? This could be due either to a critical volume of water, or due to a lake covering more fractures increasing the chances of hydrofracture occurring. This could be tested by examining the area that lakes of different drainage types reach.
- Do some lakes freeze before they can drain either through or over the ice? It could be that a lake must be in position for a certain period of time before hydrofracture to the bed is possible. This would be indicated by lakes that freeze over having a shorter duration than those that drain rapidly.
- Are lakes more likely to drain over the surface (slow draining) on steeper surface slopes? It has been found that drainage by incision of the lake spillway channel is more likely to occur on steeper slope (Raymond and Nolan, 2000). If this were the case, all other factors being equal it would be expected that slow-draining lakes would form on steeper slopes, and freezing and fast-draining lakes would form on shallower gradients.
- Are lakes more likely to drain to the bed (fast draining) if they are sited on ice in a extensional regime? Hydrofracture to the base of the ice sheet may be easier if the ice is extending i.e. there is a positive strain rate. Extensional flow would also increase the chances of fractures being available for exploitation by hydrofracture.

Lake height and ice thickness are closely related. Whilst bed topography has an influence on ice thickness at any given point, in general the ice is thicker under points of higher elevation. As the relationship is not perfectly linear, differences in both elevation and ice thickness were tested. Two hypotheses are stated here relating to ice thickness and elevation:

- Are lakes more likely to freeze at higher elevations? This is related to the point about duration, it is possible that the shorter melt season at high elevations cause lakes to freeze before either mode of drainage can be completed.

- Are lakes less likely to drain rapidly if sited on thicker ice? The thicker the ice a lake is sited on, the more difficult the process of hydrofracture becomes. Therefore, it might be the case that lake drainage to the bed can only occur at lower elevations.

6.5.1 Area

Lake area was strongly skewed (Figure 5.14a), so statistical testing was carried out on the log transformed data, and Figure 6.13 is shown with a log-scaled y axis. In all years, lakes that drained slowly were found to be smaller than those which drained rapidly and those which froze (Figure 6.13), and this difference was significant in all years (Table 6.7). Fast-draining lakes grew larger than slow-draining lakes, and freezing lakes were larger than slow-draining lakes (significant in all years). However, freezing lakes were slightly smaller than fast-draining lakes, which was significant in all years except 2005. When testing inter-regional variation in 2005, the overall pattern was true for the SW and NE regions, for other regions the difference in area between drainage types was not significant (Table 6.7).

Table 6.7: ANOVA and Tukey HSD p values comparing log transformed lake areas for different drainage types for (a) the whole ice sheet in different years and (b) different regions of the ice sheet in 2005. p values < 0.05 indicate a significant difference in geometric mean lake area at 95% confidence level, and are highlighted in *italic text.* Tukey HSD values not calculated where ANOVA test not significant

(a)	2005	2006	2007	2008	2009
ANOVA	*0.000*	*0.000*	*0.000*	*0.000*	*0.000*
Freeze vs Fast	0.114	*0.000*	*0.000*	*0.010*	*0.000*
Slow vs Fast	*0.000*	*0.000*	*0.000*	*0.000*	*0.000*
Slow vs Freeze	*0.000*	*0.000*	*0.000*	*0.000*	*0.021*

(b)	GrIS	SW	NW	N	NE	E	SE
ANOVA	*0.000*	*0.000*	0.3789	0.6735	*0.000*	0.1854	0.4814
Freeze vs Fast	0.114	0.114	-	-	0.125	-	-
Slow vs Fast	*0.000*	*0.000*	-	-	0.126	-	-
Slow vs Freeze	*0.000*	*0.000*	-	-	*0.000*	-	-

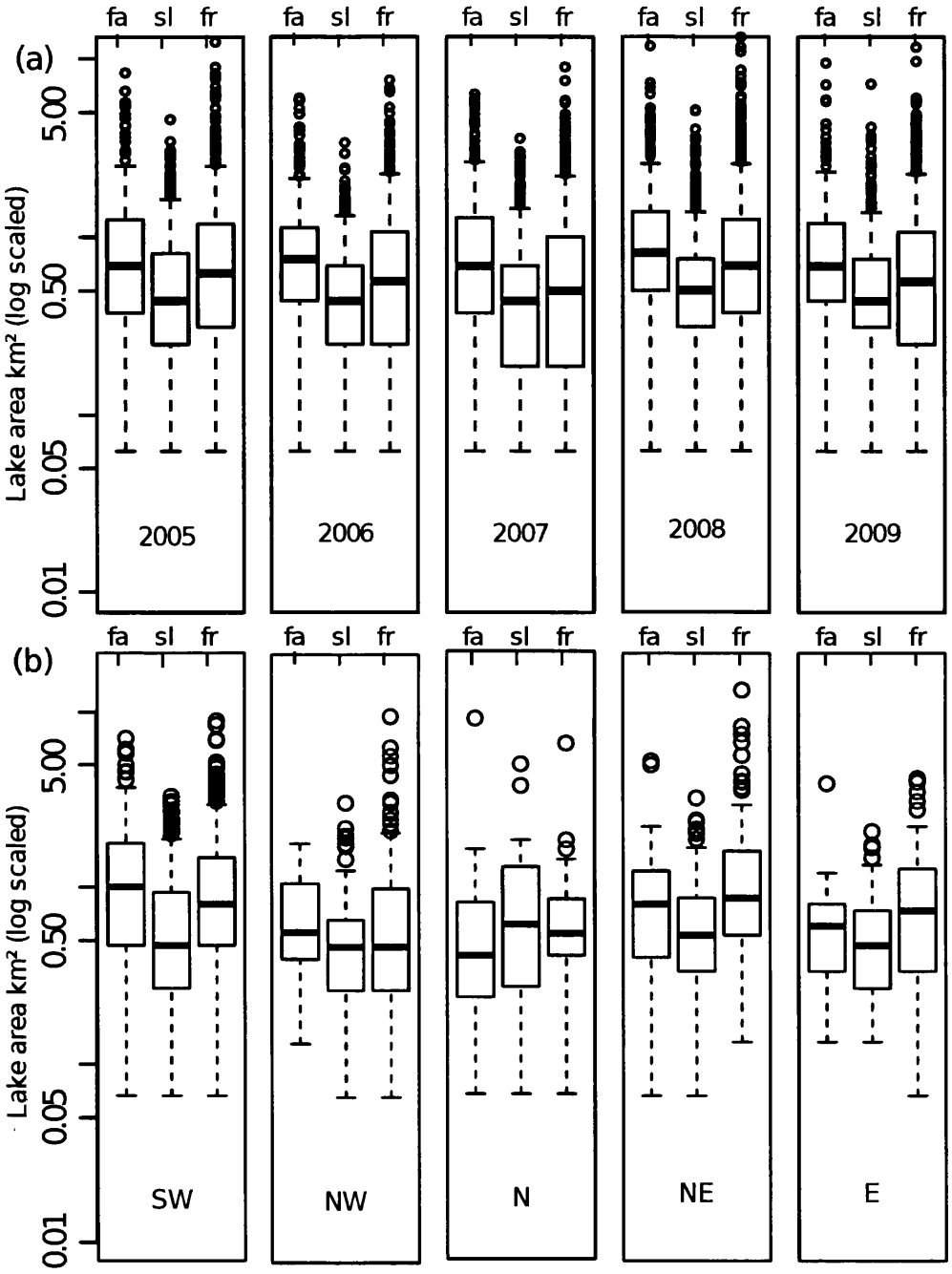

Figure 6.13: Box and whisker plots showing the differences in the areas of fast draining (Fa), slow draining (Sl), and freezing (Fr) lakes. Owing to skewness, y axes are log scaled. Lakes on the whole GrIS are shown (a), followed by separate regions (b). The SE region is omitted due to low frequency of fast drainage.

6.5.2 Duration

Duration was defined as the period between the first and last observations of each lake. While not as skewed as area, the duration data was skewed enough to require log transforming before parametric statistical tests could be performed, and the geometric mean is used as the preferred measure of central tendency (Table 6.8). In all years, fast-draining lakes had the shortest mean duration, slow-draining lakes lasted longer, and lakes that froze lasted the longest of all with a mean duration double that of fast-draining lakes (significant at 99.9% confidence level, Table 6.9, Figure 6.14). This same pattern occurred for all regions of the ice sheet. There was a significant difference in mean duration of different drainage types in all regions (in 2005), although the difference between fast and slow-draining lakes was only significant in the SW and E.

Table 6.8: Geometric mean duration (days) for different drainage types.

	2005	2006	2007	2008	2009
Fast	12.1	10.1	9.7	16.0	11.4
Slow	16.2	15.4	16.0	18.5	16.3
Freeze	32.5	28.4	38.8	25.3	31.4

Table 6.9: ANOVA and Tukey HSD p values comparing lake duration for different drainage types for (a) the whole ice sheet in different years and (b) different regions of the ice sheet in 2005. p values significant at the 95% confidence level ($p < 0.05$) are highlighted in *italics*, and represent a significant difference in geometric mean lake duration.

(a)	2005	2006	2007	2008	2009
ANOVA	*0.000*	*0.000*	*0.000*	*0.000*	*0.000*
Freeze vs Fast	*0.000*	*0.000*	*0.000*	*0.000*	*0.000*
Slow vs Fast	*0.000*	*0.000*	*0.000*	0.089	*0.000*
Slow vs Freeze	*0.000*	*0.000*	*0.000*	*0.000*	*0.000*

(b)	GrIS	SW	NW	N	NE	E	SE
ANOVA	*0.000*	*0.000*	*0.000*	*0.000*	*0.000*	*0.000*	*0.002*
Freeze vs Fast	*0.000*	*0.000*	*0.000*	*0.000*	*0.000*	*0.000*	*0.007*
Slow vs Fast	*0.000*	*0.005*	0.239	0.928	0.708	*0.001*	0.255
Slow vs Freeze	*0.000*	*0.000*	*0.000*	*0.000*	*0.000*	*0.000*	*0.020*

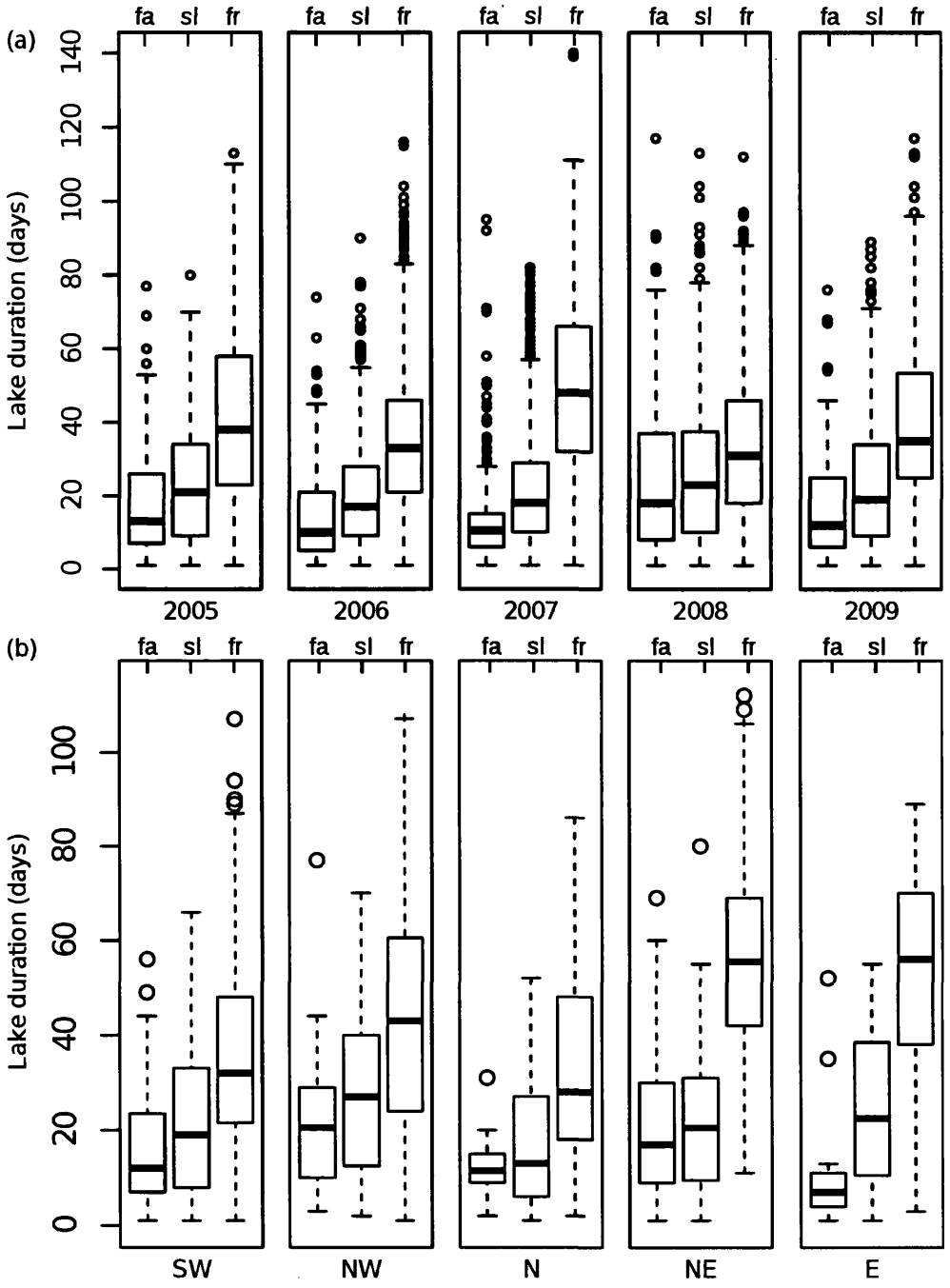

Figure 6.14: Box and whisker plots to compare the duration of lakes that drained fast (Fa), drained slowly (Sl), or froze (Fr). Freezing lakes consistently had the longest duration, and fast-draining lakes has the shortest duration. Although represented here on a linear y-axis, the data required log transforming before the ANOVA test could be performed.

6.5.3 Ice surface slope

The slope of the ice sheet at each lake was taken from the 5 km DEM described in Section 3.5.1. Due to outliers, probably the result of DEM errors, the slope data required log transformation before use. All lakes were found on shallow slopes, most of those (72%) with an incline of less than one degree (Figure 6.15, Table 6.10). For all years except 2007 (when differences in slope between drainage types were not significant), freezing lakes formed on the shallowest surface slopes. Slow-draining lakes formed on the steepest slopes in 2006, 2008, and 2009. In 2005 fast-draining lakes formed on the steepest slopes, however this was only the case for the SW region, slow-draining lakes formed on the steepest slopes in other parts of the ice sheet. Although slow-draining lakes formed on slightly steeper slopes than fast-draining lakes, this was not significant all regions except the E (Table 6.11).

Table 6.10: Geometric mean slope angle (degrees) of the ice surface at lakes of different drainage types

	2005	2006	2007	2008	2009
Fast	0.79	0.76	0.70	0.72	0.81
Slow	0.78	0.86	0.74	0.78	0.81
Freeze	0.67	0.71	0.70	0.66	0.67

Table 6.11: ANOVA and Tukey HSD p values comparing surface slope at lakes of different drainage types for (a) the whole ice sheet in different years and (b) different regions of the ice sheet in 2005. *Values in italics* represent a statistically significant difference in geometric mean slope angle at the 95% confidence level.

(a)	2005	2006	2007	2008	2009
ANOVA	*0.000*	*0.000*	0.076	*0.000*	*0.000*
Freeze vs fast	0.832	*0.005*	-	0.056	0.976
Slow vs fast	*0.001*	0.486	-	0.423	*0.000*
Slow vs freeze	*0.000*	*0.000*	-	*0.000*	*0.000*

(b)	GrIS	SW	NW	N	NE	E	SE
ANOVA	*0.000*	*0.000*	*0.000*	0.101	0.537	*0.031*	0.241
Freeze vs fast	*0.001*	*0.000*	*0.002*	-	-	0.246	-
Slow vs fast	0.832	0.995	0.604	-	-	*0.027*	-
Slow vs freeze	*0.000*	*0.000*	*0.000*	-	-	0.390	-

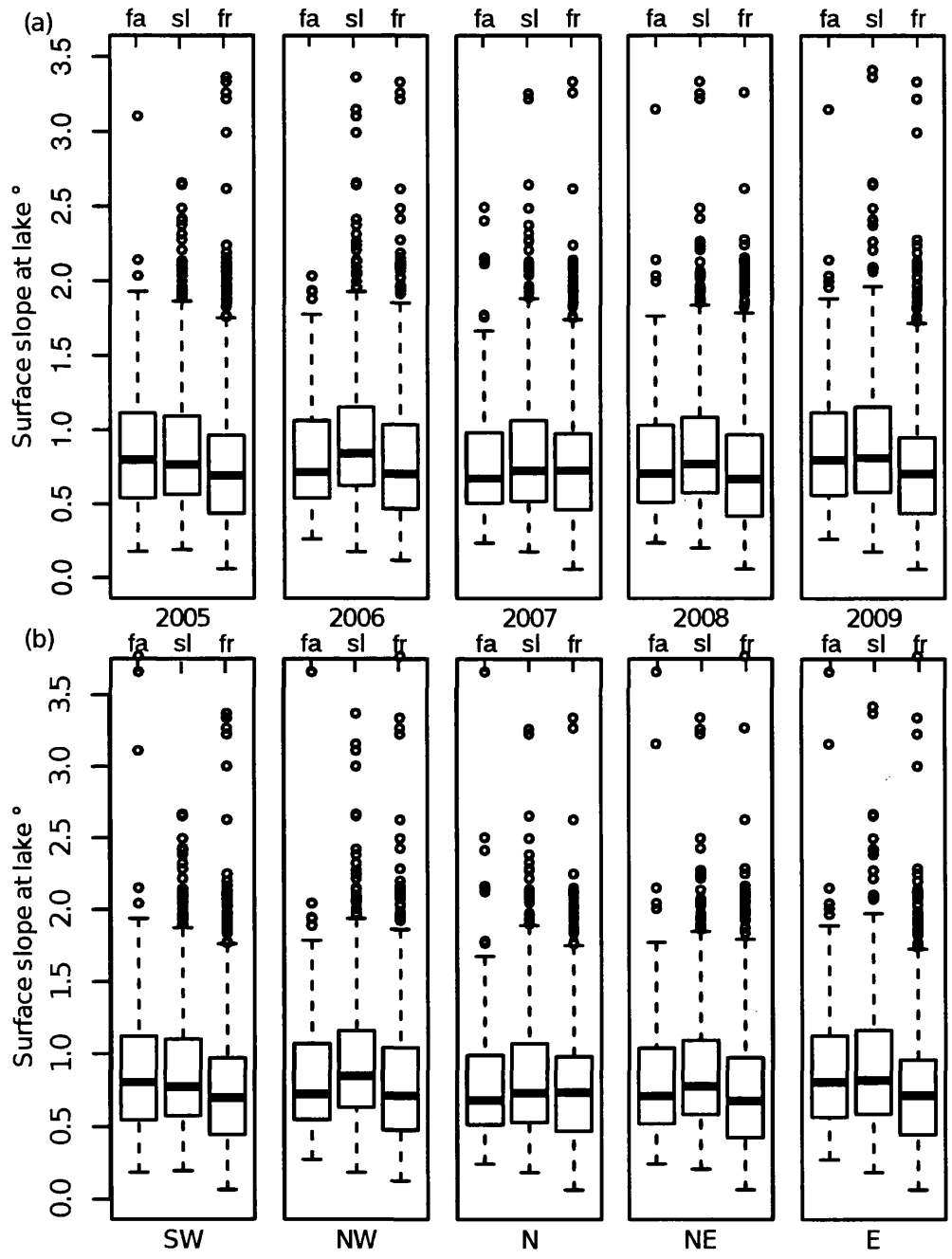

Figure 6.15: Box and whisker plots to compare the surface slope at lakes that drained fast (Fa), drained slowly (Sl), or froze (Fr). Outliers (circles) are probably a result of DEM errors.

6.5.4 Lake height above sea level and ice thickness

In all years, and in all regions, lakes that froze formed at higher elevations than those which did not (Figure 6.16, Table 6.12(a), significant at the 99.9% confidence level, see Table 6.13). In most years and regions, fast-draining lakes formed at lower elevations than slow draining and freezing lakes (usually significant at 95% confidence level, see Table 6.13). This difference in height also meant that fast-draining lakes formed over thinner ice, and freezing lakes formed over the thickest ice of all (Table 6.12(b), Figure 6.17).

Table 6.12: (a) Mean elevation (m) of lakes with different drainage types. (b) Mean ice thickness (m) below lakes with different drainage types

(a)

	2005	2006	2007	2008	2009
Fast	922	1059	1106	1032	942
Slow	1097	1063	1182	1101	1097
Freeze	1230	1198	1232	1251	1215

(b)

	2005	2006	2007	2008	2009
Fast	628	664	725	679	634
Slow	667	613	726	675	660
Freeze	873	821	870	860	835

Table 6.13: ANOVA and Tukey HSD p values comparing elevation at lakes of different drainage types for (a) the whole ice sheet in different years and (b) different regions of the ice sheet in 2005. p values below 0.05 indicate a significant difference between means at 95% confidence level, and are highlighted in *italic type.*

(a)	2005	2006	2007	2008	2009
ANOVA	*0.000*	*0.000*	*0.000*	*0.000*	*0.000*
Freeze vs fast	*0.000*	0.990	*0.009*	*0.011*	*0.000*
Slow vs fast	*0.000*	*0.000*	*0.000*	*0.000*	*0.000*
Slow vs freeze	*0.000*	*0.000*	*0.024*	*0.000*	*0.000*

(b)	GrIS	SW	NW	N	NE	E	SE
ANOVA	*0.000*	*0.000*	*0.000*	*0.000*	*0.000*	*0.000*	0.105
Freeze vs fast	*0.000*	*0.000*	*0.000*	*0.000*	*0.000*	*0.000*	-
Slow vs fast	*0.000*	*0.022*	*0.028*	*0.000*	0.152	*0.000*	-
Slow vs freeze	*0.000*	*0.000*	*0.000*	0.202	*0.001*	0.753	-

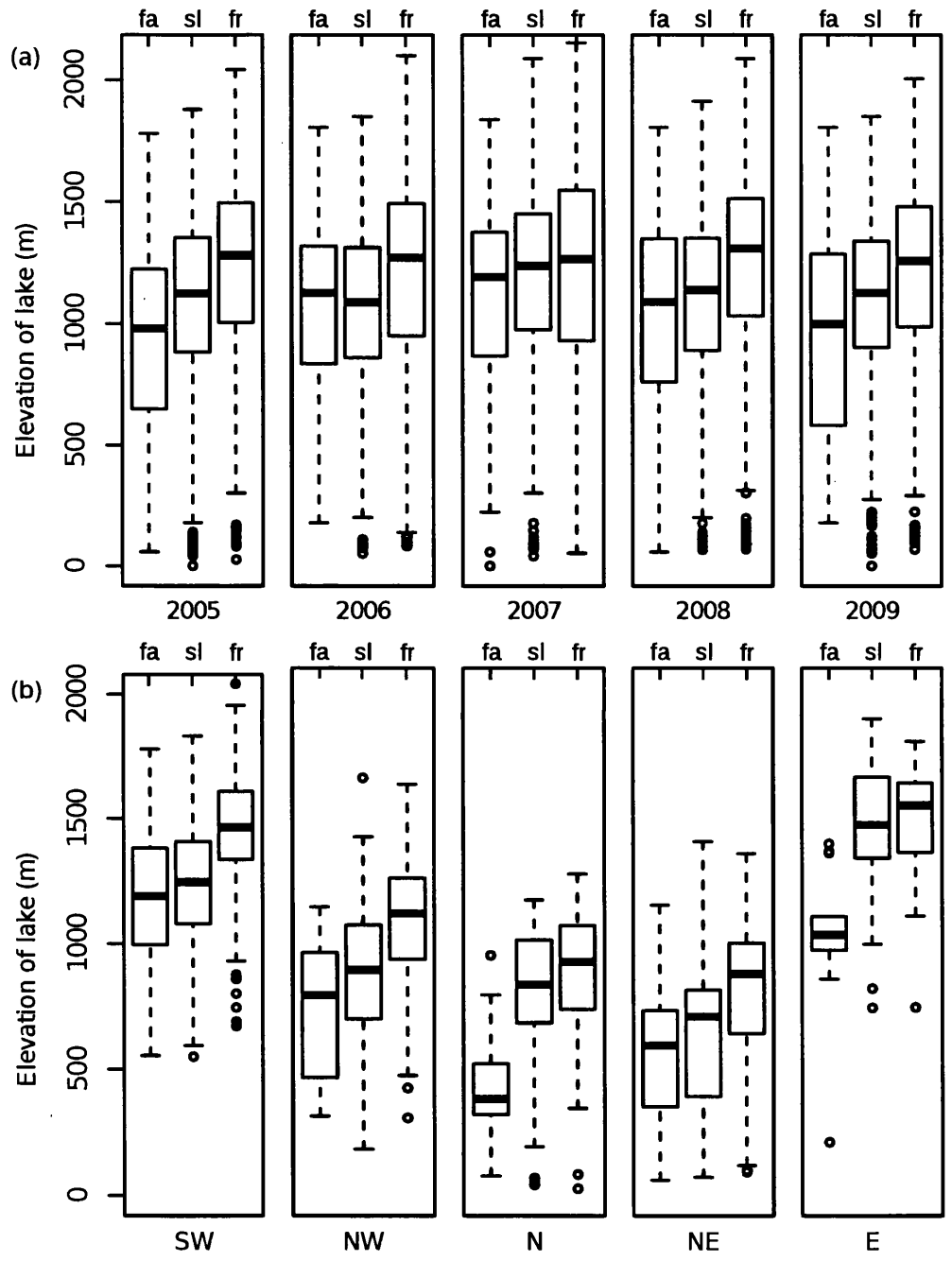

Figure 6.16: Box and whisker plots to compare the elevation of lakes that drained fast (Fa), drained slowly (Sl), or froze (Fr). Freezing lakes generally formed at higher elevations than slow or fast-draining lakes, and the range of the data shows that the highest lakes always froze

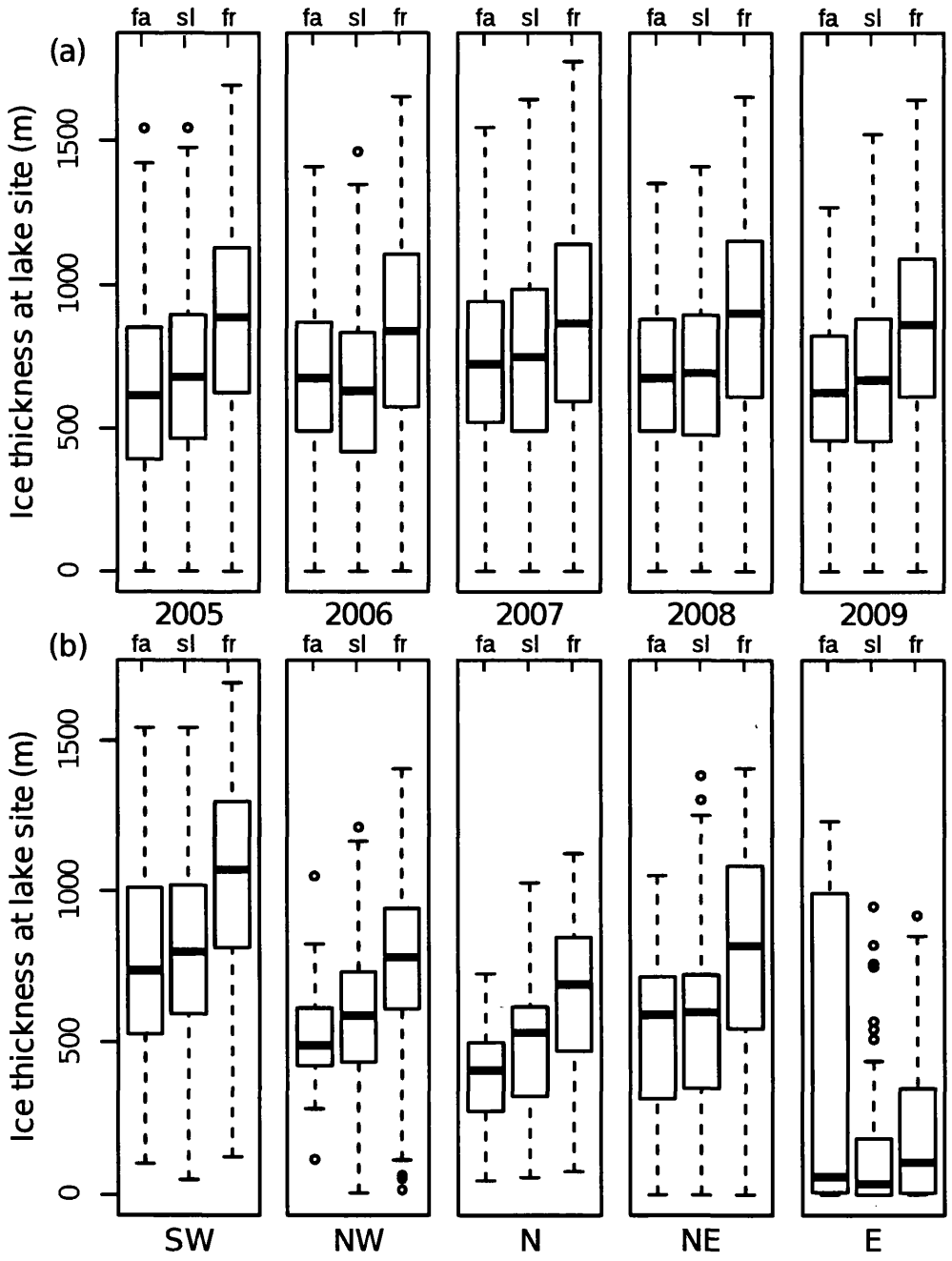

Figure 6.17: Box and whisker plots to compare the ice thickness at lakes that drained fast (Fa), drained slowly (Sl), or froze (Fr). The unusual values for the E region are presumably caused by the combination of the complexity of the E coast in that region, and the coarse resolution of the ice sheet thickness grid

6.5.5 Ice strain rate

Longitudinal strain rate ($\dot{\varepsilon}_{xx}$) calculated from the remotely sensed velocity data of Joughin *et al.* (2010) shows whether the ice at the site of a lake is extending or compressing. Positive numbers indicate that ice is accelerating in a downflow direction, and is therefore extending. Negative numbers indicate a deceleration downstream, and therefore compression. Mean strain-rate (Table 6.14) was 0.0017–0.0034 yr^{-1} for all years. In general, lakes were more likely to be experiencing positive strain rates (Figure 6.18), although many lakes were also found in compressive regimes. There were slight differences in strain rate between drainage types, with fast-draining lakes having slightly more positive mean strain-rates, and freezing lakes having the most negative, although the spread of values was large for all types (Figure 6.18). This difference in strain rates was not significant in any year studied however (Table 6.15).

Table 6.14: Mean ice strain rate $year^{-1}$ at lakes of different drainage type for the period 2005–2009. Positive numbers indicate that ice is extending due to acceleration

	2005	2006	2007	2008	2009
Fast	0.0031	0.0030	0.0031	0.0023	0.0034
Slow	0.0020	0.0026	0.0029	0.0028	0.0030
Freeze	0.0022	0.0022	0.0019	0.0017	0.0029

Table 6.15: ANOVA p values comparing strain rates at lakes of different drainage types. p values below 0.05 indicate a significant different at the 95% confidence level. No significant difference was found in strain rate between drainage type

	2005	2006	2007	2008	2009
ANOVA p	0.76	0.82	0.51	0.54	0.94

6.6 Drainage type persistence

Many lakes had the same drainage type in several years, for example some lakes almost always drained rapidly. Some lakes, however, exhibited far more variation in drainage behaviour. This variation is summarized in Figure 6.19a. This figure

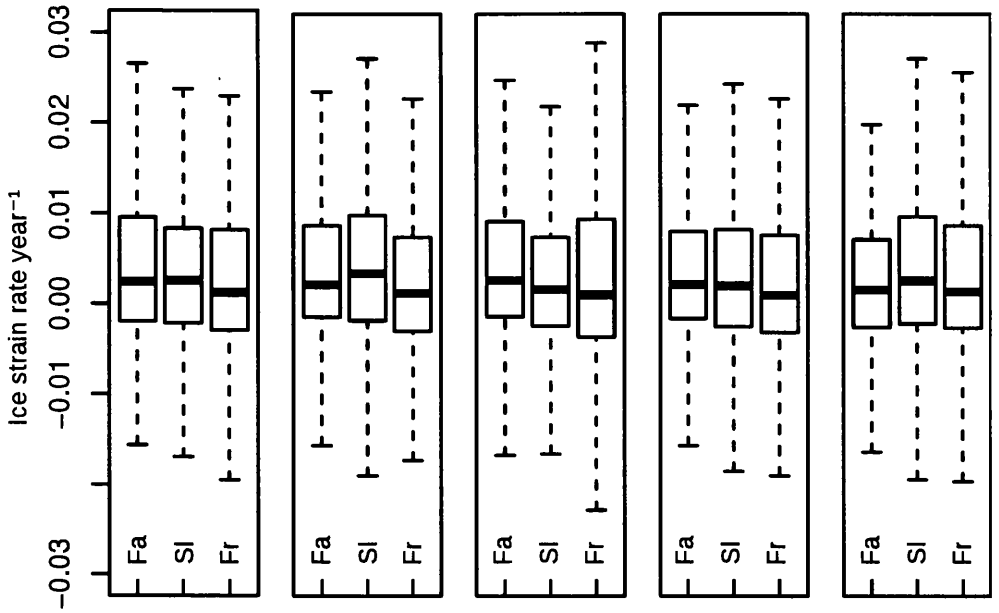

Figure 6.18: Box and whisker plots to show differences in ice strain rate between fast draining (Fa), slow draining (Sl), and freezing (Fr) lakes. Positive values indicate ice that is extending due to acceleration, negative values indicate ice under compression due to deceleration.

shows for each lake drainage type how often that drainage type reoccurred for each lake. Note that the number of times that drainage type is counted regardless of the number of years the lake formed, therefore a lake that formed in only three years but froze in every year is counted as freezing three times. This is expressed as a percentage of all the lakes of that drainage type. For example, Figure 6.19a shows that 42% of lakes than drained rapidly at some point during 2005–2009 only did so in that single year. Conversely, 6% of lakes that drained rapidly did so in every year. Lakes that froze were mostly likely to have the same termination behaviour in successive years, with 28% of lakes that froze in one year doing so in 4–5 of the years studied. Only 26% of freezing lakes only froze in one year. Lakes that drained slowly were only slightly more likely to maintain the same drainage behaviour in multiple years than fast-draining lakes.

Lakes that drained rapidly were subdivided by the number of years that fast drainage occurred, this number of years is plotted on the x axis of Figure 6.19b. For each lake that drained rapidly in 1–4 years, the probability of slow draining, freezing, or unknown drainage type being assigned to any one of the remaining years was

calculated, and is shown on the y axis of Figure 6.19b. The probability of a lake not forming was also considered, and is also included on this figure. This plot shows that lakes that were observed to drained rapidly in 1–3 out of the 5 years were most likely to drain slowly in the remaining years observed. For lakes that drained rapidly in four years out of the five studied, in the remaining year the lake was most likely to be classified as unknown, raising the possibility that several lakes drained rapidly in every year but observations were missed due to cloud in one year. Similar plots to Figure 6.19b were also calculated for lakes that drained slowly (Figure 6.19c) and lakes that froze (Figure 6.19d). Slow-draining lakes were most likely to freeze in other years, and conversely lakes that froze were most likely to drain slowly. Freezing lakes were twice as likely to not form in other years than lakes of any other drainage type, with fast and slow-draining lakes having similar probabilities of not forming in other years.

6.7 Simultaneous lake drainages

When examining the behaviour of fast-draining lakes, it was occasionally observed that two or more lakes in the same vicinity drained on the same day. While this could be coincidence, it could equally suggest some form of link between the lakes causing the simultaneous drainage.

The fact that some pairs of lakes drained with 24 hours of each other in several years suggests that in at least some cases a forcing mechanism is at work. This phenomenon was investigated further by defining a search window around each fast-draining lake, and identifying nearby lakes that drained rapidly on the same day. All fast draining lakes within 6.25 km (25 250 m MODIS pixels) were considered. To be allocated to a cluster of lakes a lake needed to be within 6.25 km of any lake in the group; therefore groups could be rather more than 6.25 km across. The spatial constraints were defined in an attempt to quantify the phenomenon as observed when scrolling through the JPEG thumbnails described in Section 4.5.2, rather than

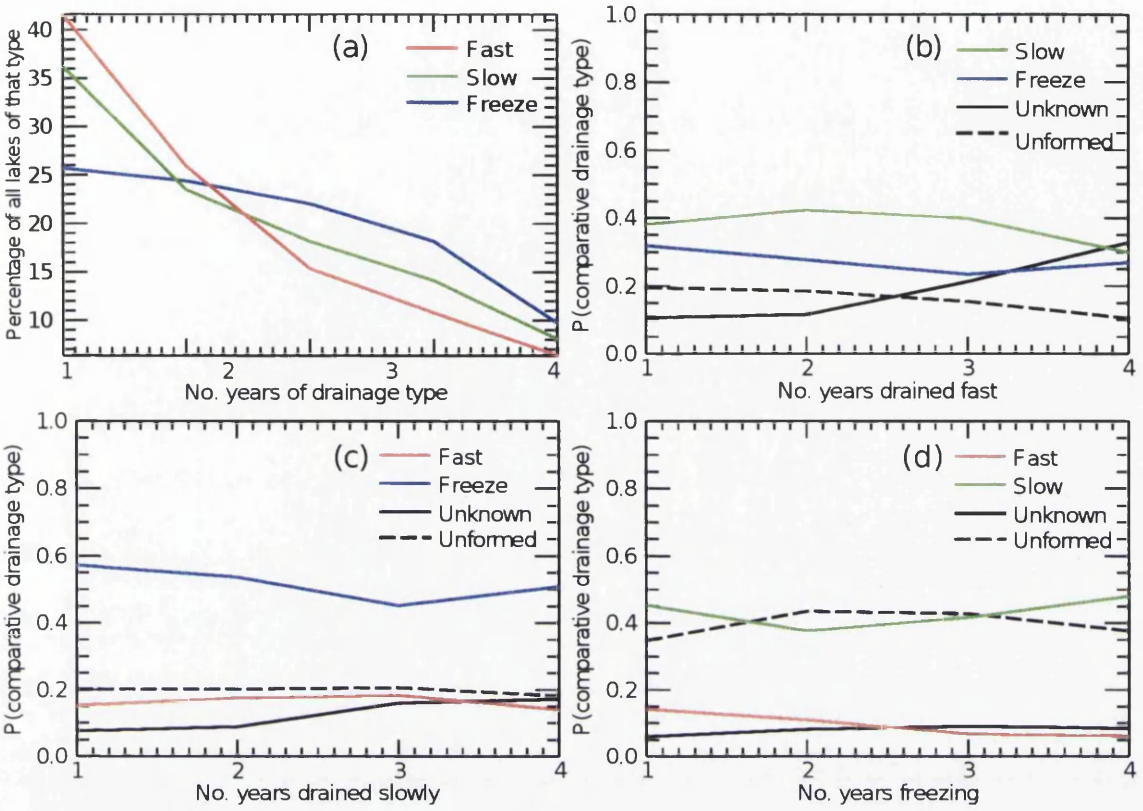

Figure 6.19: The persistence of drainage types. (a) How often each drainage type reoccurred for the same lake in different years, as a percentage of all lakes with that drainage type at least once. (b–d) For lakes that drained fast (b), slowly (c), or froze (d), the probability (P) that a lake with that drainage type in 1–4 years will have had each of the other drainage types in the remaining years is plotted.

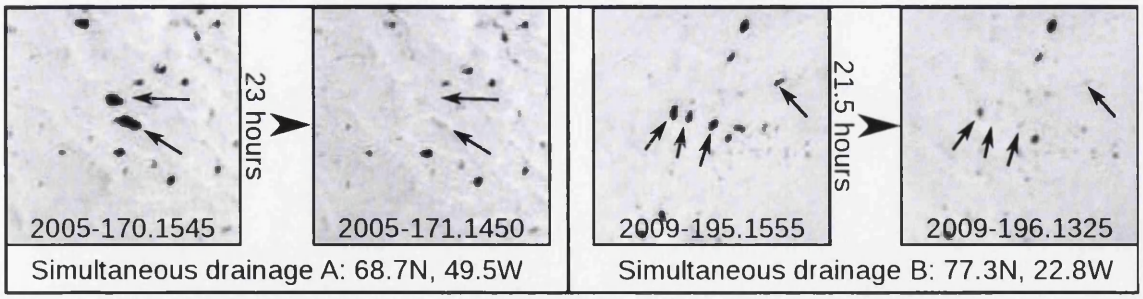

Figure 6.20: Examples of simultaneously draining lakes. Example A is in SW Greenland, involving two lakes. Example B is in NE Greenland, involving four lakes. In both examples less than 24 hours separates the before and after images. Lakes that drained are identified in both before and after images by arrows. Times are shown as YYYY-DDD.HHMM.

resulting from a prior knowledge of any underlying physical process.

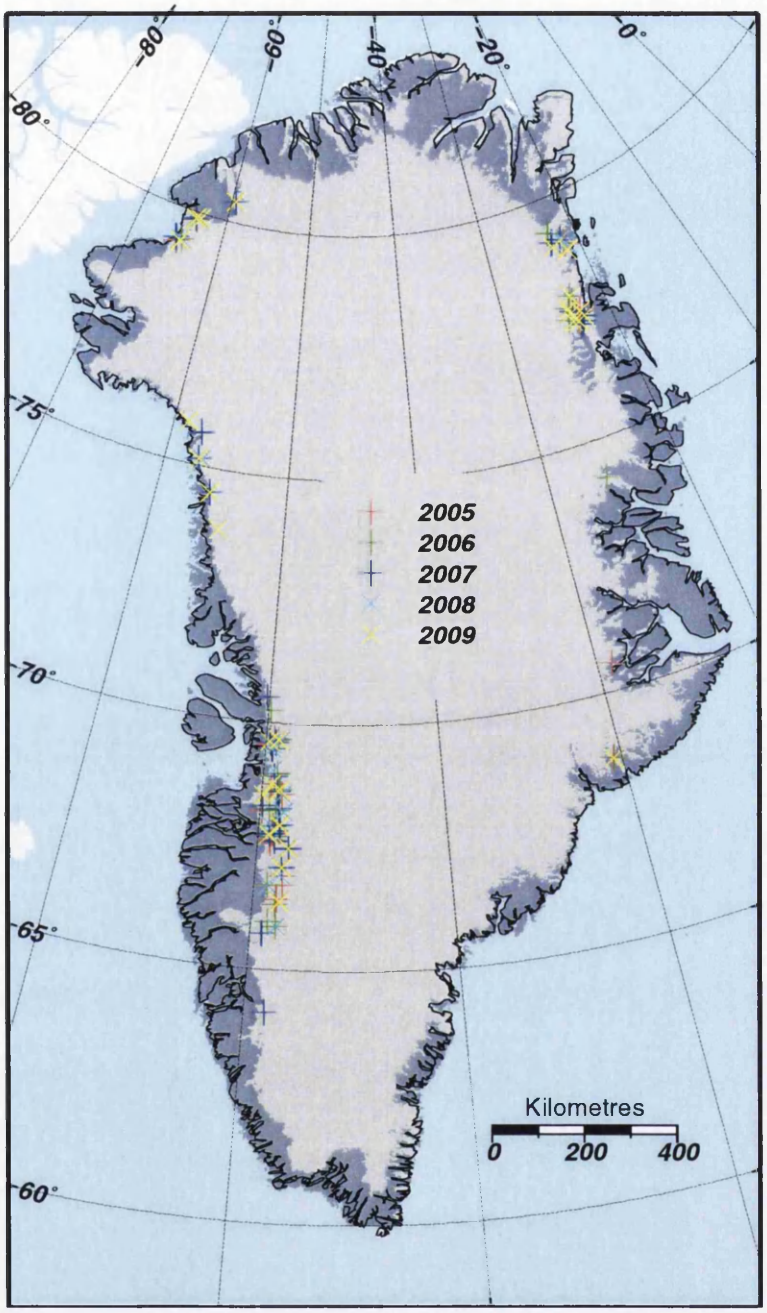

Figure 6.21: For each group of simultaneous fast-draining lakes, one lake is marked as a cross on this map.

Groups of fast-draining lakes were found in all years. In the years 2005–2009, 13, 8, 11, 11, and 15 groups of fast-draining lakes were identified respectively. These groups contained between two and four lakes per group. For each of these groups in each year, the central lake is marked as a cross on Figure 6.21. Occurrence

of these groups was rather clustered, although it should be remembered that a degree of clustering would be expected in a purely random distribution. Groups of simultaneous fast-draining lakes were found in several years in the Nordenskiöld area of the SW, around Steenstrup Glacier in the NW, on Humboldt and Petermann Glaciers in the N, on the three outlets of the NE Ice Stream, and on Kong Christian IV Glacier in the E.

This analysis was very sensitive to the spatial and temporal constraints used. Doubling the search area and allowing lakes with a one day difference in drainage date considerably increased the number of groups formed to 28–37 groups of 2–8 lakes. However, this modification would have considerably increased the risk that the groups of fast-draining lakes were due to chance.

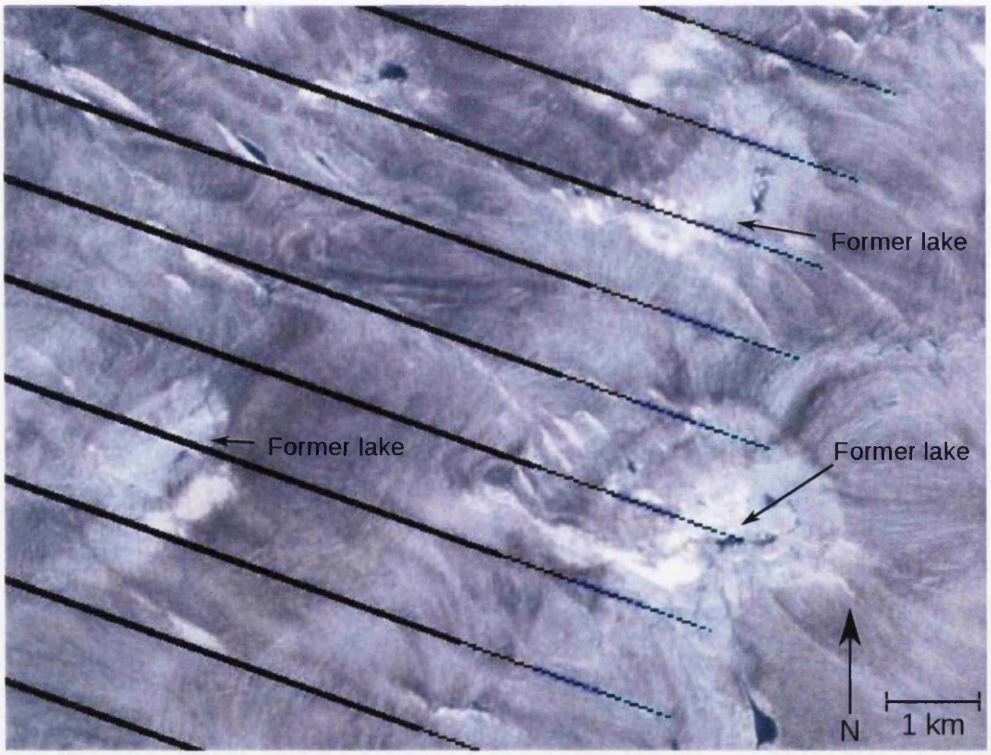

Figure 6.22: The former site of three adjacent lakes that drained on the same day as imaged by Landsat ETM+. There is no evidence of any connecting fracture at this resolution (15m). Black lines across the image are a result of the failed ETM+ scan line corrector.

The existence of adjacent lakes that drain on the same day suggests the existence of some form of link between the lakes, the most obvious being a fracture which

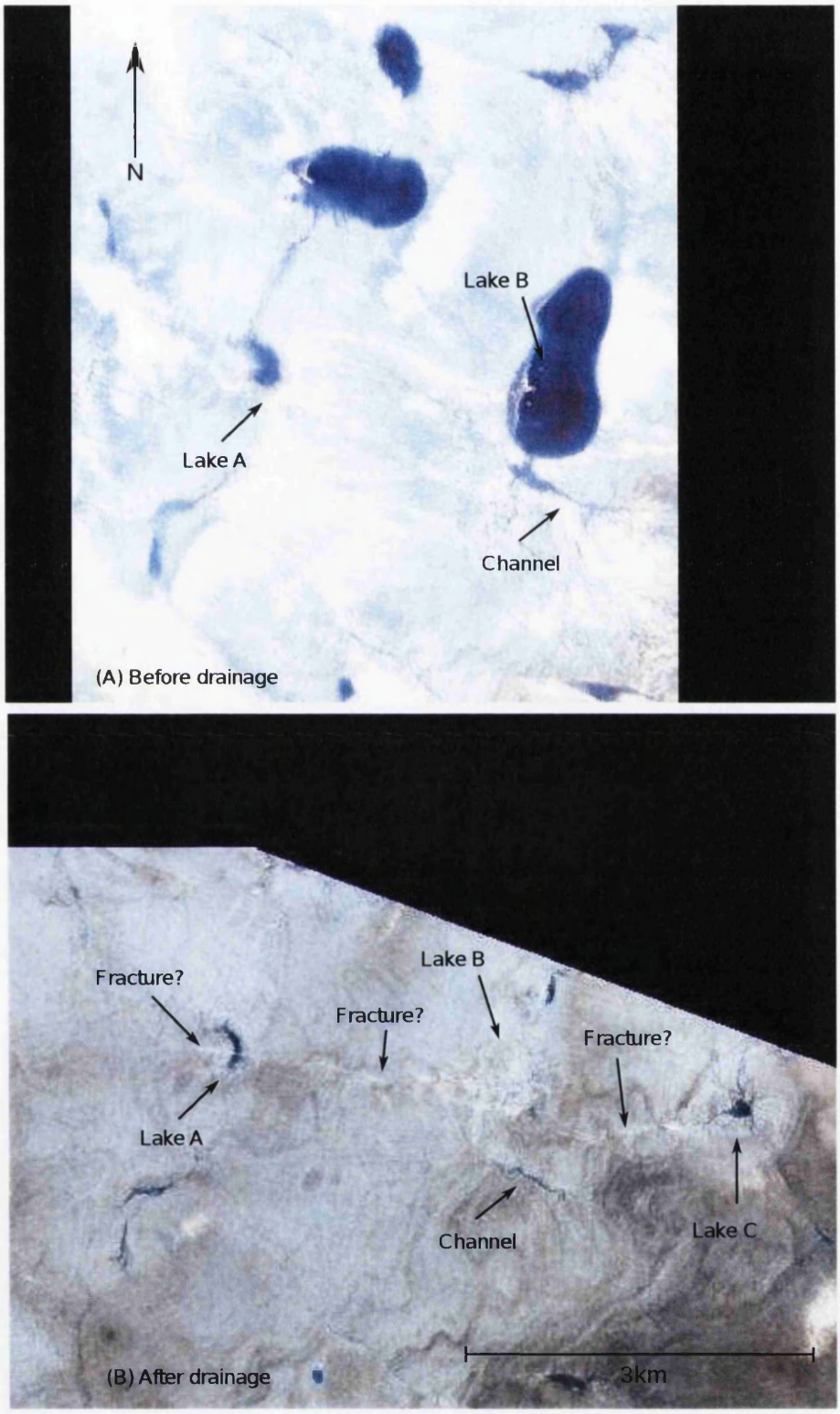

Figure 6.23: A possible fracture running through a group of lakes that drained on the same day. (A) The lakes before drainage. (B) The lakes after drainage. A new linear feature (bright white) running through the former lake beds has appeared, this may be a fracture.

both lakes can drain through. To see if any fractures were visible at sites where simultaneous drainage had occurred, all available Landsat and ASTER data for the ten day period following drainage were obtained. Only ten images met these criteria, and in nine of these images while the drained lake sites were clearly visible, no connecting fractures were visible at the available resolution (15 m). An example is shown in Figure 6.22. In this figure three adjacent lakes have drained on the same day are shown, but there is no evidence of any connecting features.

In one ASTER image of a group of lakes after simultaneous drainage, a new linear connecting feature was observed. In Figure 6.23a some of the lakes in the group are visible, and there is no evidence of any connecting features running between the lakes. Figure 6.23b shows the same lakes after drainage has occurred. A new bright white linear feature is evident running through three lakes, two of which have drained and one of which has drained partially. From the dataset presented in this thesis it is know that lakes B and C drained on the same day, lake A is too small to be visible in MODIS data so no information is available on the relative timing of drainage from that lake. The new feature observed cannot be a channel, as it crosses former lake basins and as such would be flowing uphill. Therefore the most likely explanation for this feature is that it is a new fracture that has opened or been enlarged during lake drainage.

6.8 Chapter summary

Three different means by which lakes can disappear from the ice sheet could be identified from MODIS imagery. Some lakes drained very rapidly, presumably to the bed as observed by Das *et al.* (2008). Others froze, which could be determined by the timing of the lake with regards to the stage of the melt season and ice surface temperature, and through visual keys such as the loss of area from surrounding lakes and a general increase in the albedo of the surrounding area. Finally, other lakes appeared to drain slowly over the surface, inferred by the slow reduction in lake area

during a period of plentiful melt.

Freezing was the most common reason for a lake disappearing, 46% of lakes per year froze. Slow drainage accounted for a further 34% of lakes, and 13% drained rapidly. It was found that while fast-draining lakes occurred almost everywhere lakes formed, they were far more likely to occur in some areas than others. Lakes were most likely to drain rapidly in the NE, N, and SW regions. The NE and SW regions had more fast-draining lakes than expected based on region size, and 78% of all fast-draining lakes on the GrIS were found in these two regions (with 61% in the SW). The distribution of drainage types was not always even within regions, and catchment scales variations were observed.

Lakes that drained slowly were found to generally be smaller that fast draining and freezing lakes, although this was not significant in all regions of the ice sheet. Freezing lakes persisted on the ice sheet for twice the duration of fast draining lakes, lasting approximately one month, rather than fast-draining lakes' 10–15 days. Slow-draining lakes had a geometric mean duration between those of fast draining and freezing lakes. Lakes were mostly found on slopes of approximately 0.7 degrees, and were slightly more likely to drain slowly where the slope angle was steeper, with freezing lakes forming on the shallowest slopes. A significant difference in elevation and underlying ice thickness was found between different lake types, with the lakes at higher elevations most likely to freeze. Fast-draining lakes formed at lower elevations, with mean elevations around 200 m lower than freezing lakes in most years. This also means that fast-draining lakes formed on the thinnest ice, whereas those lakes on the thickest ice usually froze. This pattern could also be seen in ice sheet wide mapping of drainage type: the band of highest lakes froze in each year, despite having the longest duration. No significant difference in ice-sheet strain-rate could be found between drainage types.

Some lakes drained in the same manner each year, whereas other lakes drained differently or froze in consecutive years. Freezing was the most likely mode of lake termination to occur in multiple years, whereas fast drainage was the least likely.

There was not equal probability of each drainage type occurring to a lake with a different drainage type in another year. Lakes that drained fast in one year, were most likely to otherwise drain slowly. Slow-draining lakes otherwise tended to freeze, and freezing lakes were most likely to drain slowly in years they did not freeze. There were some lakes that drained rapidly in every year studied (6%), and lakes that drained rapidly in four out of the five years studied were most likely to be categorised as unknown, so some of these lakes will have drained rapidly in every year as well.

Groups of adjacent lakes were found that all drained rapidly on the same day, and were found in all years and in most parts of the ice sheet where large numbers of lakes form. In one case, a possible fracture appeared connecting drained lakes, although the same fracturing could not be found for other groups of draining lakes. However, it is unsurprising that fractures would not be visible in satellite imagery considering the findings of Krawczynski *et al.* (2009) that fractures of less than one metre across are sufficient to drain a supraglacial lake through 1000 m cold ice.

Chapter 7

Discussion

7.1 Introduction

Striking differences in the occurrence of supraglacial lakes between different regions of the Greenland Ice Sheet have been presented in Chapters 5 and 6. Different modes of lake drainage have been identified, and the phenomenon of fast lake-drainage has been shown not to occur uniformly across the ice sheet. In this chapter, the controls on lake formation and drainage will be explored, and the ramifications of the findings of this thesis for the study of ice sheet hydrology and dynamics discussed.

The different drainage types described in Chapter 6 are discussed with respect to their possible role in ice sheet dynamics in Section 7.2. The controls on lake position and size are discussed in Sections 7.3.1 and 7.3.2, and controls on lake drainage are discussed in Section 7.3.3. The controls identified in these sections are brought together in Section 7.3.4 to show how they have lead to the interregional patterns in lake occurrence observed in the results of this thesis.

Possible biases in the results of this study are described and evaluated in Section 7.4. These biases include the availability of cloud-free imagery for different parts of the ice sheet, the temporal resolution used to initially identify lakes, and error in the measurement of area. The use of lake area as a proxy for lake volume is also

discussed.

The importance of the findings of this thesis are discussed in two parts. Firstly, the impact that these results should have on the future study of Greenland lakes is considered, and recommendations for future field studies are made. The implications for past and future remote sensing studies of lakes are also discussed. Previous studies have inferred that lakes drain to the bed from coarse temporal resolution data. The results of this thesis show that weekly imaging may infer that lakes have drained suddenly, when in fact they have drained more slowly over several days. The importance of high temporal resolution data for studying lake drainage is highlighted, and papers that have identified draining lakes are revisited and tested for robustness in Section 7.5.1. Secondly, the finding that the phenomenon of lakes draining suddenly is not an ice sheet wide occurrence has important ramifications for the study of ice sheet dynamics. Virtually all studies of the role of hydrology in the dynamics of the Greenland Ice Sheet have been undertaken in the SW, yet the results presented here show that the surface hydrology of the SW is not representative of the whole ice sheet. The impact of this issue is discussed further in Section 7.5.2.

7.2 Importance of different drainage types for ice sheet dynamics

In the previous chapter the concept of fast draining, slow draining, and freezing lakes was introduced, and a discussion is warranted regarding the probable role of each drainage type in the interaction of the surface and basal hydrology.

Fast-draining lakes are interpreted to drain through the ice to the ice sheet bed by the means of fracture propagation. This interpretation means that lakes of this type are delivering most of their water to the bed, and in addition are opening new conduits from the surface to the base of the ice, which may remain open if sufficient meltwater continues to flow down them. The water that reaches the bed does so

suddenly and therefore at high pressure, which can overwhelm the basal hydrology increasing subglacial water pressure and reducing the effective pressure, allowing the ice to accelerate (Paterson, 1994, p145–151). This acceleration will be possible even if the basal hydrology has developed into an efficient drainage system as the large volume of water will be sufficient to overwhelm the drainage channels (Schoof, 2010).

Slow-draining lakes are interpreted to drain over the ice surface, probably due to incision of the exit spillway. This drainage can occur over a range of timescales depending on the rate of channel incision, from a few days to over a month. Water from slow-draining lakes can still reach the bed; however this water will be delivered at a slower rate than from fast-draining lakes and so will not cause velocity increases in an efficient drainage network. Crucially lakes which drain slowly will not open a new conduit to the ice sheet base; rather to reach the bed the water would need to exploit an existing conduit, although it is possible that water from a lake with a very rapidly incising exit channel could transfer water into a crevasse fast enough to cause fracture propagation, although there is no published field evidence to support this. As meltwater running over the ice surface can enter moulins and reach the bed whether it is first stored in a lake or not, slow-draining lakes play no major role of lakes in ice sheet dynamics.

While water stored in freezing lakes clearly does not reach the bed, at least one lake identified as freezing had a substantial exit channel (pers. comms. A. Booth, 2011) meaning that to a certain extent freezing lakes may play a similar role to slow draining lakes. In the case of freezing lakes, the exit channel must not incise fast enough to empty the lake over the course of the melt season. Whereas slow-draining lakes probably have a neutral effect on ice sheet dynamics, freezing lakes store meltwater and prevent large volumes from reaching the ice sheet base, therefore reducing the potential effect of surface melt on ice sheet dynamics.

7.3 Controls on lake formation and drainage

This section discusses the controls on where lakes can form, how large they grow to, and if/how they drain. Lakes did not occur equally in all parts of the ice sheet, and in some areas did not form at all. The controls on where lakes could form are discussed in Section 7.3.1. Lakes were not of equal sizes, and the controls on lake size are discussed in Section 7.3.2. As already discussed, lakes could drain either rapidly or slowly, or could freeze over, the possible controls on which of these happens to each lake are considered in Section 7.3.3. Finally, in Section 7.3.4 the controls on lake location, area, and drainage are examined together to identify why interregional differences occurred.

7.3.1 Controls on lake locations

The finding that lakes do not advect with ice flow shows that lake position is controlled by basal topography. This lack of advection was first observed by Echelmeyer *et al.* (1991), and the findings of this thesis add support to this, with lakes being identified in the same position ten years apart despite considerable ice advection during that period (Section 5.2). Presumably subglacial depressions cause backslopes on the ice surface, and therefore produce the sites where lakes can form if meltwater is available to fill these depressions. Enhanced melt through albedo reduction may make these depressions deeper (Lüthje *et al.*, 2006).

For lakes to form there needs to be a depression in the ice (as already discussed above) and water to fill it. This observation logically leads to another first order control on lake formation: surface melt. Lake positions in 2005 were compared with observed melt extent from MODIS LST (Section 5.3). The upper margin of the lake zone was found to correspond to $\sim$ 45 days of melt in some regions, and this is shown in red on Figure 7.1(d) with lakes over-plotted in blue. Whilst this number of melt days was sufficient to form lakes in the N and E regions, in the SW region (and to a lesser extent in the NE and NW) this number of melt days considerably

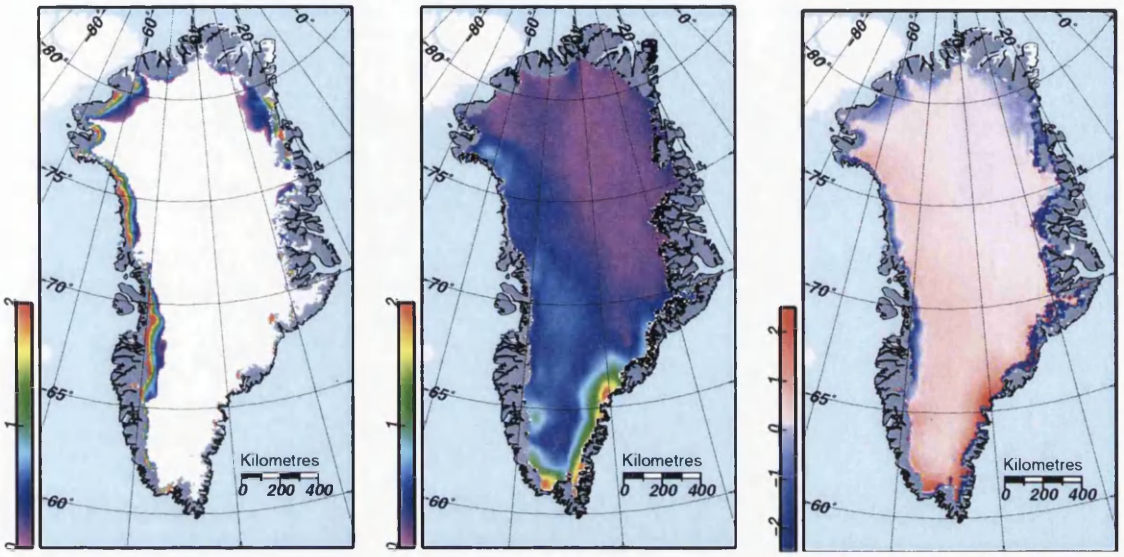

(a) Runoff (b) Snow (c) Surface mass balance

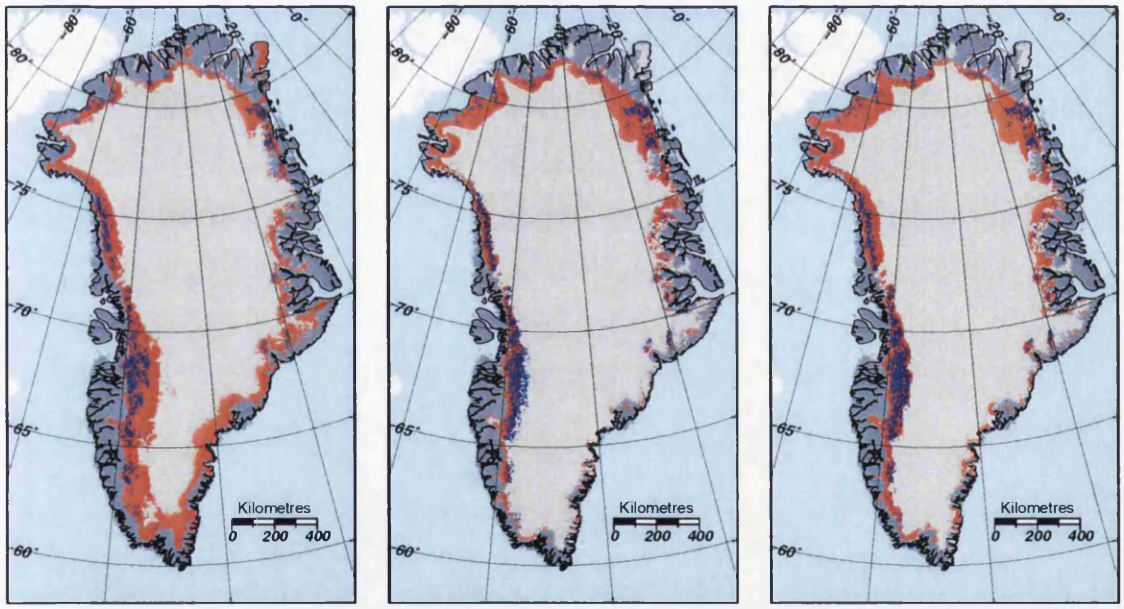

(d) 45 days melt (e) Ablation area (f) Area with runoff

Figure 7.1: 2005: modelled surface mass balance components (Section 3.5.5) (a) runoff and (b) snowfall combined into (c) surface mass balance. All plots are in m/yr. Lakes (blue) are shown over the region with > 45 days of melt observed (in red, d), modelled ablation area (in red, e) and modelled area with runoff (in red, f).

overestimates the maximum elevation of lake formation. From these melt data it would also appear that there is a wide band of melt down the SE coast that does not correspond with lake formation at all. It would seem that some regions require a different number of days of melt to form lakes than other regions. To explore the possible reasons behind this, the ablation area was calculated by taking all pixels with negative surface mass balance from modelled data (Section 3.5.5). Surface mass balance is shown in Figure 7.1(c) and the ablation area calculated from it is shown in red with lakes over-plotted in blue in Figure 7.1(e). Lakes form above the modelled equilibrium line in the SW, so the modelled ablation area underestimates the lake forming zone. Lakes forming outside of the accumulation area is to be expected in the SW region, as they were observed to do so by Echelmeyer *et al.* (1991). However, in the N and NE lakes formed only below the modelled equilibrium line. Modelled ablation area explained the extent of lakes well in the SE, NW, and E regions.

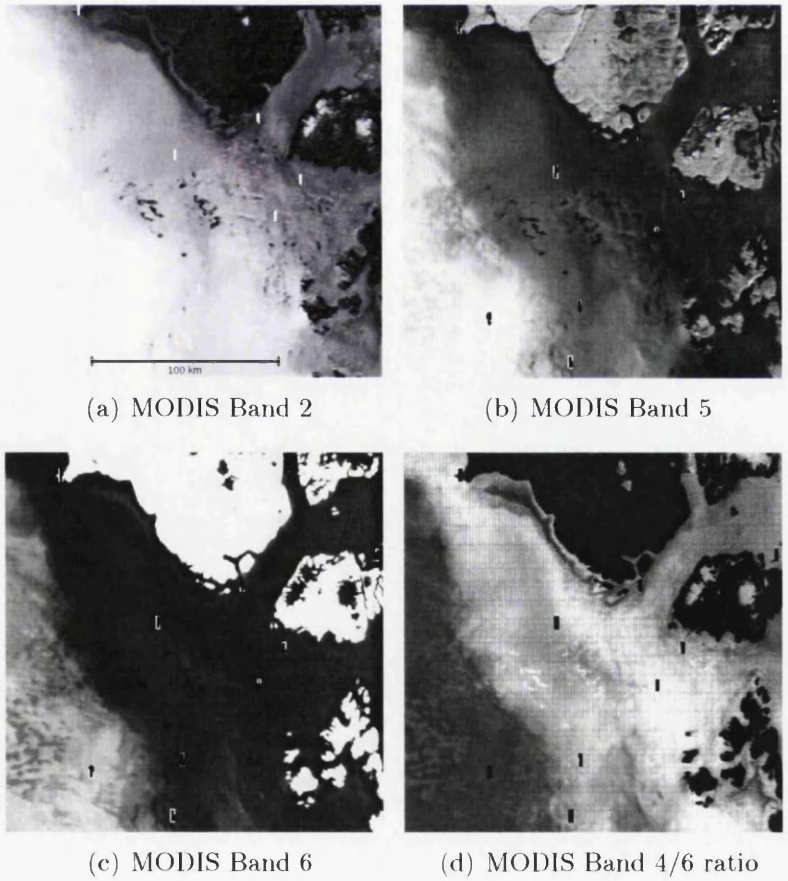

(a) MODIS Band 2 (b) MODIS Band 5

(c) MODIS Band 6 (d) MODIS Band 4/6 ratio

Figure 7.2: Snowline estimation from various infrared MODIS bands. The snowline would be estimated to be the same from each of the bands shown here

In the northern regions, lake distribution did not reach the modelled equilibrium line, this may have been due to errors in modelled runoff and accumulation, or due to another factor constraining lake development. Surface slope was similar in these regions to the SW, where lakes form in the accumulation zone, therefore terrain is unlikely to be a factor. To test the ablation area data used, the equilibrium line was measured by mapping the highest elevation that the snowline reached in 2005 using MODIS data. Several bands and band ratios were trialled (Figure 7.2), however what was interpreted to be the snowline was clearly visible in MODIS Band 2, in which lakes can also be seen. Snowline from Band 2 agreed well with that inferred from Bands 5 and 6, and a ratio of Band 4 and 6 (similar to the often used Landsat Thematic Mapper 4/5 ratio (De Angelis *et al.*, 2007)). While this mapping means that any superimposed ice will have been classed as being in the ablation area, it does provide a maximum possible equilibrium line. The results of comparing the observed highest snowline in 2005 with modelled ablation area are presented in Figure 7.3. In the SW, SE, E, and NW, the upper bound of modelled ablation area corresponded very closely to the observed highest snowline. In the N and NE the snowline never reached as high as the modelled equilibrium line, suggesting that modelled accumulation may be too low in these regions. In the SW, lakes could be seen to be forming above the snowline. In other regions the observed highest snowline provided a good upper limit for lake formation.

The patterns observed above suggest that accumulation (Figure 7.1(b)) may play an important role in controlling the locations of lakes. Lakes required more melt days for formation in the southern regions where snowfall is substantial. In the SE region lakes only formed in a small fraction of the area that received an intensity of melt that would form lakes in other parts of the ice sheet. Modelled and observed ablation area coincided with the limit of lake formation in the SE more closely than melt extent, suggesting that the high volumes of snowfall in the SE region may prevent lake formation. Lake formation on snow is more difficult than on ice (owing to the higher permeability of snow), and meltwater can refreeze in the snowpack reducing runoff. Large volumes of snow in the SW would explain why lakes take more melt

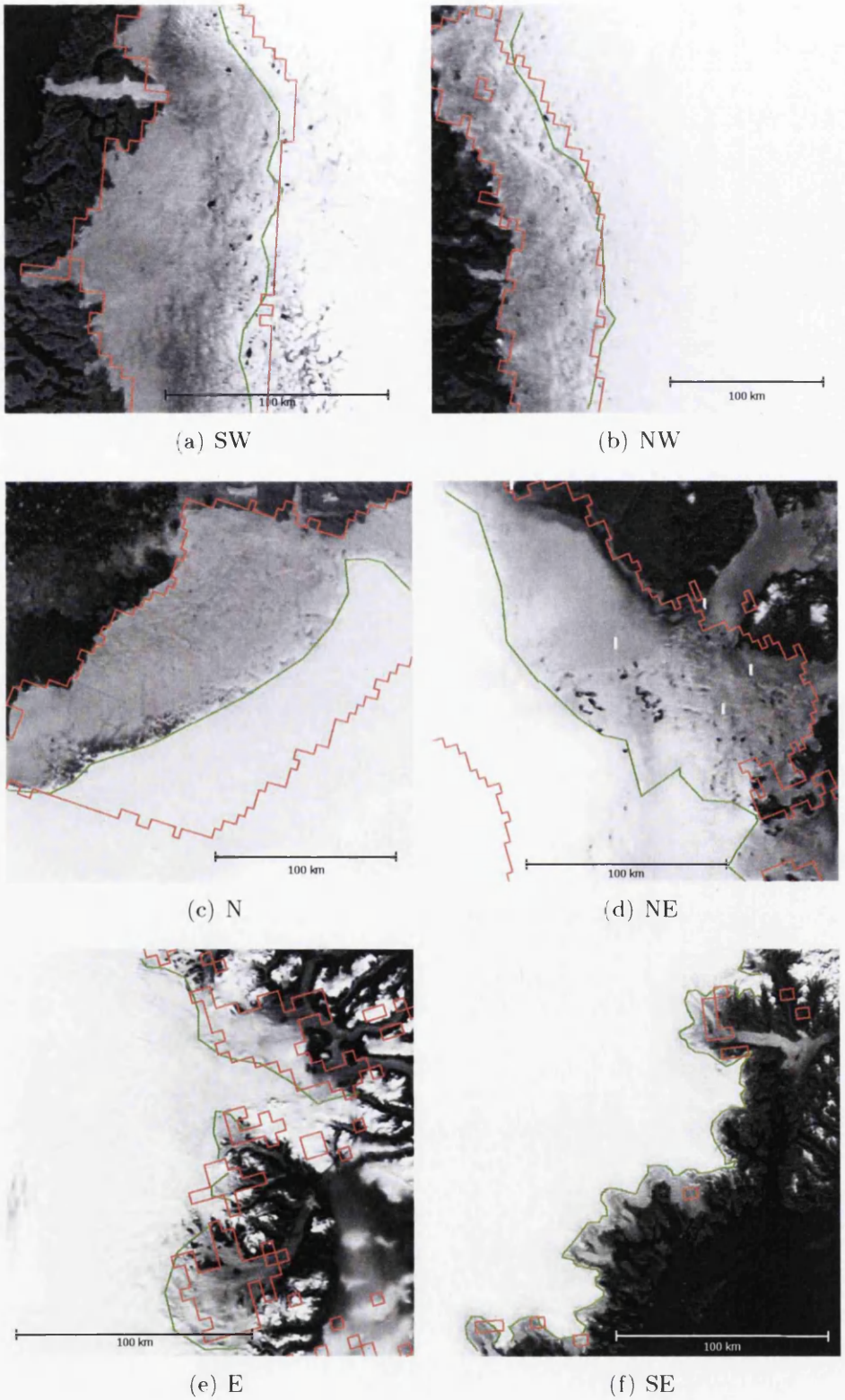

(a) SW (b) NW

(c) N (d) NE

(e) E (f) SE

Figure 7.3: Observed highest snowline (green) and modelled ablation zone (red) on MODIS Band 2 images (0.86 μm) for subsets of the six regions of the ice sheet during 2005. The modelled abalation zone outline includes the ice sheet margin.

days to form in the SW than the northern regions, however lake formation can still occur over a wide area in the SW as the melt zone in that region is widespread and long lasting. It is notable that in the SW region lake formation on snow and firn is more common than in other regions, which may be also due to the volumes of snow in that part of the ice sheet, as large areas of the melt zone are within the accumulation area. This interaction of melt and snow will result in extensive refreezing of melt water within the snowpack, forming ice layers which will help make the snowpack impermeable, which in turn will allow lake formation on snow to occur more readily. This suggestion gains further support from the fact that the SW is the only region where modelled runoff better describes the distribution of lakes than the ablation area, and the widespread occurrence of slush above the equilibrium line in the SW indicates that saturated snow is more common in this region than elsewhere. The fact that the SE region - which also has plentiful melt but also plentiful snow - does not show the same pattern of lake formation as the SW would suggest that slope also plays a role: the SE region has very steep topography near the ice margin (the steepest gradient of the ice sheet across the melt area) whereas the gradient of the SW melt area is one of the lowest on the ice sheet (Figure 7.4).

More can be learnt about the controls on lake formation from studies of small regions in greater detail. The notable absence of lakes in a small region which otherwise has many lakes may help demonstrate why lakes are common in some areas, and absent in others. An unusual "Y" shaped pattern of lake formation, shown on Figure 7.5, occurs in NE Greenland. This pattern is also one of the most striking patterns of ice-sheet scale lake distribution, visible on Figure 5.7. A sharp discontinuity is visible in Figure 7.5 (labelled A), north of which lakes do not form. This section of the ice sheet is apparently snow-free (Figure 7.2) with adequate melt for lake formation. Topography appears to control this pattern (Figure 7.6), with the area with no lakes forming corresponding to a prominent ridge. Both of the two "prongs" of the Y-shaped pattern (the S prong is labelled B in Figure 7.5) coincide with the edge of changes in topography. In addition, large lakes visible in Figure 7.5 correspond to large flatter parts of the ice showing a strong topographic control on both lake

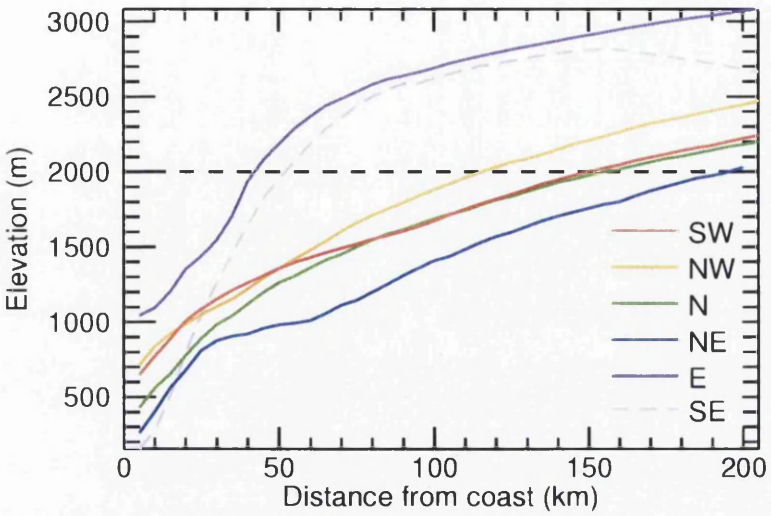

Figure 7.4: Elevation profiles for the six regions of the ice sheet. Profiles were taken up the fall line of the slope. In the SW and NW the profiles were taken from the latitudinal mid point of the ice margin of that region. The N profile was taken from Humboldt Gl. The NE profile was taken from Nioghlvfjerdsbræ. The East profile was taken from Daugaard-Jensen Gl. The SE profile was taken from Bernstorff Gl. The ice divide in the centre of the S GrIS is offset far enough to the E that it appears in the SE profile. The dotted horizontal black line represents 2000 m elevation.

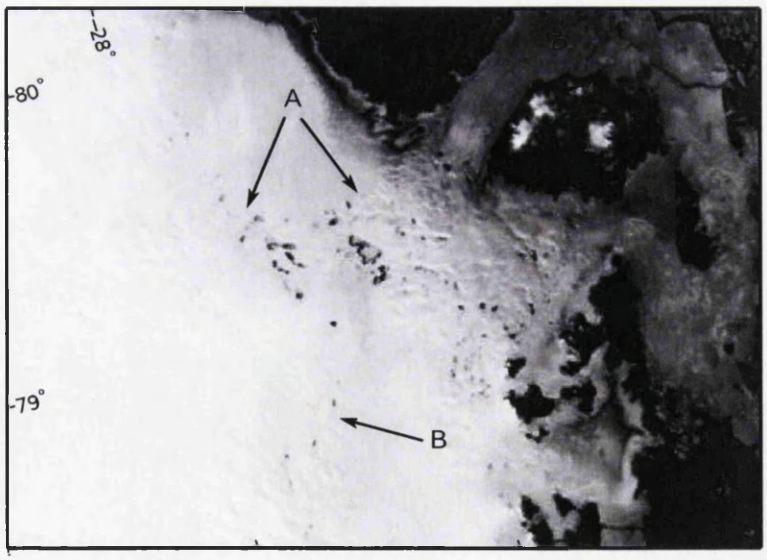

Figure 7.5: The pattern of lake formation in NE Greenland (Nioghlvfjerdsbræ), discontinuities in lake formation are shown by arrows and labelled A and B. The lake-free area north of discontinuity A is permanently lake-free.

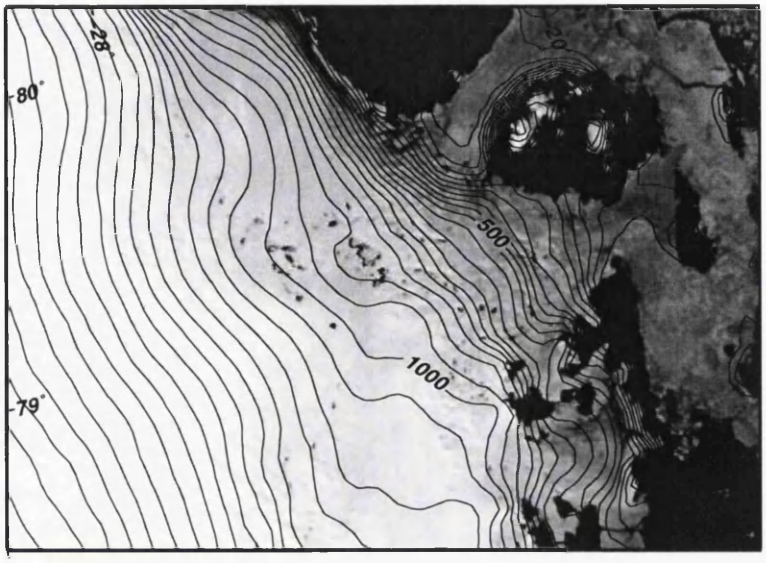

Figure 7.6: The pattern of lake formation in NE Greenland (Nioghlvfjerdsbræ) related to topography. Contour lines are drawn every 50m.

location and lake size.

7.3.2 Controls on lake area

It has already been demonstrated in Section 6.5 and will be discussed further in Section 7.3.3 that the drainage type of lakes has an effect on (or is affected by) lake area. Fast draining and freezing lakes grew to larger mean areas than slow-draining lakes. As a result of this difference, the remaining figures in this section will show all lakes coloured by drainage type (red for fast, green for slow, blue for freeze, and black for unknown) to take this relationship into account.

Figure 7.7 shows the effect of melt duration at individual lakes on individual lake areas. Data from only one year is shown (2005) to keep the plot as uncluttered as possible. The relationship between melt and individual lake area is obviously complex. Lakes are generally larger if more melt is available up to a threshold of around 60 days, beyond which increasing melt yields decreasing lake area. Despite this, even with 60 days of melt with which lakes grew largest, a spread of lake areas existed from the largest down to the smallest sizes in the dataset.

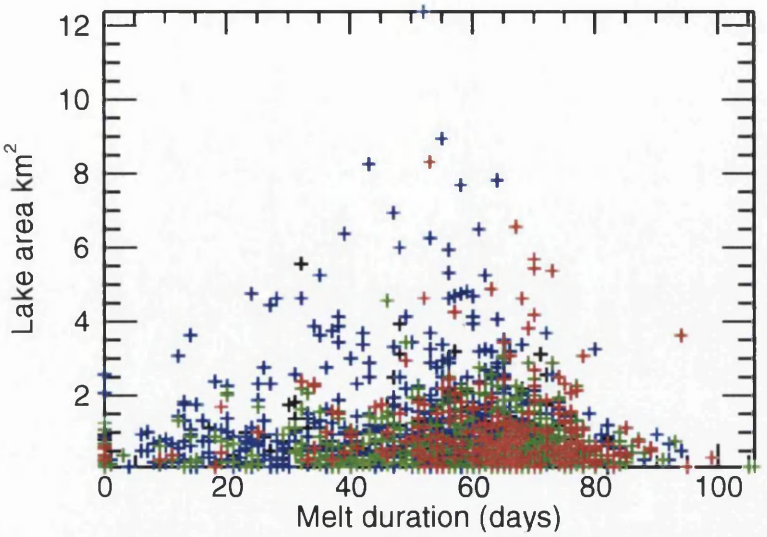

Figure 7.7: The relationship between melt extent and duration and total lake area

Lake duration (as shown in Figure 7.8) displays little relationship with lake area, with a slight peak in the occurrence of very large lakes at around 30 days. Most of the pattern in the duration/lake area relationship appears to relate to differences in drainage type, with the significant differences in lake duration between drainage types clearly apparent. Fast draining lakes can be seen in general to persist for shorter durations than slow draining lakes, which in turn had shorter durations on average than freezing lakes.

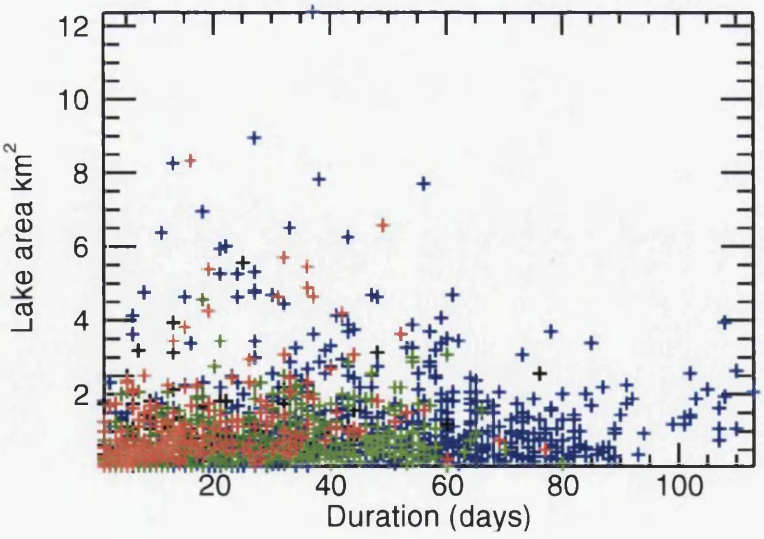

Figure 7.8: The relationship between lake duration and total lake area. Lake duration is clearly different for fast draining (red), slow draining (green), freezing (blue), and unknown (black) lakes.

Not all of the variables produced what might be considered an intuitive response in lake area. Lake size would be expected to decrease with increasing altitude due to the environmental lapse rate, however lake size generally increased with increasing elevation up to a threshold of around 1500 m elevation, above which lakes were smaller with increasing elevation (Figure 7.9), although a wide range of lake sizes occurred at most elevations. Similarly, the latitudinal temperature gradient would

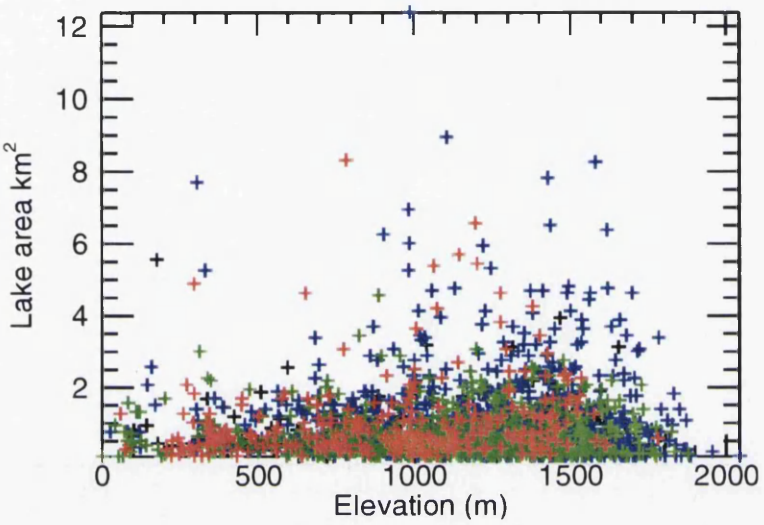

Figure 7.9: The relationship between lake elevation and total lake area for fast draining (red), slow draining (green), freezing (blue), and unknown (black) lakes. Note that for some of the ice sheet, the ice margin is at 500 m elevation.

be expected to produce smaller lakes in the most northerly parts of the ice sheet. Again, the relationship is less straightforward (Figure 7.10). Lakes clearly occur in clusters relating to the most prevalent lake forming regions, however there is no obvious decline in lake size relating to increasing latitude.

The relationship between the area of lakes and the slope angle of the ice they formed on is shown in Figure 7.11. In general, larger lakes formed on shallower slope angles. While this relationship is clearer than was evident for some of the possible controls discussed above, this relationship was also not straightforward. As with the other possible controlling factors, even at the most apparently optimal slope angles ($< 1°$) a wide range of area values occurred indicating that only part of the variation of lake area can be explained by slope angle.

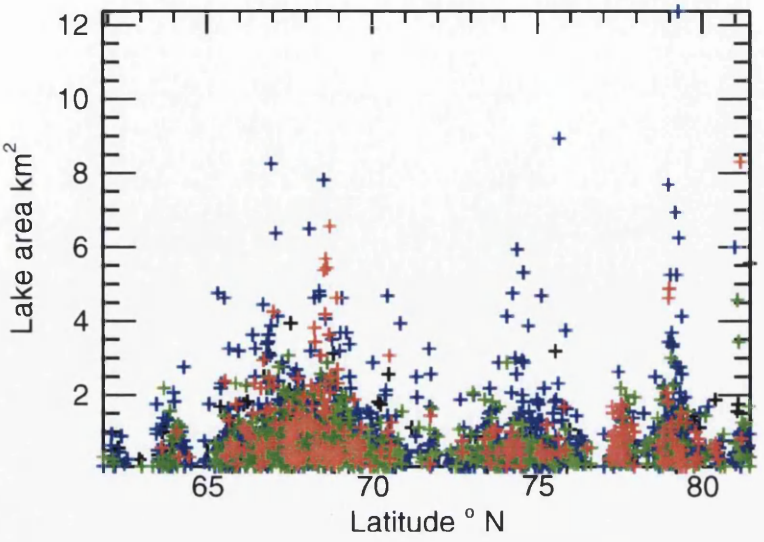

Figure 7.10: The relationship between latitude and total lake area for fast draining (red), slow draining (green), freezing (blue), and unknown (black) lakes. Clusters relate to the prominent lake forming regions of the ice sheet.

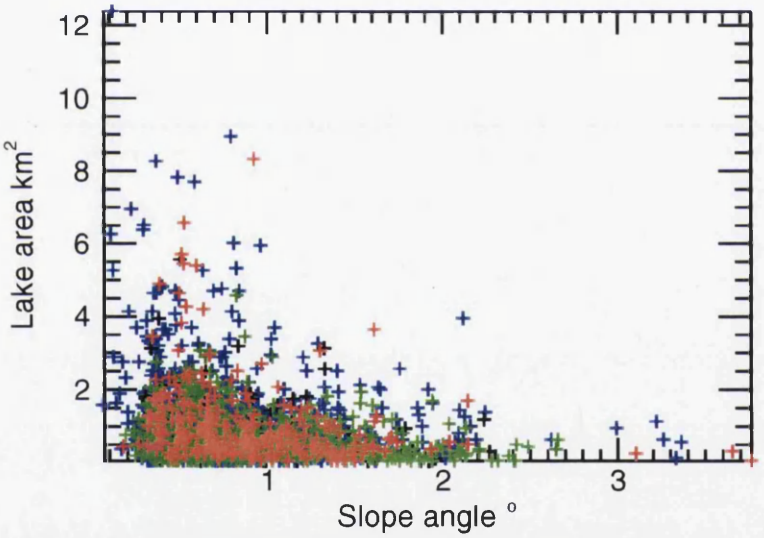

Figure 7.11: The relationship between surface slope and individual lake areas.

The large variance for all of the factors shown above indicates that no one factor alone controls lake area. Melt duration, elevation and slope angle all had a relationship with lake area. It is problematic to tell whether any of the possible controlling factors described actually have a causal relationship with lake area. Many of these factors are interrelated, making it difficult to tell which factor actually causes the variation in lake area. Elevation controls the length of the melt season owing to the environmental lapse rate (Figure 7.12(a)), and melt length is shorter at higher

elevations as expected. The GrIS has mostly convex slopes, and therefore the topographic slope is shallower at higher elevations (Figures 7.4 and 7.12(b)). Local scale variations in slope can be seen to be related to lake size (Figure 7.6) which suggests that the positive relationship between elevation and lake area could be caused by topographic slope, however this is complicated by the termination types of the lakes being studied. Lakes were found to be more likely to freeze at higher elevations and on shallower slopes, and freezing lakes were also found to have fairly large mean areas making it difficult to establish which (if any) variables are independent. The controls on lakes freezing at high elevations are discussed in Section 7.3.3; however it is worth mentioning here that shallow slopes may make unstable supraglacial drainage less likely, which would both increase the chances of a lake lasting until the end of the melt season without draining (and therefore freezing), and would also reduce the loss of water through surface drainage allowing large lakes to develop. Shallow surface slopes probably cause larger lakes by simply providing a larger lake forming surface than a similar shaped depression on steeper ground, therefore it seems likely that surface slope is a key factor in the determining the size that lakes grow to on the GrIS.

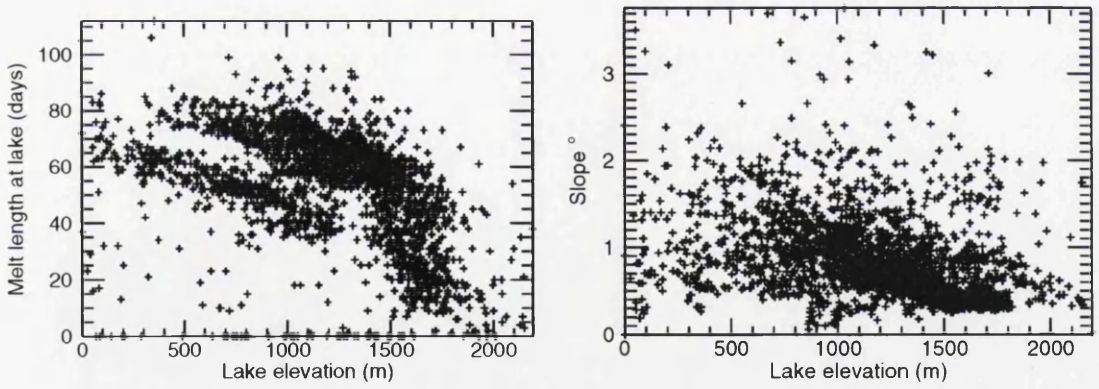

(a) Melt (b) Slope

Figure 7.12: The interplay between the various factors that may control lake area. Both melt (a,r=-0.4, p¡0.001) and slope (b, r=-0.37, p¡0.001) are negatively correlated with elevation.

The total area of lakes on the ice sheet is a function of both the number of lakes, and the individual sizes of those lakes. Therefore, those factors that control the upper limit of lake formation discussed in Section 7.3.2, namely the surface mass balance

components of melt and accumulation, also control the total area of lakes forming on the ice sheet. This result is demonstrated in Figures 7.13 and 7.14. Figure 7.13 shows the total maximum lake area per region plotted against melt extent and duration (i.e. melt extent x melt duration). A linear relationship is evident for each region between total lake area and melt, and likewise a linear trend can be fitted to the full sample of regional total lake areas and melt intensities, although the SE region stands out as having low lake area despite relatively high melt extent and duration. The gradient of each fitted line of Figure 7.13 gives an indication of the magnitude of the response of total lake area to melt extent and duration in each region. Both the NW and N show considerably less variability in lake area with melt extent and duration than the NE and SW regions, the NE in particular has the largest response of total lake area to changes in melt of any region, which means that of all the regions studied the NE is most likely to see a large increase in the number of lakes in a warming climate. Melt and total lake area were positively correlated for all regions, but the correlation was only significant in the N and NE regions. The same regional trends can also be observed in Figure 7.14, where the

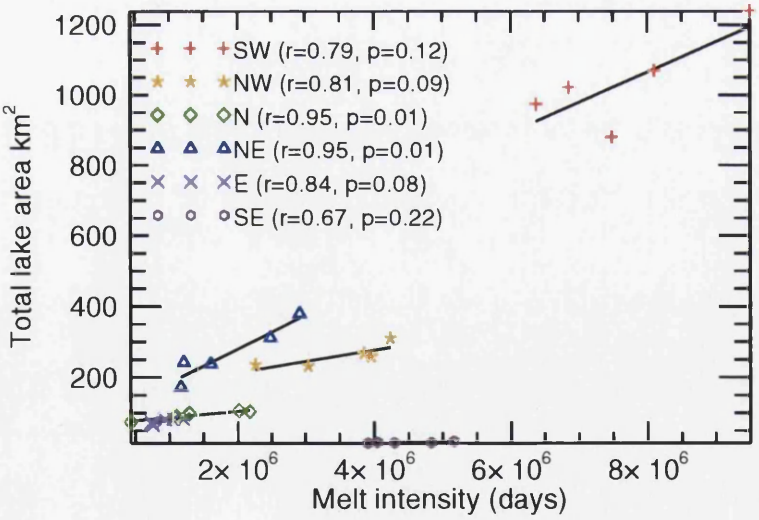

Figure 7.13: The relationship between melt extent and duration and total lake area for the regions of the GrIS over the period 2005-2009. Pearson's r and significance (p) are shown.

total-area/melt relationship can be observed for all catchments, coloured by region. Again, a generally linear trend can be fitted through the data, although the data

are strongly skewed and heteroscadastic (variance increasing with x). Some intra-regional variation can be seen e.g. some SW catchments have a total-area/melt relationship more typical of the SE.

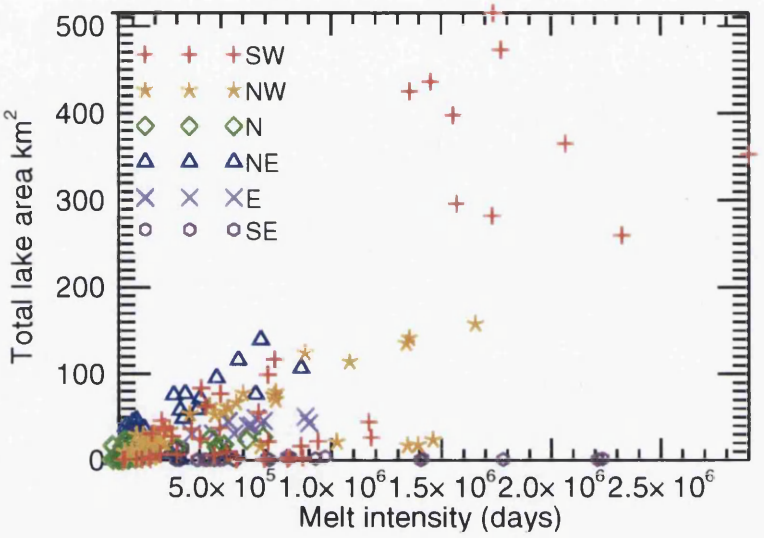

Figure 7.14: The relationship between melt extent and duration and total lake area for the catchments of the GrIS over the period 2005-2009

7.3.3 Controls on lake drainage

In Section 6.5 a set of plausible hypotheses for the occurrence of different drainage types were proposed, followed by a statistical analysis of the differences between the drainage types through the factors suggested. These hypotheses are revisited here in light of the findings of these tests. In each case the hypothesis is restated (in *italics*), and then discussed.

Do lakes need to reach a critical size before fast drainage can occur? This hypothesis was proposed as there may be a critical size which lakes must reach to drain to the bed, and larger lakes will have more potential to form over pre-existing fractures. While fast-draining lakes were found to grow larger than slow-draining lakes, the difference between fast draining and freezing lakes was smaller and not always significant, with considerably overlap in sizes between types. Therefore, it would seem that lake area is not a first order control on lake drainage. The difference between

fast and slow-draining lakes may mean that lake area has a secondary role in determining whether a lake that does not freeze drains to the bed or over the surface, although it could equally mean that constant drainage over the surface limits the growth of a lake.

Do some lakes freeze before they can drain either through or over the ice? It is be conceivable that lakes that froze would have drained (quickly or slowly) if they had not frozen first, however it was demonstrated that lakes that froze lasted twice as long as lakes that drained quickly. Slow-draining lakes lasted longer than those that drained rapidly, but were still on the ice for significantly less time than those that froze. This long duration would suggest that freezing lakes are prevented from draining by another factor rather than freezing before drainage could occur.

Are lakes more likely to drain over the surface (slow draining) on steeper surface-slopes? Slow-draining lakes were found to form on steeper slopes than lakes of other drainage types, although while the difference in mean slope between fast and slow-draining lakes was usually statistically significant, the difference was only small at a few hundredths of a degree. Considering these slope data were taken from a 5 km resolution DEM, these differences in slope angle are too small to form any real conclusions. Freezing lakes formed on the shallowest slopes, and mean slope-angle for freezing lakes was around 0.1 degree shallower than for slow-draining lakes.

Are lakes more likely to drain to the bed (fast draining) if they are sited on ice in a extensional regime? While strain rates were found to be slightly higher for fast-draining lakes than slow-draining or freezing lakes in most years, this difference was not statistically significant in any year.

Are lakes more likely to freeze at higher elevations? It seems intuitive that at higher elevations lakes would be more likely to freeze, as the shorter melt season would ensure that the lakes froze over before they had a chance to drain. Lakes were found to be more likely to freeze at higher elevations, however they were also found to have the longest duration of any drainage type and the highest elevation lakes were often the last to disappear at the end of the melt season, therefore the length of the melt

season at a lake site is not the primary control on whether or not that lake freezes.

Are lakes less likely to drain rapidly if sited on thicker ice? It was suggested in Section 6.5 that fast-draining lakes might be less likely were the ice sheet is thicker, as hydrofracture would be more difficult over thicker ice. Fast-draining lakes were found to form at the lowest mean elevation of any drainage type and were never found at the highest elevations, rather they occurred in a band nearer the ice sheet margin where the ice is thinner. Fast-draining lakes did form further up the ice sheet in higher melt years though, just never at the highest elevations (Figure 7.15).

Freezing lakes formed on thicker ice, flatter slopes, had the largest mean area. and lasted the longest. With the data presented in this thesis there is no way of telling whether any surface drainage from these lakes occurs on a lake-by lake-basis, but by communicating with researchers who have worked near lakes that have subsequently frozen, it has been possible to establish for one freezing lake that a substantial exit spillway was present. This observation would suggest that a lake that freezes may contribute further to the wider supraglacial (and possibly later basal) hydrology, however the down-wasting of the spillway never becomes unstable so the area of the lake can persist, this may be where slope is important. The low slope angles at many of the freezing lakes would make unstable surface drainage less likely (Raymond and Nolan, 2000), so the lakes can persist to the end of the melt season and subsequently freeze. As the margins of the GrIS are largely convex, this means that slow-draining lakes would be more likely to occur at lower elevations where the surface slope is steeper, and indeed slow-draining lakes were associated with lower elevation, steeper slopes.

The reason for the lack of fast-draining lakes at higher elevations, and the preferential occurrence of freezing lakes (Figure 7.15) in this region instead is potentially more complex. Research by Alley *et al.* (2005), van der Veen (2007), and Krawczynski *et al.* (2009) has shown that lake drainage to the bed is theoretically possible for any lake included in this thesis, therefore for lakes that freeze there must be a control preventing this drainage. Freezing lakes were only slightly smaller than fast

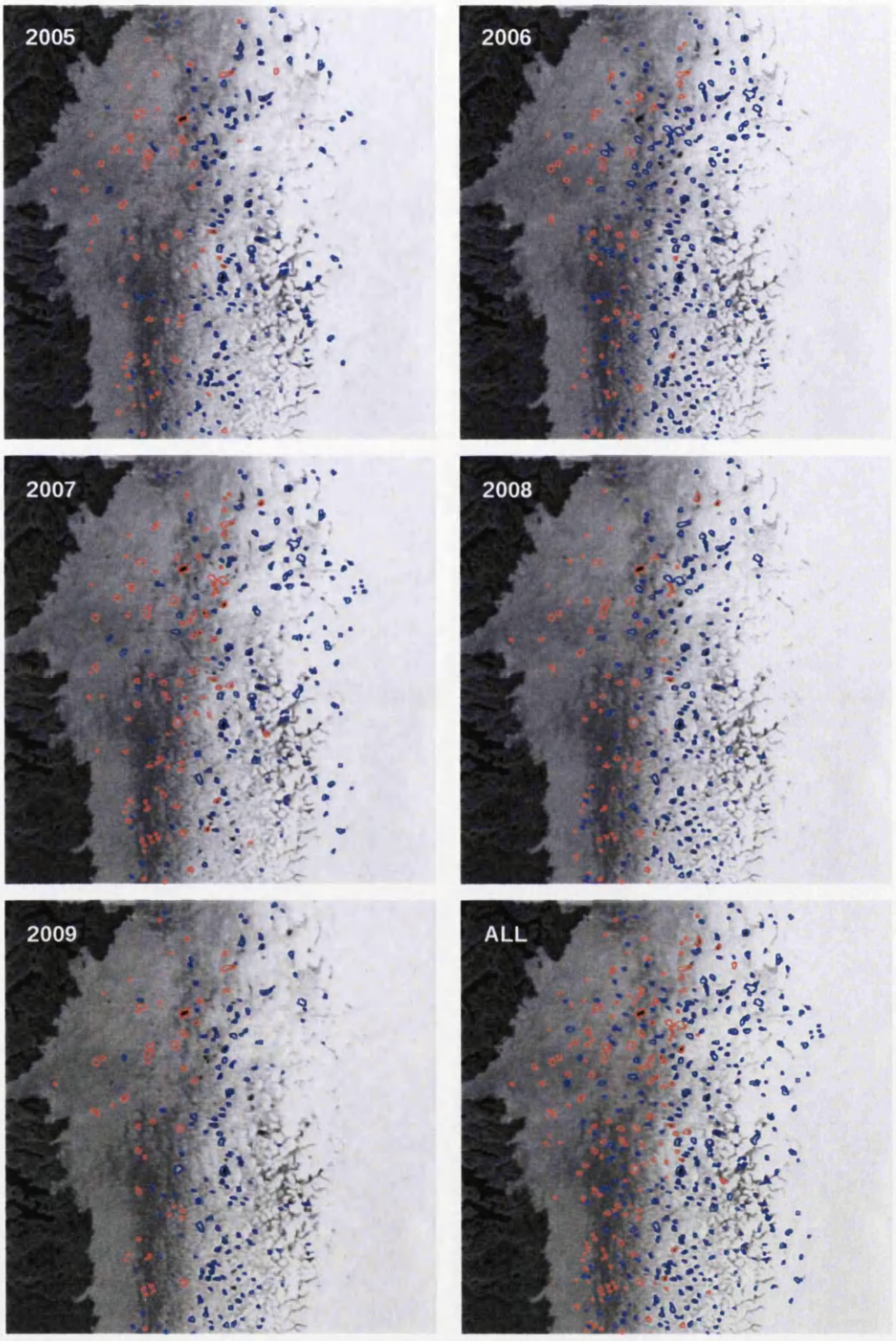

Figure 7.15: Map of part of SW Greenland, showing the locations of fast draining (red) and freezing (blue) lakes. Each year is shown, and a combined map of all years is also included. Freezing lakes occurred at all altitudes, while fast-draining lakes only occurred in a narrower band at lower elevations.

draining lakes and had longer durations, therefore lack of water or insufficient time to propagate a crack to the bed seems unlikely. However, the thicker ice underlying most freezing lakes (see below) may require more water for fracture propagation, and lower slope angles may result in shallower water in these lakes. The differences in strain rates experienced by fast draining and freezing lakes have been demonstrated to be insignificant, suggesting that if the stress regime plays an important role in determining whether or not a lake drains, it cannot be measured at the resolution at which velocity data were available. Two possible theories for the lack of drainage of these freezing lakes will be explored here.

Firstly, it is possible that hydrofracture through the full thickness of the ice sheet becomes more difficult where the ice is thicker, meaning that over the thick ice at the highest elevations fast lake-drainages would be less likely. While modelling studies suggest that hydrofracture through thick ice is straightforward, field observations by Boon and Sharp (2003) showed that this is not the case, and that hydrofracturing failing to reach the bed is common.

Secondly, it may be that lakes forming on thick firn or snow do not drain vertically through the ice as the snow provides a buffer between the lake water and fractures in the ice. If the water column never enters a fracture, then fracture propagation cannot be initiated. This is plausible in the SW where fast-draining lakes formed in the ablation area and freezing lakes above the equilibrium line (Figure 7.16), however in the N and NE freezing lakes, whilst forming at higher elevations than fast-draining lakes, were also mostly in the ablation area.

Which of these theories is closer to the truth is impossible to determine with the data presented here, however it is worth noting that if the ice thickness theory is correct this will provide an upper bound on the elevations at which hydraulic connectivity between supraglacial and subglacial hydrology is possible.

The cause of the existence of both fast and slow-draining lakes at lower elevations is also difficult to establish from the data available. Slow-draining lakes formed at a higher mean elevation (which was significant in all years), however fast and slow

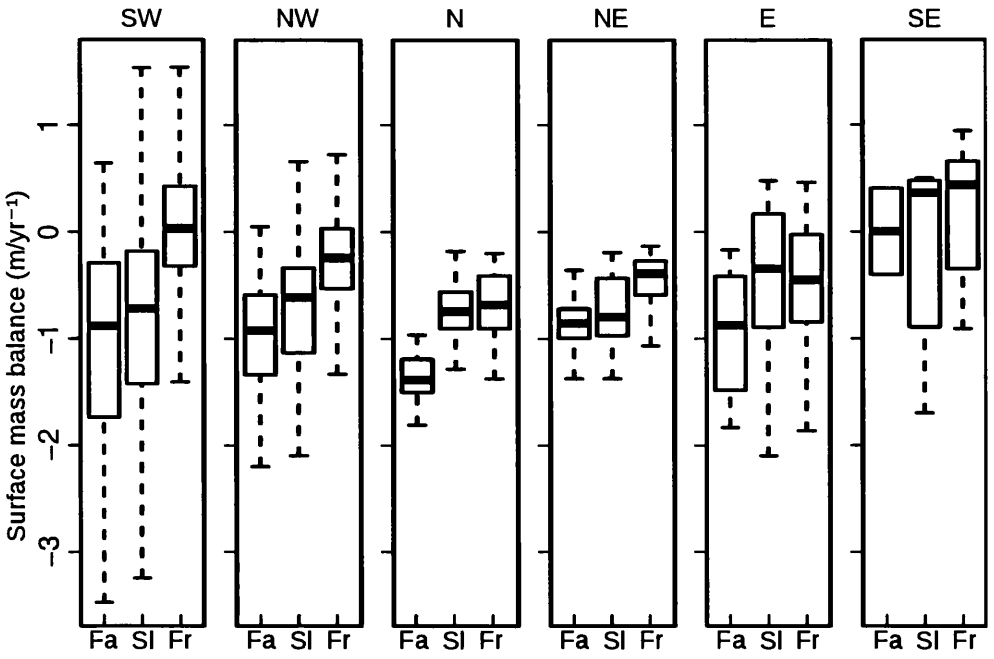

Figure 7.16: Modelled surface mass balance for lakes of different drainage types per region in 2005. Freezing lakes formed well into the accumulation area in the SW, but this pattern was less prominent in other regions.

draining lakes formed alongside each other in all years and all regions. Slow-draining lakes formed on slightly steeper slopes, however this difference was only significant in some years. No significant difference in strain rate could be found between fast and slow-draining lakes. Slow-draining lakes had significantly smaller mean area than fast-draining lakes, however this may well be due to the existence of a prominent drainage channel limiting lake area. It seems most likely that a major element of the reason for a lake draining to the bed or draining over the surface may be due to factors too local to determine remotely. This control on lake drainage could be due to local stress fields too small to be identified in the velocity data available, or likewise localized variation in slope: the DEM used had a spatial resolution of 5 km, it is quite conceivable that slow-draining lakes formed on steeper ground that cannot be detected at the available resolution. The existence of simultaneous fast-draining lakes lends weight to the argument of local forcing mechanisms. Adjacent lakes draining on the same day suggests that very local forcing factors are involved, the drainage of one lake may enlarge a fracture enough that either a nearby lake can drain through the same conduit, or in some way weaken the ice to make propagation

of another part of the same fracture easier. The fact that some lakes drain both slowly and quickly in subsequent years whilst some lakes always drain the same way implies that it is not simply local scale variations in slope forcing the difference, unless the topography is changing significantly between years. Whatever factor controls whether lakes drain rapidly or slowly can change from one year to the next, and Figure 6.19 shows lakes that drained fast in only some years were most likely to drain slowly in other years, so fast and slow-draining lakes must have some interchangeable characteristics. In contrast, few lakes drained fast in some years and froze in others.

7.3.4 Causes of interregional differences in lake area

Much of the interregional variation observed most likely came from the topography of the different regions. If latitudinal temperature gradient was ignored, lakes would be expected to form up to similar altitudes in all parts of the ice sheet. On Figure 7.4, 2000 m elevation is represented by a horizontal dotted line. If the lake area was delimited by this contour the NE would be expected to have the largest lake area (per unit of coastline), the SW and N would be similar, the NW area smaller again, and the SE and E regions the smallest of all. This difference in topography explains the obvious difference between the SW and SE regions, and the low total lake area of the E region. The NW remains steeper at higher elevations than the SW which flattens out considerably at around 1300 m providing good potential for lake formation at higher elevations, the larger surface area of ice in the SW in the potentially lake forming elevations explains the difference in the total lake area between these two regions, and the generally steeper slopes of the NW explain the smaller lakes found in that region. The SW and NE regions had the largest lakes on average, and the largest lakes in these regions were higher on the ice sheet, therefore the flatter high elevation topography in these two regions explains the larger mean lake sizes in these regions. The topography of the difference regions also explains the differing interannual variation in mean lake area between regions. Inter-annual

variations were significant in the SW, NW, N, and NE regions, where increasing melt allowed lakes to form on flatter slopes. In the E and SE regions, where variations in the mean area of lakes were not significant, the slope does not flatten out until much higher up the ice sheet than in the other regions. Topography controls the area of the ice over which melt occurs, and latitudinal variations in melt exist, with less melt occurring further north. As a result of this lakes formed at lower elevations in the northern regions, with lakes forming up to around 1400 m, whereas in the southern regions lakes reached nearly 2000 m.

7.4 Potential biases and sensitivities of the results

This section discusses possible causes of error and bias in the results of this thesis. If one region consistently had more cloud cover than other regions, then that region may have fewer fast lake-drainage events recorded, and the day of maximum area for each lake would be more likely to be missed. The possible biases from cloud are discussed in Section 7.4.1. The temporal resolution used to initially identify lakes is revisited in Section 7.4.2, and the likelihood of lakes having been missed as a result is discussed. Possible errors in area measurements resulting from the classification method used are discussed in Section 7.4.3, and two approaches to calculating errors in overall lake area are described. In both result chapters data are normalised by ice-sheet margin length. In Section 7.4.4 other possible normalisation techniques are described, and the impact of using them on the conclusions of this thesis are discussed. Finally, the relationship between lake volume and lake area (used in this thesis as a proxy for lake volume) is explored in Section 7.4.5.

7.4.1 Cloud

One of the sources of uncertainty for this thesis is the data missing due to cloud cover. Missing data from cloud means that some lakes could not be classified by drainage type, and were assigned the classification "unknown". The distribution of

unknown lakes was not spatially uniform. In particular, as noted in Section 6.3.3, a lot of unknown category lakes were located in the southernmost catchments of the SW region. From Figure 4.10 it is clear why: this part of the ice sheet had the least probability of being imaged cloud-free. Conversely the very low number of unknown lakes in the NE corresponded with a relatively high probability of cloud-free imagery. For the conclusions of this thesis to be robust, differences in the occurrence of fast-draining lakes between regions need to be examined with respect to cloud bias. In particular the contrast between the SW/NE and NW/SE with regard to total lake area and fast lake-drainage occurrence needs to be free from cloud bias.

From Figure 4.10 it is apparent that the SW and SE had similarly high rates of missing data due to cloud. The fact that these regions have the lowest potential of cloud-free imagery is reassuring as they account for the highest and lowest numbers of lakes (and fast-draining lakes) on the ice sheet. The NW and NE regions both had similarly low frequency of data loss due to cloud. The NE region had the highest percentage of lakes draining rapidly of any region. This frequency of fast lake-drainage may have been due to low accumulation (see discussion in Section 7.3.3 regarding the fast draining lake occurrence on snow and firn), or could have been due to the very low number of images lost to cloud. To consider the possible effect that the failure of lake classification due to cloud may have had on the conclusions of this thesis, the extreme scenario that all unknown category lakes actually drained rapidly whilst obscured by cloud is considered and the results of this are presented in Table 7.1. The same pattern of fast-draining lake distribution is seen in the original data (Table 7.1a) and the modified data (Table 7.1b). This pattern is backed up by performing a chi-square analysis on the modified data (Table 7.2), and the differences are found to still be highly significant; therefore the results are robust to cloud bias. Comparing the deviation from the expected frequency of fast-draining lakes in Table 7.2 with those of Table 6.2 it is apparent that the higher percentage of lakes in the NE draining rapidly than in the SW could be due to the more frequent cloud cover in the latter region.

Table 7.1: The possible effects of uncertainty on the number of fast-draining lakes in each region. (a) The original observed frequency of different drainage types in the regions of the GrIS, averaged over five years. (b) The frequency of drainage types if all unknown category lakes were actually fast draining.

(a)	Fa	Sl	Fr	Un
SW	160	420	451	91
NW	29	121	225	20
N	16	26	65	10
NE	45	70	135	10
E	9	40	42	3
SE	3	17	14	2

(b)	Fa	Sl	Fr
SW	251	420	451
NW	49	121	225
N	27	26	65
NE	56	70	135
E	12	40	42
SE	5	17	14

Table 7.2: The possible effect of uncertainty on the significance of the differences in the number of fast-draining lakes between regions. The χ^2 analysis is carried out in the same manner as in Table 6.2, but with all unknown lakes converted into fast-draining lakes. χ^2=486.37, df=5, critical value (p=0.001)=20.52, therefore there would still be a significant difference in the occurrence of fast-draining lakes between regions

Region	Ice margin length (km)	Proportion of total length	Observed freq. (O)	Expected freq. (E)	O-E	$\frac{(O-E)^2}{E}$
SW	1331	0.2134	251	85.15	165.45	321.49
NW	1193	0.1913	49	76.32	-27.32	9.78
N	923	0.1480	27	59.05	-32.25	17.61
NE	476	0.0763	56	30.45	25.15	20.77
E	985	0.1579	12	63.01	-50.61	40.65
SE	1329	0.2131	5	85.02	-80.42	76.07
Total	6237		399	399		486.37

7.4.2 Temporal resolution of initial lake identification

With the data collected in Chapter 5 it is possible to revisit an important part of the methodology: the temporal spacing of the images used to initially identify lakes in Section 4.4. Before the main lake-by-lake classification was run (Section 4.5), images approximately every five days were used to identify the position of lakes, and the positions from all five years combined. If the duration of some lakes was less then five days then the risk of having missed a lake due to drainage would be increased, although the lake would have to be missed (or not formed) in each of

the five years. Geometric mean lake duration was 21 days, and geometric standard deviation was 2.67 days, therefore the range of values equivalent to one arithmetic standard deviation either side of the mean (accounting for ~ 68% of values) was 7.8–55.5 days. The shortest lived lakes were those those drained rapidly. Fast-draining lakes had a geometric mean duration of 12.1 days and a geometric standard deviation of duration of 2.5, meaning ~ 68% of values fell in the range 5–30 days. These values, and the use of five years of data, show that the original image temporal spacing was robust.

7.4.3 Errors in area measurement

To quantify the error of classifying lakes, Sundal *et al.* (2009) took the RMSE from comparing lake areas hand digitised from ASTER data and classified from MODIS data, and for each total area multiplying the RMSE by the number of lakes. This calculation was carried out using the RMSE calculated in Section 4.2.5 (0.14 km^2). The results of applying this to the total maximum lake area per region are shown as error bars on Figure 7.17.

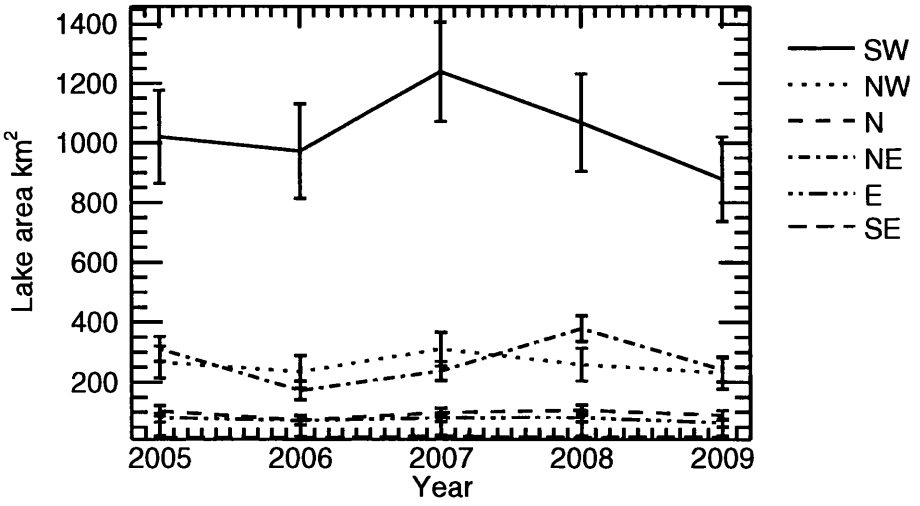

Figure 7.17: The total maximum lake area for the six regions of the ice sheet, with errors bars calculated from RMSE

Whilst the error bars for the area in the SW on Figure 7.17 are large enough to mean any interannual variation could be due to error, much interregional variation

persists, although the NW and NE, and N and E regions become difficult to separate. However, this method of error estimation assumes that all errors could have the same sign which is very unlikely; it is far more probable that errors will cancel themselves out partially, as seen in Figure 4.5 where the errors are found to be equally positive and negative, and the total area obtained from ASTER and MODIS in Section 4.2.5 was identical at the precision used. An alternative is the standard method for adding independent errors (e.g. Tinker and Lambourne, 2000). The overall error $\pm E$ of independent errors $\pm e_1$,$\pm e_2$,$\pm e_3$...$\pm e_n$ is given by

$$E = \sqrt{e_1^2 + e_2^2 + e_3^2 \ldots + e_n^2} \tag{7.1}$$

As individual errors for each lake were not available, the mean absolute error was calculated (0.11 km^2), and this was used in the following formula

$$E = \sqrt{M^2 n} \tag{7.2}$$

where M is the mean absolute error and n is the number of lakes from which total area has been calculated. This error was also applied to the total maximum lake area per region, and the resulting error bars are shown in Figure 7.18.

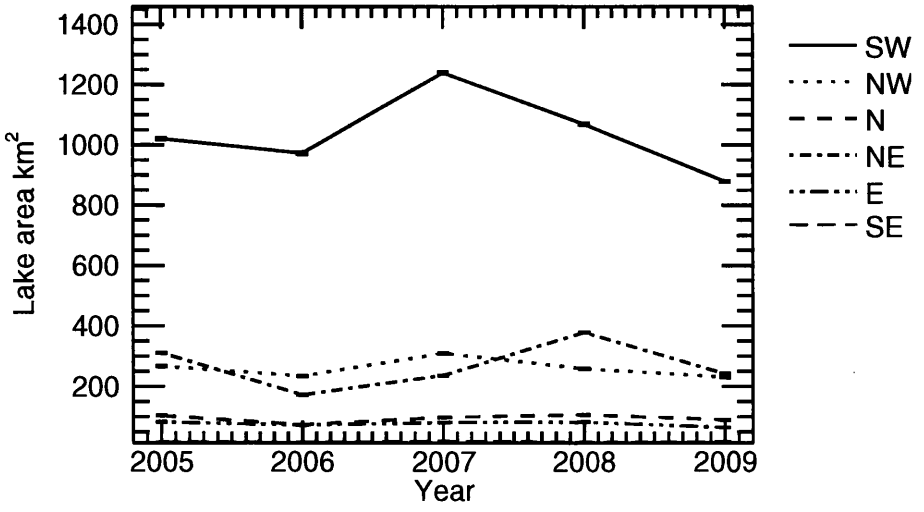

Figure 7.18: The total maximum lake area for the six regions of the ice sheet with error bars calculated from Equation 7.2. The error bars are up to 4 km^2.

The error bars in Figure 7.18 are clearly far smaller than in Figure 7.17. Without extensive ground truthing it is impossible to determine how appropriate the choice of error representation is, although the error estimation carried out using ASTER data (Section 4.2.5) gives an interesting insight. The total area of lakes in the test area from ASTER was 76.7 km^2. Using the RMSE $\times$ n method of error estimation, this would have made the total area with error 76.7 ± 14.2 km^2. Using the mean absolute error and independent errors method would have made the total area with error 76.7 ± 1.2 km^2. Considering the total area from MODIS was also 76.7 km^2, the error estimated from RMSE seems rather large. Obtaining exactly the same area from ASTER and MODIS is perhaps unrepresentative of the accuracy of the measurement as clearly there is some error, so two 50 lake sub-samples were taken from the original 100 lake test-dataset. The total areas for ASTER and MODIS for these sub-samples were 25.9 and 26.0 km^2 and 49.8 and 49.7 km^2 respectively, so well within the 0.61 km^2 error estimated from Equation 7.2 for n= 50.

Clearly the choice of error representation makes a huge difference to the errors estimated, however it must be remembered that these errors are only estimates, and the true error per lake is unknown. In addition, for the conclusions of this thesis the exact area of lakes is far less important than the relative area and frequency of lakes between regions and catchments, and from Figure 7.17 it is apparent that even with those rather conservative error bars, major interregional differences occurred.

7.4.4 Data normalisation methods

To test the effect of using different normalisation methods on the relative importance of the regions of the ice sheet in terms of total lake area and the number of fast-draining lakes, a range of different normalisation methods were tested. Data normalisation in this case can serve to either remove sampling bias, or to provide a density of lake coverage and drainage for each unit of some normalising area. The use of margin length as a normalisation method removes sampling bias resulting from the different sized regions used, but leaves any variation resulting from differ-

ences in melt and topography. If the total area of lakes and number of fast drainage events are divided by the margin length for each region, then a normalised quantity is obtained allowing regions to be rank ordered (Table 7.3).

Table 7.3: Regional results normalised by ice sheet margin length. Regions are ranked according to normalised lake area and fast drainage frequency, ranks are given in brackets.

Region	Ice margin length (km)	Total lake area (km^2)	No. fast lakes	Lake area km^2 per km of margin	No. fast-draining lakes per km of margin
SW	1331	1035.8	159.6	0.78 (1)	0.12 (1)
NW	1193	260.19	29.2	0.22 (3)	0.02 (3)
N	923	94.34	16.4	0.1 (4)	0.02 (3)
NE	476	268.02	45.4	0.56 (2)	0.1 (2)
E	985	76.48	9.2	0.08 (5)	0.01 (5)
SE	1329	16.71	2.8	0.01 (6)	0.00 (6)

The alternative to just removing sampling bias is to normalise by the zone where lakes can form, to give a density of lake coverage and drainage. As discussed in Section 7.3.1 defining such a zone is not straightforward, the most satisfactory metric to use is probably ablation area. Lake area and fast drainage frequency are shown in Table 7.4.

Table 7.4: Regional results normalised by modelled ablation area. Regions are ranked according to normalised lake area and fast drainage frequency, ranks are given in brackets.

Region	Ablation area (km^2)	Total lake area (km^2)	No. fast lakes	Lake area as % ablation area	No. fast draining lakes per 1 km^2 ablation area $x10^{-3}$
SW	68101	1035.8	159.6	1.52 (1)	2.34 (1)
NW	60406	260.19	29.2	0.43 (3)	0.48 (3)
N	48881	94.34	16.4	0.19 (4)	0.34 (4)
NE	52453	268.02	45.4	0.51 (2)	0.87 (2)
E	40389	76.48	9.2	0.19 (4)	0.23 (5)
SE	34104	16.71	2.8	0.05 (6)	0.08 (6)

To further establish the variation obtained through normalisation, lake density was also calculated by another two methods. Lakes formed below 2000 m in all parts of the ice sheet, normalising by this area removes bias from the size of catchments,

takes into account the topography of the regions, but not latitudinal temperature gradient. The data normalised by this area are shown in Table 7.5.

Table 7.5: Regional results normalised by the area below 2000 m elevation. Regions are ranked according to normalised lake area and fast drainage frequency, ranks are given in brackets.

Region	Area < 2000 m (km^2)	Total lake area (km^2)	No. fast draining lakes	Lake area as % of area < 2000 m	No. fast draining lakes per 1 km^2 < 2000 m x10^{-3}
SW	113205	1035.8	159.6	0.91 (1)	1.41 (1)
NW	110668	260.19	29.2	0.24 (4)	0.26 (4)
N	113715	94.34	16.4	0.08 (5)	0.14 (5)
NE	83298	268.02	45.4	0.32 (2)	0.55 (2)
E	28933	76.48	9.2	0.26 (3)	0.32 (3)
SE	52786	16.71	2.8	0.03 (6)	0.05 (6)

Finally the area that experienced at least 45 days of melt per year explained the distribution of lakes in some parts of the ice sheet (although not in the south). The data normalised by this area are given in Table 7.6.

Table 7.6: Regional results normalised by the area with more than 45 days of melt per year. Regions are ranked according to normalised lake area and fast drainage frequency, ranks are given in brackets.

Region	Area of melt (km^2)	Total lake area (km^2)	No. fast draining lakes	Lake area as % melt area	No. fast draining lakes per 1 km^2 melt area x10^{-3}
SW	158213	1035.8	159.6	0.65 (2)	1.01 (2)
NW	69699	260.19	29.2	0.37 (3)	0.42 (3)
N	39078	94.34	16.4	0.24 (4)	0.42 (3)
NE	35734	268.02	45.4	0.75 (1)	1.27 (1)
E	43911	76.48	9.2	0.17 (5)	0.21 (5)
SE	105128	16.71	2.8	0.02 (6)	0.03 (6)

In all of the normalisation methods presented in Tables 7.3–7.6 the regions with the highest normalised lake area and fast lake-drainage frequency are the SW and NE, with the SW highest when normalising by margin length, ablation area, and elevation below 2000 m, and the NE was highest when normalising by melt area. The SE region had the lowest normalised lake area and fast drainage frequency with each normalisation method. This analysis shows that the interregional differences reported in this thesis are robust to different normalisation methods.

The results in the previous chapters were normalised using margin length, a choice made for two reasons. Firstly, as an aim of this research was to find causes for interregional differences, normalising by a factor which will mostly likely explain part of these differences (such as topography, or ablation area) is not desirable. Secondly, as the zone of potential lake formation is difficult to delineate and not fully explained by for example ablation area (Section 7.3.1), an appropriate method for calculating lake density is not available. Even if an appropriate method was available to calculate the density of fast-draining lakes, it is not yet known whether it is more significant for ice-sheet dynamics to have a given number of fast-draining lakes closely spaced at low elevations, or more sparsely spaced but occurring at higher elevations as well. Normalising by ablation area etc will make the former case appear more significant, which may not be the case.

7.4.5 The relationship between lake area and volume

In this thesis, lake area has been used as a proxy for lake volume, this section will explore the relationship between lake depth and lake volume as reported by previous studies to determine if this proxy use was appropriate.

Several studies have attempted to remotely measure the depths of Greenland lakes based on optical depth measurement techniques, using the attenuation of light by water to estimate the depth of the water column. This has been performed using the Lambert-Beer law applied to ASTER data (Sneed and Hamilton, 2007; Georgiou *et al.*, 2009), and using an empirical approach with MODIS data (Box and Ski, 2007). Lake volumes derived both remotely and in the field by Das *et al.* (2008) are shown in Table 7.7. While a range of volume measurements are available, few of these have been verified. Sneed and Hamilton (2007) did not verify their lake depth findings at all. While Box and Ski (2007) took field measurements of lake depths, they used these depths to produce a lake-depth/MODIS reflectance function meaning that these field data cannot be used for verification. Georgiou *et al.* (2009) compared the depths of one lake obtained from ASTER data to airborne lidar measurements

of the drained lake basin, and found large uncertainties (errors up to 50% of lake depth).

Table 7.7: Lake areas and volumes from previous studies. Volumes from Box and Ski (2007) and Georgiou *et al.* (2009) were estimated remotely, the volume from Das *et al.* (2008) was measured in the field. Of two lakes measured, Das *et al.* (2008) reports the volume of one. The data from both were used by Krawczynski *et al.* (2009). Individual lake volumes were not reported by Sneed and Hamilton (2007).

Source	Area km^2	Volume km^3
Box and Ski (2007)	1.7	0.008
	2.2	0.008
	3.3	0.024
	1.8	0.010
	6.8	0.033
	6.5	0.022
	8.5	0.022
Das *et al.* (2008)	5.6	0.044
Georgiou *et al.* (2009)	3.4	0.019

The absence of reliable lake depth estimations lead Krawczynski *et al.* (2009) to compare the areas and volumes of two lakes measured by Das *et al.* (2008), and approximate lake volume by assuming lakes had a conical shape and a diameter-depth aspect ratio of 100:1. The diameter-depth ratios for the lakes in Table 7.7 were calculated and are presented in Table 7.8. While the ratio of 1:100 chosen by Krawczynski *et al.* (2009) is of the correct order of magnitude, there was substantial variation around this ratio for the lakes included here: from 88:1 to 430:1. For this reason volume approximations were not attempted in this thesis, and lake extent and drainage have been expressed as areas. If in the future a satisfactory and verified method for obtaining lake volumes from MODIS data becomes available, then the results of this thesis could be expressed as volumes instead.

Table 7.8: The diameter and depths of conical approximations of field and remotely measured lake volumes. The lakes used are the same as in Table 7.7.

Area 10^6 m^2	Volume 10^6 m^3	Conical diameter m	Conical depth m	Diameter-depth Aspect ratio
1.7	7.9	1471	13.9	106:1
2.2	8.3	1674	11.3	148:1
3.3	24.3	2050	22.1	93:1
1.8	10.3	1514	17.2	88:1
6.8	32.9	2942	14.5	203:1
6.5	21.7	2877	10.0	287:1
8.5	21.7	3290	7.7	430:1
5.6	44	2670	23.6	113:1
3.4	19	2080	16.8	124:1

7.5 Glaciological importance

The glaciological importance of the findings of this thesis are split into the implications for past and future studies of lake drainage, and the implications for the study of ice-sheet dynamics. In Section 7.5.1, the importance of these results for both field and remote sensing based studies of lakes is discussed, and the robustness of the conclusions of several previous studies of lake drainage is analysed. In Section 7.5.2, the implications of the results of this thesis for the dynamics of the Greenland Ice Sheet are discussed, in particular relating to the spatial relationship between fast lake-drainages and dynamic mass loss from the ice sheet.

7.5.1 Implications for studies of lake drainage

The results of this thesis have implications for the study of supraglacial lake-drainage both through remote sensing and in the field. A major difficulty for instrumenting sudden lake-drainage in the field, is having monitoring equipment in place at the right lake at the right time. As only around ten percent of lakes drain rapidly, choosing a lake to instrument is problematic. In addition, to study the rapid drainage of a lake, instrumentation must be in place sufficiently early so that drainage is not

missed. The results of this thesis can be used to predict which lakes are most likely to drain rapidly. Some lakes drained in every year studied: the lake studied by Das *et al.* (2008) is one such lake. These lakes would be excellent choices for field projects wanting to study a fast lake-drainage event. Similarly, if a field study wanted to find out what controls why a lake can drain to the bed in one year and over the surface in another, the results of this thesis could be used to identify a lake which frequently changed drainage types interannually in the past.

Predicting when a lake will drain rapidly is not straightforward. Taking the lake studied by Das *et al.* (2008) as an example, that lake drained rapidly on days 170, 210, 191, 192, and 167 in the five years studied in this thesis: a range of 43 days. This range shows that to capture a fast lake-drainage event in the field, instruments must be in place early. Duration values from this thesis show that from lake formation to lake drainage for fast-draining lakes was a geometric-mean period of 12 days, plus/minus one geometric standard-deviation this was 5–31 days. These values mean that it may be possible to delay instrumentation until a lake forms, but once the lake begins to grow it is reasonable to expect rapid drainage within a week.

The discovery that many lakes drain, but do so gradually over several days and probably supraglacially as opposed to the sudden drainage to the bed in a few hours of lakes like that studied by Das *et al.* (2008) has important implications for the choice of temporal resolution used to study lake drainage through remote sensing. Even if the water from slow-draining lakes reaches the bed of the ice sheet through a moulin, the dynamic effect of a given volume of water being delivered to the bed in several hours is very different to the same volume of water reaching the bed over several days, and an additional connection to the bed will not have been established in the latter case. Clearly it is important to distinguish between these drainage types, however if the time between images used to infer drainage is longer than the time it takes for a lake to drain over the ice surface, then misidentification of lake drainage is inevitable.

Drainage time for each slow draining lake was calculated as the time from when the

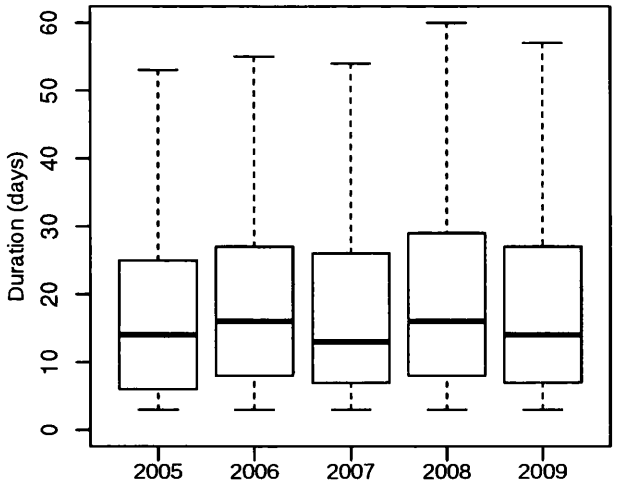

Figure 7.19: Boxplots showing the time taken for slow-draining lakes to drain in each year.

lake was largest to the day the lake disappeared, and is shown in the boxplots in Figure 7.19. The mean drainage time of slow-draining lakes (plus/minus one standard deviation) was 18.9 ± 14.8 days, a substantial range of durations. It is therefore recommended that future studies wishing to monitor lake drainage use daily imagery whenever possible, perfectly feasible using MODIS data. Obviously this temporal resolution is not always possible especially when higher spatial resolution data are required, in this case it must be understood that lakes observed to drain will not necessarily have done so either suddenly or to the bed. With this recommendation in mind, previous remote-sensing studies that consider lake drainage are revisited here to check whether adequate temporal resolutions were used to support their findings.

Howat *et al.* (2010) correlated the drainage of two lakes on Storegletscher in W Greenland with velocity slowdowns on the same glacier using images spaced up to 23 days apart. Despite this, their conclusions remain robust as the data from this thesis show that the lakes inferred to drain to the bed of the glacier did indeed drain in < 24 hours, although it is difficult to discern from the information in that paper how the more precise timings determined here would affect their conclusions regarding velocity responses.

Joughin *et al.* (1996) studied a "mini-surge" of Ryder Glacier in 1995, and noted a

change in SAR intensity values over supraglacial lakes between 22 September and 26 October 1995 (days 265 and 299). Joughin *et al.* (1996) interpreted these changes as lake drainages, and speculated that lake drainage to the glacier bed may have caused or been caused by the ice accelerating. Geographically this is plausible: fast lake-drainages were observed on Ryder Glacier in this study, one in 2006 and two in 2008. However, the timing of the images used brings this theory into question. The fast lake-drainages in 2006 and 2008 occurred on days 186, 186, and 181. While no melt data for 1995 were collected for this study, it seems most plausible given the timings of the images that the lakes in question froze over, resulting in a change of intensity values. Most lakes on Ryder Glacier in the study period of this thesis were freezing over by the date first image pair used Joughin *et al.* (1996), and all had frozen by the date of the second image pair in all years studied in this thesis. Therefore, it seems most likely that lake drainage did not play a role in the 1995 "mini-surge".

Box and Ski (2007) state that "sequential cloud-free images" were used, which is interpreted as being at least daily observations where cloud permits. In addition the duration over which each lake drained was given. Therefore, their findings regarding lake drainage were probably robust. Similarly, Bartholomew *et al.* (2011) used all available cloud-free scenes when studying rapid lake-drainage with regards to pro-glacial runoff in SW Greenland, which amounted to 40 images over a 79 day period: almost certainly sufficient to support the conclusions of that paper.

Only 12 ASTER images over the whole 2001 melt season were used by McMillan *et al.* (2007) to study lake drainage, who used these drainage data to estimate the maximum possible volume of water that could have reached the bed. While this temporal resolution is very poor, McMillan *et al.* (2007) acknowledge that is was not possible to tell how much of that water actually reached the ice-sheet bed.

Chu *et al.* (2009) did not explicitly state the temporal resolution used for their study of the link between supraglacial lake drainage and fjord sediment-plumes, but do state that at least 90% cloud-free images were used (not necessary when working

on a lake-by-lake basis). As Chu *et al.* (2009) were specifically studying drainage of lakes to the ice-sheet base, temporal resolution was important for their conclusions. While adequate imagery may have been used, this omission serves as an example of why reviewers should insist upon an explicit statement of the temporal resolution used, to allow the findings of the paper to be adequately critiqued.

7.5.2 Implications for ice sheet dynamics

It has been stated (Sundal *et al.*, 2009) that as the warming climate leads to lakes forming higher up on the ice sheet, it would in turn lead to more lake drainage events, and therefore more connections between the surface and basal hydrologies at higher elevations on the ice sheet. As demonstrated in Section 7.3.3, the relationship between lake elevation and lake drainage is not simple. If lake drainage to the bed is limited by snow cover, then the retreating snow line is more important for lake drainage than either the extent of surface melt or the upper limit of lake coverage. So far in response to global warming Greenland, whilst experiencing more melting, is also experiencing more snowfall (Hanna *et al.*, 2005) which will make the forcing of basal hydrology by a warming climate more complex than has been suggested if fast lake-drainage is inhibited by thick layers of snow. If instead lake drainage to the bed is limited by ice thickness, then lakes forming at higher elevations will have no impact on the basal hydrology at higher elevations as they will be unable to drain.

The interannual relationship between fast lake-drainage events and melt is straightforward to test. Figure 7.20 shows the relationship between melt extent and duration and the number of fast lake-drainages for each region of the ice sheet, and can be compared with Figure 7.13 which shows the relationship between the same melt extent and duration and total lake area. In many regions there is a clear relationship between melt and the number of fast lake-drainages. Strong positive correlations were found between melt and fast lake-drainage in the SW (r=0.83), NE (r=0.93), and E (r=0.59). Moderate positive correlations were found between melt and fast lake-drainage in the N and SE, and a moderate negative correlation between melt

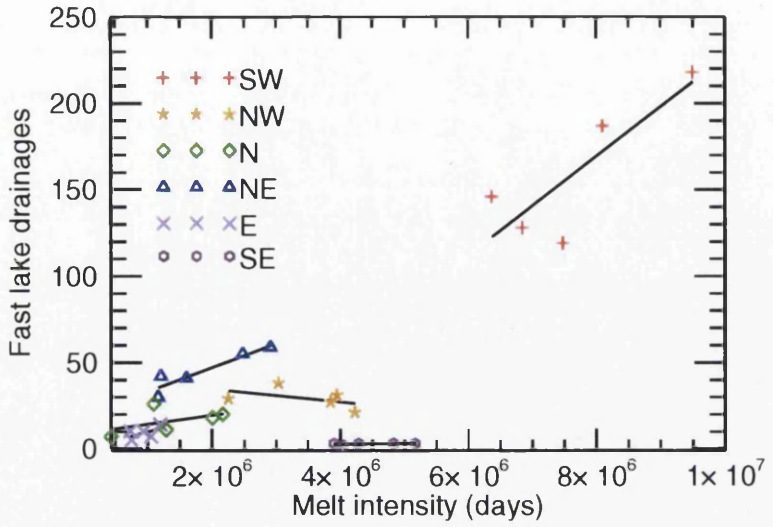

Figure 7.20: The relationship between melt extent and duration and the number of fast lake-drainages

and fast lake-drainages in the NW. Of the correlations listed however, only that for the E region was significant at the 95% confidence level ($p = 0.02$). As a result of this lack of significance, it is not possible to predict the number of fast lake-drainage events with just melt data and the results of this thesis, although with more years of lake data a predictive capability may be possible. It is therefore difficult to say with certainty that increased melt leads to more fast lake-drainage events, however the next section will demonstrate that recent mass loss from the ice sheet cannot have been caused by increased melt leading to more fast lake-drainage events, owing to the locations of the lake drainages themselves.

GRACE, ICESat, and other methods have shown that the mass loss from the GrIS is not uniform, and the causes of mass loss are spatially variable as well. As discussed in Chapter 1, GRACE results have shown the regions of greatest mass loss to be the SE and NW, with some mass loss in the SW (Velicogna and Wahr, 2006; Khan *et al.*, 2010). Only the NW and SE regions have experienced significant dynamic mass loss, with the negative mass balance of other regions attributable to surface mass balance (Pritchard *et al.*, 2009; van den Broeke *et al.*, 2009). If fast lake-drainage events were intimately linked to dynamic mass loss from the Greenland Ice Sheet, it would be reasonable to assume that those regions with the greatest dynamic mass loss would have experienced the most fast lake-drainages. In fact, the pattern of fast

lake drainage shows a striking inverse relationship with the regions of dynamic mass loss.

The SE region where mass loss has been the most significant (Velicogna and Wahr, 2006) and dynamically driven (Pritchard *et al.*, 2009; van den Broeke *et al.*, 2009) had the fewest lakes of any region, and an even smaller proportion of fast lake-drainages. Of the large glaciers responsible for dynamic mass loss in this region, only Kangerdlugssuaq Glacier experienced fast lake-drainages in each year of the observation period. As fast lake-drainages were so rare in the SE, they cannot have played a role in the dynamic mass loss observed in this region.

The NW region has been losing mass since 2005 (Khan *et al.*, 2010), the starting date for this study, and has also been highlighted as an area of dynamic thinning (Pritchard *et al.*, 2009). Whilst the NW region had the second highest number of lakes of the regions studied, this was in part due to the size of the region as shown by the expected frequencies (Table 6.2), and only a small proportion of these lakes drained (7%). Fast lake-drainages, whilst more common in the NW than the SE, were still infrequent in this region compared with the SW were five times more drainage events occurred.

In contrast the SW region, where mass loss outside of the Jakobshavn Isbræ catchment can be explained by surface mass balance (Pritchard *et al.*, 2009; van den Broeke *et al.*, 2009), had by far the greatest number of fast lake-drainages: triple the number of any other region. The lakes in the NE region, where GRACE results show the lowest mass loss of any Greenland region (Wouters *et al.*, 2008), had the second largest number and the highest proportion (17%) of lakes that drained suddenly during the observation period. The SW and NE were the only regions where the frequency of fast-draining lakes was higher than the expected distribution (Table 6.2).

This analysis is simple, but defensible because of the nature of the pattern observed. Had the high concentration of lake drainages correlated spatially with areas of dynamic mass loss, it could be insufficient to claim that fast lake-drainages were the

cause of this change owing to possible interregional differences in hydrology, and due to the re-organisation of subglacial drainage in high-discharge conditions. As discussed in Chapter 2, large influxes of water lead to more efficient subglacial drainage, and as a result the highest levels of melt observed in parts of the SW have been linked to lower than normal velocities (Sundal *et al.*, 2011). However, the scarcity of fast lake-drainages in the regions experiencing dynamic mass loss means that the conclusions made here are largely independent of these factors; if fast lake-drainages were a vital component of dynamic mass loss on the GrIS they would be prevalent in the SE and NW, which is not the case.

To ensure that these conclusions are as robust as possible, the scenario that regional differences in the dynamic effect of lake drainage exist is worth considering. All other factors being equal, fast lake-drainage events being scarcer in the SE in the NW would suggest that lake drainage has played a limited role in the dynamic mass loss from that region. However, as no studies on the dynamic effect of surface meltwater reaching the ice sheet base have been conducted in regions outside of the SW, it is conceivable that the effect of lake drainage to the bed may not be the same in all regions. The SW has a greater proportion of its margin land-terminating than other regions, and is known to develop an efficient sub-glacial drainage network. Therefore to demonstrate that fast lake-drainages could not have caused dynamic mass loss in the SE and NW, more localized mass loss and lake drainages need to be compared. For this purpose, the glacier-by-glacier dynamic mass loss calculated by Pritchard *et al.* (2009) is used. Assigning fast-draining lakes to glaciers in the SE was simple, owing to the very low number of fast-draining lakes and the wide spacing of the outlets, which tend to be well defined. In the NW region there were more fast-draining lakes and outlets flow into coastal embayments, making it harder to decided which lakes would affect which glacier. Fast lake-drainages in the NW were therefore assigned to glaciers based on flowlines from the velocities calculated by Joughin *et al.* (2010), and it was assumed that lake drainage would affect the glacier down-flow of the lake.

It is straightforward to demonstrate that dynamic mass loss on the SE was not

Table 7.9: Glaciers in the SE as studied by Pritchard *et al.* (2009), with fast-draining lakes per year listed for each glacier. Glaciers that were thinning dynamically are shown in *italics*. A fast lake-drainage occurred on Fenris Gletscher in both 2006 and 2008, however this glacier was not included in the findings of Pritchard *et al.* (2009).

Name	Lat	Lon	Dynamic thinning/yr	2005	2006	2007	2008	2009
Kangerdlugssuaq	*68.68*	*-33.29*	*-18.1*	*3*	*2*	*2*	*1*	*2*
Polaric	*67.96*	*-32.49*	*-0.4*	-	-	-	-	-
Midgardgletscher	*66.45*	*-36.77*	*-18.9*	-	-	-	-	-
Helheim	*66.35*	*-38.37*	*-21.8*	-	-	-	*1*	-
Unnamed	*65.79*	*-39.7*	*-2.3*	-	-	-	-	-
Unnamed	*65.71*	*-40.05*	*-1.5*	-	-	-	-	-
Unnamed	*65.56*	*-40.13*	*-2.85*	-	-	-	-	-
Unnamed	65.42	-49.91	0.2	-	-	-	-	-
Unnamed	65.24	-40.78	0.3	-	-	-	-	-
Unnamed	65.23	-41.09	0.45	-	-	-	-	-
Unnamed	*64.97*	*-41.44*	*-3*	-	-	-	-	-
Unnamed	*64.51*	*-40.62*	*-5.3*	-	-	-	-	-
Kangiatamunata s.	*64.18*	*-49.34*	*-1.1*	-	-	-	-	-
Gyldenlove Fj.	*64.17*	*-41.57*	*-8.2*	-	-	-	-	-
Bernstorff Isfjord N	*63.87*	*-41.75*	*-6.1*	-	-	-	-	-
Bernstorff Isfjord S	*63.66*	*-41.77*	*-5.75*	-	-	-	-	-
Unnamed	63.25	-42.29	2.1	-	-	-	-	-
Unnamed	62.96	-42.88	1.2	-	-	-	-	-
Mogens Henesen Fj. N	*62.52*	*-43.04*	*-11.5*	-	-	-	-	-
Mogens Henesen Fj. M	*62.49*	*-43.05*	*-8.2*	-	-	-	-	-
Mogens Henesen Fj. S	*62.34*	*-43.1*	*-16.2*	-	-	-	-	-
Husfjeldet	*61.68*	*-43.21*	*-2*	-	-	-	-	-
Unnamed	*61.56*	*-43.42*	*-1.85*	-	-	-	-	-
Unnamed	*61.44*	*-42.61*	*-12.3*	-	-	-	-	-
Unnamed	*61.33*	*-43.51*	*-1.1*	-	-	-	-	-
Unnamed	*61.22*	*-43.56*	*-3.2*	-	-	-	-	-
Unnamed	*60.94*	*-43.6*	*-3.8*	-	-	-	-	-

caused by lake drainage. Pritchard *et al.* (2009) found dynamic mass loss for the period 2003–2007 in 22 individual tidewater glaciers in the SE along a 1300 km long coastline. In the same area, only three fast lake-drainage events were detected per year, a comparison of dynamic mass loss and fast lake-drainage is presented in Table 7.9. Two fast lake-drainages were usually on Kangerdlugssuaq, and a second usually in the Schweizerland area, and in 2008 one fast lake-drainage occurred on Helheim. This pattern means that 19 of the SE glaciers found to be losing mass dynamically by Pritchard *et al.* (2009) had no fast lake-drainage events at all during the period 2005–2009, therefore fast lake-drainages cannot have played a role in dynamic mass loss from the SE region.

Table 7.10: NW glaciers as measured by Pritchard *et al.* (2009). The number of fast-draining lakes per year in the catchment area of each glaciers is shown. All dynamically thinning glaciers are shown in *italics*, the ten most rapidly thinning glaciers are also in ***bold***.

Glacier Name	Lat	Lon	Dynamic thinning/yr	2005	2006	2007	2008	2009
Tracy	***77.66***	***-65.73***	***-7***	-	-	-	-	-
Heilprin	*77.52*	*-65.36*	*-0.54*	*2*	*1*	*1*	*1*	*1*
Harald Moltke Br.	***76.55***	***-57.5***	***-13.1***	-	-	***1***	***1***	-
Store Landglet.	76.49	-58.05	0	-	-	-	-	-
Unnamed 1	76.44	-64.53	0.3	-	-	-	-	-
Unnamed 2	*76.44*	*-63.08*	*-2.8*	-	-	-	-	-
Unnamed 3	*76.41*	*-63.58*	*-0.5*	-	-	-	-	-
Gade Gl.	*76.4*	*-62.87*	*0.2*	-	-	-	-	-
Unnamed 4	***76.34***	***-62.41***	***-4.1***	-	-	-	-	-
Docker Smith Gl.	***76.33***	***-51.98***	***-11.2***	-	-	-	-	-
Unnamed 5	*76.22*	*-67.57*	*-1.9*	-	-	-	-	-
Peary Gl.	*76.16*	*-50.54*	*-1.8*	-	-	-	-	-
Unnamed 6	*76.1*	*-58.08*	*-2.3*	-	-	-	-	-
Unnamed 7	***76.1***	***-59.82***	***-3.2***	-	-	-	-	-
Kong Oscar Gl.	*76.07*	*-59.51*	*-1.5*	-	-	-	-	-
Nansen Gl.	*75.83*	*-58.84*	*-0.1*	*2*	-	*1*	*2*	*2*
Unnamed 8	***75.59***	***-58.1***	***-9.5***	***1***	-	-	-	***2***
Steenstrup N	***75.36***	***-57.82***	***-5.1***	***1***	***4***	***4***	***4***	***5***
Steenstrup S	*75.14*	*-57.55*	*-0.5*	*3*	*4*	*3*	*4*	*5*
Hayes north	*75.05*	*-57.42*	*-1*	*1*	*1*	-	*1*	*2*
Hayes central	*75*	*-55.84*	*-0.3*	-	-	-	-	*1*
Hayes south	***74.88***	***-55.73***	***-2.9***	-	-	***1***	***1***	***1***
Unnamed 9	74.62	-56.43	-	-	1	-	1	1
Unnamed 10	*74.31*	*-55.06*	*-1.5*	-	-	-	-	*1*
Cornell Gl.	*74.21*	*-55.99*	*-1*	-	-	*1*	*2*	*3*
Ussing Braeer	*73.97*	*-55.54*	*-2.5*	-	-	*2*	*1*	*1*
Ussing Braeer S	73.88	-55.19	-	1	-	1	1	-
Qeqertarssup s.	*73.62*	*-55.42*	*-1.5*	*2*	*2*	*1*	*1*	*2*
Kakivfait sermiat	*73.5*	*-55.18*	*-1.15*	*1*	*1*	-	-	-
Nunatakavsaup s.	73.28	-55.02	2.9	1	3	2	4	1
Alangorssup s.	73.16	-54.98	0	1	-	-	-	-
Uperrnavik Isstrom	***73.01***	***-54.43***	***-15***	-	***1***	-	-	***1***
Umiamako Isbrae	***71.76***	***-52.43***	***-9.2***	-	-	-	-	-

In the NW region it was not as clear cut as in the SE, with 29 fast-draining lakes in a region where Pritchard *et al.* (2009) found 27 glaciers to be thinning dynamically (Table 7.10). However, of these 27 glaciers, 12 had no fast draining lakes in any year, and a further 7 had no fast lake-drainages in three years of the five studied. Of the ten glaciers in the NW that have had the highest rates of dynamic thinning, five had no fast lake-drainages events in any year studied, meaning that the dynamic mass loss that has been observed in GRACE data since 2005 (Khan *et al.*, 2010)

cannot have been a result of fast lake drainages.

7.6 Chapter summary

Lake location is controlled by subglacial topography, the availability of melt and the volume of snowfall. In some parts of the ice sheet lakes form only below the equilibrium line, in other regions (especially the SW) lakes form well into the accumulation zone. The total area of lakes is also well explained by melt. As total area depends on both the number of lakes present and the size of those lakes, it also relies on all the controls on lake location. Controls on the sizes of individual lakes are complex, but melt duration and slope appear to be important controls.

Chapter 6 introduced three modes by which lakes disappear from the from ice sheet, and these were interpreted further in this chapter. Fast-draining lakes most likely drain through the ice to the bed, and could cause localized ice accelerations and new connections to the bed. Water from slow draining and freezing lakes may reach the bed, but unless the drainage system is inefficient the water will have no effect on ice sheet dynamics. Freezing lakes appear to have different controls to fast and slow-draining lakes, occurring on flatter ice and at higher altitudes. Freezing lakes also last the longest of any lakes suggesting that lake drainage is impeded, possibly by snow layers or thicker ice making hydrofracture more difficult.

The drainage of supraglacial lakes was previously thought to play an important role in dynamic mass loss from the Greenland Ice Sheet, but the results of this thesis show that this cannot be the case. Regions of dynamic thinning had very few fast lake drainages during the observation period, and many dynamically thinning glaciers had not fast lake-drainages at all. In the regions where fast lake-drainage was common, mass loss has been shown to be entirely attributable to surface mass balance, therefore fast lake-drainage cannot be responsible for dynamic mass loss from the Greenland Ice Sheet.

Chapter 8

Summary and Suggestions for Further Work

8.1 Summary

Supraglacial lakes have been identified as having a possible role in dynamic mass loss from the Greenland Ice Sheet, however little is known about their occurrence and drainage behaviour away from a well studied section of SW Greenland. The aim of this research was to discover where on the ice sheet lakes occur, and how many of these lakes apparently drain to the bed.

The desirable characteristics of a satellite sensor for mapping and monitoring lakes on the Greenland Ice Sheet were considered, and the MODIS sensor was chosen owning to the compromise between spatial resolution and regular coverage of the ice sheet, and all necessary preprocessing steps were undertaken. Previously used methods for classifying lake occurrence in satellite imagery were evaluated, and a problem with a resolution sharpening algorithm common to all previous studies using MODIS data was discovered. A new method using a single band of MODIS imagery and a region growing algorithm based on a threshold of the reflectance of the surrounding ice was developed. The new method was tested against lake

areas classified in higher resolution ASTER imagery, and compared with previous methodologies. The method performed well, with a RMSE of 0.14 km^2. 2600 lakes were identified using weekly MODIS data and substantial manual editing to avoid classification errors, and the positions of these lakes were used to seed the classification of 3704 MODIS images. From the time series of area obtained, each lake was classified by its drainage behaviour.

8.2 Conclusions

Lakes were identified in all parts of the ice sheet, reforming in the same hollows each year. However, substantial differences in the spatial distribution of lakes were discovered. 55% of all lakes occurred in the SW region (59% of the total lake area). The NW and NE accounted for 19 and 13 % of lakes respectively, although the lakes in the NE were larger so the two regions accounted for 14.9 and 15.3% of total lake area. The SE region accounted for only 2% of all lakes, and only 1% of lake area, despite the region accounting for 15% of the area of the Greenland Ice Sheet, and having 21% of the ice sheet margin length. Of the lakes in the SE region, 65% occurred on only one glacier: Kangerdlugssuaq. An expected frequency was calculated for each region based on the margin length of each region and only the SW and NE regions had more lakes than expected. Lakes in the NE and SW regions were the largest, and lakes in the SE were the smallest. Lake size did not vary significantly between the remaining regions. Melt extent was calculated for each of the five years studied, 2007 was a year of very high melt in the SW, and 2008 was the year of maximum melt in the north. In most regions, 2006 and 2009 were generally low melt years. Melt extent and duration explained the inter-annual variation in lake occurrence, and some inter-regional variation. Controls on the sizes of individual lakes were complex, but melt duration and slope appeared to be important controls. Inter-regional differences in the size and occurrence of lakes were a result of the different topography of each region, the latitudinal temperature gradient, and accumulation. In some parts of the ice sheet lakes formed only below

the equilibrium line, in other regions (especially the SW) lakes formed well into the accumulation zone.

Three modes by which lakes could disappear from the ice sheet surface were identified. Some lakes drained suddenly, presumably to the bed. Other lakes had a slow decline in lake area over several days despite plentiful melt, these lakes were interpreted to be draining over the ice surface. Finally some lakes froze at the end of the melt season, inferred from the time a lake disappeared compared with the stage of the melt season, the disappearance of surrounding lakes, and evidence such as ice visibly forming on the lake surface.

The most common cause for lake disappearance was freezing, accounting for 46% of lakes per year. Slow drainage accounted for a further 34% of lakes, and 13% drained rapidly. The occurrence of fast-draining lakes was not uniform. Lakes were most likely to drain in the NE, N, and SW regions. The NE and SW regions accounted for 68% of fast draining lakes, and were the only regions to have more fast draining lakes than expected based on region size (measured by margin length). In the SE region only $\sim$ 3 lakes drained rapidly per year, along a 1300 km long coastline. Of the 22 glaciers of the SE identified by Pritchard *et al.* (2009) as experiencing dynamic thinning, 19 had no fast lake-drainages in any year. In the NW region, of the 27 glaciers that have been identified to be thinning dynamically, 12 were not affected by fast-draining lakes, including 5 of the 10 glaciers with the most rapid dynamic thinning.

Lakes that drained slowly were found to generally be smaller that fast draining and freezing lakes, although this was not significant in all regions of the ice sheet. Freezing lakes persisted on the ice sheet for twice the duration of fast draining lakes, lasting approximately one month, rather than fast draining lakes' 10–15 days. Slow draining lakes had a geometric mean duration between those of fast draining and freezing lakes. Lakes were mostly found on slopes of approximately 0.7 degrees, and were slightly more likely to drain slowly where the slope angle was steeper, with freezing lakes forming on the shallowest slopes. A significant difference in the

elevation and underlying ice thickness was found between different lake types, with the lakes a higher elevations most likely to freeze. Fast draining lakes formed at lower elevations, with mean elevations around 200 m lower than freezing lakes in most years. This also means that fast draining lakes formed on the thinnest ice, whereas those lakes on the thickest ice usually froze. This pattern could also be seen in ice sheet wide mapping of drainage type: the band of highest lakes froze in each year, despite having the longest duration. No significant difference in ice strain rate could be found between drainage types, with nearly all lakes forming in areas of extensional flow.

Freezing lakes appear to have different controls to fast and slow draining lakes, occurring on flatter ice and at higher altitudes. Freezing lakes also last the longest of any lakes suggesting that lake drainage is impeded, possibly by snow layers or thicker ice making hydrofracture more difficult. No plausible reason for some lakes draining slowly and others draining rapidly could be found, it may be that these two different drainage types are controlled by very local factors, a theory supported by the existence of groups of adjacent lakes that all drained rapidly on the same day. These groups of lakes were found in all years and in most parts of the ice sheet where large numbers of lakes formed. In one case, a possible fracture was observed to appear connecting drained lakes, although such fractures could not be identified in the imagery available for other groups of drained lakes.

Some lakes drained in the same manner each year, whereas other lakes drained differently or froze in consecutive years. Freezing was the most likely mode of lake termination to occur in multiple years, whereas fast drainage was the least likely. There was not equal probability of each drainage type occurring at a lake with a different drainage type in another year. Lakes that drained fast in one year, were most likely to otherwise drain slowly. Slow draining lakes otherwise tended to freeze, and freezing lakes were most likely to drain slowly in years they did not freeze. Freezing lakes were also the most likely type to not form in other years. The combination of fast draining in some years and slow draining in others was very common, and this would suggest that the difference between fast and slow draining

lakes cannot be controlled by an factor that changes little between years, such as slope or ice thickness.

The drainage of supraglacial lakes was previously thought to play an important role in dynamic mass loss from the Greenland Ice Sheet, but the results of this thesis show that this cannot be the case. Regions of dynamic thinning had very few fast lake drainages during the observation period, and many dynamically thinning glaciers had not fast lake drainages at all. In the regions where fast lake drainage was common, mass loss has been shown to be entirely attributable to surface mass balance, therefore fast lake drainage cannot be responsible for dynamic mass loss from the Greenland Ice Sheet.

8.3 Suggestions for further work

Unanswered questions relating supraglacial lakes still remain that warrant investigation. Some of these could be investigated remotely, others would require a field based approach.

8.3.1 The role of surface hydrology in ice dynamics in regions with few supraglacial lakes

The link between surface hydrology and ice velocity has been well studied in the SW region, however the number of lakes and the number of fast draining lakes in that region are unusual for the ice sheet, therefore similar studies carried out in regions of the ice sheet away from supraglacial lakes would be interesting. Land terminating ice should be selected to avoid any oceanic forcing of velocity, suitable sites for a study like this exist along the northern coast of the ice sheet. Only with observations from regions with a range of different hydrologies can an adequate representation of the dynamic effects of hydrology be suitably incorporated in ice sheet models.

8.3.2 Controls on lake drainage

The reason for some lakes draining suddenly to the bed when surrounding lakes do not has not been answered, and would be difficult to do remotely. A remote sensing based approach could involve ordering very high resolution imagery (e.g. Ikonos on Quickbird) of lakes that always have the same drainage type, and possibly try to time an acquisition for after lake drainage. The timing of this would be very difficult as the date of the start of lake growth and of drainage varies by up to a month from year-to-year. It is possible more advanced statistical methods applied to the results of this thesis would yield more information on drainage controls. The use of multiple regression analysis would be interesting, and could be applied to datasets such as surface slope, surface melt, and ice strain rate. Alternatively field visits to lakes that often changed drainage types inter-annually would be a more reliable method of determining the controls. Spillway incision should be monitored, local topography mapped, and strain rates up and downstream from the lakes measured. Geophysical observations may help detect the presence of fractures, and a survey of the ice sheet bed may reveal differences in the controlling subglacial basin. Also of interest would be geophysical surveys of pairs of lakes that drained on the same day, to see if linking fractures do in fact exist. Several pairs of lakes that frequently drained together exist, so there would be a fairly high probability of this field work succeeding.

8.3.3 Calculation of lake volume

As discussed in Section 7.4.5, at present there is not a satisfactory method for calculating lake depth (and hence volume) from MODIS data, and methods using other optical data have not been adequately verified. Should a method become available to accurately calculate lake depth, the dataset from this thesis could be updated to give the volume of water draining to the bed. The calculation of lake depth from MODIS data is, at the time of writing, currently the focus of another PhD project at Swansea University, therefore this data may become available in the

future.

8.3.4 Other regions of the Arctic

Supraglacial lakes in other regions of the Arctic have been observed to drain to the bed (Liestøl *et al.*, 1980; Boon and Sharp, 2003), so the occurrence and drainage of supraglacial lakes outside of Greenland could be studied using the methodology of this thesis. While Svalbard would be an obvious choice given the body of work that exists for those islands, the strongly maritime climate means that cloud-free imaging may be problematic, so any such study would be advised to thoroughly investigate the frequency of cloud-free imagery when choosing a site.

References

Abdalati, W. (2007). Greenland Ice Sheet melt characteristics derived from passive microwave data. Boulder, Colorado USA: National Snow and Ice Data Center, 2003-2007. Digital media.

Abdalati, W., W. Krabill, E. Frederick, S. Manizade, C. Martin, J. Sonntag, R. Swift, R. Thomas, W. Wright, and J. Yungel (2001). Outlet glacier and margin elevation changes: Near-coastal thinning of the Greenland Ice Sheet. *J. Geophys. Res.*, **106**(D24):33729–33742.

Abdalati, W. and K. Steffen (2001). Greenland Ice Sheet melt extent: 1979-1999. *J. Geophys. Res.*, **106**:33983–33988.

Ackerman, S., K. Strabala, W. Menzel, R. Frey, C. Moeller, L. Gumley, *et al.* (1998). Discriminating clear sky from clouds with MODIS. *J. Geophys. Res.*, **103**(D24):32–141.

Alley, R. B., T. K. Dupont, B. R. Parizek, and S. Anandakrishnan (2005). Access of surface meltwater to beds of sub-freezing glaciers: preliminary insights. *Ann. Glaciol.*, **40**:8–14.

Anderson, R., S. Anderson, K. MacGregor, E. Waddington, S. O'Neel, C. Riihimaki, and M. Loso (2004). Strong feedbacks between hydrology and sliding of a small alpine glacier. *J. Geophys. Res*, **109**:F03005.

Bamber, J., R. Layberry, and S. Gogineni (2001). A new ice thickness and bed data set for the Greenland Ice Sheet. measurement, data reduction, and errors. *Journal of Geophysical Research. D. Atmospheres*, **106**:33.

Bartholomew, I., P. Neinow, A. Sole, D. Mair, T. Cowton, S. Palmer, and J. Wadham (2011). Supraglacial forcing of subglacial drainage in the ablation zone of the Greenland Ice Sheet. *Geophys. Res. Lett.*

Bartholomew, I., P. Nienow, D. Mair, A. Hubbard, M. King, and A. Sole (2010). Seasonal evolution of subglacial drainage and acceleration in a Greenland outlet glacier. *Nature Geoscience.* ISSN 1752-0894.

Benn, D., J. Gulley, A. Luckman, A. Adamek, and P. Glowacki (2009). Englacial drainage systems formed by hydrologically driven crevasse propagation. *J. Glaciol.*, **55**(191):513–523. ISSN 0022-1430.

Boon, S. and M. Sharp (2003). The role of hydrologically-driven ice fracture in drainage evolution on an Arctic glacier. *Geophys. Res. Lett.*, **30**(18):1916. doi:10.1029/2003GL018034.

Box, J. E., D. H. Bromwich, B. A. Veenhuis, L. S. Bai, J. C. Stroeve, J. C. Rogers, K. Steffen, T. Haran, and S. H. Wang (2006). Greenland Ice Sheet surface mass balance variability (1988-2004) from calibrated polar mm5 output. *J. Climate*, **19**:2783–2800.

Box, J. E. and K. Ski (2007). Remote sounding of Greenland supraglacial melt lakes: implications for subglacial hydraulics. *J. Glaciol.*, **53**(181):257–265.

van den Broeke, M., J. Bamber, J. Ettema, E. Rignot, E. Schrama, W. J. van de Berg, E. van Meijgaard, I. Velicogna, and B. Wouters (2009). Partitioning recent Greenland mass loss. *Science*, **326**(5955):984–986. doi: 10.1126/science.1178176.

Catania, G., T. Neumann, and S. Price (2008). Characterizing englacial drainage in the ablation zone of the Greenland Ice Sheet. *J. Glaciol.*, **54**(187):567–578. ISSN 0022-1430.

Chu, V., L. Smith, A. Rennermalm, R. Forster, J. Box, and N. Reehy (2009). Sediment plume response to surface melting and supraglacial lake drainages on the Greenland ice sheet. *J. Glaciol.*, **55**(194):1072–1082. ISSN 0022-1430.

Clark, P. U., N. G. Pisias, T. F. Stocker, and A. J. Weaver (2002). The role of the thermohaline circulation in abrupt climate change. *Nature*, **415**:863–869. ISSN 0028-0836. doi:10.1038/415863a.

Cuffey, K. M. and S. J. Marshall (2000). Substantial contribution to sea-level rise during the last interglacial from the Greenland Ice Sheet. *Nature*, **404**:591–594. ISSN 0028-0836. doi:10.1038/35007053.

Das, S. B., I. Joughin, M. D. Behn, I. M. Howat, M. A. King, D. Lizarralde, and M. P. Bhatia (2008). Fracture propagation to the base of the Greenland Ice Sheet during supraglacial lake drainage. *Science*, **320**(5877):778–781. doi: 10.1126/science.1153360.

De Angelis, H., F. Rau, and P. Skvarca (2007). Snow zonation on Hielo Patagónico Sur, Southern Patagonia, derived from Landsat 5 TM data. *Global and Planetary Change*, **59**(1-4):149–158. ISSN 0921-8181. doi:DOI:10.1016/j.gloplacha.2006.11.032. Mass Balance of Andean Glaciers.

Dimarzio, J., A. Brenner, B. Schutz, C. A. Schuman, and H. J. Zwally (2007). *GLAS/ICESat 1 km laser altimetry digital elevation model of Greenland.* National Snow and Ice Data Center, Boulder, Colorado, USA. Digital media.

Echelmeyer, K., T. Clarke, and W. Harrison (1991). Surficial glaciology of Jakobshavns Isbræ, West Greenland: Part I. surface morphology. *J. Glaciol.*, **37**(127):368–382.

Georgiou, S., A. Shepherd, M. McMillan, and P. Nienow (2009). Seasonal evolution of supraglacial lake volume from ASTER imagery. *Ann. Glaciol.*, **50**(52):95–100.

Green, E., P. Mumby, A. Edwards, and C. Clark (1996). A review of remote sensing for the assessment and management of tropical coastal resources. *Coastal management*, **24**(1):1–40.

Gumley, L., J. Descloitres, and J. Schmaltz (2007). Creating reprojected MODIS true color images: a tutorial. `ftp://ftp.ssec.wisc.edu/pub/IMAPP/MODIS/TrueColor/` (Accessed May 2011).

Hall, D. K., J. R. S. Williams, S. B. Luthcke, and N. E. DiGirolamo (2008). Greenland Ice Sheet surface temperature, melt and mass loss: 2000-6. *J. Glaciol.*, **54**(184):81–93.

Hall, D. K., R. S. Williams, K. A. Casey, N. E. DiGirolamo, and Z. Wan (2006). Satellite-derived, melt-season surface temperature of the Greenland Ice Sheet (2000-2005) and its relationship to mass balance. *Geophys. Res. Lett.*, **33**.

Hambrey, M. (1984). Sudden draining of ice-dammed lakes in Spitsbergen. *Polar Record*, **22**(137):189–194. ISSN 1475-3057.

Hanna, E., J. Cappelen, X. Fettweis, P. Huybrechts, A. Luckman, and M. Ribergaard (2009). Hydrologic response of the greenland ice sheet: the role of oceanographic warming. *Hydrological Processes*, **23**(1):7–30.

Hanna, E., P. Huybrechts, I. Janssens, J. Cappelen, K. Steffen, and A. Stephens (2005). Runoff and mass balance of the Greenland Ice Sheet: 1958-2003. *J. Geophys. Res.*, **110**:D13108. doi:10.1029/2004JD005641.

Hanna, E., P. Huybrechts, K. Steffen, J. Cappelen, R. Huff, C. Shuman, T. Irvine-Fynn, S. Wise, and M. Griffiths (2008). Increased runoff from melt from the Greeland Ice Sheet: a response to global warming. *J. Climate*, **21**.

Hanna, E., J. McConnell, S. Das, J. Cappelen, and A. Stephens (2006). Observed and modeled greenland ice sheet snow accumulation, 1958-2003, and links with regional climate forcing. *Journal of Climate*, **19**(3):344–358.

Hansen, J., M. Sato, P. Kharecha, G. Russell, D. W. Lea, and M. Siddall (2007). Climate change and trace gases. *Philosophical Transactions of the Royal Society*, **365**:1925–1954. doi:10.1098/rsta.2007.2052.

Hodgkins, R. (1997). Glacier hydrology in Svalbard, Norwegian high arctic. *Quaternary Science Reviews*, **16**(9):957–973.

Holland, D., R. Thomas, B. De Young, M. Ribergaard, and B. Lyberth (2008). Acceleration of Jakobshavn Isbrae triggered by warm subsurface ocean waters. *Nature Geoscience*, 1(10):659–664.

Howat, I. and A. Eddy (2011). Multi-decadal retreat of Greenland's marine-terminating glaciers. *Journal of Glaciology*, **57**(203):1.

Howat, I. M., J. E. Box, A. Yushin, A. Herrington, and E. McFadden (2010). Seasonal variability in the dynamics of marine-terminating outlet glaciers in Greenland. *J. Glaciol.*, **56**(198).

Howat, I. M., I. Joughin, M. Fahnestock, B. E. Smith, and T. A. Scambos (2008). Synchronous retreat and acceleration of southeast Greenland outlet glaciers 2000-06: ice dynamics and coupling to climate. *J. Glaciol.*, **54**(187):646–660.

Hsu, J. (1996). *Multiple comparisons: theory and methods.* Chapman & Hall/CRC.

Hu, A., G. A. Meehl, W. Han, and J. Yin (2011). Effect of the potential melting of the Greenland Ice Sheet on the Meridional Overturning Circulation and global climate in the future. *Deep Sea Research Part II: Topical Studies in Oceanography*, **In Press**:–. ISSN 0967-0645. doi:DOI:10.1016/j.dsr2.2010.10.069.

Iken, A. and R. Bindschadler (1986). Combined measurements of subglacial water pressure and surface velocity of Findelengletscher, Switzerland: conclusions about drainage system and sliding mechanism. *Journal of Glaciology*, **32**(110):101–119.

Iken, A., H. Röthlisberger, A. Flotron, and W. Haeberli (1983). The uplift of unteraargletscher at the beginning of the melt season–a consequence of water storage at the bed. *Journal of Glaciology*, **29**(101):28–47.

IPCC (2001). *Climate Change 2001: The Scientific Basis. Contribution of Working Group I to the Third Assessment Report of the Intergovernmental Panel on Climate Change.* Cambridge University Press, Cambridge, UK.

IPCC (2007). *Climate Change 2007 - The Physical Science Basis: Working Group I Contribution to the Fourth Assessment Report of the IPCC.* Cambridge University Press, Cambridge, UK and New York, NY, USA. ISBN 0521880092.

Janssens, I. and P. Huybrechts (2000). The treatment of meltwater retention in mass-balance parameterizations of the greenland ice sheet. *Annals of Glaciology*, **31**(1):133–140.

Johannessen, O. M., K. Khvorostovsky, M. W. Miles, and L. P. Bobylev (2005). Recent ice-sheet growth in the interior of Greenland. *Science*, **310**:1013–1016.

Joshi, M., C. Merry, K. Jezek, and J. Bolzan (2001). An edge detection technique to estimate melt duration, season and melt extent on the Greenland ice sheet using passive microwave data. *Geophys. Res. Lett.*, **28**(18):3497–3500.

Joughin, I., W. Abdalati, and M. Fahnestock (2004). Large fluctuations in speed on Greenland's Jakobshavn Isbræ glacier. *Nature*, **432**:608–610.

Joughin, I., I. M. Howat, M. Fahnestock, B. Smith, W. Krabill, R. B. Alley, H. Stern, and M. Truffer (2008). Continued evolution of Jakobshavn Isbræ following its rapid speedup. *J. Geophys. Res.*, **113**:F04006. doi: 10.1029/2008JF001023.

Joughin, I., B. Smith, I. Howat, T. Scambos, and T. Moon (2010). Greenland flow variability from ice-sheet-wide velocity mapping. *Journal of Glaciology*, **56**(197):415–430.

Joughin, I., S. Tulaczyk, M. Fahnestock, and R. Kwok (1996). A mini-surge on the Ryder Glacier, Greenland, observed by satellite radar interferometry. *Science*, **274**(5285):228.

Kamb, B. (1987). Glacier surge mechanism based on linked cavity configuration of the basal water conduit system. *Journal of Geophysical Research*, **92**(B9):9083–9100.

Khan, S., J. Wahr, M. Bevis, I. Velicogna, and E. Kendrick (2010). Spread of ice mass loss into northwest Greenland observed by GRACE and GPS. *Geophys. Res. Lett.*, **37**(6):L06501. ISSN 0094-8276. doi:10.1029/2010GL042460.

Krabill, W., W. Abdalati, E. Frederick, S. Manizade, C. Martin, J. Sonntag, R. Swift, R. Thomas, W. Wright, and J. Yungel (2000). Greenland Ice Sheet: High-elevation balance and peripheral thinning. *Science*, **289**:428–430.

Krabill, W., E. Frederick, S. Manizade, C. Martin, J. Sonntag, R. Swift, R. Thomas, W. Wright, and J. Jungel (1999). Rapid thinning of parts of the southern Greenland Ice Sheet. *Science*, **283**:1522–1524.

Krabill, W., E. Hanna, P. Huybrechts, W. Abdalati, J. Cappelen, B. Csatho, E. Frederick, S. Manizade, C. Martin, J. Sonntag, R. Swift, R. Thomas, and J. Jungel (2004). Greenland Ice Sheet: increased coastal thinning. *Geophys. Res. Lett.*, **31**:L24402. doi:10.1029/2004GL021533.

Krawczynski, M. J., M. D. Behn, S. B. Das, and I. Joughin (2009). Constraints on the lake volume required for hydro-fracture through ice sheets. *Geophys. Res. Lett.*, **36**:L10501. doi:10.1029/GL036765.

Lappegard, G. and J. Kohler (2005). Determination of basal hydraulic systems based on subglacial high-pressure pump experiments. *Annals of Glaciology*, **40**(1):37–42.

Lappegard, G., J. Kohler, M. Jackson, and J. Hagen (2006). Characteristics of subglacial drainage systems deduced from load-cell measurements. *Journal of Glaciology*, **52**(176):137–148.

Liestøl, O., K. Repp, and B. Wold (1980). Supra-glacial lakes in Spitsbergen. *Nor. Geogr. Tidsskr*, **34**(2):89–92.

Lüthje, M., L. Pedersen, N. Reeh, and W. Greuell (2006). Modelling the evolution of supraglacial lakes on the West Greenland ice-sheet margin. *J. Glaciol.*, **52**(179):608–618.

MacGregor, K., C. Riihimaki, and R. Anderson (2005). Spatial and temporal evolution of rapid basal sliding on Bench Glacier, Alaska, USA. *Journal of Glaciology*, **51**(172):49–63.

McMillan, M., P. Nienow, A. Shepherd, T. Benham, and A. Sole (2007). Seasonal evolution of supra-glacial lakes on the Greenland Ice Sheet. *Earth Planet. Sc. Lett.*, **262**:482–492.

Moon, T. and I. Joughin (2008). Changes in ice front position on Greenland's outlet glaciers from 1992 to 2007. *J. Geophys. Res.*, **113**:F02022. doi:10.1029/2007JF000927.

Murray, T., K. Scharrer, T. James, S. Dye, E. Hanna, A. Booth, N. Selmes, A. Luckman, A. Hughes, S. Cook, and P. Huybrechts (2010). Ocean regulation hypothesis for glacier dynamics in southeast Greenland and implications for ice sheet mass changes. *J. Geophys. Res.*, **115**(F3):F03026. ISSN 0148-0227.

Nick, F., A. Vieli, I. Howat, and I. Joughin (2009). Large-scale changes in Greenland outlet glacier dynamics triggered at the terminus. *Nature Geoscience*, **2**(2):110–114.

Nienow, P., M. Sharp, and I. Willis (1998). Seasonal changes in the morphology of the subglacial drainage system, Haut Glacier d'Arolla, Switzerland. *Earth Surface Processes and Landforms*, **23**(9):825–843.

Nye, J. (1957). The distribution of stress and velocity in glaciers and ice-sheets. *Proceedings of the Royal Society of London. Series A. Mathematical and Physical Sciences*, **239**(1216):113.

Oswald, G. K. A. and S. Gogineni (2008). Recovery of subglacial water extent from Greeland radar survey data. *J. Glaciol.*, **54**(184):94–106.

Parizek, B. R. and R. B. Alley (2004). Implications of increased Greenland surface melt under global-warming scenarios: ice-sheet simulations. *Quaternary Sci. Rev.*, **23**:1013–1027.

Partington, K. (1998). Discrimination of glacier facies using multi-temporal SAR data. *Journal of Glaciology*, **44**(146):42–53.

Paterson, W. S. B. (1994). *The Physics of Glaciers*. Butterworth Heinemann, Oxford.

Pritchard, H., R. Arthern, D. Vaughan, and L. Edwards (2009). Extensive dynamic thinning on the margins of the Greenland and Antarctic ice sheets. *Nature*, **461**(7266):971–975. ISSN 0028-0836.

Raymond, C. and M. Nolan (2000). Drainage of a glacial lake through an ice spillway. *IAHS PUBLICATION*:199–210.

Ridley, J. K., P. Huybrechts, J. M. Gregory, and J. A. Lowe (2005). Elimination of the Greenland Ice Sheet in a high CO_2 climate. *J. Climate*, **18**:3409–3427.

Riggs, G. and D. Hall (2004). Snow mapping with the MODIS Aqua instrument. In *Proceedings of the 61st Eastern Snow Conference*, volume 9.

Rignot, E., J. Box, E. Burgess, and E. Hanna (2008). Mass balance of the Greenland Ice Sheet from 1958 to 2007. *Geophysical Research Letters*, **35**(10.1029).

Rignot, E., I. Velicogna, M. Van den Broeke, A. Monaghan, and J. Lenaerts (2011). Acceleration of the contribution of the Greenland and Antarctic ice sheets to sea level rise. *Geophysical Research Letters*, **38**(5):L05503.

Schaepman-Strub, G., M. Schaepman, T. Painter, S. Dangel, and J. Martonchik (2006). Reflectance quantities in optical remote sensing–definitions and case studies. *Remote Sensing of Environment*, **103**(1):27–42.

Schoof, C. (2010). Ice-sheet acceleration driven by melt supply variability. *Nature*, **468**(7325):803–806. ISSN 0028-0836.

Schrama, E. J. O. and B. Wouters (2011). Revisiting Greenland ice sheet mass loss observed by GRACE. *J. Geophys. Res.*, **116**. doi:10.1029/2009JB006847.

Scorer, R. S. (1988). Sunny Greenland. *Quarterly Journal of the Royal Meteorological Society*, **114**(479):3–29. ISSN 1477-870X. doi:10.1002/qj.49711447902.

Selmes, N., T. Murray, and T. D. James (2011). Fast draining lakes on the Greenland Ice Sheet. *Geophys. Res. Lett.*, **38**:L15501. doi:10.1029/2011GL047872.

Shepherd, A., A. Hubbard, P. Nienow, and M. King (2009). Greenland Ice Sheet motion coupled with daily melting in late summer. *Geophys. Res. Lett.*, **36**:L01501. doi:10.1029/2008GL035758.

Smith, R. C. and K. S. Baker (1981). Optical properties of the clearest natural waters (200-800 nm). *Applied Optics*, **20**:177.

Sneed, W. and G. Hamilton (2007). Evolution of melt pond volume on the surface of the Greenland Ice Sheet. *Geophys. Res. Lett.*, **34**:L03501. doi:10.1029/2006GL028697.

Sørensen, L., S. Simonsen, K. Nielsen, P. Lucas-Picher, G. Spada, G. Adalgeirsdottir, R. Forsberg, and C. Hvidberg (2011). Mass balance of the Greenland Ice Sheet (2003-2008) from ICESat data-the impact of interpolation, sampling and firn density. *Cryosphere*, **5**(1):173–186.

Steffen, K., S. V. Nghiem, R. Huff, and G. Neumann (2004). The melt anomaly of 2002 on the Greenland Ice Sheet from active and passive microwave satellite observations. *Geophys. Res. Lett.*, **31**.

Stern, N. (2007). *The Economics of Climate Change: The Stern Review*. Cambridge University Press. ISBN 0521700809.

Stroeve, J., A. Nolin, and K. Steffen (1997). Comparison of AVHRR-derived and in situ surface albedo over the Greenland Ice Sheet. *Remote Sensing of Environment*, **62**(3):262–276.

Sundal, A., A. Shepherd, P. Nienow, E. Hanna, S. Palmer, and P. Huybrechts (2011). Melt-induced speed-up of Greenland Ice Sheet offset by efficient subglacial drainage. *Nature*, **469**(7331):521–524. ISSN 0028-0836.

Sundal, A. V., A. Shepherd, P. Nienow, E. Hanna, S. Palmer, and P. Huybrechts (2009). Evolution of supra-glacial lakes across the Greenland Ice Sheet. *Remote Sens. Environ.*, **113**:2164–2171.

Thomsen, H., L. Thorning, and O. Olesen (1989). Applied glacier research for planning hydro-electric power, Ilulissat/Jakobshavn, West Greenland. *Ann. Glaciol*, **13**:257–261.

Tinker, M. and R. Lambourne (2000). *Further mathematics for the physical sciences*. Chichester: Wiley.

Toniazzo, T., J. M. Gregory, and P. Huybrechts (2004). Climatic impact of a Greenland deglaciation and its possible irreversibility. *J. Climate*, **17**:21–33.

Townend, J. (2002). *Practical statistics for environmental and biological scientists*. John Wiley & Sons.

van de Wal, R. S. W., W. Boot, M. R. van den Broeke, C. J. P. P. Smeets, C. H. Reijmer, J. J. A. Donker, and J. Oerlemans (2008). Large and rapid melt-induced velocity changes in the ablation zone of the Greenland Ice Sheet. *Science*, **321**:111–113.

van der Veen, C. J. (2007). Fracture propogation as means of rapidly transferring surface meltwater to the base of glaciers. *Geophys. Res. Lett.*, **34**:L01501. doi:10.1029/2006GL028385.

Velicogna, I. (2009). Increasing rates of ice mass loss from the Greenland and

Antarctic ice sheets revealed by GRACE. *Geophys. Res. Lett.*, **36**(19):L19503. ISSN 0094-8276. doi:10.1029/2009GL040222.

Velicogna, I. and J. Wahr (2006). Acceleration of Greenland ice mass loss in spring 2004. *Nature*, **443**:329–331.

Vermote, E., N. El Saleous, C. Justice, Y. Kaufman, J. Privette, L. Remer, J. Roger, and D. Tanré (1997). Atmospheric correction of visible to middle-infrared EOS-MODIS data over land surfaces: Background, operational algorithm and validation. *J. Geophys. Res.*, **102**(D14):17131–17141. doi:10.1029/97JD00201.

Wan, Z. (2004). Land surface temperature measurements from EOS MODIS data. Technical Report NAS5-31370, NASA.

Wan, Z. and J. Dozier (1996). A Generalized Split-Window Algorithm for Retrieving Land-Surface Temperature from Space. *IEEE T. Geosci. Remote.*, **34**(4).

Wan, Z. and Z. Li (1997). A physics-based algorithm for retrieving land-surface emissivity and temperature from eos/modis data. *Geoscience and Remote Sensing, IEEE Transactions on*, **35**(4):980–996.

Wan, Z., Y. Zhang, Q. Zhang, and Z. Li (2002). Validation of the land-surface temperature products retrieved from Terra Moderate Resolution Imaging Spectroradiometer data. *Remote Sens. Environ.*, **83**(1-2):163–180.

Weertman, J. (1973). Can a water-filled crevasse reach the bottom surface of a glacier? symposium on the hydrology of glaciers: Water within glaciers ii. *International Association of Scientific Hydrology Publication*, **95**:139–145.

Wientjes, I. and J. Oerlemans (2010). An explanation for the dark region in the western melt zone of the Greenland Ice Sheet. *The Cryosphere*, **4**(3):261–268.

Wouters, B., D. Chambers, and E. Schrama (2008). GRACE observes small-scale mass loss in Greenland. *Geophys. Res. Lett.*, **35**:L20501. doi:10.1029/2008GL034816.

Zwally, H. J., W. Abdalati, T. Herring, K. Larson, J. Saba, and K. Steffen (2002). Surface melt-induced acceleration of Greenland Ice Sheet flow. *Science*, **297**:218–222.

Appendix A

Lake maps

This section contains maps of the lakes detected on the Greenland Ice Sheet for each of the five years studied. Fast draining (red), slow draining (green), freezing (blue), and unknown (black) lakes are coloured. These figures are relevant to the analyses in Sections 5.4.1 and 6.3.1; these figures were omitted from those sections to prevent repetition of similar figures.

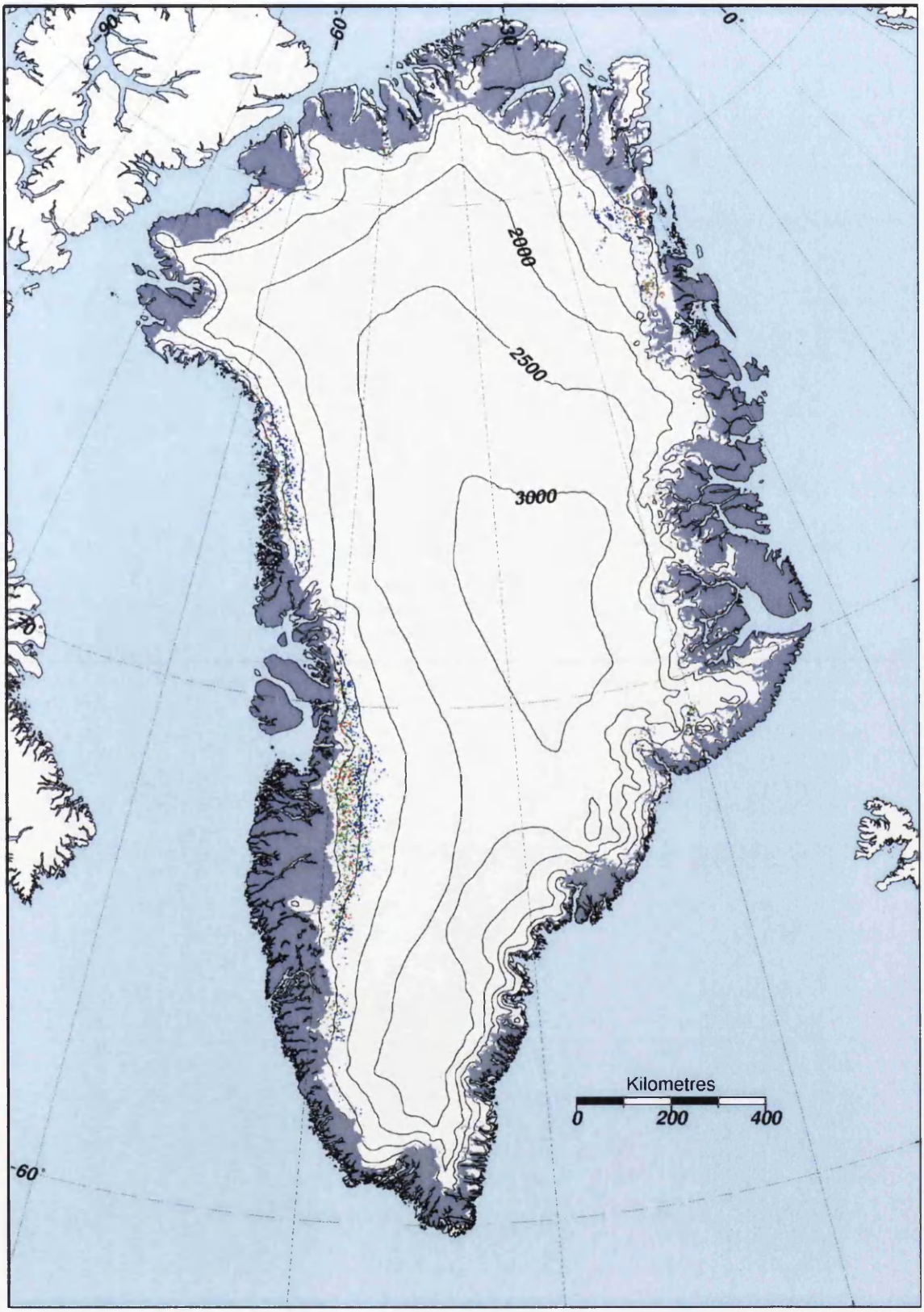

Figure A.1: Distribution of different drainage types in 2005, showing fast draining lakes (red), slow draining lakes (green), freezing lakes (blue), and lakes of unknown drainage type (black).

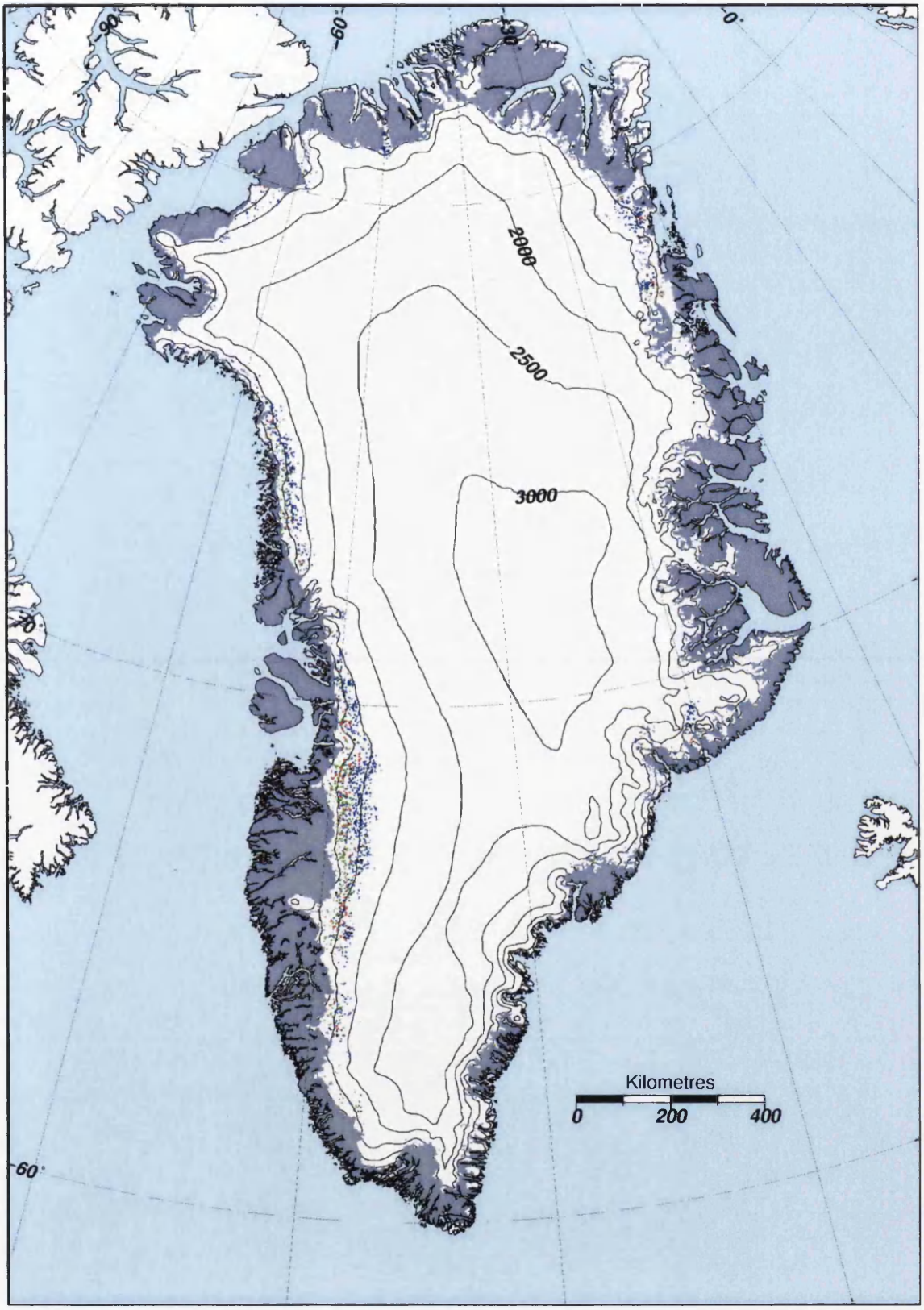

Figure A.2: Distribution of different drainage types in 2006, showing fast draining lakes (red), slow draining lakes (green), freezing lakes (blue), and lakes of unknown drainage type (black).

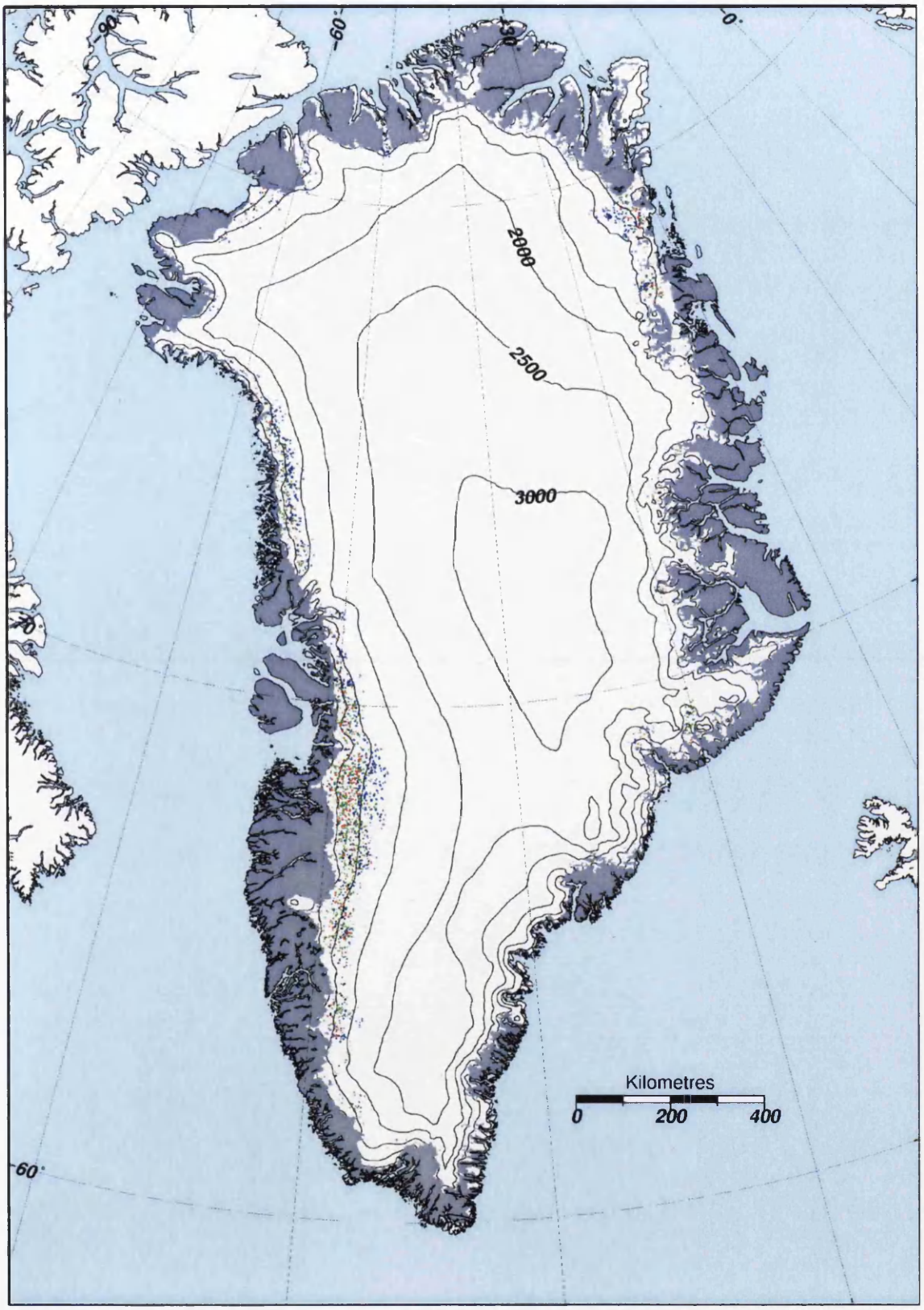

Figure A.3: Distribution of different drainage types in 2007, showing fast draining lakes (red), slow draining lakes (green), freezing lakes (blue), and lakes of unknown drainage type (black).

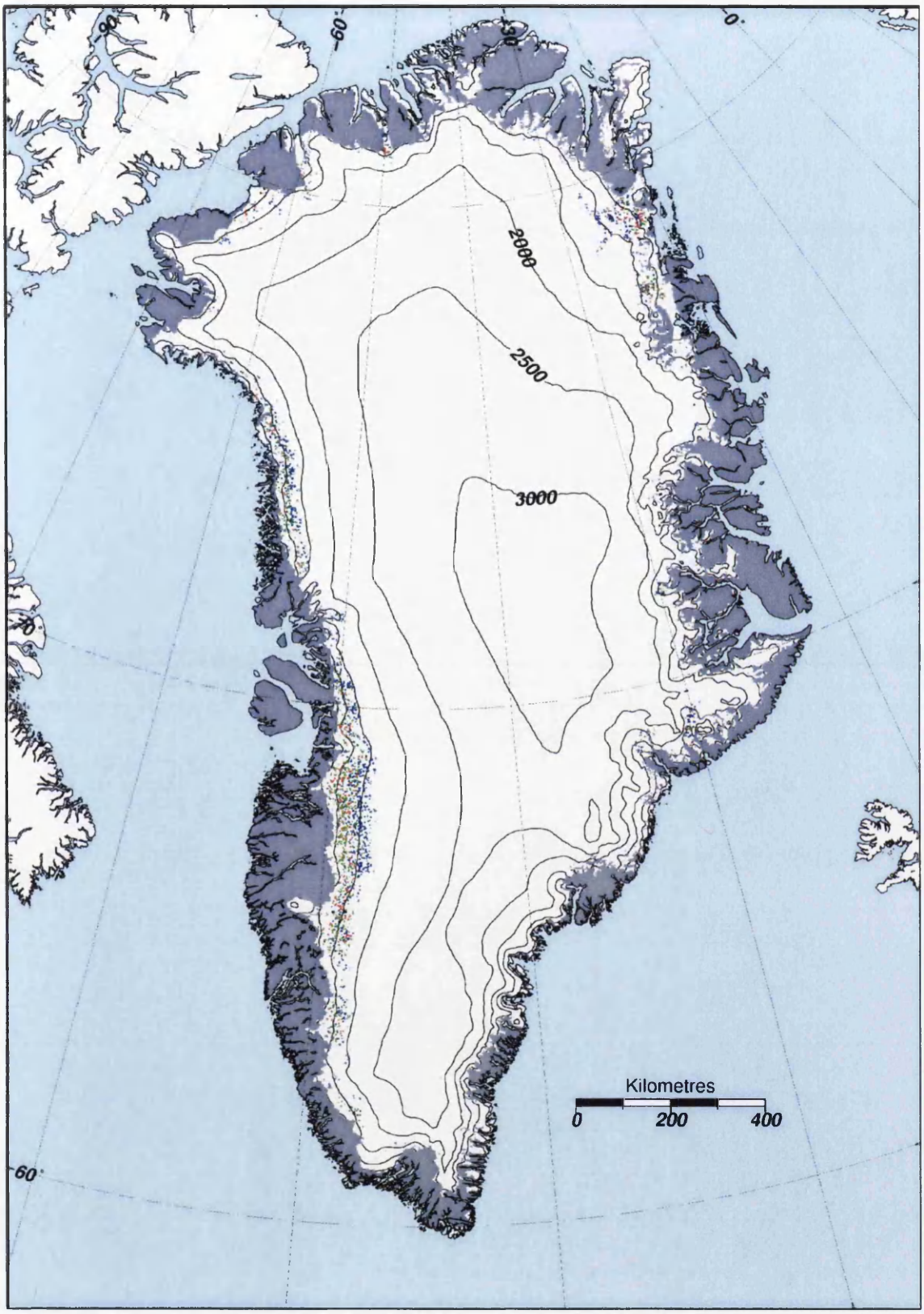

Figure A.4: Distribution of different drainage types in 2008, showing fast draining lakes (red), slow draining lakes (green), freezing lakes (blue), and lakes of unknown drainage type (black).

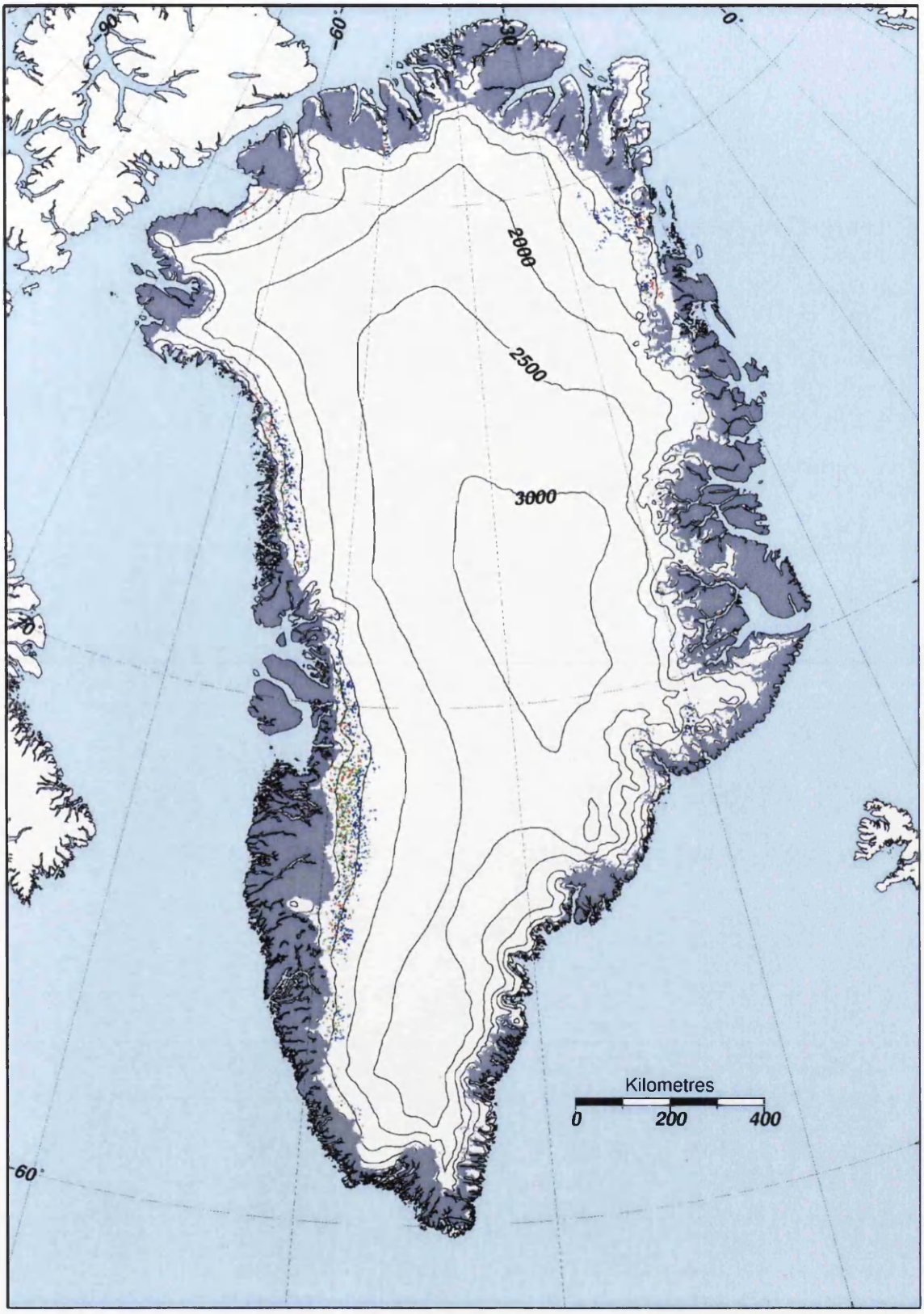

Figure A.5: Distribution of different drainage types in 2009, showing fast draining lakes (red), slow draining lakes (green), freezing lakes (blue), and lakes of unknown drainage type (black).

Appendix B

Additional results tables

This section contains addition results tables omitted from the main matter of this thesis for easier reading. Tables B.1–B.4 show expected frequencies and chi square analysis for the differing proportions of drainage types. Where each test is significant ($\chi^2 >$ the critical value) there was a significant difference between regions i.e. lakes were more likely to be of that drainage type in some regions than in others. These tables show that there was a significant difference for fast draining, slow draining, and freezing lakes, but not for lakes of unknown types. See Section 6.3.2 for more details.

Tables B.5–B.7 show expected frequencies and chi square analysis for the difference in frequency between regions for slow draining, freezing, and unknown lakes, and are discussed in Section 6.3.2.

Tables B.8–B.10 show the frequency of occurrence of slow draining, freezing and unknown lakes, and are equivalent to Table 6.6.

Table B.1: Observed and expected frequencies for fast-draining lakes, normalised by the total number of lakes in each region. χ^2=15.8, df=5, critical value (p=0.01)=15.086

Region	Total no. all lakes	Proportion of lakes	Observed freq. (O)	Expected freq. (E)	O-E	$\frac{(O-E)^2}{e}$
SW	1126	0.55	160	145	14.4	1.4
NW	390	0.19	29	50	-21.0	8.8
N	117	0.06	16	15	1.3	0.1
NE	267	0.13	45	34	11.0	3.5
E	101	0.05	9	13	-3.8	1.1
SE	37	0.02	3	5	-2.0	0.8
Total	2038		263	263		15.8

Table B.2: Observed and expected frequencies for slow draining lakes, normalised by the total number of lakes in each region. χ^2=16.7, df=5, critical value (p=0.01)=15.086

Region	Total no. all lakes	Proportion of lakes	Observed freq. (O)	Expected freq. (E)	O-E	$\frac{(O-E)^2}{e}$
SW	1126	0.55	420	384	36.0	3.4
NW	390	0.19	121	133	-12.1	1.1
N	117	0.06	26	40	-13.6	4.6
NE	267	0.13	70	91	-20.8	4.8
E	101	0.05	40	34	5.7	1.0
SE	37	0.02	17	13	4.8	1.8
Total	2038		694	263		16.7

Table B.3: Observed and expected frequencies for freezing lakes, normalised by the total number of lakes in each region. χ^2=17.8, df=5, critical value (p=0.01)=15.086

Region	Total no. all lakes	Proportion of lakes	Observed freq. (O)	Expected freq. (E)	O-E	$\frac{(O-E)^2}{e}$
SW	1126	0.55	470	529	-58.4	6.5
NW	390	0.19	221	183	37.7	7.8
N	117	0.06	64	55	8.9	1.4
NE	267	0.13	140	125	14.4	1.7
E	101	0.05	48	47	0.4	0.0
SE	37	0.02	14	17	-3.0	0.5
Total	2038		957	263		17.8

Table B.4: Observed and expected frequencies for unknown lakes, normalised by the total number of lakes in each region. χ^2=5.6, df=5, critical value (p=0.05)=11.070

Region	Total no. all lakes	Proportion of lakes	Observed freq. (O)	Expected freq. (E)	O-E	$\frac{(O-E)^2}{e}$
SW	1126	0.55	76	69	7.9	0.9
NW	390	0.19	19	24	-4.5	0.9
N	117	0.06	11	7	3.5	1.7
NE	267	0.13	12	16	-4.6	1.3
E	101	0.05	4	6	-2.3	0.9
SE	37	0.02	2	2	0.1	0.0
Total	2038		124	263		5.6

Table B.5: Observed and expected frequencies for slow draining lakes, normalised by margin length. χ^2=721, df=5, critical value (p=0.001)=20.52

Region	Ice margin length (km)	Proportion of total length	Observed freq. (O)	Expected freq. (E)	O-E	$\frac{(O-E)^2}{E}$
SW	1331	0.21	420	148	272	498
NW	1193	0.19	121	133	-12	1
N	923	0.15	26	103	-76	57
NE	476	0.08	70	53	17	5
E	985	0.16	40	110	-70	44
SE	1329	0.21	17	148	-131	115
Total	6237	1.00	694	694		721

Table B.6: Observed and expected frequencies for freezing lakes, normalised by margin length. χ^2=705, df=5, critical value (p=0.001)=20.52

Region	Ice margin length (km)	Proportion of total length	Observed freq. (O)	Expected freq. (E)	O-E	$\frac{(O-E)^2}{E}$
SW	1331	0.21	470	204	266	347
NW	1193	0.19	221	183	38	8
N	923	0.15	64	142	-78	42
NE	476	0.08	140	73	67	61
E	985	0.16	48	151	-103	71
SE	1329	0.21	14	204	-189	176
Total	6237	1.00	957	957		705

Table B.7: Observed and expected frequencies for unknown drainage type lakes, normalised by margin length. χ^2=133, df=5, critical value (p=0.001)=20.52

Region	Ice margin length (km)	Proportion of total length	Observed freq. (O)	Expected freq. (E)	O-E	$\frac{(O-E)^2}{E}$
SW	1331	0.21	76	26	50	94
NW	1193	0.19	19	24	-5	1
N	923	0.15	11	18	-8	3
NE	476	0.08	12	9	2	0
E	985	0.16	4	20	-16	13
SE	1329	0.21	2	26	-24	22
Total	6237	1.00	124	124		133

Table B.8: Frequency of slow lake drainages for all years studied (2005–2009), presented by catchment.

No.	Name	2005	2006	2007	2008	2009
14	Nordbogletscher	-	-	-	-	-
27	Arsuk Bræ	1	-	2	1	1
16	Sermilik	2	5	8	4	3
22	Frederikshab Isblink	5	5	16	16	14
13	Narssap	14	12	24	17	10
21	Narssap Sermia	118	106	141	151	109
15	Nordenskiöld	211	138	221	198	197
25	Jakobshavn	21	12	24	27	23
29	Unnamed	22	14	27	28	14
28	Sermeq Avangnardleq	11	3	11	8	6
30	Unnamed	23	16	26	25	19
9	Rinks	2	5	3	4	3
31	Unnamed	65	62	84	85	57
3	Hayes	9	3	13	12	6
32	Steenstrup	19	17	34	33	31
5	Kong Oscar	2	-	3	4	5
33	Unnamed	9	3	7	10	16
4	Humboldt	7	5	8	9	7
34	Unnamed	-	-	-	-	-
8	Petermann	8	3	6	8	8
35	Unnamed	4	-	-	3	4
10	Ryder	6	-	1	7	6
36	Unnamed	2	2	-	-	1
7	Ostenfeld	-	1	-	-	-
37	Unnamed	1	-	-	-	-
1	Academy	-	-	-	1	1
38	Unnamed	3	1	1	2	4
39	Unnamed	2	-	2	1	-
6	Nioghlvfjerdsbræ	13	2	6	15	9
40	Unnamed	12	2	6	10	3
12	Zachariae	13	4	6	11	6
11	Storstrømmen	40	22	37	47	26
41	Walterhausen	29	15	26	23	32
2	Daugaard-Jensen	4	5	5	5	3
42	K. Christian IV	30	10	30	15	12
26	Kangerdlugssuaq	9	7	11	10	13
19	Schweizerland	4	4	4	4	6
23	Helheim	-	1	3	1	1
20	Johan Peterson	-	-	-	-	-
24	Ikertivaq	-	-	-	-	-
17	Koge	-	-	-	-	-
18	SE Fjords	2	3	-	1	2

Table B.9: Frequency of freezing lakes for all years studied (2005–2009), presented by catchment.

No.	Name	2005	2006	2007	2008	2009
14	Nordbogletscher	-	-	-	-	-
27	Arsuk Bræ	1	2	4	3	1
16	Sermilik	5	3	5	4	6
22	Frederikshab Isblink	20	18	24	24	20
13	Narssap	23	26	20	28	19
21	Narssap Sermia	128	140	78	120	146
15	Nordenskiöld	170	245	115	174	142
25	Jakobshavn	53	59	57	46	34
29	Unnamed	23	23	12	15	17
28	Sermeq Avangnardleq	20	28	13	18	18
30	Unnamed	39	53	48	41	48
9	Rinks	12	11	12	12	9
31	Unnamed	117	122	95	91	110
3	Hayes	26	29	23	21	26
32	Steenstrup	63	63	57	42	46
5	Kong Oscar	3	5	4	4	2
33	Unnamed	16	31	23	25	19
4	Humboldt	17	24	22	23	17
34	Unnamed	-	-	-	-	-
8	Petermann	14	14	14	11	8
35	Unnamed	5	10	7	6	4
10	Ryder	8	13	11	4	11
36	Unnamed	-	1	3	-	-
7	Ostenfeld	3	2	1	1	3
37	Unnamed	-	-	-	-	-
1	Academy	4	1	2	4	2
38	Unnamed	7	2	1	11	8
39	Unnamed	-	2	-	-	1
6	Nioghlvfjerdsbræ	57	34	34	59	63
40	Unnamed	24	27	23	18	26
12	Zachariae	16	27	16	14	23
11	Storstrømmen	25	50	28	26	30
41	Walterhausen	20	27	19	25	15
2	Daugaard-Jensen	12	11	10	10	9
42	K. Christian IV	13	35	10	31	30
26	Kangerdlugssuaq	13	14	13	12	11
19	Schweizerland	2	3	1	1	-
23	Helheim	-	-	-	-	-
20	Johan Peterson	-	-	-	-	-
24	Ikertivaq	-	-	-	-	-
17	Koge	-	-	-	-	-
18	SE Fjords	-	1	-	1	-

Table B.10: Frequency of unknown lakes for all years studied (2005–2009), presented by catchment.

No.	Name	2005	2006	2007	2008	2009
14	Nordbogletscher	-	-	-	-	-
27	Arsuk Bræ	-	1	-	2	-
16	Sermilik	-	3	-	4	-
22	Frederikshab Isblink	9	11	7	4	1
13	Narssap	3	4	9	1	1
21	Narssap Sermia	29	38	50	12	23
15	Nordenskiöld	28	18	33	14	17
25	Jakobshavn	7	3	4	1	2
29	Unnamed	2	7	4	-	7
28	Sermeq Avangnardleq	-	-	2	-	2
30	Unnamed	8	1	5	2	4
9	Rinks	-	-	2	-	-
31	Unnamed	8	5	16	13	11
3	Hayes	1	-	-	-	-
32	Steenstrup	2	7	4	6	3
5	Kong Oscar	-	1	1	-	1
33	Unnamed	5	-	2	4	3
4	Humboldt	4	5	7	6	-
34	Unnamed	-	-	-	-	-
8	Petermann	3	2	1	1	1
35	Unnamed	1	-	-	-	-
10	Ryder	4	2	2	2	1
36	Unnamed	-	-	-	-	-
7	Ostenfeld	-	-	-	-	-
37	Unnamed	-	2	-	1	-
1	Academy	-	5	-	-	-
38	Unnamed	1	-	-	-	-
39	Unnamed	-	-	-	-	1
6	Nioghlvfjerdsbræ	3	2	2	3	4
40	Unnamed	1	-	2	2	5
12	Zachariae	2	1	-	1	2
11	Storstrømmen	1	1	1	5	12
41	Walterhausen	2	-	1	3	6
2	Daugaard-Jensen	-	-	-	-	-
42	K. Christian IV	5	2	1	2	3
26	Kangerdlugssuaq	1	-	-	-	1
19	Schweizerland	2	-	-	2	-
23	Helheim	1	1	-	-	-
20	Johan Peterson	-	-	-	-	-
24	Ikertivaq	-	-	-	-	-
17	Koge	-	-	-	-	-
18	SE Fjords	-	-	1	1	-